HAL
open science

Contribution to the experimental and theroretical study of phase-change heat transfer for the thermal management of electronics

Stéphane Lips

To cite this version:

Stéphane Lips. Contribution to the experimental and theroretical study of phase-change heat transfer for the thermal management of electronics. Thermics [physics.class-ph]. Institut National des Sciences Appliquées de Lyon; Université Claude Bernard Lyon 1, 2018. tel-01858451

HAL Id: tel-01858451

https://hal.science/tel-01858451

Submitted on 6 Sep 2018

HAL is a multi-disciplinary open access archive for the deposit and dissemination of scientific research documents, whether they are published or not. The documents may come from teaching and research institutions in France or abroad, or from public or private research centers.

L'archive ouverte pluridisciplinaire **HAL**, est destinée au dépôt et à la diffusion de documents scientifiques de niveau recherche, publiés ou non, émanant des établissements d'enseignement et de recherche français ou étrangers, des laboratoires publics ou privés.

N° 2018 HDR 004 Année 2018

HABILITATION A DIRIGER DES RECHERCHES

présentée devant

l'Institut National des Sciences Appliquées de Lyon
et l'Université Claude Bernard LYON I

Contribution à l'étude expérimentale et théorique des transferts thermiques avec changement de phase pour le contrôle thermique des composants électroniques

SPECIALITE : Thermique et Energétique

Par

Lips Stéphane

Soutenue le 06 Juin 2018 devant la Commission d'examen

Bertin Yves	Professeur, ENSMA, Institut P Prime,	rapporteur
Bonjour Jocelyn	Professeur, INSA de Lyon,	examinateur
Colin Catherine	Professeur, INP/ENSEEIHT, IMFT Toulouse,	rapporteur
Jallut Christian	Professeur, Université Lyon 1,	président
Khandekar Sameer	Professeur, IIT Kanpur, India,	rapporteur
Laraqi Najib	Professeur, Université Paris-Nanterre	examinateur

CETHIL

Résumé

Le contrôle thermique des composants électroniques est un enjeu majeur dans de nombreuses applications industrielles. L'augmentation des puissances thermiques à dissiper sur des surfaces toujours plus petites rend les solutions de refroidissement traditionnelles, basées sur un refroidissement par air ou par liquide sans changement de phase, souvent obsolètes. Les solutions de contrôle thermique par voie diphasique peuvent permettre de répondre à ces besoins, sous réserve d'un dimensionnement fiable des systèmes concernés.

Cette habilitation à diriger les recherches est donc une contribution à l'étude expérimentale et théorique des phénomènes et des transferts thermiques au sein de systèmes de contrôle thermique avec changement de phase. Trois grands types de systèmes sont abordés : les caloducs, les condenseurs ou évaporateurs, et les amortisseurs thermiques (basés sur le changement de phase solide-liquide).

Mon parcours scientifique ainsi que son contexte scientifique est résumé dans l'introduction. Un état de l'art des solutions de contrôle thermique pour les composants électroniques, ainsi que les différentes problématiques scientifiques associées y sont aussi discutés de manières très globale. Les chapitres 2 à 4 représentent chacun un volet des recherches que j'ai pu effectuer tout au long de mon parcours.

Les caloducs constituent des solutions particulièrement intéressantes pour le refroidissement de composants électroniques. Dans ce domaine, mes recherches sont essentiellement axées sur des analyses phénoménologiques des systèmes, ce qui permet de mieux appréhender leur comportement. L'utilisation de systèmes transparents, couplée au développement de modèles inverses et/ou mécanistiques, représente une des particularités du CETHIL dans ce type d'analyse. Quelques exemples d'études sont présentés dans le chapitre 2.

Lorsque les solutions passives ne suffisent plus, les phénomènes d'ébullition et de condensation convectives peuvent être utilisés au sein d'évaporateurs et de condenseurs. Dans le chapitre dédié, l'effet de forces de frottements, de capillarité, de gravité et d'inertie sur la structure de ce type d'écoulements, les pertes de charges et les transferts thermiques sont discutés, en particulier dans le cas d'écoulements en tubes inclinés. La synthèse permet de mettre en avant les similitudes et différences des écoulements en ébullition et en condensation convectives.

Dans certaines applications, les sollicitations thermiques sont extrêmement fluctuantes. L'enjeu n'est alors plus d'évacuer la chaleur, mais de limiter les pics de températures dues aux sollicitations transitoires. Le concept d'amortisseur thermique, couplant un matériau à changement de phase solide-liquide et une matrice à haute conductivité thermique, peut être utilisé pour augmenter l'inertie thermique apparente du système à contrôler. Le dernier chapitre est donc consacré à l'étude de l'un de ces types de système, composé de paraffine dans une structure de nanotubes de carbone densifiés, elle-même insérée dans une cavité en silicium.

Au sein de chacun de ces chapitres, un bref état de l'art est proposé et les différentes approches, théoriques, de modélisation et expérimentales sont présentées. Des perspectives sont proposées à la fin de chaque chapitre, puis synthétisées et priorisées dans la conclusion finale.

Abstract

Thermal management of electronic components is a major issue in many industrial applications. The continuous increase of the heat power to be dissipated on smaller surfaces makes many traditional cooling systems obsolete. Two-phase cooling systems can be used to cater to such cooling specifications, but have to be carefully designed.

The present habilitation thesis to supervise research (HDR) is thus a contribution to the experimental and theoretical study of heat transfer in two-phase cooling systems. Three types of systems are considered: Heat pipes, condensers or evaporators, and thermal dampers (involving solid-liquid phase change).

My research path and its scientific context are presented in the introduction. The general overview of the various systems for the cooling of electronics, as well as the main scientific issues involved are also outtired. Chapters 2 to 4 then present the three components of my research, linked to the three types of systems.

Heat pipes are very interesting solutions to the thermal management of electronic component. In this field, my work consists mainly in phenomenological analyses of the various systems, in order to achieve a better understanding of their behaviour. One of the specificities of the approaches followed by the CETHIL is the coupling between transparent device characterisations and the development of inverse or mechanistic models. Examples are presented in chapter 2.

When passive cooling solutions cannot fit the specifications, convective boiling and condensation phenomena can be used to increase the thermal efficiency of the systems. In the dedicated chapter, the effects of the frictional, inertial, capillary and gravitational forces on the flow regime, the heat transfer and the pressure drops are discussed, particularly in inclined configurations. As a conclusion, the similitudes and differences between condensing and evaporating flows are discussed.

In applications such as telecommunications, electronics components are subject to large thermal transients. In order to limit their temperature variation, thermal dampers can be used in order to increase the apparent thermal inertia of the system. They consist in the coupling between a solid-liquid phase-change material with a high thermal conductivity structure. The last chapter is devoted to the study of such a system, made of paraffin inserted in an array of densified carbon nanotubes ; the integrated unit directly inserted into the silicon substrate of an electronic component.

In each chapter, a brief literature review is presented and the various scientific approaches, which I followed, are presented (theoretical, modelling, and experimental). Perspectives are discussed at the end of each chapter, and are then summarised and prioritised in the final conclusion.

Contents

RESUME ..... **III**

ABSTRACT ..... **IV**

CONTENTS ..... **V**

LIST OF FIGURES ..... **VII**

LIST OF TABLES ..... **XI**

NOMENCLATURE ..... **XIII**

CHAPTER 1: INTRODUCTION AND CONTEXT **1**

1.1 Personal context 1

1.2 Industrial and scientific challenges in the thermal management of electronic components 2

1.3 Overview of my research 3

CHAPTER 2: PASSIVE SYSTEMS BASED ON THE LIQUID-VAPOUR PHASE CHANGE: HEAT PIPES AND RELATED **5**

2.1 Working principle, history and applications 5

2.2 General approach of the scientific community 7

2.2.1 Research motivated by the heat pipe characterization *8*

2.2.2 Scientific issues linked to the working Fluid behaviour *10*

2.2.3 Studies aiming to predict the phase change heat transfer in thin films *12*

2.2.4 The development of new heat pipe models *14*

2.2.5 Summary and Conclusions *14*

2.3 The heat pipe: an old concept full of scientific challenges 14

2.3.1 Heat pipe modelling *15*

2.3.2 A research strategy based on a phenomenological analysis *19*

2.3.3 On the difficulty of characterizing a heat pipe *21*

2.3.4 Example of theoretical study: Definition of an utility criterion *25*

2.4 When heat pipe scientific issues meet technological issues (or maybe the opposite?) 28

2.4.1 The case of the loop heat pipes *28*

2.4.2 Toward new heat pipe designs? *31*

2.4.3 Example of active control of heat pipes: application of EHD forces *33*

2.4.4 Plastic heat pipe: expectations and limits *36*

2.5 Conclusions and perspectives 38

CHAPTER 3: ACTIVE COOLING SYSTEMS: CONVECTIVE BOILING AND CONDENSATION **39**

3.1 Scientific context 39

3.1.1 General description of two-phase flows *39*

3.1.2 Characterisation techniques for two-phase flows *41*

3.1.3 Force balance in two-phase flows: effect of the tube inclination *43*

3.2 Experimental test benches and flow pattern characterisation 45

3.2.1 Description of the experimental test benches *45*

3.2.2 Effect of the tube inclination on the flow pattern map *46*

3.2.3 Database analysis for the construction of a symmetry correlation *49*
3.2.4 Conclusions *53*
3.3 Effect of the tube orientation on the heat transfer 53
3.3.1 Experimental determination of the heat transfer coefficient *53*
3.3.2 Convective condensation *54*
3.3.3 Convective boiling *57*
3.3.4 Conclusions *59*
3.4 Effect of the tube orientation on the pressure drops 59
3.4.1 Pressure drops measurements *60*
3.4.2 The notion of apparent gravitational pressure drop and void fraction *62*
3.4.3 Theory or philosophy? Discussion on the physical meaning of a pressure drop decomposition *64*
3.4.4 An optimum inclination angle in terms of Entropy generation? *71*
3.5 Conclusions and perspectives 72
CHAPTER 4: PASSIVE SYSTEMS USING THE SOLID-LIQUID PHASE CHANGE: THE NOTION OF THERMAL DAMPER 75
4.1 Principle and general overview of the applications 75
4.2 The need for the notion of ideal thermal damper 76
4.3 Experimental characterisation of a thermal damper 80
4.3.1 Samples and test benches *80*
4.3.2 Optical approach and calibration *81*
4.3.3 Heat storage capacity characterisation *82*
4.3.4 Thermal resistance characterisation *83*
4.4 Optical non-destructive testing 85
4.5 Conclusions and perspectives 88
CHAPTER 5: CONCLUSIONS AND PERSPECTIVES 89
5.1 Conclusions of the present analysis 89
5.2 Research perspectives 90
REFERENCES 91
LIST OF PUBLICATIONS 103
CURRICULUM VITAE (IN FRENCH) 107

List of figures

Figure 1-1. Simplified timeline of the various projects and supervisions in which I have been involved 2
Figure 1-2. Evolution of the transistors number per chip and the clock speed of microprocessors (Waldrop, 2016) 2
Figure 1-3. Evolution of the size of the electronic component (Waldrop, 2016) 2
Figure 1-4. 3D electronic component (sources left: Fraunhofer IZM; centre: ITRS 2009; right: AES, Samsung) 2
Figure 1-5. Example of 3D electronic component manufactured by ST-Ericsson / CEA (Vivet and Guérin, 2011) .. 3
Figure 1-6. Maximal admissible temperature on various location of a cell phone (Kinkelin, 2016) 3
Figure 1-7. Various systems used for the thermal management of electronic components. In green, the systems which I had the opportunity to study. In blue, the systems I used commonly as an engineer tool 4
Figure 2-1. Different heat pipe technologies (Lips, 2015) 5
Figure 2-2. Number of papers dedicated to heat pipes according to the database of Web of ScienceTM (Lips, 2015) 7
Figure 2-3. Experimental characterization of the operating regime of a PHP by means of a thermal camera (Karthikeyan et al., 2014) 10
Figure 2-4. Visualisation and modelling of the vapour region in the evaporator of a LHP (Mottet et al., 2015) .. 10
Figure 2-5. Possible clogging of nanoparticles in a nucleating cavity affecting the boiling phenomenon (Khandekar et al., 2008) 12
Figure 2-6. Number of publications dedicated to nanofluids in heat pipes according to the database of Web of Science™ 12
Figure 2-7. Example of the effect of the nanostructuration of the wall on the boiling curve obtained with γ-Fe_2O_3 nanoparticle on a 100 µm platinum wire. τ_c is the nano-particle coating duration with pure water (Stutz et al., 2011) 13
Figure 2-8. Distribution of the heat transferred from the wall to the fluid during the passage of a meniscus (Chauris et al., 2015) 13
Figure 2-9. Various levels of nodal models 15
Figure 2-10. Geometries and corresponding domains for three heat pipe configurations (Lips and Lefèvre, 2014) 16
Figure 2-11. Example of thermal and hydrodynamic results obtained with the analytical model for a flat plate heat pipe with three heat sources and two heat sinks (Lips and Lefèvre, 2014) 17
Figure 2-12. Example of phenomena occurring in heat pipes and difficult to consider in a 3D model 17
Figure 2-13. Schematic of the evaporator with double layer wick (Giraudon et al., 2017a) 18
Figure 2-14. Capillary limit as a function of the bottom layer pore radius (left) and of the top and bottom layer permeabilities (right) (Giraudon et al., 2017a) 19
Figure 2-15. Flat heat pipe configurations tested by Alba Fornells-Vernet , adapted from (Fornells-Vernet, 2012) 20
Figure 2-16. Example of heat pipe performance for various configurations (Lips et al., 2013) 20
Figure 2-17. Example of comparison between an experimental temperature profile and the corresponding profile calculated by the inverse method (Q = 20 W; horizontal orientation) (Revil-Baudard and Lips, 2015) 21
Figure 2-18. Example of equivalent thermal conductivity determination by means of the inverse method (L_{evap} = 140 mm, horizontal orientation) (Revil-Baudard and Lips, 2015) 21
Figure 2-19. Example of evolution of the gravitational pressure drop as a function of the heat transfer rate transferred by phase change (Levap = 140 mm) (Revil-Baudard and Lips, 2015) 22
Figure 2-20. Example of the frictional pressure drop as a function of the heat transfer rate (Levap = 140 mm) (Revil-Baudard and Lips, 2015) 22
Figure 2-21. Example of sample manufactured by Rémi Giraudon during his PhD (Giraudon et al., 2017b) 22
Figure 2-22. 3D view of the experimental test bench (Giraudon et al., 2017b) 22
Figure 2-23. Operating principle of the test bench when measuring the permeability (Giraudon et al., 2017b) . 23
Figure 2-24. Example of determination of the permeability for two samples (Giraudon et al., 2017b) 23
Figure 2-25. Operating principle when measuring the effective pore radius (Giraudon et al., 2017b) 23
Figure 2-26. Example of evolution of the water level during the test (Giraudon et al., 2017b) 23
Figure 2-27. 3D view and schematic of the thermal test bench (Giraudon et al., 2017b) 24
Figure 2-28. Example of a sample thermal characterisation (Giraudon et al., 2017b) 24
Figure 2-29. Evolution of the heat transfer coefficient for each sample with water (Giraudon et al., 2017b) 24
Figure 2-30. Evolution of the heat transfer coefficient for each sample with pentane (Giraudon et al., 2017b) .. 24

Figure 2-31. Comparison of the maximum heat flux of the various samples between water and pentane (Giraudon et al., 2017b) 25
Figure 2-32. Comparison of the maximum heat transfer coefficient of the various samples between water and pentane (Giraudon et al., 2017b) 25
Figure 2-33. Example of studied configuration. The heat sink is not represented (Lips et al., 2017b) 25
Figure 2-34. Examples of temperature fields in the PCB, calculated by CFD modelling for two different heat transfer coefficient with the heat sink (Q = 25 W/components and T_{amb} = 0°C) (Lips et al., 2017b) 26
Figure 2-35. Heat spreading efficiency of the PCB presented on figure 2-33 (In the present example, $R_{cond,0}$ = 0.4 K/W) (Lips et al., 2017b) 27
Figure 2-36. Thermal gain of a flat heat pipe for S_b/S_{tot} = 1 (Lips et al., 2017b) 27
Figure 2-37. Thermal gain of a flat heat pipe for S_b/S_{tot} = 0.25 (Lips et al., 2017b) 27
Figure 2-38. Thermal gain for various PCB spreading efficiency, characterized by $R_{cond,0}$ (Lips et al., 2017b) 27
Figure 2-39. Configuration characterized, with and without flat heat pipe (left) and its thermal resistance measured with various heating and cooling conditions (right) (D: heating spot diameter, CN: Natural convection, CF: forced convection, sans DTD: without flat heat pipe, avec DTD: with flat heat pipe) (Lips et al., 2017b) 28
Figure 2-40. Heat leaks in a cylindrical evaporator (Giraudon, 2017) , adapted from (Siedel, 2014)) 28
Figure 2-41. Thermal expansion coefficient for various polymers, metals and ceramics (Giraudon, 2017). 30
Figure 2-42. SEM pictures of a sintered samples made of zircone (left) and copper (right) (Giraudon, 2017) 30
Figure 2-43. SEM pictures of a freeze casted sample: top view (left) and side view (right) (Giraudon, 2017) 30
Figure 2-44. Experimental set-up with the confined thermosiphon (Narcy et al., 2017) 31
Figure 2-45. Flow visualizations with the transparent heat spreader. Initial filling ratio: 30% of the spreader volume, Q = 500 W in (b) and (c) (Narcy et al., 2017) 32
Figure 2-46. Influence of inclination on the heat spreader thermal performance (Narcy et al., 2017) 32
Figure 2-47. Evolution of the spreader thermal resistance for various filling ratios (Narcy et al., 2017) 32
Figure 2-48. Schematic of a two-phase heat spreader with integrated fins 33
Figure 2-49. Example of condensation pattern in an array of transparent tube (Berut, 2016) 33
Figure 2-50. Example of the effect of electric field on the interface shape (Cardin et al., 2017) 34
Figure 2-51. Effect of an electric field at meniscus recession for FC-72 (Cardin et al., 2017) 34
Figure 2-52. Effect of an electric field on the pressure jump for FC-72 (Cardin et al., 2017) 34
Figure 2-53. Effect of an electric field on the maximal pressure for FC-72 (Cardin et al., 2017) 34
Figure 2-54. Schematic of the experimental set up of Cardin et al. (2018) 35
Figure 2-55. Evolution of the hydrostatic pressure drop along central groove an angle of 5° and a partial electrode. The solid blue line represents the analytical solution in the absence of electric field. The blue dots are the experimental results in the absence of electric field, the red dots the experimental results in presence of the electric field (Cardin et al., 2018) 35
Figure 2-56. Comparison between measurements (marks) and the numerical prediction (solid lines) of the effect of an electric field on the curvature evolution of a meniscus in an inclined groove (Cardin et al., 2018) 35
Figure 2-57. Example of prototype manufactured by Elise Berut (Berut, 2016) 37
Figure 2-58. Example of contribution of the various thermal resistance of the system (conv: convection ; c,cond: conduction at the condenser ; c,évap: conduction at the evaporator) (Berut, 2016) 37
Figure 3-1. Flow pattern map of Wojtan et al. (2005) 40
Figure 3-2. The different types of flow patterns considered in the study of Lips and Meyer (2012a). Discrimination were performed only visually 40
Figure 3-3. Flow patterns considered by Layssac et al. in his PhD (2018a). The determination of the top and bottom liquid thicknesses enables to use quantitative indicators 40
Figure 3-4. Geometry considered by Taitel and Dukler (1976) for stratified flow 40
Figure 3-5. Pumping action of the disturbance waves, adapted from Fukano and Ousaka (1989) 40
Figure 3-6. Example of comparison between experiments and simulations of a growing bubble in a subcooled convective flow (Lal et al., 2015) 41
Figure 3-7. Example of boiling modelling taking into account the bubble merging (Sato and Niceno, 2017) 41
Figure 3-8 Example of heated transparent test section by means of an ITO coating (Narcy et al., 2014) 41
Figure 3-9 Superposition of IR and visible images of a saturated R11 flow for increasing heat fluxes (Ozer et al., 2011) 41
Figure 3-10 Example of liquid film LIF visualization (Schubring et al., 2010) 42
Figure 3-11 Three-dimensional wavy structure for entrainment regimes (Alekseenko et al., 2012) 42
Figure 3-12. Flow pattern amp of Bhagwat et Ghajar (2016b) for upward air-water flow in a 12,7 mm inner diameter smooth tube 43

Figure 3-13. Flow pattern amp of Bhagwat et Ghajar (2017) for downward air-water flow in a 12,7 mm inner diameter smooth tube 43
Figure 3-14. Example of pressure drop evolution as a function of the inclination angle (air-water flow in a 4.55 mm inner diameter pipe) (Spedding et al., 1982) 44
Figure 3-15. Example of evolution of the heat transfer coefficient as a function of the tube inclination for convective boiling of HFE 7100 in a 0.44 mm inner diameter channel (Hsu et al., 2015a) 44
Figure 3-16. Picture and schematic diagram of the experimental setup of Lips and Meyer (2011b) for the study of convective condensation in an inclined orientation 45
Figure 3-17. Schematic of the test bench of Layssac et al. (2018a) for the study of convective boing in inclined orientation 45
Figure 3-18. Schematic of the test section of Charnay et al. (2014) 46
Figure 3-19. Photo and schematic of the evaporator of Layssac et al. (2018a) 46
Figure 3-20. Effect of the inclination angle on the flow pattern for different mass fluxes (R134a, d = 8.38 mm, x = 0.5) (Lips and Meyer, 2012a) 47
Figure 3-21. Evolution of flow patterns (pink: intermittent; blue: stratified; green: annular) and time representative frames for various vapour qualities and inclination angles (R245fa, d = 1.6 mm, G = 150 kg.m^{-2}.s^{-1}) (Layssac et al., 2018a) 47
Figure 3-22. Example of experimental flow pattern map of Lips and Meyer (2012c) (R134a, d = 8.38 mm, G = 200 kg/m²s) 47
Figure 3-23. Example of experimental flow pattern map of Layssac et al. (2018a) (R245fa, d = 1.6 mm, G = 150 kg.m^{-2}.s^{-1} ; φ = 0 kW.m^{-2}) 47
Figure 3-24. Comparison of experimental flow patterns of Lips and Meyer (2012a) and Layssac et al. (2018a) with the Barnea (1987) flow pattern map (An = Annular, I = Intermittent, S = Stratified) 48
Figure 3-25. Example of the heat flux effect on the flow pattern (Layssac et al., 2018a) 49
Figure 3-26. Flow patterns with φ = 13,5 kW.m^{-2} compared to the adiabatic conditions (G = 150 kg.m^{-2}.s^{-1}) (Layssac et al., 2018a) 49
Figure 3-27. Position of the vapour core centre for a horizontal two-phase flow (Layssac et al. (2017)) 50
Figure 3-28. Base parameters correlation (Layssac et al., 2017) 51
Figure 3-29. Evolution of the Mean Squared Error with the imposed exponents (Layssac et al., 2017) 51
Figure 3-30. Correlation with the Bond number, the Froude number and the Lockhart-Martinelli parameter (Layssac et al., 2017) 52
Figure 3-31. Evolution of the Mean Squared Error with imposed dimensionless number exponents (Layssac et al., 2017) 52
Figure 3-32. Measured symmetry as a function of predicted symmetry for Bd, χ and Fr_{vo} correlation (Layssac et al., 2017) 52
Figure 3-33. Top and side view of the IR test section. Polycarbonate plates enables to measure the equivalent temperature of the test section surroundings (Layssac et al., 2018b) 54
Figure 3-34. Black body temperature field of the test section. The edges of the tube appear hotter because of the angle dependence of the ITO coating emissivity (Layssac et al., 2018b) 54
Figure 3-35. Variations of the ITO deposit emissivity with abscissa for sapphire outer wall temperature of 70°C, 80°C and 90°C (Layssac et al., 2018b) 54
Figure 3-36. Thermal model at abscissa z and electric equivalent schematic (Layssac et al., 2018b) 54
Figure 3-37. Experimental heat transfer coefficient during convective condensation of R134a in a 8.38 mm tube (G = 200 kg/m²s, -90° : downwards, 0° : horizontal; 90° vertical upwards) (Lips and Meyer, 2012c) 55
Figure 3-38. Inclination effect on heat transfer coefficients during convective condensation of R134a in a 8.38 mm tube for various mass fluxes (x = 0.5) (Lips and Meyer, 2012a) 55
Figure 3-39. Map of the inclination effect on heat transfer coefficients drawn on the Thome-El Hajal-Cavallini (El Hajal et al., 2003) flow pattern map (Lips and Meyer, 2012a) 55
Figure 3-40. Flow patterns and heat transfer coefficients for downward flows at low mass fluxes and low vapour qualities (Lips and Meyer, 2012a) 55
Figure 3-41. Pressure drops predicted by the model of Taitel and Dukler compared with experimental results obtained for convective condensation of R134a in a 8.38 mm tube (Lips and Meyer, 2012b) 56
Figure 3-42. Modified model of Taitel and Dukler (1976) for convective condensation in inclined tubes (Lips and Meyer, 2012c) 56
Figure 3-43. Scheme of the thermal model for the heat transfer coefficient determination for convective condensation in inclined tubes (Lips and Meyer, 2012c) 56

Figure 3-44. Comparison of the model predictions with experimental results (G = 200 kg/m²s). Dashed lines mean that the flow is not stratified according to Crawford et al. (1985)(Lips and Meyer, 2012c) 57
Figure 3-45. Influence of different assumptions on the model predictions. FFHTC: Falling film heat transfer coefficient (G = 200 kg/m²s ; x = 0.3; ΔT = 2 K) (Lips and Meyer, 2012c) 57
Figure 3-46. Variations of the heat transfer coefficient with the inclination angle for various mass fluxes (x = 0.06) (Layssac, 2018) 57
Figure 3-47. Variations of the heat transfer coefficient with the vapour quality for various inclination angle (G = 148 kg/m²s) (Layssac, 2018) 57
Figure 3-48. Variations of the heat transfer coefficient with the inclination angle for various heat fluxes (x = 0.12; G = 150 kg/m²s) (Layssac, 2018) 58
Figure 3-49. Prediction of the variations of the nucleate and convective heat transfer mode with vapour quality from Bertsch et al. (2009) model for a mass velocity of 150 kg.m^{-2}.s^{-1} (Layssac, 2018) 59
Figure 3-50. Measured pressure drops for different vapour qualities (R134a, d = 8.38 mm; G = 300 kg/m²s) (Lips and Meyer, 2012b) 60
Figure 3-51. Measured pressure drops for different mass fluxes (R134a, d = 8.38 mm; x = 0.5) (Lips and Meyer, 2012b) 60
Figure 3-52. Evolution of total pressure gradient as a function of the inclination angle for convective boiling of R245fa in a 1.6 mm tube and a mass velocity of 150 kg.m^{-2}.s^{-1} (Layssac et al., 2018a) 61
Figure 3-53. Comparison of pressure gradient evolution with inclination angle with an imposed heat flux of 13.5 kW.m^{-2} (filled lines) and without heat flux (dot lines) (Layssac et al., 2018a) 61
Figure 3-54. Evolution of the frictional pressure gradient as a function of the inclination angle (R134a, d = 8.38 mm; G = 200 kg/m²s) 62
Figure 3-55. Evolution of the frictional pressure gradient as a function of the inclination angle for a mass velocity of 150 kg.m^{-2}.s^{-1} (Layssac et al., 2018a) 62
Figure 3-56. Apparent gravitational pressure drops for various vapour qualities and mass fluxes as a function of inclination angle (R134a, d = 8.38 mm) (Lips and Meyer, 2012b) 63
Figure 3-57. Effect of inclination angle on the apparent void fraction and comparison with different correlations (R134a, d = 8.38 mm, G = 300 kg/m²s). The thick horizontal lines represent the mean apparent void fraction between -5° and 90° (Lips and Meyer, 2012b) 63
Figure 3-58. Apparent void fraction for horizontal and upward flows and comparison with different correlations (R134a, d = 8.38 mm, G = 300 kg/m²s) (Lips and Meyer, 2012b) 64
Figure 3-59. Comparison of the momentum pressure drop calculated by the traditional and the energy approach (Lips and Revellin, 2013) 66
Figure 3-60. Comparison of the gravitationnal pressure drop calculated by the traditional and the energy approach (Lips and Revellin, 2013) 66
Figure 3-61. Impact of the approach for the frictional pressure drop determination (Lips and Revellin, 2013) ... 67
Figure 3-62. Thermodynamic cycle of a heat pump. Solid lines: optimal cycle. Dashed lines: cycle considering irreversibilities in the condenser (Lips and Meyer, 2012d) 71
Figure 3-63. Determination of the initial temperature difference of condensation for L = 5 m (Lips and Meyer, 2012d) 71
Figure 3-64. Effect of the condenser length (G = 200 kg/m²s) (Lips and Meyer, 2012d) 72
Figure 3-65. Determination of the condenser length for an initial temperature difference of condensation equal to 5 K (Lips and Meyer, 2012d) 72
Figure 3-66. Map of the inclination effect on the flow pattern (R134a, d = 8.38 mm) (Lips and Meyer, 2012e) .. 72
Figure 3-67. Map of the inclination effect on the heat transfer coefficient (R134a, d = 8.38 mm) (Lips and Meyer, 2012e) 72
Figure 3-68. Map of the inclination effect on the apparent void fraction (R134a, d = 8.38 mm) (Lips and Meyer, 2012e) 73
Figure 3-69. General map of the inclination effect (R134a, d = 8.38 mm) (Lips and Meyer, 2012e) 73
Figure 4-1. Classification of the various material used for thermal storage applications (Kinkelin, 2016; after Zalba et al., 2003) 75
Figure 4-2. Design of the thermal damper (Kinkelin et al., 2017) 76
Figure 4-3. Thermal impedance in the single-phase zone of the ideal thermal damper associated to the geometry considered in figure 4-2 (Kinkelin et al., 2017) 77
Figure 4-4. Thermal behaviour of an ideal thermal damper subjected to a sinusoidal heat flux (Kinkelin et al., 2017) 78
Figure 4-5. Gain of the equivalent filter of an ideal thermal damper (Kinkelin et al., 2017) 79

Figure 4-6. Impedance of an ideal thermal damper in the two-phase zone (Kinkelin et al., 2017) 79
Figure 4-7. Attenuation due to the phase change (Kinkelin et al., 2017) 79
Figure 4-8. Non-ideal thermal damper behavior compared to the ideal one (p = 25 µm, σ_T = 5 K) (Kinkelin et al., 2017) 80
Figure 4-9. Effect of the honeycomb dimension p (δq = 1 W cm^{-2}; h_{ref} = 0 W m^{-2} K^{-1}; σ_T = 5 K) (Kinkelin et al., 2017) 80
Figure 4-10. Typical pictures of the studied thermal dampers (Kinkelin et al., 2017) 81
Figure 4-11. SEM images of different configurations of the CNT array: edge of a standard CNT array (a), array with holes (b), array with holes and hexagonal splits before (c) and after (d) densification (images and fabrication: CEA-Liten) (Kinkelin et al., 2017) 81
Figure 4-12. Main components of the test bench (top view, not to scale) (Kinkelin et al., 2017) 81
Figure 4-13. Picture of the test bench for the thermal cycle characterization (Kinkelin, 2016) 81
Figure 4-14. Schematic view of an experimental configuration used to measure the transmittance of the black paint layer and summarizing the various contributions seen by the IR camera (Kinkelin, 2016) 82
Figure 4-15. Equivalent emissivity of the painted silicon plate as a function of the plate temperature, for various integration times, acquisition frequency and various dates (day 1, 2 or 3) (Kinkelin, 2016) 82
Figure 4-16. Estimation of the temporal shift due to the black paint layer (solid line: measured thermogramm after a laser crenel of 11 ms. dotted line: simulation of the behaviour without the paint layer) (Kinkelin, 2016) 82
Figure 4-17. Thermal boundary conditions for the TIM-TS (Kinkelin et al., 2015) 83
Figure 4-18. Temperature history of prototype thermal dampers with and without PCM (Kinkelin et al., 2017) 83
Figure 4-19. Estimated total apparent thermal capacity $(mc_p)_{tot}$ of the samples with and without PCM versus DSC measurements (Kinkelin et al., 2017) 83
Figure 4-20. Latent heat storage capacity of the CNT/PCM material as a function of the number of fusion/solidification cycles (Kinkelin et al., 2017) 83
Figure 4-21. Measured temperature history of the back side of a prototype thermal damper subjected to a 10 ms laser crenel (DL: digital level of the IR camera) (Kinkelin et al., 2017) 84
Figure 4-22. Thermal model of the thermal damper subjected to a laser flash (Kinkelin et al., 2017) 84
Figure 4-23. Total thermal resistance of Si/CNT/Si samples with various lengths of CNTs (Kinkelin et al., 2017) 85
Figure 4-24. Estimated total thermal resistance of the best THERMA3D samples (A-F) compared to those of the CNT arrays reported in the review article of Marconnet et al. (2013) (Kinkelin et al., 2017) 85
Figure 4-25. Samples SI-PCM-SI placed in vertical orientation and heated up to the complete fusion of the PCM. The IR visualization of the front and back side are presented as a function of the time (Kinkelin, 2016) 86
Figure 4-26. Example of IR visualization for a sample above the ambient temperature (Kinkelin, 2016) 87
Figure 4-27. Schematic illustration of the contributions to the infrared signal measured by the IR camera (Kinkelin et al., 2015) 87
Figure 4-28. IR radiation of the upstream silicon and the stamping layer of unpainted samples "CNT-P" and "CNT-A" (Kinkelin et al., 2015) 88
Figure 4-29. IR radiation of the downstream silicon and the CNT array of unpainted samples "CNT-P" and "CNT-A" (Kinkelin et al., 2015) 88

List of tables

Table 2-1. Specifications for the wick characteristics (Giraudon et al., 2017a) 19
Table 2-2. Chemical compatibility between various fluids and various materials (Giraudon, 2017) 29
Table 2-3. Summary of the studies dedicated to heat pipes made of polymer (Berut, 2016) 36
Table 3-1. Applications of fluorescence and phosphorescence techniques for the two-phase flow characterisation (Martel et al., 2018) 42
Table 3-2. Summary of the studies dealing with the effect of inclination angle on the heat transfer (Layssac, 2018) 44
Table 3-3. Summary of the characteristics and range of experimental conditions for each test-sections 46
Table 3-4. Database used by Layssac et al. (2017) for the symmetry correlation construction 50
Table 3-5. Correlation coefficients of the present database flow parameters (Layssac et al., 2017) 51
Table 3-6. Heat transfer coefficient prediction accuracy of various models (Layssac et al., 2018b) 59
Table 4-1. Influence of the manufacturing process on the thermal resistance of two silicon plates linked by non-densified CNTs (Kinkelin, 2016) 84

Nomenclature

A	Cross section	m²
A_{mn}, A'_{mn}, B_{mn}, B'_{mn}	Fourier coefficient	-
Bo	Bond number	-
c_p	Heat capacity	J/kgK
d	Diameter	m
E	Electric field	V/m
f	Frequency	Hz
f	Fanning friction factor	-
Fr	Froude number	-
g	Gravity acceleration	m²/s
G	Gain	-
G	Mass flux	kg/m²s
G	Thermal conductance	W/K
h	Heat transfer coefficient	W/m²K
h, $h°$	Specific enthalpy, total specific enthalpy	J/kg
H	Enthalpy	J
H	Hydraulic head	m
I	Inclination effect	-
K	Permeability	m²
L	Length	m
L	Luminance	W
m, n, M, N	Integer	-
m,	Mass	kg
$\dot{m}$	Mass flow rate	kg/s
N_{mcp}	Non-dimensional total thermal capacity	-
N_{mhls}	Non-dimensional latent heat of phase change	-
MAPE	Mean Absolute Percentage Error	variable
MPE	Mean Percentage Error	variable
MSE	Mean squared error	variable
p	Perimeter	m
P	Pressure	Pa
PEDCx	Percentage of Data Captured within ± x%	variable
q	Heat flux	W/m²
Q	Heat transfer rate	W
r	Radius	m
R	Thermal resistance	K/W
s	Symmetry parameter	-
s	Specific entropy	J/kg
S	Area	m²
S'	Entropy generation	W
t	Time	s
t	Thickness	m
T	Temperature	K
u	Velocity	m/s
v	Specific volume	m³/kg
V	Voltage	V
w	Relative weight	-
W_t	Mechanical work	W
x	Vapour quality (for two-phase flows)	-
x	Liquid fraction (for PCM)	-
x, y, z	Coordinates	m
X, Y, Z	Non-dimensional coordinates	-
Z_{th}	Thermal impedance	K/W

Greek symbols

α	Heat transfer coefficient	W/m²K
β	Inclination angle	rad
ε	Porosity	-
ε	Void fraction	-
ε	Emissivity	-
η	Efficiency	-
λ	Thermal conductivity	W/mK
μ	Dynamic viscosity	kg/m/s
φ	Heat flux	W/m²
φ	Phase	rad
ρ	Density	kg/m^3
ρ	Reflectivity	-
σ	Surface tension	N/m
τ	Shear stress	Pa
τ	Transmissivity	-
χ	Martinelli parameter	-

subscript

abs	absorbed
amb	ambient
b	base
b	back
c, cond	condenser
cond	conduction
conv	convection
dyn	dynamic
e, evap	evaporator
f	front
ff	face to face
fric	frictional
fus	fusion
grav	gravitational
h	homogeneous
i	internal
i, int	interface
irr	irreversible
l, liq	liquid
m	mean
min	minimum
max	maximum
mom	momentum
opt	optimal
p	pore
PCM	phase change materiel
ref	reference
s	solid
Si	silicon
sat	saturation
tot	total
tp	Two-phase
v, vap	vapour
vo	vapour only
w	wall
ΔP	pressure lines

Chapter 1: Introduction and context

1.1 Personal context

My first research experience was a 5-month internship performed in the CEA of Grenoble in 2005 in the Fuel Cell Laboratory. It gave me a preview of what can be research. I confirmed my interest the following year through my Master research project performed in the CETHIL from January to September 2006 on pulsating saturated two-phase flows, for instance encountered in pulsating heat pipes (PHP). I think this Master project was the trigger of the rest of my research. Heat pipes fascinated me as a way to get around the physical limitations of conductive heat transfer and the field of possibilities only seemed to be limited by imagination and manufacturing technologies. The specific case of PHP gave me an idea of the numerous scientific questions that still had to be answered. From this project, I also kept my "plumber" approach: I discovered that in experimental studies of saturated two-phase systems, the main problem is often the tightness of the experimental set-up, the rest being only a question of quality of result analyses.

I must admit I had a lot of chance: this "innocence" was permitted to me thanks to the very favourable environment in which I was inserted. The two-phase research group of the CETHIL gave me the opportunity to develop my research skills, during my research project but also during my PhD that followed. Under the day-to-day supervision of Frederic Lefèvre and the more global supervision of Jocelyn Bonjour, I studied the thermal and hydrodynamic performance of grooved flat heat pipes by means of a phenomenological approach, both experimentally and numerically. My PhD was also an opportunity to try to understand the national and international scientific community in which I am involved today.

I said luck… After my PhD, I had the chance to perform an 18-month postdoctoral project in the University of Pretoria, in South Africa, under the supervision of Josua Meyer. This amazing experience brought me a new vision of the research field, more based on the Anglo-Saxon way of thinking. It developed my autonomy and I learned the necessity to have a global overview of the scientific advances in a specific domain. I choose to study the convective condensation in inclined tubes, in order to broaden my research fields, while focusing on experimental approaches.

Luck always… I was at the right place at the right moment… and probably with the right persons around me. An assistant professor position opened in the two-phase flow research group at CETHIL in September 2011 and I had the chance to get the position. My carrier was then definitely linked with INSA Lyon, in which I did my studies, my PhD, and thus my current research since 7 years now… It can be a weakness; it can be strength… I think it is both of them. It anyway enabled me to be quickly associated to the research projects of the group and to the teaching team of the energetic department. I kept my strategy: broadening my research field on two-phase systems, in general, and developing my experimental skills. I tried to give a coherence to my research by focusing on the cooling of electronic components. A specific application indeed gives a frame to the research and enables to study various systems, from the heat pipe systems to the thermal dampers and two-phase flows without dispersing too much. Of course, it does not prevent me to study two-phase systems for other applications, but I rather see it as a way to open the researchers mind to new constraints and new industrial contexts than to try to become a "universal" expert of two-phase systems.

This strategy also enabled me to work with various people. I had the chance (once more) to co-supervise 5 PhD students, of which 3 have completed, with 4 different professors of HDR assistant professors of the group, namely Frederic Lefèvre, Valérie Sartre, Jocelyn Bonjour and Remi Revellin. This diversity of people, in terms of scientific approach, skills and human behaviour is very rich and I believe that it enabled me to reflect on my own approaches. Co-supervisors of other laboratories (MATEIS in INSA and SIMAP in Grenoble) also enabled me to broaden my point of view and to compensate a little bit my "INSA centred" environment. Of course, I did not perform my research alone, the results presented in the manuscript are the outcomes of the work of all the master students, PhD students, co-authors, technicians, engineers, and administrative staff I had the pleasure to work with. Figure 1-1 presents a simplified timeline of the various projects and supervision in which I have been involved. More details are available in the Curriculum Vitae provided at the end of the present document.

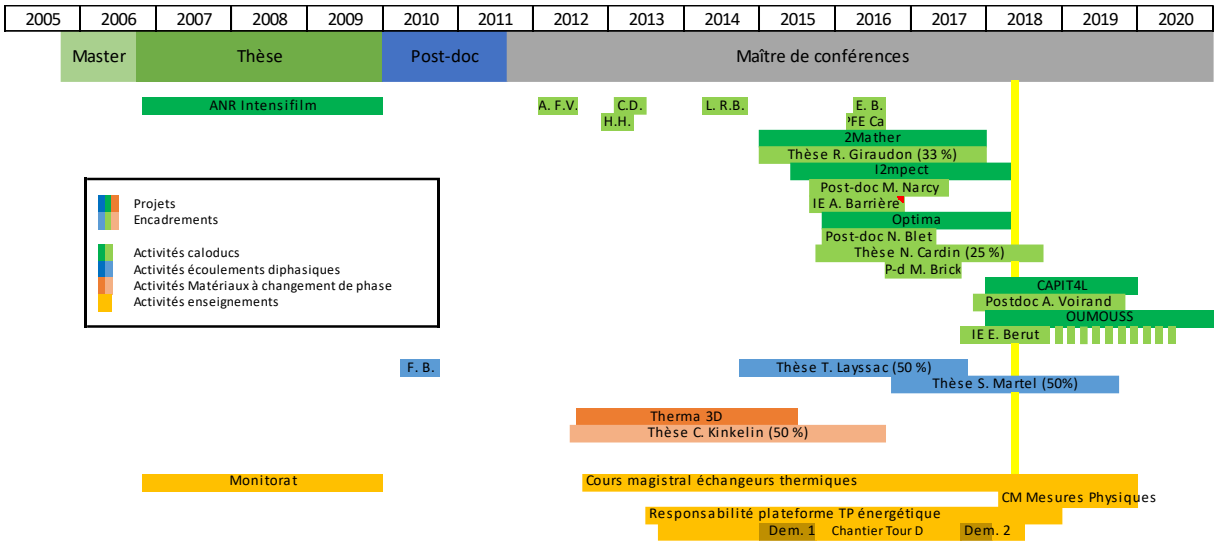

Figure 1-1. Simplified timeline of the various projects and supervisions in which I have been involved

1.2 Industrial and scientific challenges in the thermal management of electronic components

Before presenting my research activities, it is useful to give a brief industrial context of the thermal management of electronic components. The industrial and scientific challenges are of course linked to the continuous increase of transistor performance (figure 1-2), coupled to the remarkable decrease of the size of the electronic components (figure 1-3), which leads to increasing heat fluxes, up to 100 to 200 W/cm² nowadays.

However, the cooling of electronic components cannot be viewed only through the heat flux that needs to be dissipated. The structure of these systems tends to become more and more complex and the trend is to try to achieve 3D electronic components in order to limit the length of the electrical connections between the various parts of the electronic systems (figure 1-4).

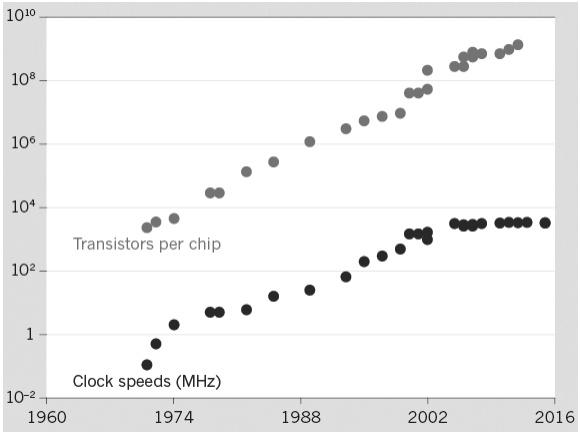

Figure 1-2. Evolution of the transistors number per chip and the clock speed of microprocessors (Waldrop, 2016)

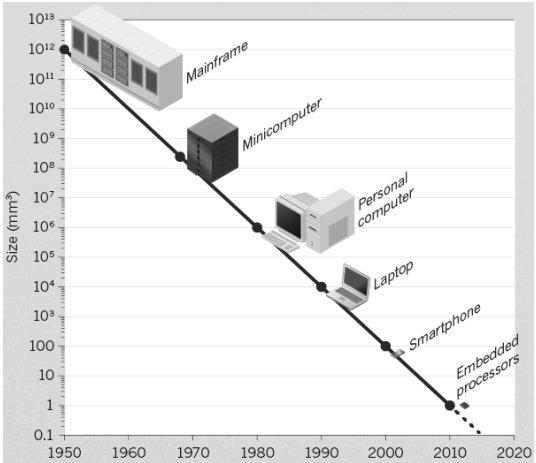

Figure 1-3. Evolution of the size of the electronic component (Waldrop, 2016)

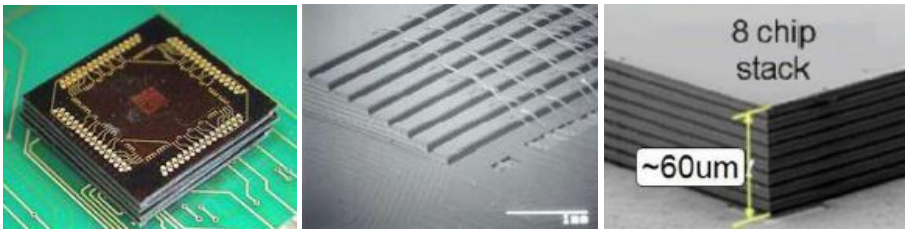

Figure 1-4. 3D electronic component (sources left: Fraunhofer IZM; centre: ITRS 2009; right: AES, Samsung)

An example of advanced 3D structure is presented in figure 1-5: the memory is located directly on the microprocessor. This kind of architecture improves the system performance but increases the complexity of the system cooling, as the memory needs to be cooled through the microprocessor itself, which is often hotter. In the present example, thermal vias made of copper were added through the microprocessors layer. Even without adding phase-change heat transfer device, temperature prediction in this kind of structure is challenging (Monier-Vinard et al., 2016).

Together with the electrical connections, the thermal links between the various parts that need to be cooled and the heat sink is a major constraint of these systems. The maximum admissible temperature of the electronic components itself often depending on its structure and function (Figure 1-6), the thermal issues should be taken into account as early as possible in the design of the architecture of the electronic component and the complete system. However, it is unfortunately rarely the case today. More links are thus required between the electronic and the thermal scientific communities.

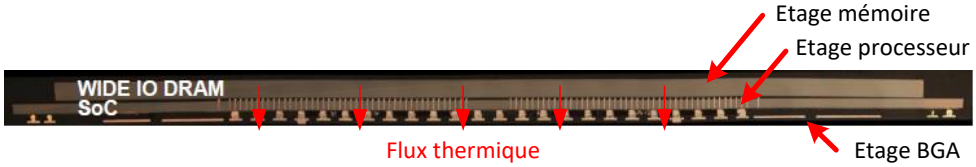

Figure 1-5. Example of 3D electronic component manufactured by ST-Ericsson / CEA (Vivet and Guérin, 2011)

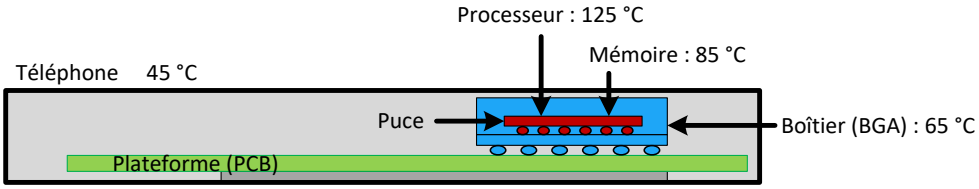

Figure 1-6. Maximal admissible temperature on various location of a cell phone (Kinkelin, 2016)

Because of the important diversity of the electronic components sizes, constraints and heat fluxes, many cooling systems can be used for the thermal management. Many recent review articles are available in the literature on this topic, with specific reference to CFD modelling (Monier-Vinard et al., 2017), advanced cooling material (Qu et al., 2011; Tong, 2011), two-phase systems (Irissou et al., 2008; Saidur et al., 2011; Tadrist, 2007) or phase change materials (Ling et al., 2014). Other reviews are dedicated to specific applications, as automotive (Mallik et al., 2011), power battery (Rao and Wang, 2011) or military applications (Price, 2003). To have a global overview of the cooling technologies and their scientific challenges, the interested readers can refer to the very pertinent PhD thesis literature surveys of Lachassagne (2009), Hodot (2015) and Charnay (2014).

As a consequence, the goal is not to present here an exhaustive review of the work performed on the thermal management of the electronic components, but rather to draw a global overview of the various technologies that exist. Figure 1-6, which is strongly inspired by the literature survey cited above, gives a summary of these technologies. A distinction is made between three types of systems:

- The cooling system themselves, that can be directly considered as a heat sink, even if the heat will be eventually released with another system. Air cooling, liquid cooling and two-phase cooling systems can be implemented.
- The heat transfer systems that aims at transferring the heat from the electronic component to a distant heat sink. Contrarily to the previous type of systems, interactions can occur between the phenomena localised at the heat source and at the heat sink. Active systems and passive systems can be used for this purpose.
- The other thermal management systems whose goal is not to cool directly the electronic components, but rather to play on the thermal spreading and thermal damping phenomena.

1.3 Overview of my research work

Figure 1-6 highlights the richness of the scientific field linked to the thermal management of electronic components. Even if I try to maintain a general scientific culture of the various topics listed in this figure, for instance through international conferences and review articles, I am directly involved in only a very little number of scientific questions.

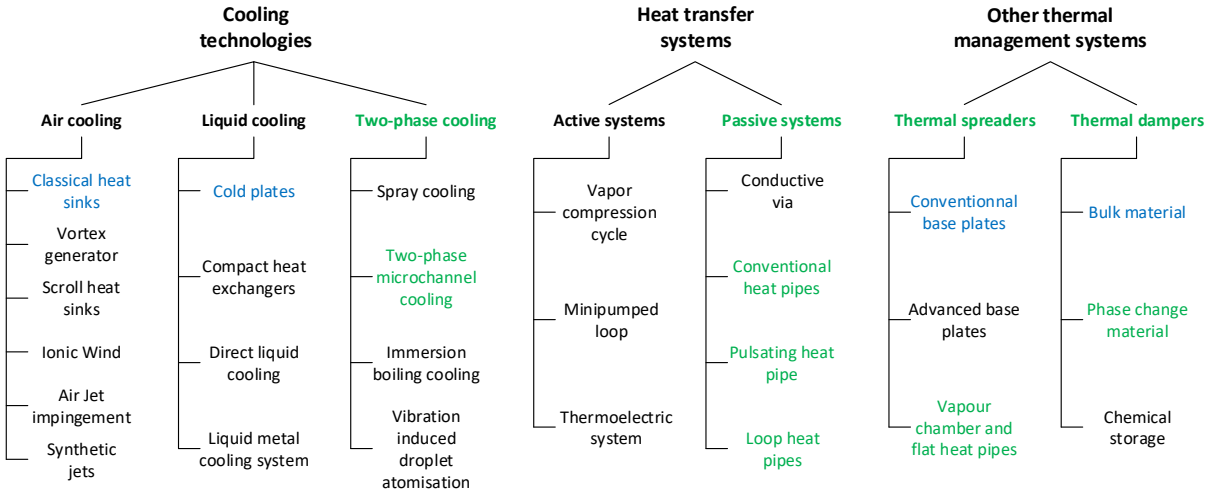

Figure 1-7. Various systems used for the thermal management of electronic components. In green, the systems which I had the opportunity to study. In blue, the systems I used commonly as an engineer tool

Amongst the various systems presented in figure 1-7, and beyond the systems highlighted in blue and corresponding to classical thermal management systems, I had the opportunity to work on three main types of systems, highlighted in green: the heat pipes, the two-phase flows and the thermal dampers using phase-change material.

In the present thesis, I will try to draw an overview of my research outcomes since my PhD defence in 2009. As many aspects of my research are discussed, I have tried not to enter too much into the details, except for specific scientific points. Each chapter corresponding to a different research field, I also tried to vary the philosophy of each of them. It may affect the uniformity of the present document, but the goal is rather that any concerned reader can find something interesting in it than to dedicate the whole document to a specific audience.

Chapter 2 is dedicated to the studies on heat pipes. In this field, my research consisted mainly in phenomenological analyses of various systems, in order to achieve a better understanding of their behaviour. I will firstly try to give the reader a short overview of the working principle, history and applications of these systems. The word “heat pipe” referring to multiples systems, a literature survey of the various type of studies available in the literature is then proposed. The scientific questions being numerous, I will not enter into the details but rather try to draw a global view of the scientific context and of the various approaches the scientific community uses to study these systems. With the same philosophy, I will then present my own approaches and outcomes on this field. A specific discussion on the link between thermal and materials sciences will close this chapter.

Chapter 3 is dedicated to my research work on two-phase flows. I am mainly interested in inclined two-phase flows with the idea of using this configuration to study the balance between the various forces involved in these systems. Contrary to Chapter 2, I will try to go a little bit deeper in the scientific questions linked to this domain. After a brief scientific context and the presentation of the test benches I have used to study inclined two-phase flows, some experimental results are presented and discussed in terms of flow patterns, heat transfer and pressure drops.

The last Chapter is a summary of the work on thermal dampers in which I was involved, mainly through the PhD thesis of Christophe Kinkelin. In this chapter, the idea is to present the complete analyses of this type of system, from the theoretical work consisting in defining and studying the notion of ideal thermal damper, to the characterisation of prototypes.

In each chapter, a brief literature review is presented. Perspectives are discussed at the end of each chapter, and are then summarised and prioritised in the global conclusion.

Chapter 2: Passive systems based on the liquid-vapour phase change: Heat pipes and related devices

2.1 Working principle, history and applications

A heat pipe is a system able to transfer high heat fluxes from a heat source to a heat sink with a low thermal resistance using liquid-vapour phase-change. It consists of a cavity filled by a fluid at saturation. The liquid evaporates at the contact of the heat source and condenses close to the heat sink. The way the vapour and the liquid flow to the condenser and to the evaporator, respectively, depends on the type of heat pipe.

The main types of heat pipes are summarised in figure 2-1. A distinction can be made between conventional heat pipes, loop heat pipes and oscillating heat pipes. The family of conventional heat pipes comprises thermosiphons, cylindrical heat pipes, flat plate heat pipes and rotating heat pipes. The liquid and vapour flows are counter-current within the heat pipe body. The liquid flows from the condenser to the evaporator owing to either gravity, capillary, centrifugal forces or a combination of these forces. In capillary heat pipes, the capillary structure (grooves, meshes or porous medium) has to be continuous from the condenser to the evaporator.

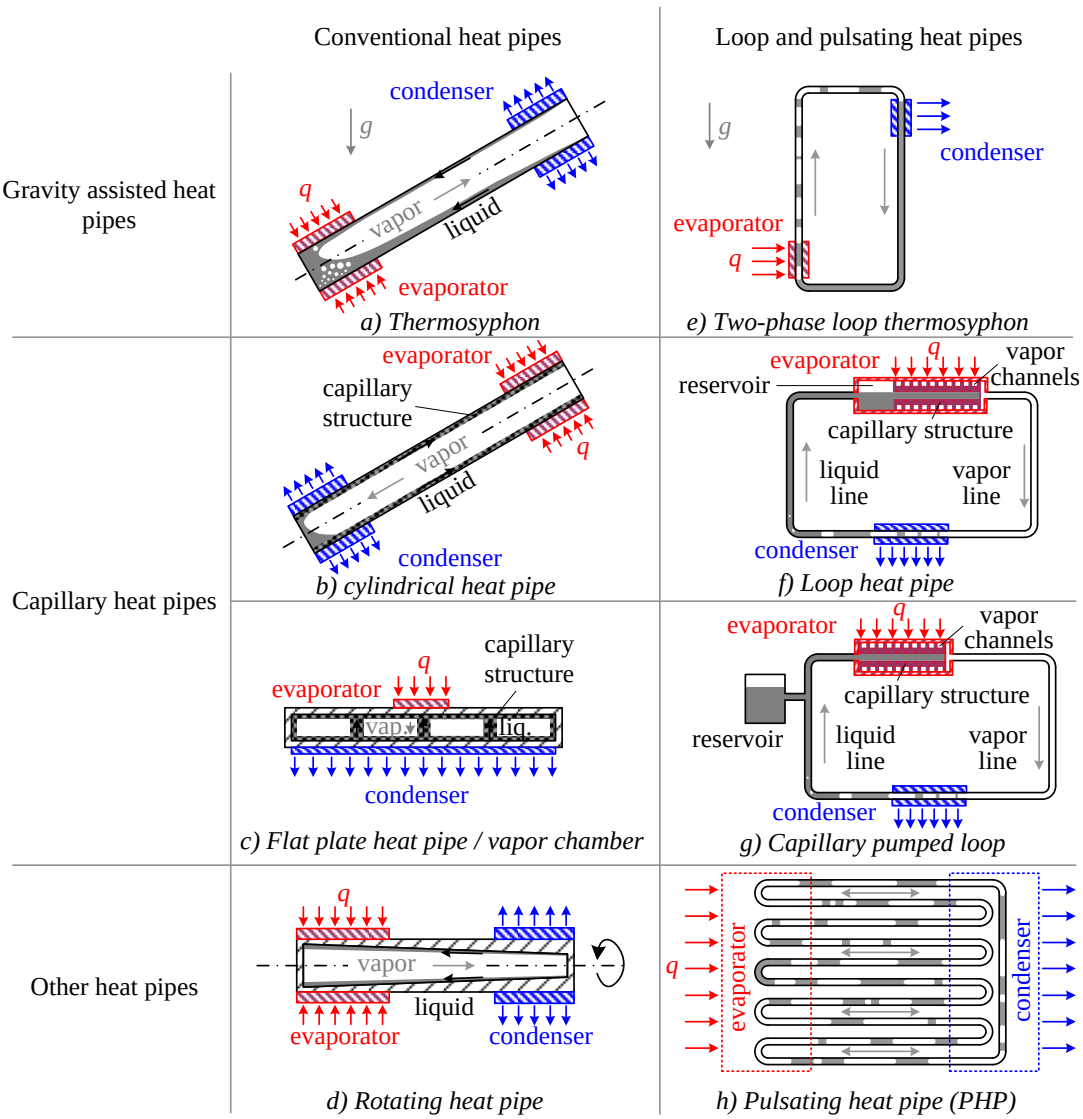

Figure 2-1. Different heat pipe technologies (Lips, 2015)

In figure 2-1, the generic term ‘loop heat pipes’ refers not only to loop heat pipes themselves (LHPs), but also capillary pumped loops (CPLs) and two-phase loop thermosiphons (also called closed-loop thermosiphons). In these systems, the liquid and vapour flows in separate lines. For LHPs and CPLs, the sum of frictional and gravitational pressure drops are compensated by the capillary forces in the capillary structure placed at the evaporator only. A CPL differs from a LHP by the place of the reservoir, which has a great importance on the overall system behaviour. In closed-loop thermosiphons, the gravitational forces compensate for the frictional pressure drop.

The oscillating heat pipes (figure 2-1h), also called pulsating heat pipes (PHPs) are made of a single meandering tube placed between the heat source and the heat sink. Its diameter, close to the fluid capillary length, leads to a distribution of the fluid within the tube into liquid plugs and vapour slugs. The violent vaporisation of multiple liquid slugs in the evaporator, associated to the condensation of multiple vapour plugs at the condenser, generates self-sustained oscillations of the fluid. It leads to an efficient heat transfer from the heat source to the heat sink, both by latent and sensible heat. These systems are cheap and easy to manufacture, but their behaviour is difficult to predict and they are currently sparsely used in the industry.

Despite the strong differences between the various heat pipe technologies, there are several phenomena shared by these systems. Obviously, liquid-vapour phase-change heat transfer is present in all heat pipes. The phase-change occurs at the scale of the capillary structure or at the scale of the thin liquid films present in the system. The capillary forces are indeed almost never negligible. Moreover, as the fluid is always heated through a wall, the interactions between the working fluid and the wall, mainly wetting effects, are of great importance. Lastly, there is always a coupling between hydrodynamic and thermal phenomena, as the working fluid follows a thermodynamic cycle in the systems.

The similarity of the phenomena involved in all heat pipes induces that the progress in understanding of one kind of heat pipe generally helps to progress on the other kinds. Indeed, heat pipes are the topic of many research programs. Figure 2-2 presents the evolution of the number of articles related to heat pipes indexed on the Web of ScienceTM database between 1975 and 2014 (Lips, 2015).

The heat pipe science began during the sixties and conventional heat pipes were soon widely used in space applications, for instance to transfer the heat dissipated by the electronic components to the radiators. To try to reduce the weight of the systems, CPLs and LHPs were invented by the NASA during the sixties and by the Russian Federal Space Agency during the seventies, respectively. However, these technologies were not reliable enough during this period.

During the eighties, terrestrial applications of heat pipes were developed, mainly with thermosiphons because of the difficulty in overcoming the gravity forces. Thermosiphons have been widely used in industrial applications, as well as in the heat exchangers. The development of electric locomotives also motivated the use of heat pipes in mobile applications.

During the nineties, new types of heat pipes were invented and more and more studied. Micro heat pipes appeared, thanks to the progress in micro technologies. They aimed to reduce the thermal contact resistance between the electronic component and the heat sink by directly integrating the heat pipe into the silicon substrate of the electronic component. At the same time, the progresses in porous material technologies enabled the implementation of CPLs and LHPs in spacecrafts.

Since 2000, the number of papers dedicated to heat pipes has increased continuously and now stands at about 250 papers per year. According to Larsen and von Ins (2010), the general annual growth rate of scientific publications is close to 5%, which implies a doubling time of about 15 years. With a doubling time of about 8 years, the growth rate of publications dedicated to heat pipes is much higher than the growth rate of all scientific publications. This enhanced research effort is mainly motivated by the increase of the heat flux density dissipated by electronic components, which creates a need for efficient and reliable cooling systems. Heat pipes, especially CPLs and LHPs, are thus developed for terrestrial applications and the systems need to be optimised and perfectly understood in order to deal with gravitational forces and acceleration forces for on-board vehicle applications. At the same time, rising energy prices favour the use of heat pipes in numerous applications, either as a passive system to remove heat, to improve the efficiency of heat recovery systems, or to homogenise the temperature of various

systems. In parallel, the continuous progress in new materials and manufacturing processes enables the spreading of heat pipes in many other industrial applications.

In figure 2-2, one can note the important development of research on CPLs / LHPs over the last 15 years, and on PHPs over the last 10 years. Together, they represent currently one third of the papers devoted to heat pipes. The development of reliable LHP would open the use of heat pipes in many applications, as they enable to transfer heat over a longer distance than other types of heat pipes, while having a low sensitivity to gravitational and acceleration forces. The development of PHPs is mainly motivated by the low cost of these kinds of systems. One can also note the remaining importance of research on thermosiphons, despite the age of the early research on this field. These systems are more and more optimised and studies aim to push their operating limits, especially in terms of heat power, heat flux density and operating temperature.

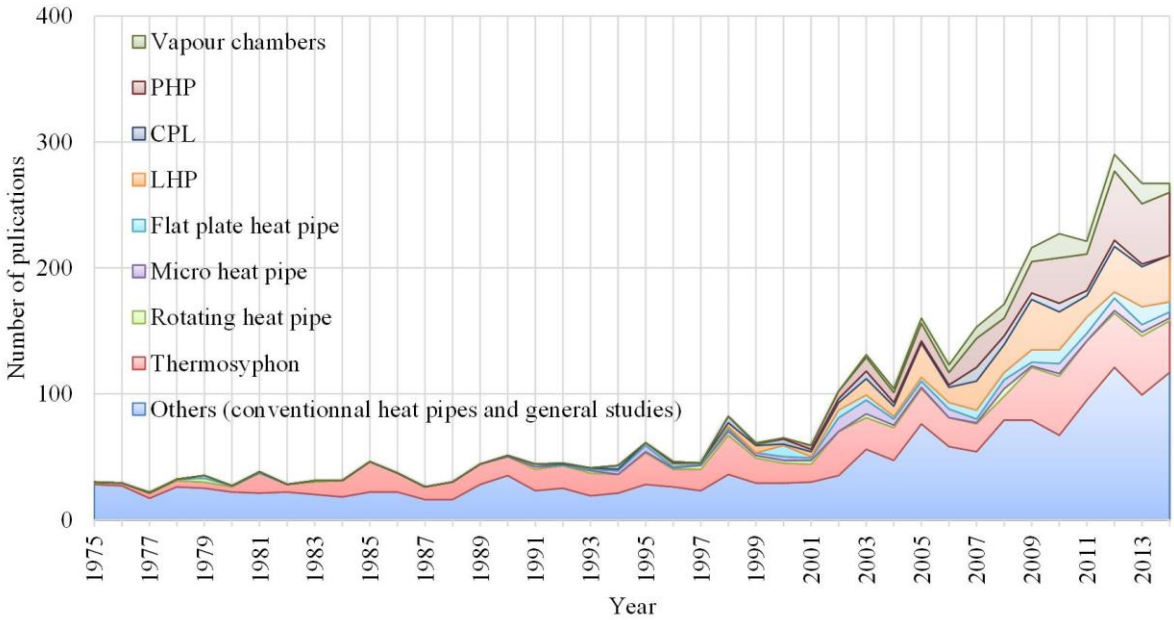

Figure 2-2. Number of papers dedicated to heat pipes according to the database of Web of ScienceTM (Lips, 2015)

Since my Master thesis in 2006, I had the opportunity to work on several research projects linked to heat pipes. They led to several scientific papers in international journals and communications in international conferences. In the following of the present chapter, the goal is not to list every scientific studies and results, but rather to try to give an overview of the various research strategies I have used to improve the understanding of the phenomena involved in heat pipes. I will first give a brief overview the general approaches encountered in the heat pipe scientific community (section 2.2). I will then focus briefly on my research concerning heat pipe modelling and give some examples of specific experimental or theoretical studies in which I were involved in order to illustrates the various approaches and justify the need of research projects on heat pipes (section 2.3). Section 2.4 will be specifically dedicated to the links between the progress in material sciences and those in heat pipe sciences. Eventually, conclusions and perspectives on heat pipes sciences will be given in section 2.4.3.

2.2 General approach of the scientific community

This section is mainly drawn from of a keynote lecture, I had the opportunity to present at the HEFAT conference in 2015, and is devoted to the heat pipe studies presented in the literature between 2010 and 2015 (Lips, 2015). It has been completed with more recent studies. This brief summary will help to understand my own contributions to the community.

Scientific issues involved in heat pipes are usually classified in four categories: evaporation heat transfer, condensation heat transfer, flow patterns in heat pipes and capillary flows. In the present section, another classification of the studies available in the literature is proposed:

- The research motivated by heat pipe characterisation,

- The scientific issues linked to the working fluid behaviour,
- The studies aiming to predict the phase-change heat transfer in thin films,
- The development of new heat pipe models.

This classification enables to highlight not only the different scientific issues but also the different scientific approaches that are used by the various research teams working on heat pipes.

2.2.1 Research motivated by heat pipe characterization

From an industrial point of view, an important outcome of heat pipe studies is the determination of the overall performance of the various heat pipes. The performance can be typically expressed in terms of system thermal resistance and of system capacity to operate in given operating conditions (imposed heat flux, ambient temperature, acceleration, orientation…). Many studies are thus devoted to the determination of the heat pipe performance and the numerous prototypes that are tested enable to build important databases for each type of heat pipes. The thermal resistance of a heat pipe usually depends on the heat transfer at the evaporator and at the condenser, and thus, on many parameters, such as the working fluid, the fluid fill charge and the effective thermal conductivity of the wick (when exists), but also on other phenomena as the operating regime, or the partial or total dry-out of the evaporator. For instance, the thermal performance of LHPs is often characterized by their operating curve (vapour or reservoir temperature as a function of the heat power) and not by their thermal resistance. Determining a heat pipe performance also leads to determine its operating limits, often detected by a sudden increase of the thermal resistance or of the operating temperature. If the different limits are well known from decades, it is not so trivial to link the observed heat pipe behaviour to a particular limit.

Many review articles on heat pipes are available in the literature. They are of a great interest as they enable to summarize the data scattered in a large number of articles. For instance, Maydanik et al. (2014) recently proposed a review on the performance of loop heat pipes with flat evaporators. The performance of the various geometries is compared, as well as the impact of the working fluid and the materials. Recommendations are then proposed in order to achieve a good performance when designing the evaporator of a LHP.

Other reviews are focused on specific applications instead of a specific type of heat pipe, as that of Srimuang and Amatachaya (2012), who proposed a review on heat pipe heat exchangers presented in the literature. It highlights the fact that the main design parameters strongly depend on the application in which the heat pipe is used and not only on the type of heat pipe itself.

Moreover, the performance of a heat pipe is not only limited to its thermal performance. For instance, Zhang et al. (2014) studied the socio-economic performance of a solar water heating system that includes a heat pump and a new type of two-phase loop thermosiphon. This example shows that reducing the heat pipe performance to its only thermal resistance minimizes the challenges that are to be faced by the heat pipe scientific community.

Besides academic papers, many patents are filed, in which specific geometries and configurations are proposed. Patents can deal with specific parts of heat pipe, as condensers (Fried et al., 2013) or wicks (Asfia et al., 2014). Additional parts are also proposed, as a reservoir filled with adsorbent material in order to deal with freezing problems (Bonjour et al., 2013). The large number of patents filed each year shows the strong links between the academic research on heat pipes and their industrial applications.

In a general way, each time a new heat pipe design is proposed, the first step in studying a prototype is to determine its performance. As an example, Lachassagne et al. (2013, 2012) proposed a new kind of LHP, called CPLIP (Capillary Pumped Loop for Integrated Power), with a reservoir located above the evaporator. In their first paper they determined its performance, and subsequently proposed a model in steady-state conditions. Heat pipes also have to be tested in various operating conditions. For instance, Mameli et al. (2014) characterised a closed loop pulsating heat pipe in microgravity conditions. They showed that their heat pipe is more affected by the variation of the gravity than by the level of gravity itself. They also concluded that the performance of their heat pipe is similar in microgravity and when it is placed horizontally in normal gravity conditions. This kind of conclusion is important for the community to limit the number of tests required in microgravity, as they are expensive and difficult to perform.

Eventually, the last step, after prototype characterisation, is to study its behaviour in the real system. Studies can be found, for instance, for solar applications (Zhang et al., 2014), HVAC applications (Wang et al., 2015) or electronic cooling applications (Kim and Kim, 2014). Most of the time, this kind of study focuses on the transient behaviour of the systems and the authors often compare their measurements with the results of transient numerical models. Indeed, the scientific goals of these studies are often to check the relevance of the models that are developed to predict the heat pipe performance for each specific application.

For capillary heat pipes, the development of models requires the knowledge of the properties of their capillary structure filled with the working fluids as they have a direct effect on the heat pipe performance. Consequently, the capillary structures are the object of great attention in heat pipe science. New ways of manufacturing new capillary structures are developed continuously. For instance, Singh et al. (2014) presented their fabrication technique for a sintered aluminium evaporator of a Loop Heat Pipe. Santos et al. (2012) proposed an evaporator made of ceramic. Their experience helps in developing evaporators that will be more advanced in the future.

Besides developing new capillary structures with new techniques and new materials, a strong challenge is to determine the properties of existing capillary structures and to develop predictive tools that can be used in heat pipe models. The measurement of the permeability of a porous medium can be performed easily (Ameli et al., 2013; Hansen et al., 2015). However, the effective permeability of the capillary structure inside a heat pipe may be different from the bulk permeability of the medium because of the influence of the liquid-vapour interface.

The measure of the global porosity can be easily performed knowing the mass and the volume of the wick. This method was used by Deng et al. (2013), as an example. However, it does not give any information about the distribution of the porosity in the wick, which is important to know in some configurations like biporous wicks. The measurement of the effective pore radius is also complicated because the contact angle between the fluid and the wick affects its value. For instance, Singh et al. (2014) used the bubble point testing method, which enables to determine the largest pore radius whereas Becker et al. (2011) characterized their wick by the measure of the smallest radius of curvature of the interface before the depriving of the wick. To characterize the pore size distribution, other methods need to be used, as the mercury injection or the imbibition (Dullien, 2012) but these methods remain challenging in practice.

From a thermal point of view, the determination of the equivalent thermal conductivity of the capillary structure is even more difficult. It can be performed with a flash method, for instance (Ababneh et al., 2014), but the measured value takes into account only conduction through the capillary structure and does not consider evaporation or condensation phenomena. More sophisticated set-ups have to be developed to take into account these phenomena (Iverson et al., 2007) but there is a lack of experimental data and studies in this field.

When direct measurements cannot be performed, another approach consists in using inverse methods. For instance, Mehta and Khandekar (2014) used an inverse method to determine the heat transfer coefficient between the wall and a Taylor bubble train flow in a mini-channel of square cross-section (5 mm x 5 mm). They coupled experimental data from IR visualisation with a numerical model that takes into account the 3D conduction in the wall. The protocol for measuring the local heat transfer coefficient was far from being simple and they concluded that the major challenges were to get a sufficient spatial resolution to determine local temperature gradients and to minimise the conjugate heat transfer effect in the system. This effect depends strongly on the wall thickness, but also on the frequency and length of the bubbles in the flow.

As a conclusion, even if a large number of papers are devoted to the determination of the heat pipe performance and/or the capillary structure properties, there is often a need in understanding the phenomena that take place in the heat pipe itself, as the models often assume a given heat pipe behaviour, which is not always verified experimentally.

2.2.2 Scientific issues linked to the working fluid behaviour

The performance of a heat pipe often depends on numerous parameters and specific studies focus on the understanding of the heat pipe behaviour itself. For conventional capillary heat pipes, the operating conditions are bounded by several limits that all lead to a dry-out at the evaporator. For thermosiphons, pulsating heat pipes and loop heat pipes, several operating regimes can be observed and recent progresses have been made in their characterization. As an example, Miscevic et al. (2012) and Kaled et al. (2012) studied the flow regimes and the transient behaviour of a CPL, respectively. Karthikeyan et al. (2014) characterized the different operating regimes of a PHP and their impact on the heat pipe performance by means of an infrared camera (figure 2-3).

Thermal measurements help to characterise the heat pipe behaviour, but it is often important to deal with the behaviour of the working fluid inside the capillary structure itself. Heat pipes are often studied as black boxes, and thus, no direct observation can be performed inside the system. For the last ten years, many research teams studied transparent heat pipes, which enables a better understanding of the physical phenomena that take place inside the system, for instance thermosiphons (Smith et al., 2014), pulsating heat pipes (Ji et al., 2013) and loop heat pipes (Xu et al., 2014).

In order to study the liquid-vapour interface shape in details, some studies focus on a sub-system of the heat pipe only. For instance, El Achkar et al. (2012) studied the condensation of n-pentane in a micro-channel that represents the condenser of a LHP,. and Mottet et al. (2015) developed a test bench dedicated to the study of partial dry-out in the evaporator of a LHP (figure 2-4). These examples of experimental works highlight the importance of the direct visualization in these kinds of systems: the distribution of the liquid and vapour phases in the capillary structure of a heat pipe is far from being trivial and the numerical models are often limited by an imperfect understanding of the fluid behaviour. This lack of knowledge directly affects the accuracy of the design tools of heat pipes as the prediction of their thermal performance mainly depends on the liquid film thicknesses in the condenser and evaporator.

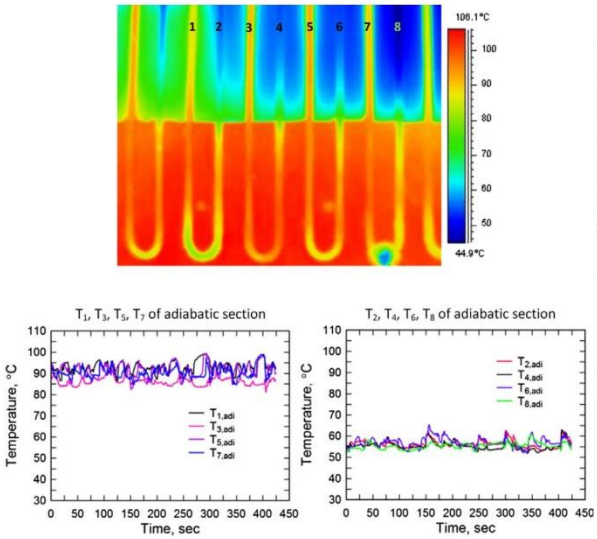

Figure 2-3. Experimental characterization of the operating regime of a PHP by means of a thermal camera (Karthikeyan et al., 2014)

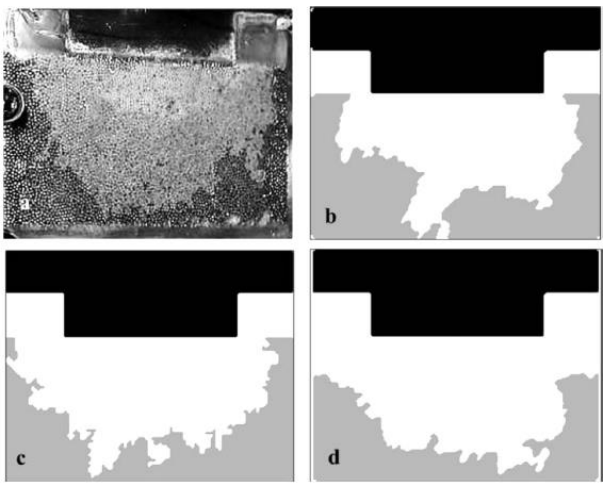

Figure 2-4. Visualisation and modelling of the vapour region in the evaporator of a LHP (Mottet et al., 2015)

Besides research on the fluid behaviour inside the heat pipe, some studies are dedicated to new kinds of fluids themselves. The choice of the fluid is indeed of a great importance and it is not so trivial to choose a compatible fluid for the pertinent heat pipe technology for a specific application. The fluid properties must show a good trade-off between high latent heat of vaporisation, surface tension and thermal conductivity and a low viscosity for the whole range of operating temperatures. A given operating temperature corresponds to a given operating pressure that the heat pipe must be able to withstand. The compatibility between the working fluid and the other materials must also be perfect. This problem currently limits the use of flexible and/or lightweight heat pipes because of the poor chemical stability

of materials like plastics or polymer composites. Other criteria, like toxicity for the humans and the environment must also be taken into account. As an example, water can be an appropriate working fluid for an operating temperature range from 50°C to 150°C, but problems of low pressure and high pressure can occur out of this range. Moreover, freezing can also be a problem for heat pipes with certain kinds of capillary structures. Studies on new fluids are thus necessary.

For instance, MacGregor et al. (2013) proposed a comparison of different working fluid performances for thermosiphons in order to replace R134a, which is widely used, but subjected to a ban in the near future. Other authors also tested their prototypes with new refrigerants, as R1234ze, which was found to be an efficient working fluid for loop heat pipes (Yeo et al., 2014). For cryogenic applications, superfluid helium was also tested (Gully, 2015). In a general way, the definition of an efficient working fluid is still a subject of discussion. Since the initial approach of Chi (1976) to define a figure of merit for cylindrical grooved heat pipes, other figures of merit have been proposed. For instance, Launay et al. (2010) proposed figures of merit for the working fluid in loop heat pipes, whereas Arab and Abbas (2014) proposed a model to predict the thermal performance of a trapezoidal grooved heat pipe when changing the working fluid.

Besides new fluids themselves, contemporary heat pipe research is mainly focusing on two new fluid families: the self-rewetting fluids and the nano-fluids.

The self-rewetting fluids exhibit an increase of their surface tension when their temperature increases. They often consist of a dilute aqueous solution of alcohol: in a certain range of temperatures, a concentration gradient occurs at the evaporator and the Marangoni effect adds to the temperature effect, and helps in draining the fluid from the condenser to the evaporator. Previously studied for space applications (Savino et al., 2010), self-rewetting fluids have now been successfully tested in conventional pipes (Senthilkumar et al., 2012), thermosiphons (Karthikeyan et al., 2013) and even oscillating heat pipes (Hu et al., 2014). The self-rewetting fluids have proven their potential efficiency, but more studies are still required to accurately predict their behaviour.

A nanofluid consists in a conventional liquid base in which nanometric size metallic/ non-metallic/ ceramic particles are incorporated, quite often with surfactants to ensure their stability. Depending on their material, the nanoparticles enable to get a working fluid with enhanced or tailor-made thermo-physical properties. In the last years, numerous studies on nanofluids in heat pipes have been published. Liu and Li (2012) performed a review of the dedicated studies and concluded that depending on the type of nanoparticles, their size and their concentration, nanofluids could significantly increase the heat pipe performances, both in terms of thermal resistance and of maximum heat removal capacity. The major effect of nanofluids seems to be the surface structuration of the evaporator, which affects the wettability of the wall, as well as the boiling phenomenon (Stutz et al., 2011). These conclusions are shared by other review articles recently published (Alawi et al., 2014; Sureshkumar et al., 2013). At present however, there are conflicting results and opinions on the efficacy of such fluids in heat pipe and thermosiphon systems. For instance, Khandekar et al. (2008) observed a decrease of the thermal performance of a PHP when nanofluids are used as working fluids. The nanoparticle clogging affected the boiling phenomenon and the authors tried to quantify the effects of the various mechanisms (figure 2-5). More focussed research is this area needs to be undertaken for clarity (Buschmann, 2013).

Figure 2-6 shows the number of publications dedicated to nanofluids in heat pipes between 2002 and 2014 according to the database of Web of Science™. The number of papers increased rapidly between 2006 and 2010, but has decreased since then. Finally, the studies on nanofluids can be considered as studies on liquid-vapour phase-change heat transfer on nanostructured surface. However, the change in structural morphology of the wall depends on numerous parameters, as it is time-dependent and involves many aging phenomena of the nanofluid (aggregation, deposition, etc.). As a conclusion, if the positive effect of nanofluids on heat pipe performance is well admitted, they mainly affect the heat transfer coefficient during the phase-change heat transfer and the pressure drops in the capillary structure. No fundamental phenomena specific to heat pipes has been observed, which could explain the decrease of the number of articles dedicated to nanofluids in heat pipes since 2010.

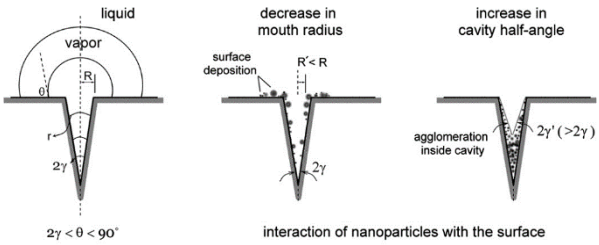

Figure 2-5. Possible clogging of nanoparticles in a nucleating cavity affecting the boiling phenomenon (Khandekar et al., 2008)

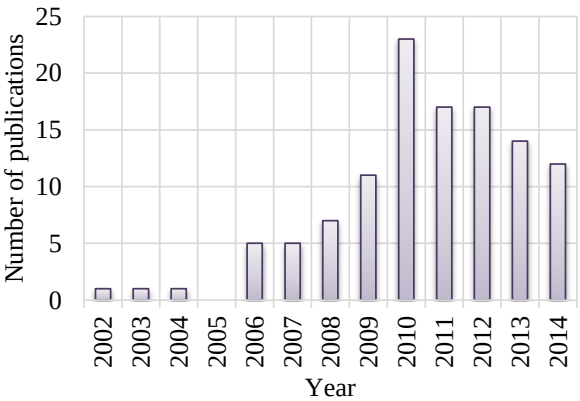

Figure 2-6. Number of publications dedicated to nanofluids in heat pipes according to the database of Web of Science™

2.2.3 Studies aiming to predict the phase-change heat transfer in thin films

Yet, wall texturing (should it be nano-texturing or micro-texturing) can still be viewed as a promising track for the improvement of the efficiency of heat pipes. Heat pipes are certainly one motivation of many research works on the boiling or condensation heat transfer enhancement using structured surfaces. Regarding condensation, the objective is quite often to promote dropwise condensation by modifying the fluid wettability: making a surface (super-) hydrophobic facilitates the roll-off of the droplets, which improves the overall condensation heat transfer. (Super-) hydrophobic surfaces are generally obtained by altering the surface morphology to obtain a chemical or physical texture to decrease the surface energy (Bisetto et al., 2014). Different processes of chemical coating of the solid substrate with a low surface-energy substance are currently being developed and evaluated, as explained by Sikarwar et al. (2011).

Regarding boiling (i.e. for an application to thermosiphons), heat transfer enhancement techniques have been studied for decades, from the emergence of extended surfaces in the 1970ies-1990ies to the development, like for condensation, of microstructured surfaces and more recently nanostructured surfaces. Extended surfaces are manufactured based on standard machining and metal processing. Microstructured surfaces can be obtained by means of porous coating, or by deformation of extended surfaces (e.g. low fins compression, fin bending and cutting, etc.), as described by Poniewski and Thome (2008). Nanostructuration relies on chemical processes (oxidation, etching, silanisation, etc.) or nanoelectromechanical systems (NEMS). Enhanced surfaces are usually used for two distinct purposes: either to increase the critical heat flux, or to increase the heat transfer coefficient.

Beyond a simple increase in heat transfer area, extended surfaces can be employed to optimise the distribution of active nucleation sites or to favour the liquid flow around the heated wall. In addition, when reducing the size of the structures that form the extension down to micrometre or nanometre size, additional phenomena can come into play, as reviewed by (Kim et al., 2015) among many other reviews on the subject of interest. For instance, while nucleation takes place within the pores of a porous coating, liquid can be fed to the nucleation site by means of capillary pumping. Micro- or nanoscale geometric effects (size, but also liquid flow distribution) can also favour the bubble initiation, growth or detachment, while the micro- or nanostructure will modify the fluid wetting characteristics, which will ultimately affect both the heat transfer coefficient and CHF. As an example, the effect of the nanostructuration with a Fe_20_3 nanofluid on the boiling curve of a 100 µm platinum wire is presented in figure 2-7 (Stutz et al., 2011): depending on the nano-particle coating duration (and thus, on the shape of the nanostructuration), the heat transfer coefficient can be increased or decreased but the CHF is always increased by this nano-particle coating.

Lastly, there are also many attempts to take the benefit of the new possibilities offered by micro- and nanotechnologies to improve the wick structures that come into play in all the capillary heat pipes (Ranjan et al., 2011) where capillary evaporation occurs, especially LHPs. As a matter of fact, while the performance of these heat pipes is usually limited by both the ability of the wick to ensure capillary

pumping and by its thermal resistance, micro- or (probably better) nanoscale objects (e.g. nanowires, nanotubes, etc.) should help improve both wicks characteristics as leading to smaller menisci (i.e. increased capillary pumping), as they usually have a greater thermal conductivity, and as they allow for an enhancement of evaporation (Plawsky et al., 2014).

However, the difficulty in predicting the thermal performance of a heat pipe actually lies in the predominance of heat transfer through very thin liquid films. Numerous studies aim to determine the heat transfer coefficients during condensation or evaporation, but the models fail to reproduce the measurements, even for simple geometries as grooves (Lips et al., 2010a). Studies dealing with micro-heat pipes (and thus with very simple geometries) are often limited to theoretical considerations and there is a lack of experimental validation (Liu and Chen, 2013). For PHPs, Khandekar et al. (2010) pointed that too many fundamental phenomena still need to be understood to achieve a complete model because of the pulsating and/or oscillating character of the Taylor bubble flow. Experimental set-ups were developed to study the evaporation and condensation phenomena in capillary tubes. For instance, Chauris et al. (2015) studied the evaporation of the thin film deposited by a moving meniscus. They highlighted the phenomena involved in the process and quantified the impact of each phenomenon on the global heat transfer by comparing their experimental results with a numerical model. They concluded that during the transit of a meniscus, most of the energy is transferred through the thin liquid film deposited by the meniscus, but the impact of the meniscus itself is not negligible (figure 2-8).

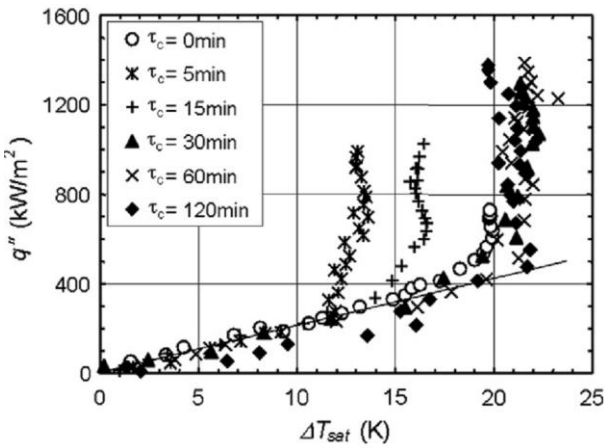

Figure 2-7. Example of the effect of the nanostructuration of the wall on the boiling curve obtained with γ-$Fe_2 0_3$ nanoparticle on a 100 µm platinum wire. τ_c is the nano-particle coating duration with pure water (Stutz et al., 2011)

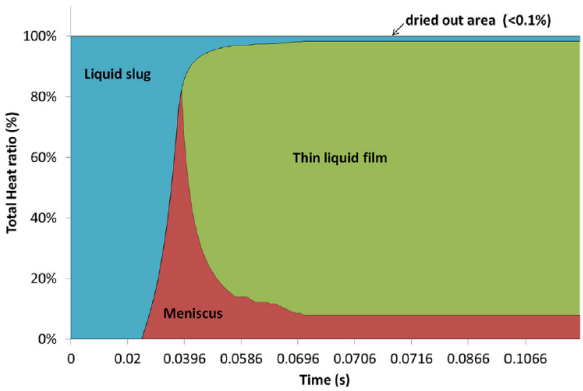

Figure 2-8. Distribution of the heat transferred from the wall to the fluid during the passage of a meniscus (Chauris et al., 2015)

Other recent studies focus on heat transfer in thin films, but with no direct application to heat pipes. As an example, Srinivasan et al. (2015) performed an experimental study that aims to understand the mechanisms occurring during the evaporation of an isolated liquid slug. They focused particularly on the drainage of the thin liquid film and found a good agreement with the Taylor's law predictions. Kunkelmann et al. (2012) studied experimentally and theoretically the effect of the three-phase contact line velocity on the heat transfer. They concluded that the heat transfer in the contact line zone mainly depends on the micro-layer evaporation and on the transient conduction in the wall. At the scale of the liquid thin film, the properties of the wall are indeed found to be not negligible and the coupling of the phenomena is complex. A study performed by Rao et al. (2015) and dedicated to the understanding of a single-branch pulsating heat pipe also illustrates the coupling of thermal and hydrodynamic phenomena, which could lead to self-sustained oscillations. This coupling is particularly important in a pulsating heat pipe, but also in all kinds of heat pipes where evaporation through thin liquid films occurs. In the case of a pulsating heat pipe, no complete model is able to predict their behaviour, but the progress in the understanding of the phenomena contributes to models that are more realistic.

2.2.4 The development of new heat pipe models

During the past few years, heat pipe models have indeed been improved. Both analytical and numerical models were proposed at the scale either of a single phenomenon or of the system. Concerning conventional heat pipes (thermosiphons and capillary heat pipes), the progress in CFD modelling enabled the development of 3D thermal and hydrodynamic models (Wang, 2012). Some other specific studies aim to determine the wick properties by means of detailed thermal and hydrodynamic models at the pore scale (Ranjan et al., 2012). These different approaches are very complementary and each of them leads to a better understanding of the phenomena involved in each type of conventional heat pipe.

Several studies are devoted to the modelling of loop heat pipes. Siedel et al. (2015a) proposed a comprehensive review of the steady-state modelling works. They highlighted the high number of models available and noted that most of them are numerical. The same authors proposed, in another article, a complete analytical model, requiring a low computational time compared to numerical ones (Siedel et al., 2015b). These models are able to reproduce the experiments, but their limit lies in the lack of knowledge of the wick properties (permeability and effective thermal conductivity), of the accommodation coefficient of the working fluid and of the thermal contact resistance between the wall and the wick structure. The presence, or absence, of a vapour zone at the contact between the porous medium and the heat source is also a source of discussion. Mottet et al. (2015) developed a 3D model of a wicked LHP evaporator. They used a mesoscale approach with a pore network model. Their model enabled to highlight phenomena that a 2D model could not reproduce and the authors made the distinction between different regimes governed by different phenomena. The best regime is found to be when a two-phase liquid-vapour zone forms just at the contact of the evaporator casing. Their simulation enables to guide the design of new wicks for LHPs.

At the scale of the system, transient models of LHPs have been proposed. For instance, Kaled et al. (2012) proposed a model classically based on the energy, mass and momentum balances for the evaporator-reservoir, the condenser and the transport lines. They concluded that the fluid motion participates in the pseudo-periodic behaviour of the system. In parallel, Nishikawara et al. (2013) proposed a transient model that correctly predicts the experimental data, despite the presence of an overshoot temperature when the heat load changes, which is not observed experimentally.

An important part of the modelling works published in the last few years are devoted to pulsating heat pipes. On one side, the increasing number of experimental databases enables the development of empirical correlations (Qu and Wang, 2013). On the other side, some 3D CFD models are proposed (Lin et al., 2013) and phenomenological models are implemented. They show a good ability to reproduce the chaotic behaviour of PHPs (Nikolayev, 2011), as well as the influence of the fluid properties (Mameli et al., 2012a) and the orientation (Mameli et al., 2012b). In all cases, these models still have to be improved in order to take into account all physical phenomena, especially at the scale of the thin liquid film and the triple contact line. Detailed models already exist to understand these phenomena, but their experimental validation remains challenging (Nikolayev, 2010).

2.2.5 Summary and Conclusions

This brief review of recent studies focused on heat pipes enables to highlight the main approaches used by the research teams to increase the understanding of the various types of systems. Both experimental and theoretical works have been proposed and the scale of interest of the studies varies from the system size itself to the scale of the very thin liquid film present in the evaporation and condensation zones.

Since 2006, I participated modestly to the improvement of the understanding of the phenomena occurring in heat pipes. A brief summary of the various approaches I followed are presented in terms of scientific questions (section 2.3) and technological issues, which requires crossing the skills of the various scientific communities (section 2.4).

2.3 The heat pipe: an old concept full of scientific challenges

A heat pipe is often defined as a system, meaning its behaviour depends on the coupling between its various parts and between the various phenomena occurring inside this system. In the present section, the various scientific challenges I tried to asses during my research work are highlighted, in a first step through the various modelling strategies I followed, and then through the various phenomenological

analyses I performed. Specific attention will be given to the difficulty of characterising heat pipes, which is a good representation of the strong coupling between the various phenomena identified. At the end of the section, an example of purely theoretical study is presented, showing that even if research on heat pipes lasts from decades, there is still a need for developing notions specific to heat pipes.

2.3.1 Heat pipe modelling

The development of heat pipe models is a major challenge for the heat pipes communities. The first reason is because there is a huge need of design tools to help the industrial community to adapt heat pipes to their specific applications. The second reason is that a model can often be considered as a summary of the knowledge of the phenomena governing the system. From this point of view, it can be an interesting tool to study the balance and the coupling between various phenomena, once the model is validated with experimental results.

In this section, two examples illustrating these reasons are presented for the case of two-phase heat spreader and loop heat pipes.

2.3.1.1 Two-phase heat spreader modelling

When a model is developed in order to help design a system, the difficulty lies in findings the good trade-off between the simplicity of the model and the accuracy of the simulations. In the various heat pipe projects in which I have been involved, I had the opportunity to use and/or develop flat heat pipe models at various scales, using nodal, analytical and numerical modelling.

When a heat pipe is introduced in a complex system, the easiest way to implement it is to use only a thermal nodal model. The level of discretisation can vary following the model purpose, but they are all based on the assumption that the temperature in the vapour zone is homogenous and equal to the saturation temperature of the fluid. A heat pipe can thus be modelled by only three nodes: the wall evaporator temperature, the saturation temperature and the wall condenser temperature. They are linked with two thermal resistances corresponding to the evaporation zone and the condensation zone respectively (figure 2-9 a)). When one wants to account for the global longitudinal conduction heat transfer in the wall, for instance to calculate the fluid mass flow inside the system, a third resistance can be added (figure 2-9 b)). Of course, this kind of model can be discretised as much as needed (figure 2-9 c)). To calculate the capillary limit of a flat heat pipe, it is possible to couple a hydrodynamic model to each of the thermal models, either by integrating the pressure drops along the capillary structure, either by solving the momentum equation for each discretised heat pipe cross section.

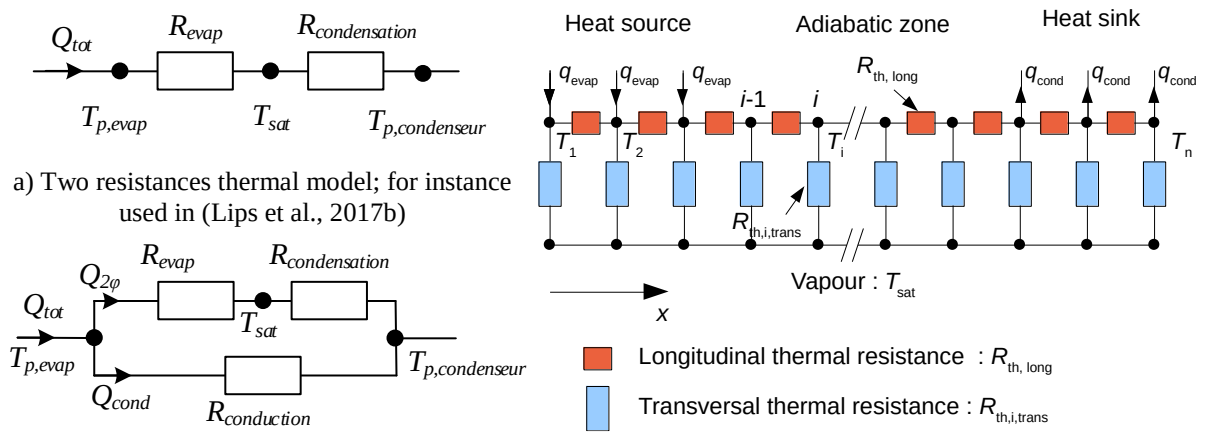

a) Two resistances thermal model; for instance used in (Lips et al., 2017b)

b) Three resistances thermal model; for instance used in (Lips et al., 2009a)

c) Discretized thermal model; for instance used in (Lips, 2009)

Figure 2-9. Various levels of nodal models

Nodal models are very easy to use and implement, but the determination of each thermal resistance can be very difficult and are subjected to many simplifications. A way to take into account the heat conduction in the heat pipe wall more accurately is to use analytical models based on Fourier transformations. In this type of model, the temperature field is written under the shape of an infinite sum of sines and cosines functions (Lips and Lefèvre, 2014):

$$T^*(X,Y,Z) = \sum_{m=1}^{\infty}\sum_{n=1}^{\infty} A_{mn}(Z)\sin(m\pi X)\sin(n\pi Y)$$
$$+\sum_{m=1}^{\infty}\sum_{n=0}^{\infty} A'_{mn}(Z)\sin(m\pi X)\cos(n\pi Y)$$
$$+\sum_{m=0}^{\infty}\sum_{n=1}^{\infty} B'_{mn}(Z)\cos(m\pi X)\sin(n\pi Y) \qquad (2\text{-}1)$$
$$+\sum_{m=0}^{\infty}\sum_{n=0}^{\infty} B_{mn}(Z)\cos(m\pi X)\cos(n\pi Y)$$

X and Y are the non-dimensional coordinates of any point on the wall of the heat pipe and A_{mn}, A'_{mn}, B'_{mn} and B_{mn} are functions of the non-dimensional coordinate $Z = z / c$ and c is the thickness of the heat pipe walls. Their expression can be explicitly found when solving the heat equation analytically. This model can be used for various heat pipe geometries by adjusting the considered axes of symmetry when building the domain for the Fourier transformations (figure 2-10). The heat pipe hydrodynamic behaviour can be determined in the same way by solving Darcy's equation. An example of results obtained with the analytical model is presented on figure 2-11. This kind of model is rather fastidious to implement but very convenient to use as it requires very little computational power.

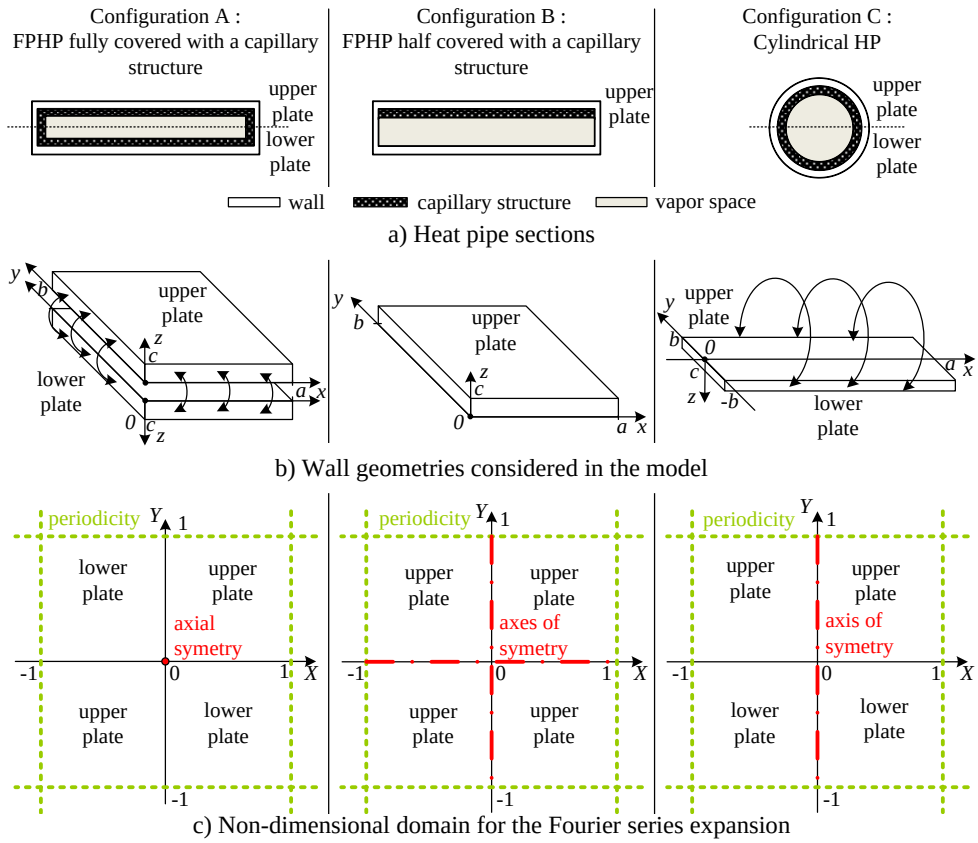

Figure 2-10. Geometries and corresponding domains for three heat pipe configurations (Lips and Lefèvre, 2014)

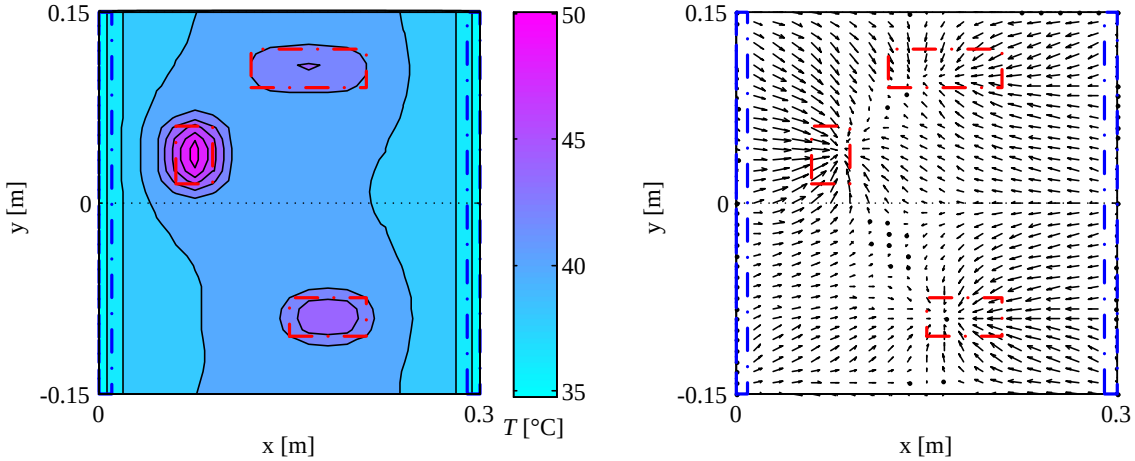

a) Wall temperature field

b) Liquid velocity field (u_{max} = 3.7 10^{-4} m/s)

Figure 2-11. Example of thermal and hydrodynamic results obtained with the analytical model for a flat plate heat pipe with three heat sources and two heat sinks (Lips and Lefèvre, 2014)

Analytical models can be very accurate, but are limited to conventional geometries and to homogenized equations (heat transfer in a solid, Darcy's law in the capillary structure). To take into account more complex geometry or to consider a more physical liquid-vapour interface shape, 3D numerical modelling is required. However, the difficulty is to consider all the phenomena occurring into a heat pipe, often acting at different scales. For instance, the meniscus shape will have to be determined at the scale of a pore of the capillary structure (figure 2-12a) whereas the nucleation of a bubble will have to be considered at the scale of the surface roughness (figure 2-12b). The boundary effects, which are far from being negligible in a heat pipe will have to be considered at the scale of the whole system (figure 2-12c).

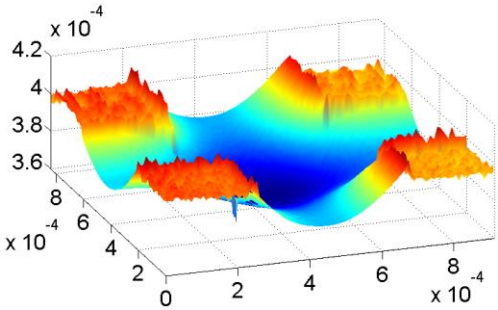

a) Capillary phenomena: example of experimental visualisation of the liquid-vapour interface in crossed grooves capillary structure by means of confocal microscopy (Lips et al., 2010b)

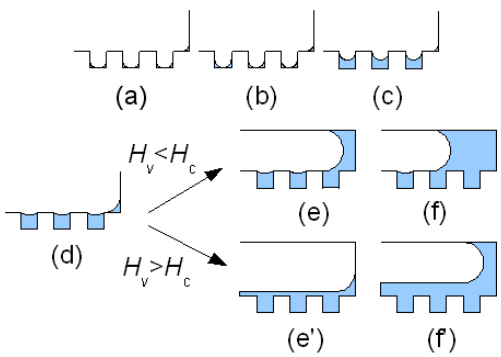

c) Distribution of the liquid inside a FPHP: role of the boundary effect (Lips et al., 2010c)

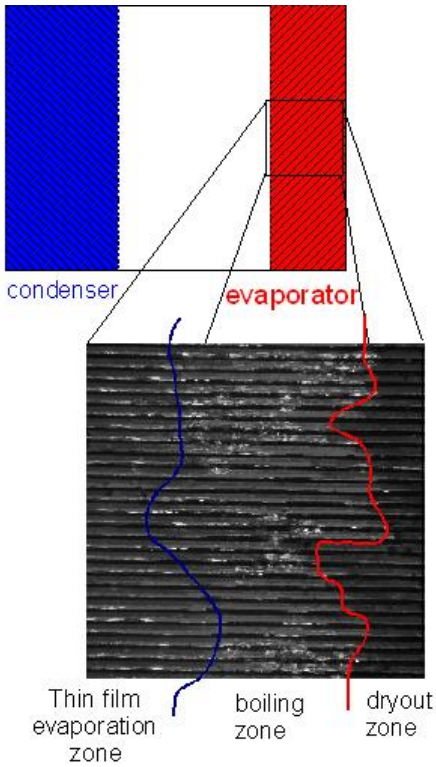

b) Example of boiling and dry-out observed in a flat heat pipe (Lips et al., 2009b)

Figure 2-12. Example of phenomena occurring in heat pipes

In practice, there is so far no complete numerical model able to predict a complete heat pipe behaviour. Even the determination of the evaporation and condensation heat transfer coefficient in a simple rectangular groove is not achievable yet (Lips et al., 2010a). Attempts of CFD modelling are done in the literature, and many of them are involving reduced equations to try to account for various phenomena. However, the parameters involved in these equations are often badly known and can only be fitted with experimental data. The main way to improve this type of model is to continue to perform experimental and theoretical works to understand each phenomena, as well as their coupling, and to develop reliable reduced models. Together with the improvement of the computational power of computers, 3D reliable heat pipe models may be available in one or two decades.

2.3.1.2 LHP modelling

The challenges in the heat pipe modelling differ depending on the type of heat pipe considered. In loop heat pipes, the presence of the liquid and vapour lines facilitates the pressure drop calculations, but the inverted menisci at the evaporator, the condensing menisci in the tube condenser and the presence of subcooled and superheated zones increase the complexity of the thermal models. Consequently, LHP models available in the literature are not able to predict accurately their performance without fitting various parameters with experimental results, for instance the heat transfer coefficient at the evaporator and at the condenser. However, they are robust enough to analyse the global behaviour of a LHP and to study the trends of its performance. They can thus be used as a tool, from a research point of view.

For instance, the goal of the 2MATHER project (2014-2017), granted by the Institut Carnot I@L was to understand the effect of the manufacturing parameters of the evaporator of a LHP on its performance. Remi Giraudon, co-supervised by Valerie Sartre and myself, completed his doctoral dissertation as part of the 2MATHER project. The first step of his work was to draw the specifications of an optimal double layer wick. He adapted the nodal model of Siedel et al. (2015b) to this configuration (figure 2-13) and performed a parameter analyses to study the effect of the top and bottom wick parameters. For instance, figure 2-14 presents the effect of the bottom layer pore radius and of the top and bottom layer permeability on the LHP capillary limit. It can be seen that if an optimum pore radius can be determined, there is no real threshold in terms of permeability. This kind of study enabled Remi Giraudon to determine the specifications of the wicks that will be manufactured and characterized (table 2-1). The latter will be presented and discussed in the sections 2.4.1 and 2.3.3 respectively.

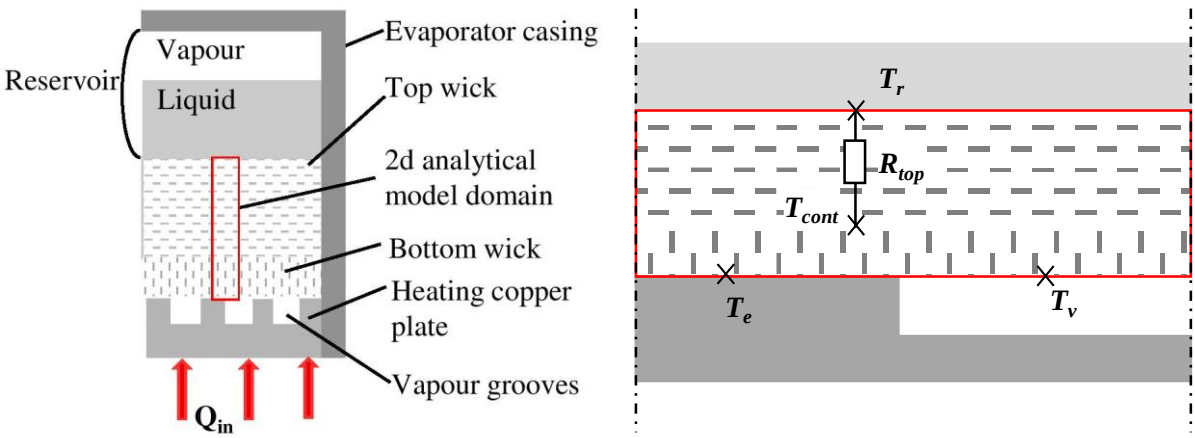

Figure 2-13. Schematic of the evaporator with double layer wick (left) and a representative control volume with imposed temperatures and symmetric boundary conditions (right) (Giraudon et al., 2017a)

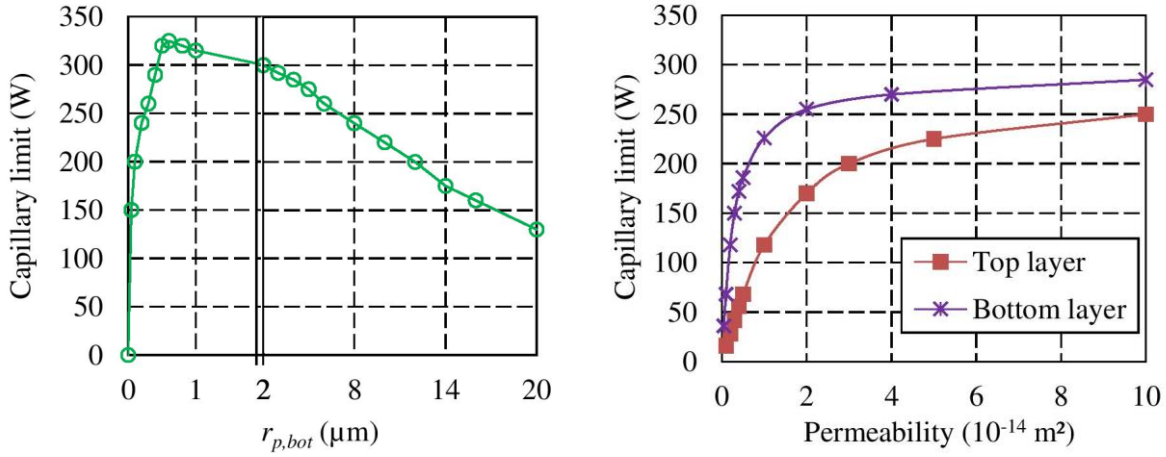

Figure 2-14. Capillary limit as a function of the bottom layer pore radius (left) and of the top and bottom layer permeabilities (right) (Giraudon et al., 2017a)

Table 2-1. Specifications for the wick characteristics (Giraudon et al., 2017a)

Layer	t	ε	K	r_p	λ
Top	10 mm	No influence in the range 0.2 – 0.7	> 3.10^{-14} m²	15 µm	< 0.1 W/m.K
Bottom	As low as possible while ensuring a sufficient mechanical strength	No influence in the range 0.2 – 0.7	> 2.10^{-14} m²	10 µm	> 10 W/m.K

As a conclusion, the development of heat pipe models can be motivated by different reasons but real predictive models are still not available in the literature. The main reason is that many phenomena are still not really understood and further experimental analyses are still necessary, whatever the type of heat pipes. Personally, most of my research works are experimental studies, and I mainly used models I develop as tools to analyse the systems behaviour and to check the validity of the experimental conclusions.

2.3.2 A research strategy based on a phenomenological analysis

Both fundamental and applied research can be led on heat pipes. The applied character is obvious, as many studies aims at understanding the system behaviour or performance. The fundamental characters lies in the fact that some physical principles occurring in heat pipes are still not well understood. “What really governs the growing of a vapour nucleus before the onset of nucleate boiling?”; “What is the real meaning of the accommodation coefficient in the phase change kinetic theory?”; “Does the phase change affects the intrinsic contact angle at the triple contact line?”; “Do triple contact lines exist?” are fundamental questions that are still discussed in the heat pipe community.

In my research, I am constantly trying to follow an intermediate approach by focusing on the phenomena and their couplings. Physical phenomena indeed link the physical principles to the behaviour of the systems. To do so, I mainly performed two-types of studies: The experimental studies based on visualisations inside the systems and the studies based on the global behaviour analyses.

Visualisations require to use transparent systems and to develop image processing tools. For instance, I studied during my Master project the shape of the liquid plug menisci oscillating in a capillary tube (Lips and Bonjour, 2007). During my PhD, I used a confocal microscope to determine the radius of curvature of the liquid-vapour interface inside a grooved capillary structure. It enabled the determination of the capillary pressure along the capillary structure and thus the understanding of the various capillary effects affecting the heat pipe performance (Lips et al., 2010b, 2010a, 2010c). In the remaining part of the manuscript, various examples of studies realized by means of transparent systems, will be presented.

The internship of Alba Fornells-Vernet which I co-supervised with Frederic Lefèvre in 2012, is a typical example of phenomena study based on the measurement of global performance of a system. She was interested in the behaviour of flat heat pipe with capillary structure made of meshes, grooves, or a combination of the two (figure 2-15). The experimental determination of the thermal and hydrodynamic performance of the various configurations under different experimental conditions enabled to study

several phenomena specifically linked to the use of metallic meshes. For instance, the heat pipe behaviour presented on figure 2-16 showed that the meshes can provide a high capillary pressure, but exhibit a low permeability (configuration A). When coupling meshes with grooves, a very early dry-out occurs because bubbles generated by boiling in the grooves lead to the depriming of the wick (configuration B). An alternative can be the use of an inverted meniscus system, which could couple the advantage of the grooves and of the meshes. However, more studies are required to enhance heat transfer between the grooves and the meshes (configuration C).

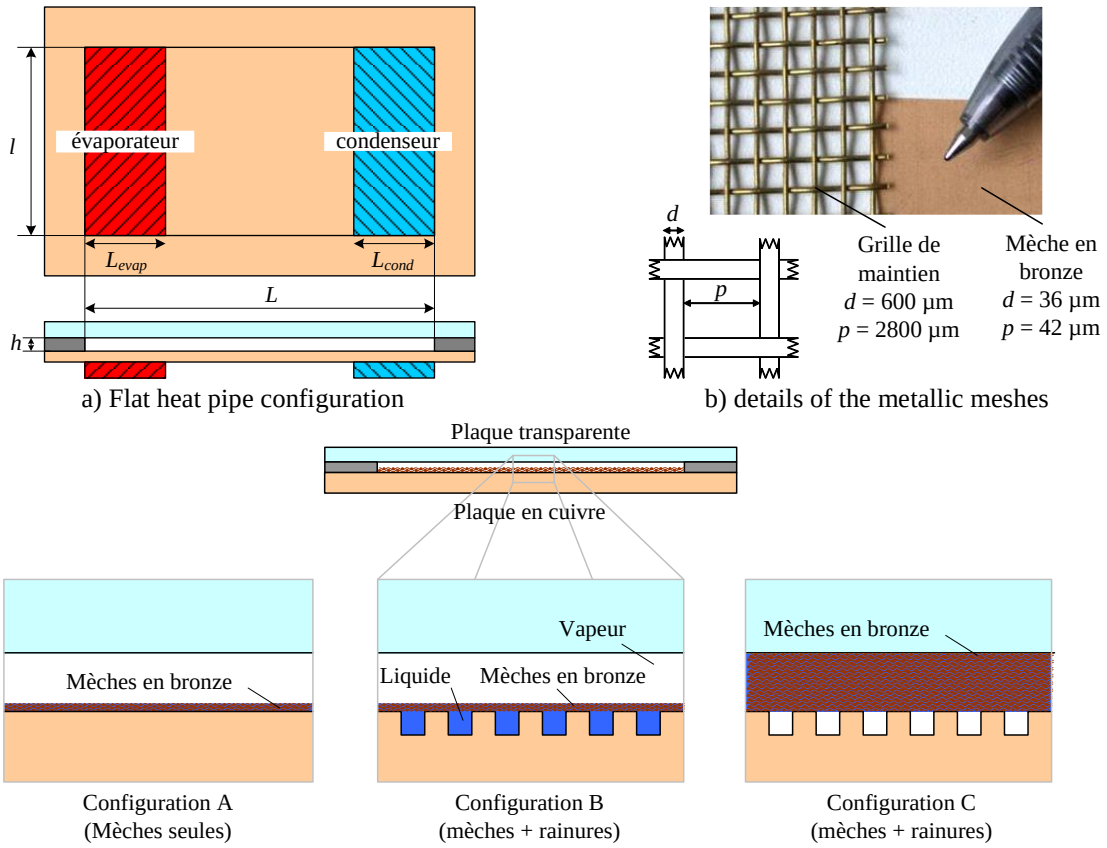

Figure 2-15. Flat heat pipe configurations tested by Alba Fornells-Vernet, adapted from (Fornells-Vernet, 2012)

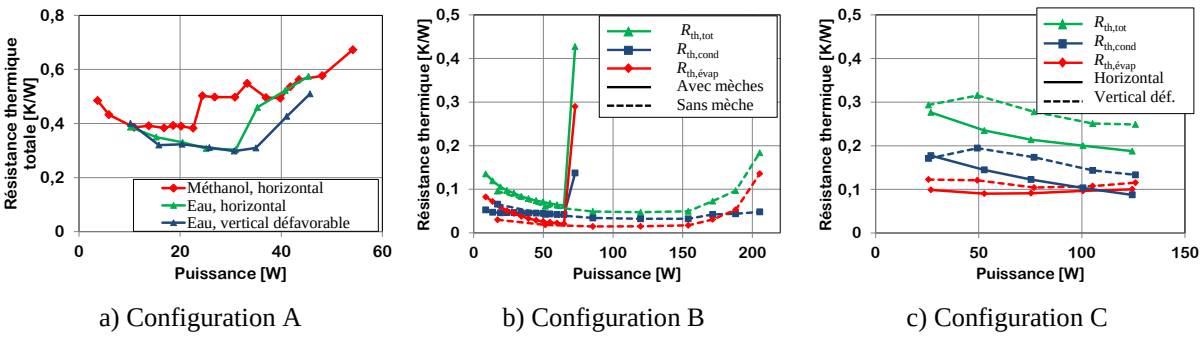

Figure 2-16. Example of heat pipe performance for various configurations (Lips et al., 2013)

As a conclusion, the type of research studies I performed aim at providing a better understanding of the phenomena occurring in the systems. I did not try to extend my work toward molecular dynamic studies or the development of new numerical algorithms for the modelling of two-phase flows for instance. This positioning enables to focus on the development of experimental skills and advance analyses tools that are both highly required when studying heat pipes.

2.3.3 On the difficulty of characterizing a heat pipe

Many research teams characterize heat pipes as a black box and their experimental results can often be categorised as the evolution of the global thermal resistance of the system in various working conditions (imposed heat flux, orientation, filling ratio, etc.). Without denying the importance of this kind of results, it is often very frustrating because it provides relatively poor information on the phenomena occurring inside the systems. Even the definition of the global thermal resistance can be subjected to discussions, depending on which temperature difference is considered.

The various results presented in the literature are thus very difficult to compare and general conclusions are hard to draw. For instance, it has been shown in section 2.3.1.1 that the thermal resistance and the capillary limit of a capillary heat pipe mainly depend on the effective thermal conductivity and the permeability of its capillary structure. Determining these properties if often more useful to the community than giving only the global heat pipe performance. In this section, two approaches aiming at giving more comparable properties are thus presented, depending whether the characterization of the heat pipe component is made in-situ or in a specific test bench.

2.3.3.1 In-situ characterization by means of inverse methods

The direct measurements of the capillary structure properties is often not possible and inverse methods have to be used. This kind of approach is illustrated in this section with the new method presented in (Revil-Baudard and Lips, 2015). The aim was to determine the capillary structure properties from measurements of the overall performance of a flat plate heat pipe under different inclination angles. The determination of the thermal properties was based on an analytical method that was directly inverted: the equivalent thermal conductivities of the capillary structure at the condenser and at the evaporator were thus the outputs of the inverse method, whereas the temperature measurements along the heat pipe were the inputs (figure 2-17). This technique enabled a direct comparison between the properties of the capillary structure of various heat pipes, even if the global thermal resistances of the systems were different. This kind of approach may be the first step for the construction of an experimental equivalent thermal conductivity database for the development of predictive tools (figure 2-18).

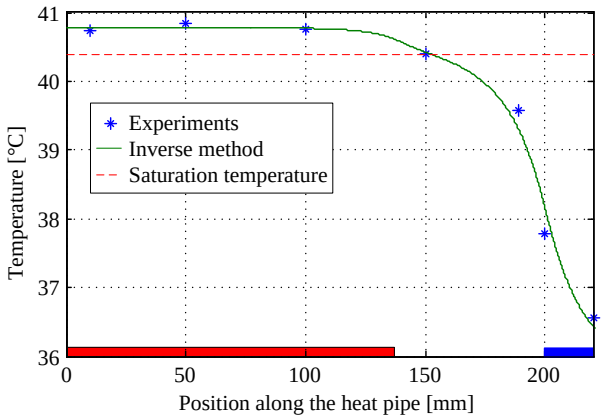

Figure 2-17. Example of comparison between an experimental temperature profile and the corresponding profile calculated by the inverse method ($\dot{Q}$ = 20 W; horizontal orientation) (Revil-Baudard and Lips, 2015)

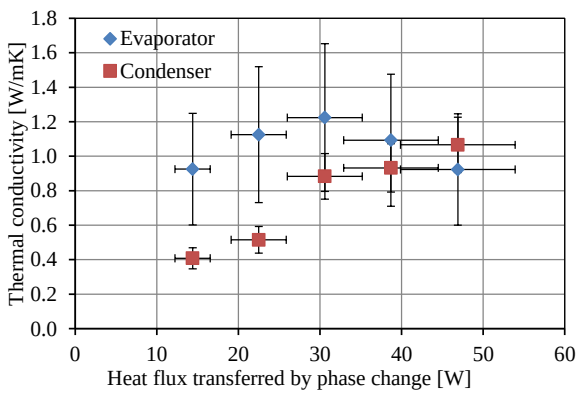

Figure 2-18. Example of equivalent thermal conductivity determination by means of the inverse method (L_{evap} = 140 mm, horizontal orientation) (Revil-Baudard and Lips, 2015)

The determination of the hydrodynamic properties of the capillary structure, i.e. its effective permeability and its effective pore radius is more difficult, as no direct measurement can be performed in a non-transparent heat pipe. The method is based on the measurement of the capillary limit for different inclination angles. The capillary limit is reached when the sum of the gravitational and frictional pressure drops is equal to the maximum capillary pressure that the wick structure can sustain. It leads to a dry-out at the evaporator, and thus to an increase of the thermal resistance of the heat pipe. When the heat pipe is tilted in unfavourable positions, the capillary limit decreases because of the effect of the gravitational pressure drop (figure 2-19). The frictional pressure drop and the effective pore radius of the capillary structure can be estimated by assuming that the capillary pressure at the capillary limit is constant whatever the inclination angle (figure 2-20). This method has been successfully tested on a

grooved flat plate heat pipe and validated by means of microscopy measurements. However, it has been shown that more studies are required to use this method with other capillary structures, as the assumption of a constant capillary pressure at the capillary limit of the heat pipe is not trivial.

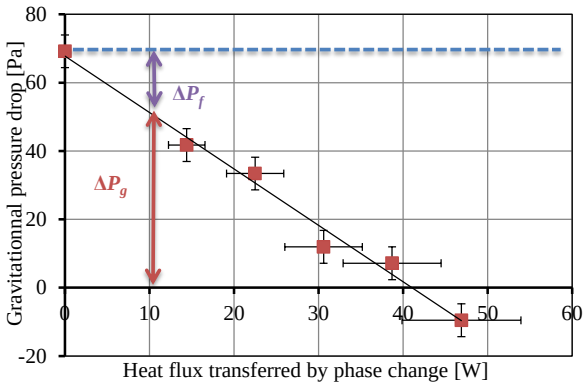

Figure 2-19. Example of evolution of the gravitational pressure drop as a function of the heat transfer rate transferred by phase change (Levap = 140 mm) (Revil-Baudard and Lips, 2015)

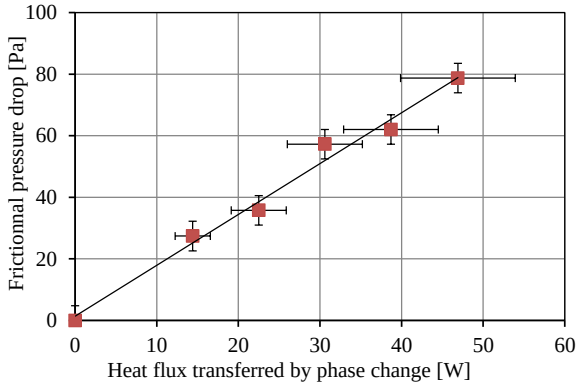

Figure 2-20. Example of the frictional pressure drop as a function of the heat transfer rate (Levap = 140 mm) (Revil-Baudard and Lips, 2015)

2.3.3.2 Direct component characterization: example of an LHP evaporator

Inverse methods enable to characterize the properties of the various heat pipe components in real working conditions, but it appears that there is often a strong coupling between the phenomena occurring at the evaporator and at the condenser of a heat pipe. It can thus be interesting to study the properties of each component out of the system. During his PhD, Rémi Giraudon studied, among others, copper sintered wicks that he manufactured himself (figure 2-21).

The main properties of this kind of wick are its permeability, its effective pore radius and its effective thermal conductance. The two first parameters were determined by means of a hydrodynamic test bench consisting in two concentric tubes: the test tube and the reservoir (figure 2-22). The tested wick is placed at one of the extremity of the test tube depending on the property that is being measured.

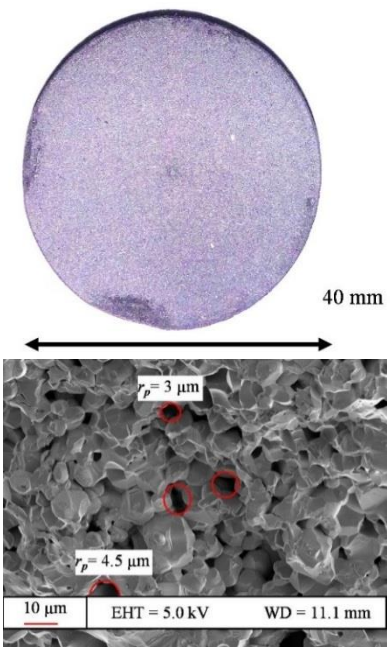

Figure 2-21. Example of sample manufactured by Rémi Giraudon during his PhD (Giraudon et al., 2017b)

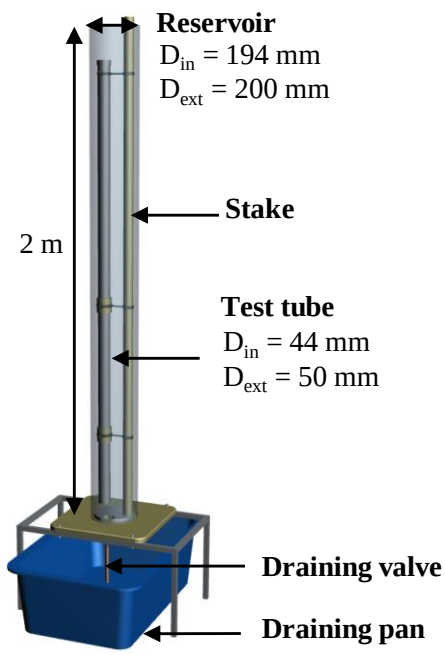

Figure 2-22. 3D view of the experimental test bench (Giraudon et al., 2017b)

When measuring its effective permeability, the sample is located at the bottom of the test tube. The test tube is then filled with the working fluid and the evolution of the water levels in the test tube and the reservoir are recorded (figure 2-23). The latter enables to determine the velocity of the fluid through the wick as well as the pressure drop across it. The permeability can then be deduced by means of Darcy's law (figure 2-24).

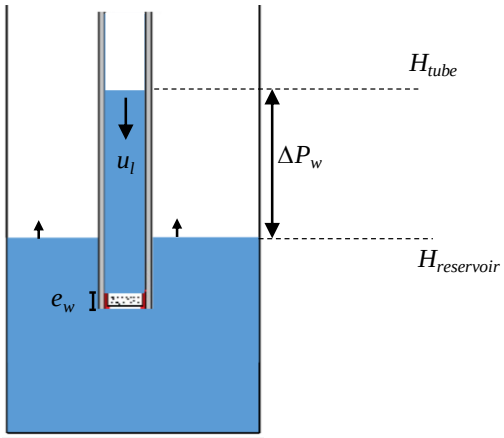

Figure 2-23. Operating principle of the test bench when measuring the permeability (Giraudon et al., 2017b)

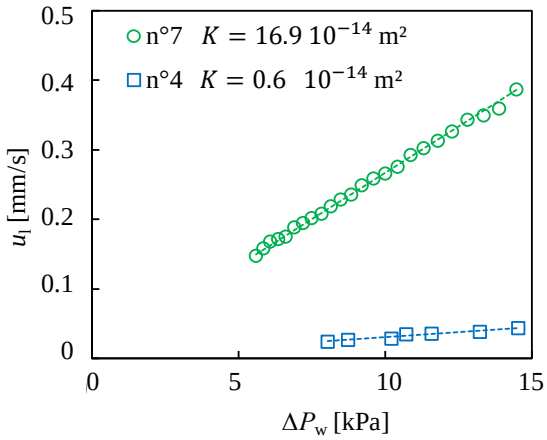

Figure 2-24. Example of determination of the permeability for two samples (Giraudon et al., 2017b)

When measuring its effective pore radius, the wick is located at the top of the test tube. Firstly, the reservoir and the test tube are filled up to the top so that the wick is saturated with fluid. Then, the reservoir is emptied step-by-step (figure 2-25). This procedure enables to create a pressure difference between both sides of the porous medium. The meniscus curvature, which is inversely proportional to pressure difference across the interface, increases up to its maximum value, linked to the fluid/material wettability and to the pore radius. Then, the liquid recedes inside the capillary structure, the liquid column falls, as highlighted in Figure 2-26 by the sudden drop of the water level in the test tube. The maximum difference between the two water levels enables the determination of the effective pore radius of the capillary structure my means of Laplace's Law.

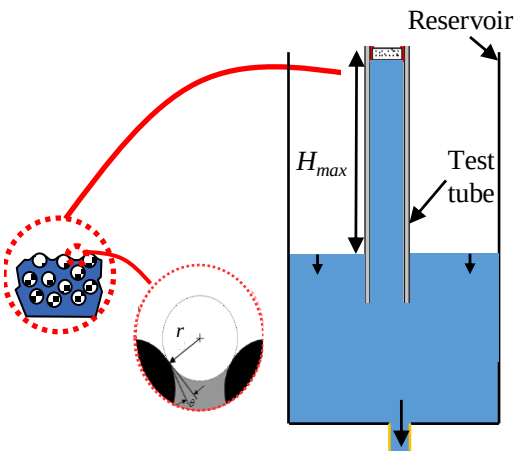

Figure 2-25. Operating principle when measuring the effective pore radius (Giraudon et al., 2017b)

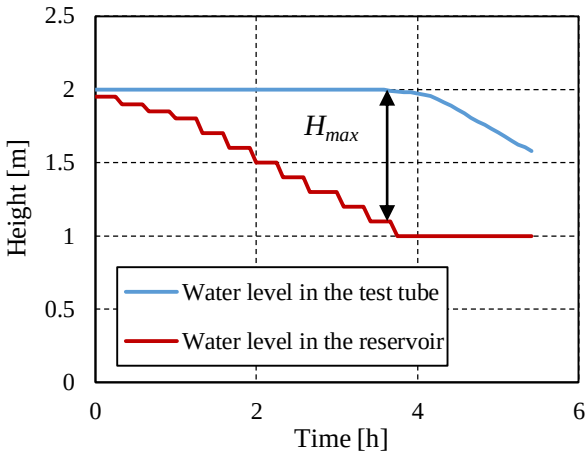

Figure 2-26. Example of evolution of the water level during the test (Giraudon et al., 2017b)

The goal of 2MATHER project was to understand the effect of the wick manufacturing parameters on its thermal performance. To do so, Remi Giraudon also designed a thermal test bench, presented in figure 2-27. The wick was located in a sealed temperature controlled enclosure enabling to simulate the thermal behaviour of a LHP. An example of sample thermal characterisation is presented on figure 2-28. From the measurement of the heat transfer coefficient as a function of the heat flux, the optimal working point of the sample could be determined.

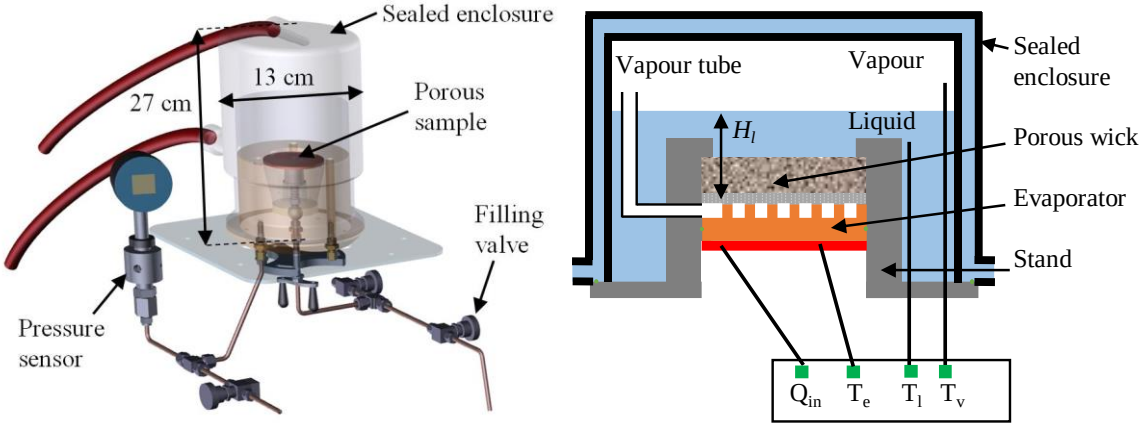

Figure 2-27. 3D view and schematic of the thermal test bench (Giraudon et al., 2017b)

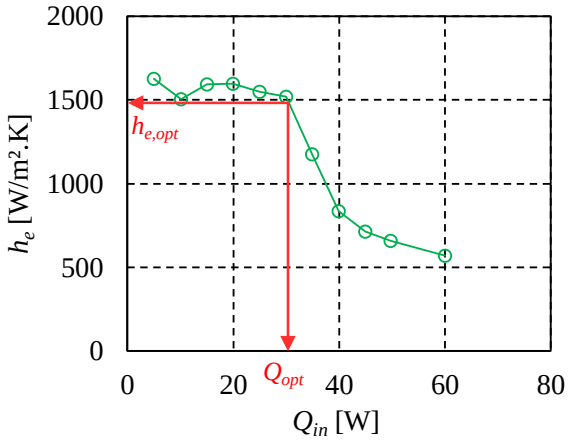

Figure 2-28. Example of a sample thermal characterisation (Giraudon et al., 2017b)

Remi Giraudon tested differents samples manufactured following a design of experiment and managed to link the hydrodynamic performances to the manufacturing process (more details are available in (Giraudon et al., 2017b)). However, the thermal behaviour of each samples, tested with water (Figure 2-29) and pentane (Figure 2-30) were more difficult to understand. He showed that the permeability and the effective pore radius had an effect on the maximum heat transfer coefficient because of the capillary limit occurring in the wick. However, the strong difference of behaviour of the samples with water and pentane, both in terms of maximum heat flux (figure 2-31) and of maximum heat transfer coefficient (figure 2-32) showed that another limit, probably linked to the boiling limit, was strongly affecting the wick performance.

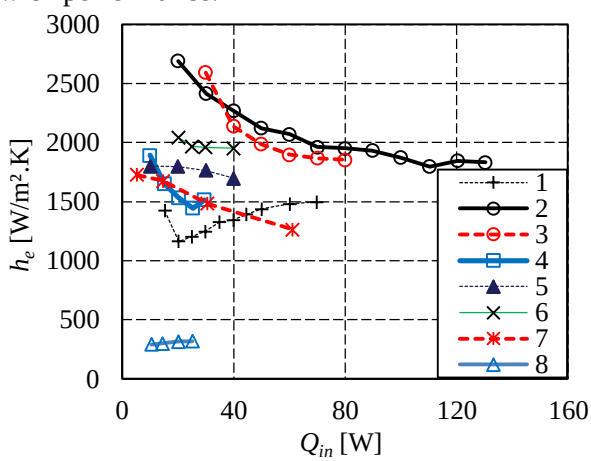

Figure 2-29. Evolution of the heat transfer coefficient for each sample with water (Giraudon et al., 2017b)

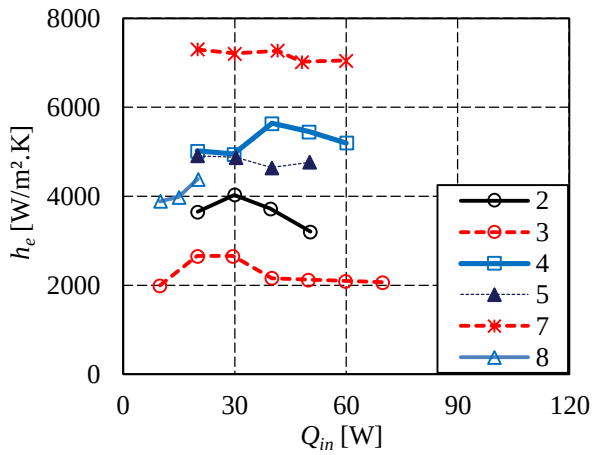

Figure 2-30. Evolution of the heat transfer coefficient for each sample with pentane (Giraudon et al., 2017b)

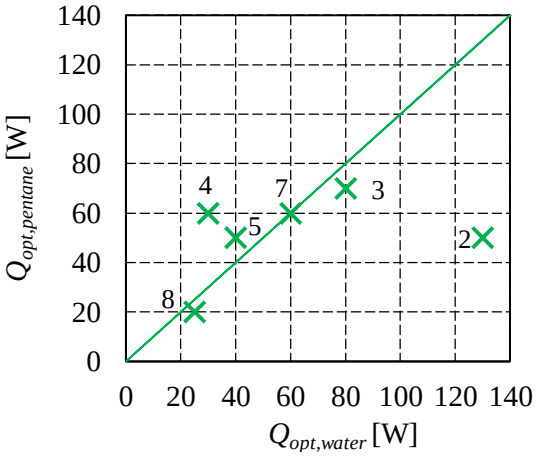

Figure 2-31. Comparison of the maximum heat flux of the various samples between water and pentane (Giraudon et al., 2017b)

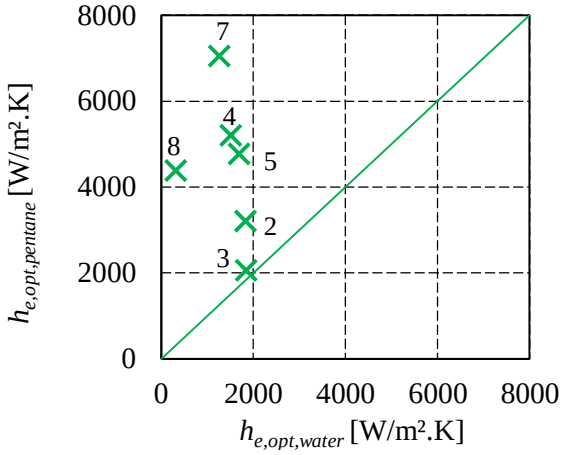

Figure 2-32. Comparison of the maximum heat transfer coefficient of the various samples between water and pentane (Giraudon et al., 2017b)

This type of experimental studies show how difficult it is to characterise the behaviour of a heat pipe component. The global performance of a system are always the result of the interactions of several phenomena and the understanding of all these possible interactions requires conducting many various experimental studies with complementary approaches.

2.3.4 Example of theoretical study: Definition of a heat pipe utility criterion

Experimental and numerical studies represent most of the heat pipe studies available in the literature, but theoretical aspects are also considered. To illustrate this kind of study, here is an example of the development of a heat pipe utility criterion. This study was performed in the European project I2MPECT and was presented in the 2017 SFT conference (Lips et al., 2017b) and is currently being adapted as an article for an IEEE journal.

In many industrial applications, the use of flat heat pipes, also called two-phase heat spreaders, is discussed but there is surprisingly no generic tool that helps to evaluate the interest of adding such type of component to an existing system. Consequently, a specific study has to be performed for each application, which can be very time consuming. The present method aims at evaluating quickly the thermal advantage of adding a two-phase thermal spreader to the system in the type of configuration presented on figure 2-33: electronic components are located on a printed circuit board (PCB) which is cooled by a heat sink on the opposite side.

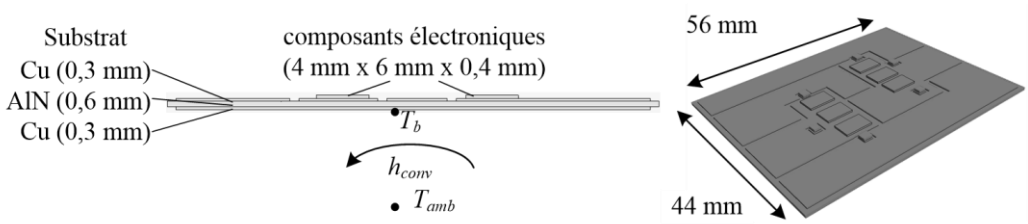

Figure 2-33. Example of studied configuration. The heat sink is not represented (Lips et al., 2017b)

In this kind of configuration, the shape of the temperature field in the PCB depends strongly on the heat transfer coefficient between the PCB and the cooling fluid. As an illustration, figure 2-33 presents two temperature fields of a PCB (with no flat heat pipe) calculated by CFD modelling for two different heat transfer coefficients. It can be seen on figure 2-33 b) that an important part of the PCB is close to the ambient temperature (0°C), the heat transfer between the heat sink and the cooling fluid in this area is thus very small. A flat heat pipe aims at spreading the heat flux to the heat sink in order to use effectively most of the heat sink surface. In this case, the addition of a flat plat heat pipe can thus be of interest to improve the total thermal resistance of the system. The interest is lower in the case of figure 2-33 a) for which the temperature field is more homogenous (even if the general temperature level is higher).

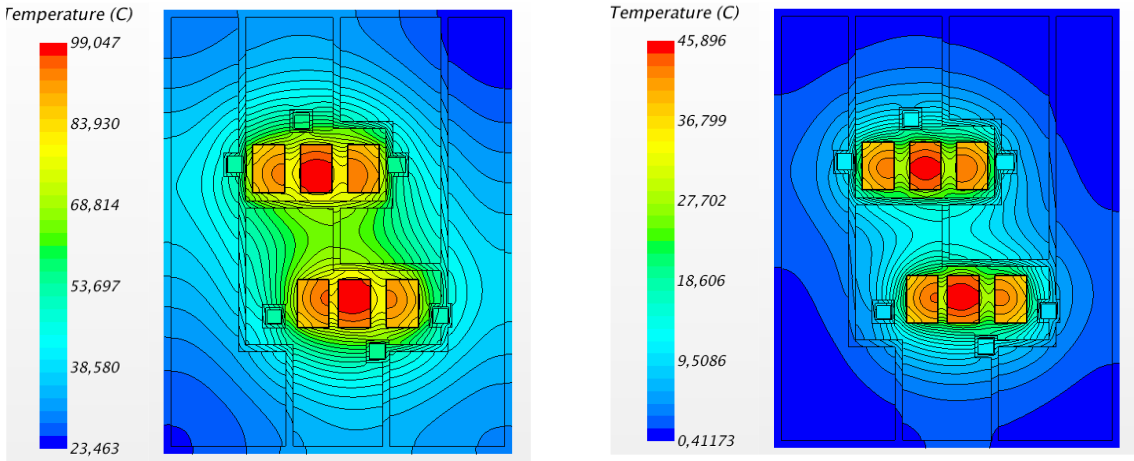

a) h_{conv} *= 1500 W/m²K* *b)* h_{conv} *= 10 000 W/m²K*

Figure 2-34. Examples of temperature fields in the PCB, calculated by CFD modelling for two different heat transfer coefficient with the heat sink (Q = 25 W/components and T_{amb} = 0°C) (Lips et al., 2017b)

The formalisation of this principle involves the notion of thermal spreading efficiency of the PCB, by similitude to the thermal efficiency of a fin. It can be calculated by the ratio between the convection thermal resistance between the PCB and the cooling fluid to the total thermal resistance of the system:

$$\eta = \frac{R_{conv}}{R_{tot}} = \frac{1}{1 + R_{cond}/R_{conv}} \tag{2-2}$$

The notion of spreading efficiency enables to quantify the total thermal resistance of a given power module cooled down with a given heat sink, compared to that of a power module with infinite thermal conductivity cooled down with the same heat sink. η is equal to 1 when the conductive thermal resistance is negligible compared to the convective thermal resistance. η is equal to 0 when the convective thermal resistance is negligible compared to the conductive thermal resistance. The thermal spreading efficiency of a given PCB can be calculated numerically or analytically by means of asymptotic considerations (figure 2-35). The lower the thermal spreading efficiency of the PCB is, the higher will be the interest of adding a heat pipe between the PCB and the heat sink.

The notion of thermal gain G due to the addition of a flat heat pipe can be defined as the relative diminution of the global thermal resistance of the system when adding a flat heat pipe to a given PCB. By modelling the heat pipe as two-thermal resistances at the evaporator and at the condenser, it can be shown (Lips et al., 2017b) that the gain is equal to:

$$G = \frac{R_{tot,\emptyset} - R_{tot,d}}{R_{tot,\emptyset}} = 1 - \eta_\emptyset \frac{S_b}{S_{tot}} - \frac{\eta_\emptyset}{\eta_d}\frac{h_{conv}}{h_{evap}}\left(1 + \eta_d \frac{S_b}{S_{tot}}\right) \tag{2-3}$$

where $\eta_\emptyset$ and η_d are the heat spreading efficiencies of the PCB with no heat pipe and with heat pipes respectively. h_{evap} is the heat transfer coefficient at the evaporator and at the condenser of the heat pipe (see two-resistance model in section 2.3.1.1) and S_b/S_{tot} is the ratio between the surface of the PCB and the surface of the heat pipe, which may be larger than the PCB. When an analytical expression is used to calculate the spreading efficiencies, the thermal gain of the heat pipe can thus be directly estimated. Figure 2-36 presents an example of evolution the gain as a function of the convective heat transfer coefficient for several heat pipe performance, modelled by h_{evap}, and for the PCB corresponding to the spreading efficiency presented on figure 2-35. It can be seen that the thermal gain can be higher or lower than zero and that the addition of a heat pipe can be interested only if the latter is very efficient (high h_{evap}), and only for a given range of heat transfer coefficient between the PCB and the cooling fluid. The addition of a heat pipe could be more interesting when the heat pipe (and thus the heat sink) is larger than the PCB (figure 2-37) or when the PCB has a lower spreading efficiently (figure 2-38).

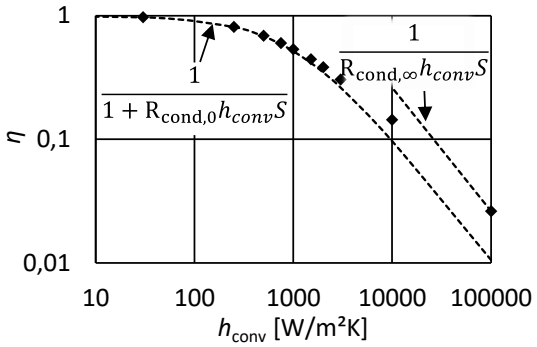

Figure 2-35. Heat spreading efficiency of the PCB presented on figure 2-33 (In the present example, $R_{cond,0}$ = 0.4 K/W) (Lips et al., 2017b)

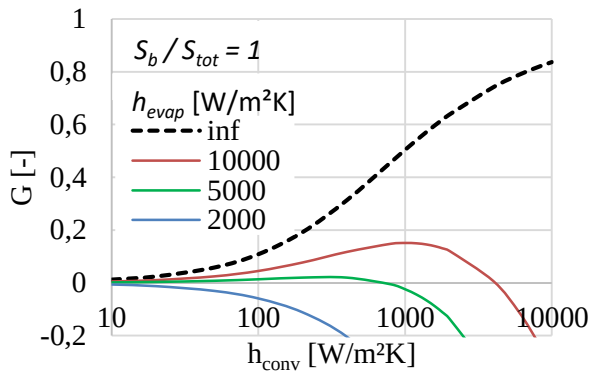

Figure 2-36. Thermal gain of a flat heat pipe for S_b/S_{tot} = 1 (Lips et al., 2017b)

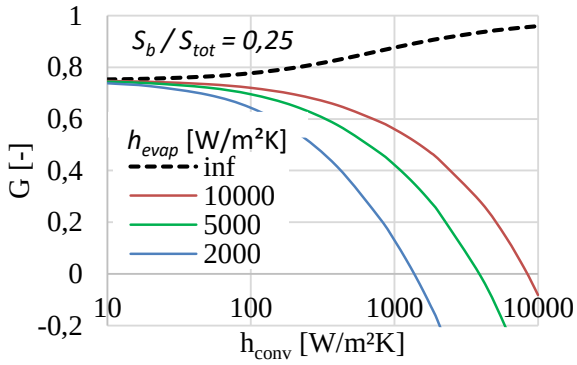

Figure 2-37. Thermal gain of a flat heat pipe for S_b/S_{tot} = 0.25 (Lips et al., 2017b)

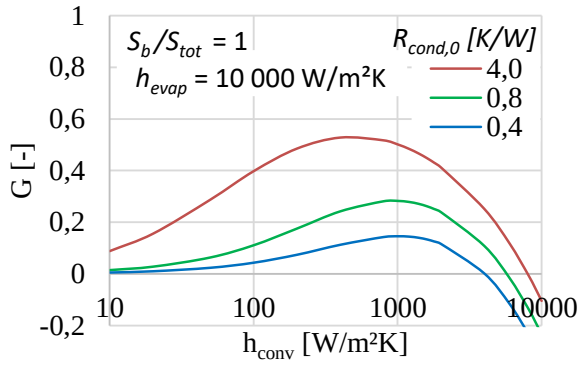

Figure 2-38. Thermal gain for various PCB spreading efficiency, characterized by $R_{cond,0}$ (Lips et al., 2017b)

In order to illustrate the results predicted by the formalization of the thermal gain due to the addition of a flat heat pipe, an experimental characterization of a heat sink with or without a heat pipe was performed under various heating and cooling configuration. The heat sink consisted of copper fins brazed on a 0.16 mm copper plate (figure 2-39 left). A flat plate heat pipe could be included in the system. The heat sink was heated on the upstream side by means of a laser with a varying spot diameter and cooled on the downstream side, either by natural or forced convection. The measured thermal resistance of the system are summarized in figure 2-39 (right), as well as the thermal gain due to the presence of the flat heat pipe. The latter is highest when the heat sink is cooled by forced convection and when the imposed heat flux is the highest. These configurations indeed correspond to those for which the spreading efficiency of the copper plate are the lowest. For other conditions, and especially when natural convection is used with a low imposed heat flux, the heat pipe gain is smaller. The heat is indeed already spread in the copper plate even without any heat pipe, the conductive thermal resistance in the plate being less important compared to the convective thermal resistance between the heat sink and the cooling fluid.

This kind of theoretical study on a very classical type of heat pipe is just an example highlighting the lack of engineering tools helping industries in choosing and designing heat pipes for their specific applications. The role of the research laboratories in the industrials project remains important despite some of the technologies being available for decades. This is mainly due to two important factors: firstly, a heat pipe indeed has often to be designed specifically for a given application, which complicates the manufacturer product catalogue. Secondly, in many sectors, like in transport applications, the industry personnel are not used to heat pipes yet. Hence, the notion specific to heat pipes (evolution of the pressure with the saturation temperature, their non-linear behaviour, their various working limits, their orientation dependent behaviour, etc.) are not well understood and thus become a barrier in their industrial applications. The increasing industrial need for efficient heat transfer devices will probably popularize heat pipes in the future in many different fields (almost every laptop already includes capillary heat pipes) but it will require a strong knowledge transfer from research laboratories and the heat pipe manufacturers to the thermal system designers.

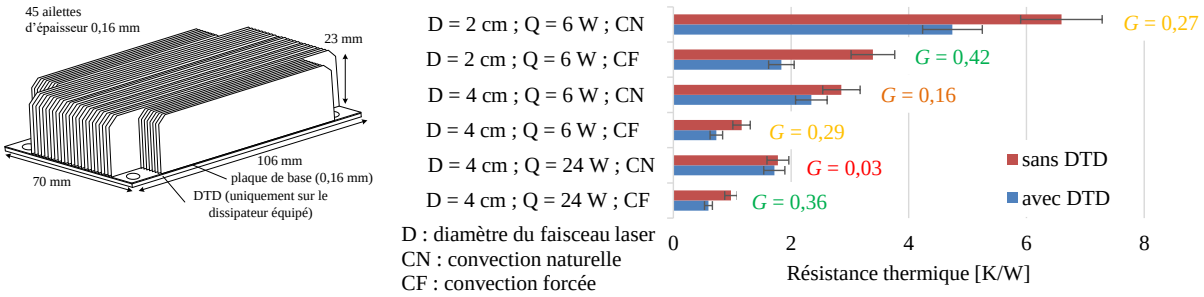

Figure 2-39. Configuration characterized, with and without flat heat pipe (left) and its thermal resistance measured with various heating and cooling conditions (right) (D: heating spot diameter, CN: Natural convection, CF: forced convection, sans DTD: without flat heat pipe, avec DTD: with flat heat pipe) (Lips et al., 2017b)

2.4 When heat pipe scientific issues meet technological issues (or may be the opposite?)

Heat pipe science belongs to the field of applied sciences. Therefore, there is a strong link between the improvement of the manufacturing technologies and the scientific advances, whatever the considered heat pipe technology. In the present section, this reality is firstly highlighted through the example of loop heat pipes. New ideas of heat pipe designs are then presented in section 2.4.2 and the examples of EHD enhanced heat pipes and polymer heat pipes are finally discussed in order to try to foresee what could be the future of heat pipes.

2.4.1 The case of the loop heat pipes

Loop heat pipes are a good example of the need for cooperation between material and heat pipe sciences. Indeed, the evaporator of a LHP can be a very complex component from a technological point of view. It contains the wick of the system, but many thermal, mechanical and chemical constraints have to be respected.

An example of the structure of a cylindrical evaporator is presented on figure 2-40. The primary wick is supplied by liquid through a secondary wick and a bayonet. The system has to be tight and axial and radial heat leaks have to be reduced as much as possible. The secondary wick and the casing have to exhibit a low thermal conductivity whereas the primary wick has to exhibit a high thermal conductivity. Consequently, at least three different materials are often present in an LHP evaporator wick. It leads to several technological issues.

One of the most important constraint when choosing the heat pipe materials is their perfect chemical compatibility with the working fluids. Any small chemical reaction, leading to non-condensable gases, will indeed decrease irremediably the heat pipe performance. Remi Giraudon summarized the compatibility tables proposed by Mishkinis et al. (2010) and Hodot (2015) in table 2-2. It shows that studies on fluid/material compatibilities can be contradictory and the variety of considered materials and working fluids is quite limited. Until now, most of the compatibility tests were realized by the heat pipe research community itself, but cooperation should be performed with chemical research laboratories to get a complete knowledge of the possible interactions between the working fluids and the wick and structural materials (including joining, welding and brazing materials), and maybe to synthetize new working fluids.

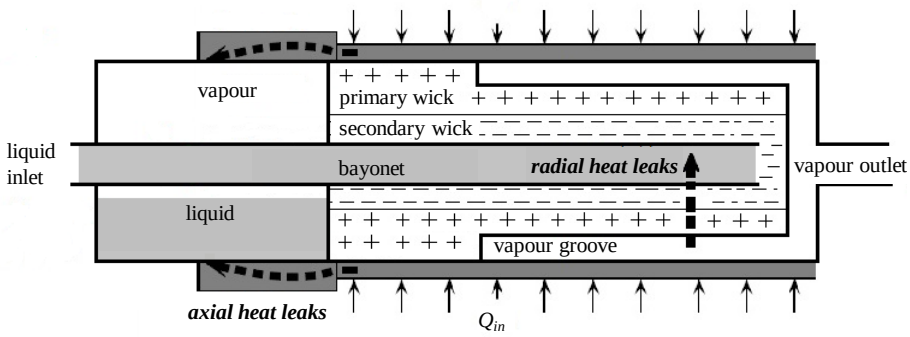

Figure 2-40. Heat leaks in a cylindrical evaporator (Giraudon, 2017) , adapted from (Siedel, 2014))

Table 2-2. Chemical compatibility between various fluids and various materials (Giraudon, 2017)

A , A-	Excellent compatibility	**A**	Excellent compatibility
AB, A, A-	Probable compatibility	**A-**	Probable compatibility
A to B	Conflict between two or more authors	**AB**	Probable incompatibility
AB, B, B+	Probably incompatible	**B+**	Incompatibility for a long period of use and above 125°C
B, B+	Incompatible	**B**	Incompatibility

	Nickel	Hastelloy	Titanium	Copper	SS 316	SS 304	Bronze	Aluminium
Ethanol	**A** [13M] **AB** [23M] **B+** [10H]	**A** [1H, 2H, 5H, 6H]	**A** [5H, 6H]	**A** [5H, 10H, 13M]	**A** [1H, 2H, 4H, 5H, 6H]	**A** [1H, 2H, 5H, 6H, 13M] **A-**[1M, 2M]	**A** [5H, 6H] **B** [1M, 2M]	**A**[1H] **A-**[1H, 5H, 6H] **B** [13M]
Methanol	**A** [7H, 8H, 1M, 13M] **A-**[16H, 2M] **B+** [10H] **B** [9H, 7M]	**A** [2H, 5H, 6H]	**A** [6H] **A-**[2H, 5H]	**A** [8H, 16H, 1M, 2M, 12M, 13M] **A-**[5H, 8M]	**A** [1H, 2H, 4H, 5H, 6H 7H]	**A** [1H, 2H, 5H, 6H, 7H, 13M] **A-**[1M,2M, 10M,18M, 19M] **AB**[14M]	**A** [5H, 6H]	**A** [5H] **A-**[4H, 6H] **B** [8H, 16H, 1M, 2M]
Acetone	**A** [13M] **A-**[16H] **AB** [5M, 24M] **B+** [10H]	**A** [1H, 2H, 5H, 6H]	**A** [2H, 5H, 6H]	**A** [5H, 8H, 16H, 1M, 5M, 12M, 13M]	**A** [2H, 4-7H, 1M, 13M] **A-**[1H, 8H, 16H, 2M]	**A** [2H, 5H, 6H, 7H, 8H, 1M, 13M] **A-**[1H, 16H, 2M] **AB** [18M]	**A** [1H, 5H, 6H]	**A** [4-6H, 8H, 1M, 13M] **A-**[1H, 16H, 2M, 21M] **AB** [18M]
Ammonia	**A** [7H, 8H, 16H]	**A** [1H, 2H, 5H, 6H] **A-**[5H]	**A-**[2H, 6H] **B+**[5H]	**B** [3H, 8H, 16H]	**A** [1H-8H, 16H]	**A** [1H, 3H, 5H-8H, 16H] **A-**[2H]	**B** [1H, 5H, 6H]	**A** [3H, 5H, 7H, 8H, 16H] **A-**[1H, 4H, 6H]
Toluene	**AB** [23M]	**A** [1H, 2H, 5H, 6H]	**A**[2H, 5H, 6H] **A-**[2M]	**A** [5H]	**A** [1H, 2H, 4H-6H]	**A** [1H, 2H, 5H, 6H] **A-**[15M]	**A** [1H, 5H, 6H]	**A** [1H, 4H, 5H, 6H] **A-**[15M]
Water	**A** [7H, 8H, 1M, 13M] **A-**[16H] **AB** [2M] **B+** [15M, 20M] **B** [9H, 7M, 17M]	**A** [1H, 2H, 5H]	**A** [8H, 16H, 1M, 2M, 12M] **A-**[22M] **B** [17M]	**A** [8H, 16H, 1M, 2M, 12M] **A-**[5H]	**A** [1H, 2H, 4H, 5H, 6H, 7H, 13M] **A-**[1M, 2M] **B+** [11M, 16M] **B** [17M]	**A** [1H, 2H, 5H, 6H, 7H, 13M] **A-**[1M, 2M]	**A** [1H, 5H, 6H]	**A** [1H, 5H] **A-**[4H, 6H] **B** [8H, 16H, 1M, 2M, 7M, 13M, 17M]

A reference noted [1M] means that this is the reference [1] coming from the work of Mishkinis *et al.* (2010), and a reference noted [1H] means that this is the reference [1] coming from the work of Hodot (2015). Boo and Chung (2005) used four fluids with a propylene wick. They found that ethanol, methanol and acetone is compatible with the propylène whereas R134a is not.

Another constraint when choosing the various materials of a LHP is the mechanical stress due to the difference of thermal expansion between the materials (figure 2-41). The necessity of a perfect thermal contact between the evaporator and the primary wick indeed requires a good adjustment between the various parts of the evaporator and prevent any mechanical play in between. Once more, cooperation with mechanical research laboratories can be interesting to develop materials, which allow a good thermal contact (i.e. a low interface thermal resistance) with low mechanical stresses.

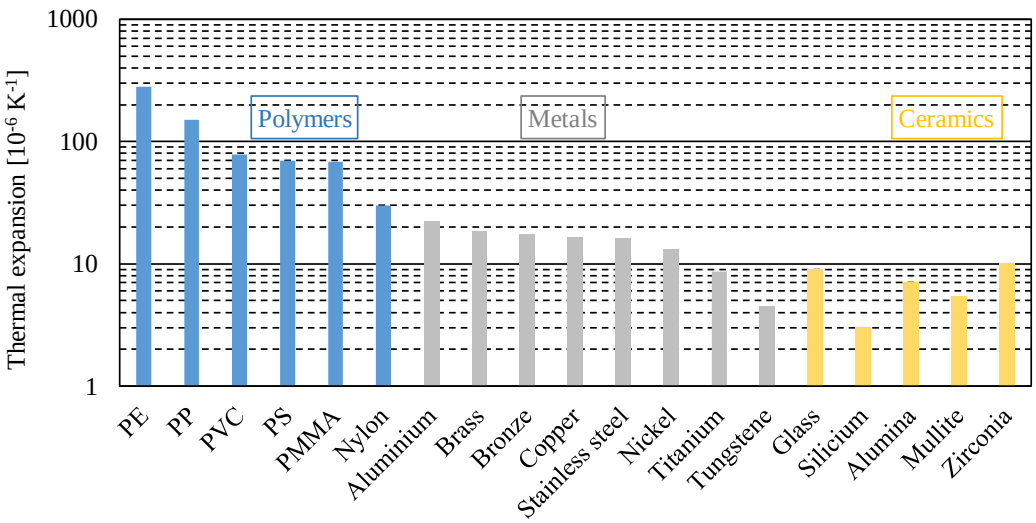

Figure 2-41. Thermal expansion coefficient for various polymers, metals and ceramics (Giraudon, 2017).

Another example of cooperation with a material research laboratory is the 2MATHER Project in which the laboratory MATEIS is involved. During his PhD, Remi Giraudon had to manufacture and characterise himself various wick samples using sintering process (Figure 2-42). It was necessary in order to adjust each manufacturing parameters and to understand the various phenomena affecting the thermal performance of the samples. The collaboration with MATEIS also enabled to imagine alternative manufacturing method, as the freeze casting process, which enables to obtain very interesting properties to the wick (Figure 2-43).

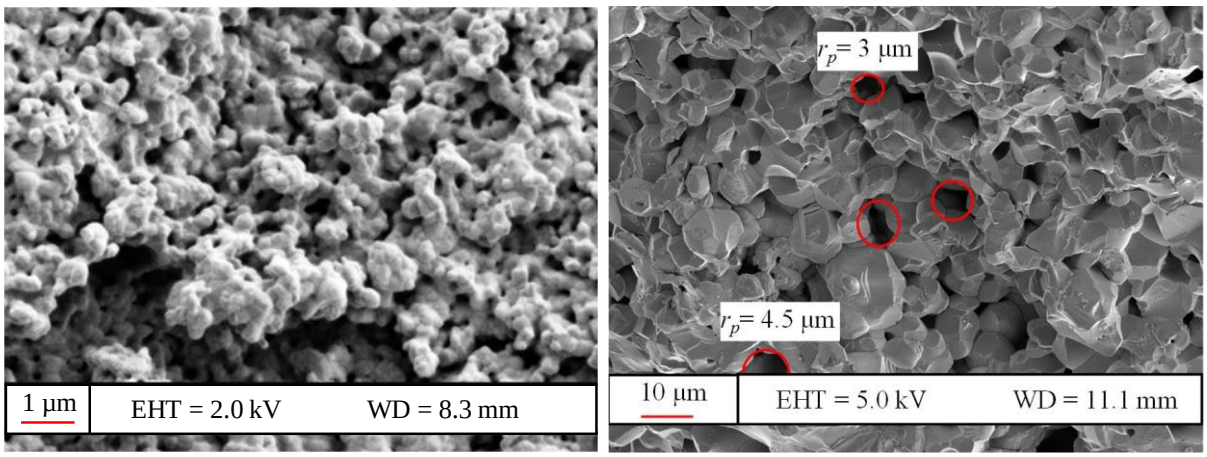

Figure 2-42. SEM pictures of a sintered samples made of zircone (left) and copper (right) (Giraudon, 2017)

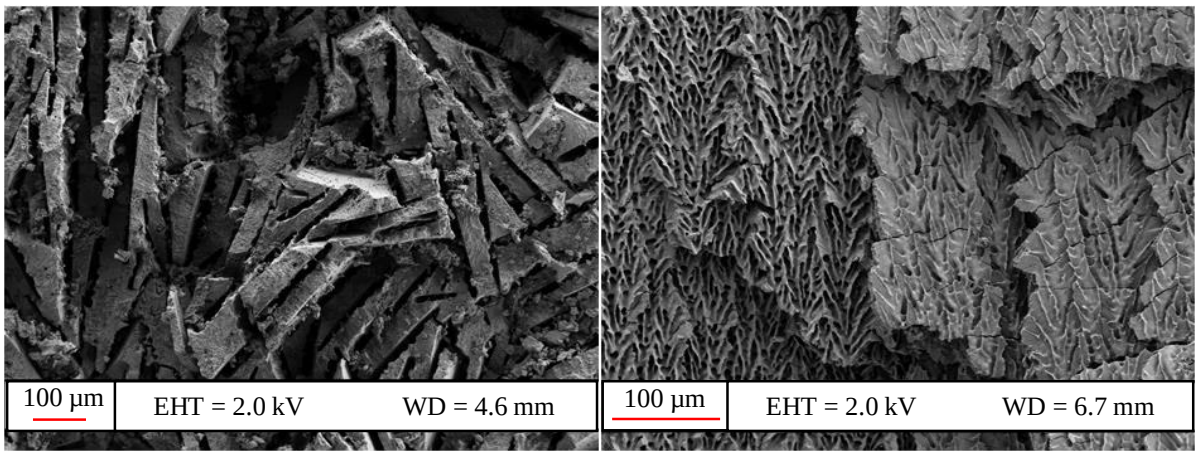

Figure 2-43. SEM pictures of a freeze casted sample: top view (left) and side view (right) (Giraudon, 2017)

As a conclusion, even if CETHIL is focused on thermal sciences, working at the system level requires a good understanding of the various phenomena affecting the heat pipe thermal performance. In heat pipes, it involves chemical, mechanical and material science skills that a single laboratory cannot develop itself. Collaborations with other communities is thus of a great importance in order to achieve a global understanding of the thermal phenomena involved in heat pipes.

2.4.2 Toward new heat pipe designs?

The technology advances in electronics brings new thermal challenges for heat pipes, but other technology advances also enable to conceive innovative designs for heat pipes. In this section two illustrations are presented: a novel thermosiphon configuration, developed as part of the European project I2mpect and patented and a novel configuration of integrated fin heat pipe.

2.4.2.1 Example of development of a confined thermosiphon

The goal of the European I2MPECT project (2015-2018) is to develop an innovating and lightweight electrical power module for aeronautic applications. The CETHIL is in charge of proposing, designing and studying the cooling system. The use of air as cooling fluid, the constraints in terms of mass, space, orientation, heat fluxes and thermal performance required to use two-phase thermal systems. However, classical capillary heat pipes, loop heat pipes and pulsating heat pipes appears not to be suited for the given specifications. We thus proposed a new type of configuration enabling to use the advantage of thermosiphons (simplicity, lightweight, low thermal resistance …) without its drawbacks (locations of the heat sources and heat sinks). It basically consists of a flat confined thermosiphon in which the heat sources are located on one side and the heat sink on the other side (figure 2-44). It can almost be seen as a vertical vapour chamber but the motion of the fluid is provided by both, the gravity and the confinement phenomena. An example of working principle is presented on figure 2-45 with a transparent system. When no heat flux is applied, the level of working fluid does not enable to flood all the evaporator area, which would lead to a dry-out in a non-confined system. When heat flux is applied, the bubble generation enables to wet an important part of the system, enabling to cool down electronic component located almost at the top of the system. During his post-doctoral position, Marine Narcy studied the behaviour of this system and showed that it is surprisingly almost unaffected by the gravity (figure 2-46) or the filling ratio (figure 2-47). Even before any thermal optimization, the system exhibits rather good thermal performance and a good ability to deal with variable heat sources locations. This kind of system was patented (Lips et al., 2017a) but further experiments are still ongoing to fully understand the working principle of such a system and especially the effect of the cavity thickness and the non-heated zones that allow recirculation of the fluid. From a scientific point of view, the study of novel type of system is indeed very interesting because it often involves new couplings between the various phenomena.

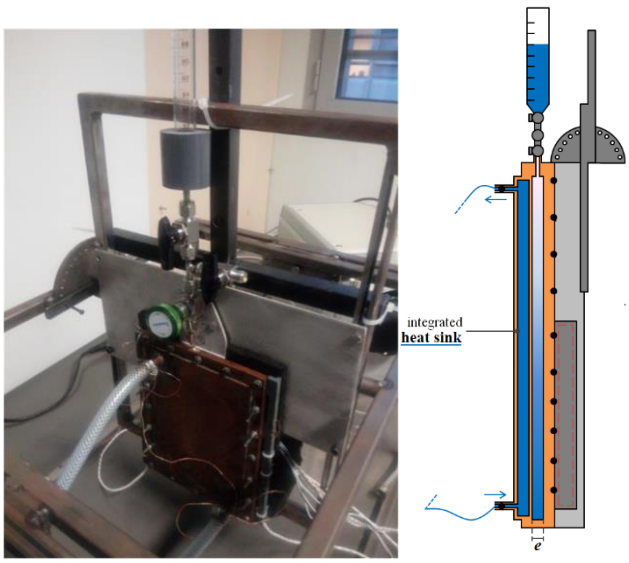

Figure 2-44. Experimental set-up with the confined thermosiphon (Narcy et al., 2017)

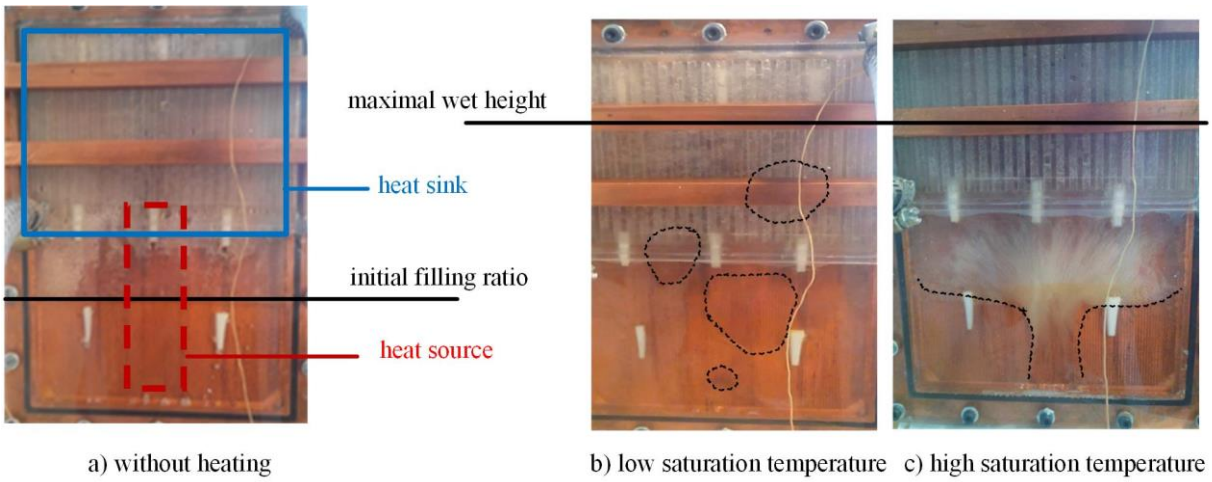

Figure 2-45. Flow visualizations with the transparent heat spreader. Initial filling ratio: 30% of the spreader volume, Q = 500 W in (*b*) and (*c*) (Narcy et al., 2017)

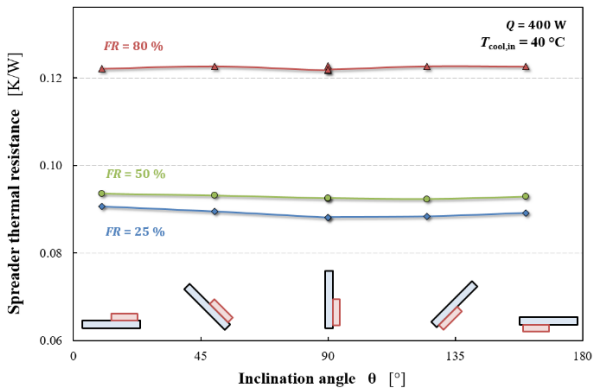

Figure 2-46. Influence of inclination on the heat spreader thermal performance (Narcy et al., 2017)

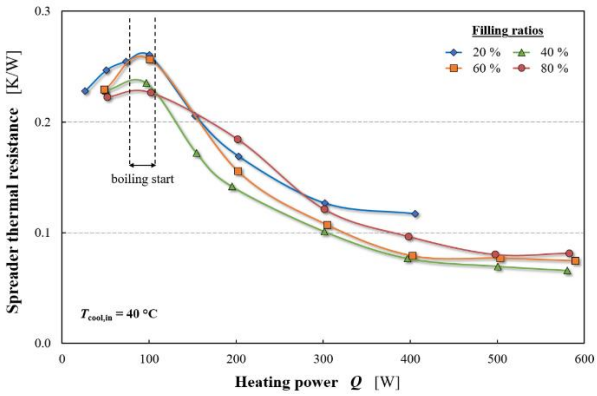

Figure 2-47. Evolution of the spreader thermal resistance for various filling ratios (Narcy et al., 2017)

2.4.2.2 Technological perspectives: experimental study of an integrated fins heat spreader

Another example of innovative configuration is an integrated fins heat spreader. It consists of a vapour chamber, but with a condensation zone made of hollow fins (figure 2-48). This type of configuration may be interesting for plastic heat pipes (see section 2.4.4) in order to avoid fins made of metals, always heavy, when the heat pipe is cooled with natural of forced air convection. This type of configuration has been barely studied in the literature (Michels et al., 2012, 2007) and never with transparent systems.

During her internship, Elise Berut began the experimental study of a prototype made of glass tubes and observed quite a few interesting working regimes depending on the working fluid, the heat flux and the saturation temperature. Film-wise and drop-wise condensation were observed as well as oscillating plug and slug flows. Partial or complete flooding of the tubes could occur depending on the configuration. Further experiments will be performed in the frame of project CAPIT4L, funded by the Institut Carnot Ingénerie @ Lyon and which began in January 2018, to understand the various phenomena occurring in the system and their impact on the system performance.

As a conclusion, confined flat thermosiphons and integrated fins heat spreaders are good examples of systems that may be very interesting for real cooling applications and in the same time that feed the heat pipe research community with new scientific challenges to understand their singular behaviour.

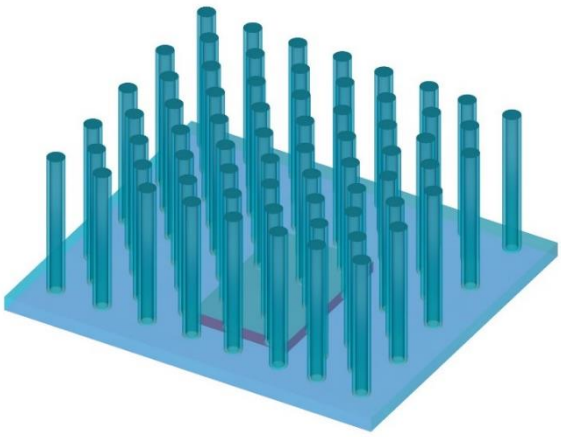

Figure 2-48. Schematic of a two-phase heat spreader with integrated fins

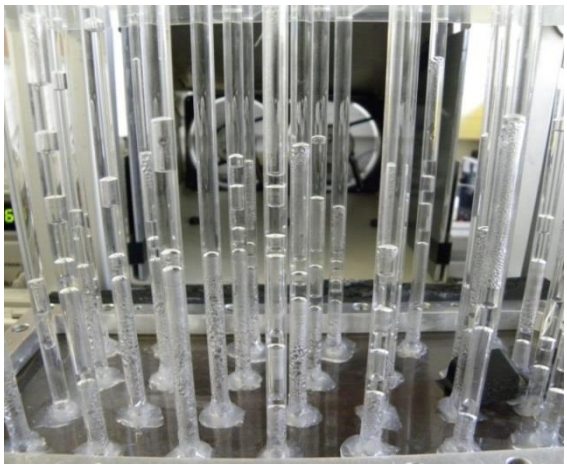

Figure 2-49. Example of condensation pattern in an array of transparent tube (Berut, 2016)

2.4.3 Example of active control of heat pipes: application of EHD forces

Besides new configurations, the continuous technology improvements also enable to gives new perspectives to old ideas. For instance, the utilisation of electric fields for the active control of boiling and condensation phenomena was studied since the beginning of the nineties (Al-Dadah et al., 1992; Cooper, 1990; Damianidis et al., 1990) but very few experimental and theoretical studies were led to evaluate its interest for heat pipes (Bryan and Seyed-Yagoobi, 1997; Suman, 2006; Yu et al., 2002) because of the difficulty to manufacture EHD heat pipe but also because of the lack of computational power.

The democratisation of coating deposition processes and the improvement of the computer performance justified to attempt again a study of the application of EHD forces in heat pipes and motivated the PhD thesis of Nicolas Cardin, started in 2016, funded by the Rhone-Alpes Region and cosupervised by the CETHIL (Jocelyn Bonjour and myself) and by the SIMAP laboratory (Laurent Davoust and Samuel Siedel). Nicolas Cardin is following in parallel both, theoretical and experimental approaches.

The theoretical approach aims at numerically evaluating the effect of the electric field on the meniscus of a grooved flat heat plate. A coupling between a Comsol code, calculating the electric field and the resulting electric stress on the liquid-vapour interface, and a Matlab code, calculating the resulting meniscus shape in the meniscus was developed and used to understand the EHD effect at the scale of a groove. It appears that the electric field was acting essentially at the corner of the grooves (figure 2-50) and increases the maximal pressure jump across the interface that the capillary structure can sustain, i.e. just before the meniscus recession in the groove (figure 2-51). This result can be explained by two phenomena:

- For a given meniscus radius of curvature, the electric field adds an electric stress to the capillary stress and thus increases the pressure jump across the liquid-vapour interface (figure 2-52). This well-known phenomenon is called the electro-pumping effect.
- The intense electric field at the corner changes the curvature of the interface locally. It has very little influence on the global shape of the meniscus but increases the curvature of the interface for a given contact angle between the fluid and the wall. It thus increases the maximum interface curvature, and therefore the maximum pressure jump, before the recession of the meniscus in the groove. The numerical results show that this effect is even dominant compared to the classical electro-pumping effect (figure 2-53).

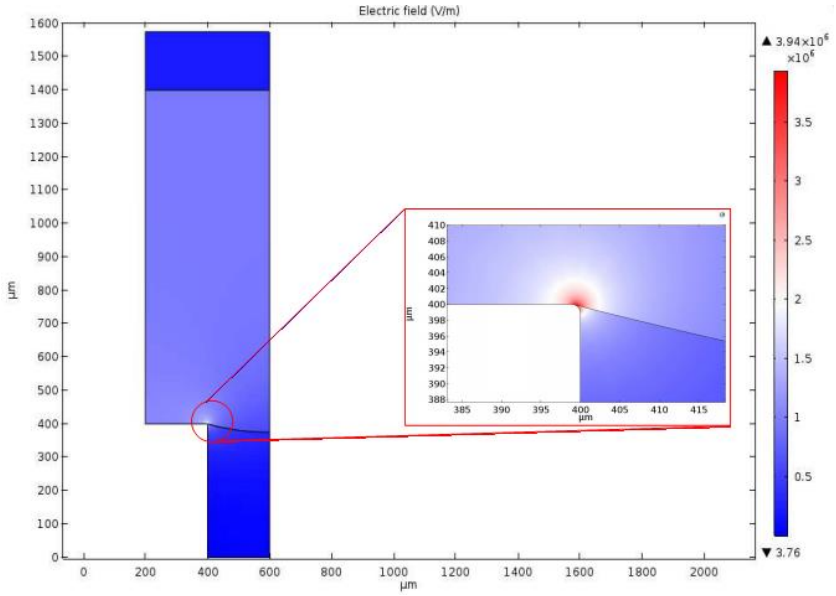

Figure 2-50. Example of the effect of electric field on the interface shape (Cardin et al., 2017)

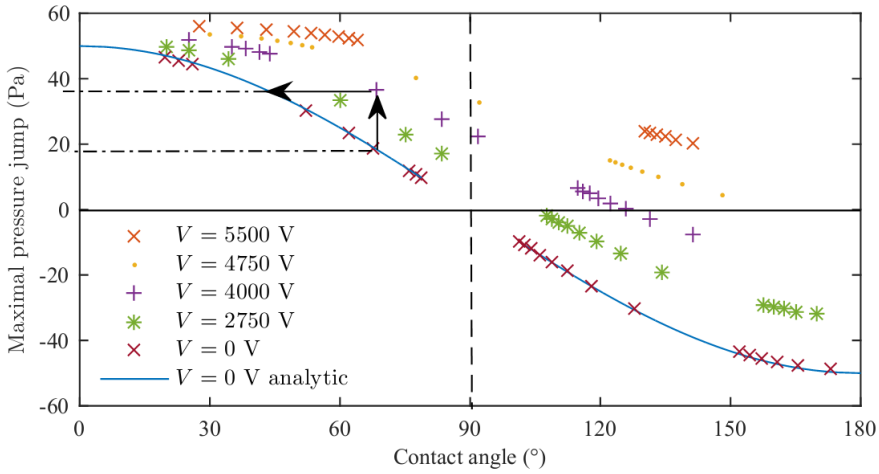

Figure 2-51. Effect of an electric field at meniscus recession for FC-72 (Cardin et al., 2017)

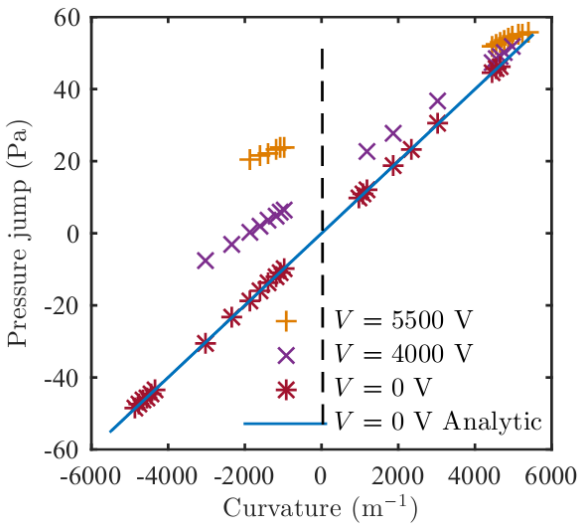

Figure 2-52. Effect of an electric field on the pressure jump for FC-72 (Cardin et al., 2017)

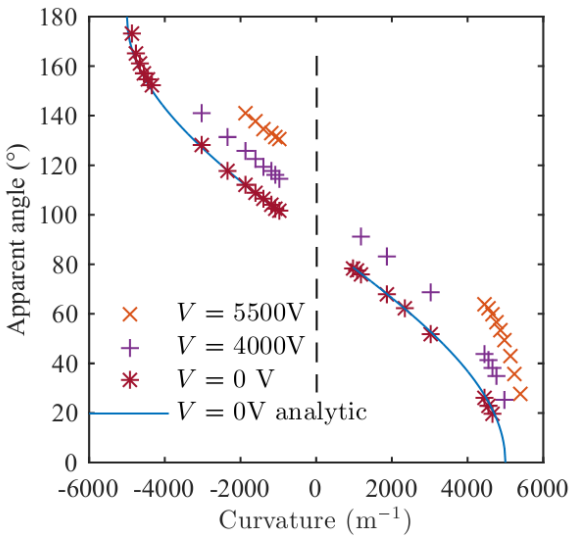

Figure 2-53. Effect of an electric field on the maximal pressure for FC-72 (Cardin et al., 2017)

In order to verify the validity of the numerical mode, Nicolas Cardin designed and built an experimental setup consisting of a sealed cavity made of five grooves (figure 2-54). An ITO layer is coated on a transparent plate, which enables to impose an electric field on the liquid-vapour menisci and to measure the shape of the latter by means of confocal microscopy. The evolution of the menisci curvature along the grooves in tilted configuration were measured with and without electric field for various experimental conditions (inclination angles, filling ratios, shape of the electrode, history of the electric field…). It has been showed that the electric field has a strong effect on the interface in the zone of the electrode, but it surprisingly also affect the menisci in the area not covered by the electrode (figure 2-55). This effect could be due to a recirculation of the fluid owing to a tangential stress generated by the electric field, but more experimental and theoretical works are still required to be able to understand this phenomenon.

The slope of the curvature evolution in the zone of the electrode measured by confocal microscopy and predicted by the numerical model were compared and a good agreement was found even if a high scattering of the experimental data is observed (figure 2-56). However, macroscopic effects on the global organisation of the fluid inside the system were observed experimentally but could not be predicted by the numerical models. Iterations between experiments and modelling are still required to identify all phenomena involved in the studied configuration.

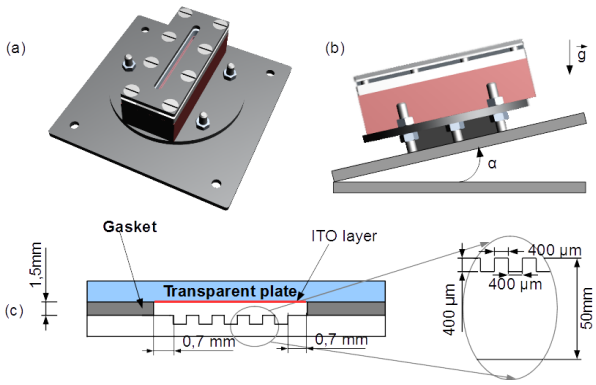

Figure 2-54. Schematic of the experimental set up of Cardin et al. (2018)

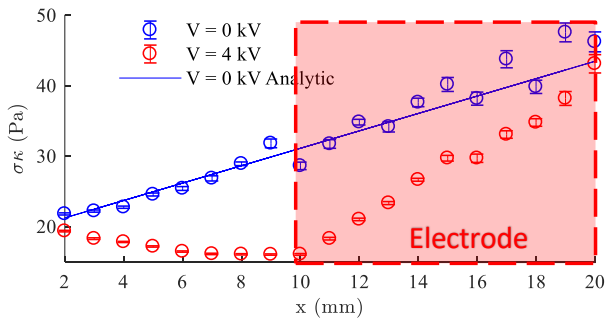

Figure 2-55. Evolution of the hydrostatic pressure drop along central groove an angle of 5° and a partial electrode. The solid blue line represents the analytical solution in the absence of electric field. The blue dots are the experimental results in the absence of electric field, the red dots the experimental results in presence of the electric field (Cardin et al., 2018)

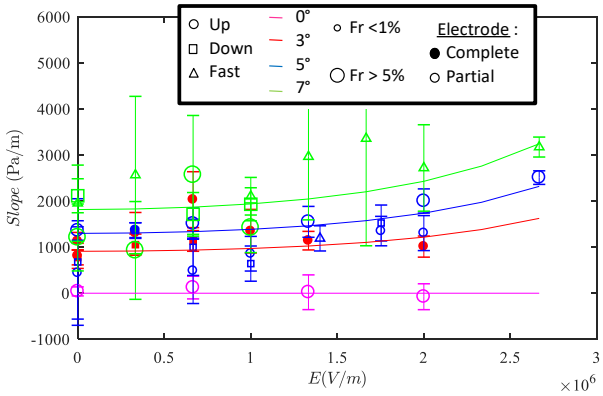

Figure 2-56. Comparison between measurements (marks) and the numerical prediction (solid lines) of the effect of an electric field on the curvature evolution of a meniscus in an inclined groove (Cardin et al., 2018)

In my opinion, this kind of study is very interesting from a scientific and technologic perspective. It brings a new tool to study the phenomena occurring in heat pipe by changing the balance between the various forces involved in the fluid behaviour. If further studies are still required to use the EHD effects in real heat pipe applications, the advance of the electronic technology enables us to dream of high frequency controlled heat pipes, enabling to smoothen the temperature variations of the electronic components during their transient situations.

2.4.4 Plastic heat pipe: expectations and limits

If heat pipe active control solutions are very interesting from a technology point of view, the most important industrial need lies in lightweight thermal solutions. Sometimes, heat pipes help to reduce the weight of the cooling systems but they remain quite heavy compared to the system that need to be cooled. Heat pipes are indeed made of metal, and most of them are made of copper. Aluminium heat pipes are currently mainly used for spatial applications as the need to use ammonia as the working fluid is a major drawback for transport applications. A real technology breakthrough can come from heat pipes made of plastics. The idea is old but the manufacturing of a reliable plastic heat pipe is not yet achievable because of two major issues: the low thermal conductivity of polymers and their high permeability.

The spectacular progresses in the last decade in polymer sciences may enable to overcome these issues in a close future and the heat pipe research community start to study plastic heat pipes for a couple of years. At CETHIL, I cosupervised with Mhamed Boutaous (head of the CETHIL research group on heat transfer in polymers and composites), two internships funded by the CETHIL as an interdisciplinary research. Their goal was to evaluate the feasibility of polymer heat pipes. From a scientific point of view, polymer heat pipes bring new challenges, as evaporation and condensation on non-wetting surfaces and they would enable completely innovative geometries.

Elise Berut performed in 2016 an extensive literature review on heat pipes made of polymers and of the technological and scientific issues that still have to be overcome. Table 2-3 summarizes the recent studies dedicated to heat pipes made of polymer. Several types of polymers were tested, all of them having some advantages and drawbacks. To fulfil the heat pipe requirements, the polymer should exhibit a good mechanical resistance, good barrier properties, a good chemical and thermal stability and most importantly a not to low thermal conductivity. Amongst the various polymer families, two of them are particularly of interest: the LCP (Liquid Crystal Polymer) and the PET (PolyEthylene Terephtalate).

Table 2-3. Summary of the studies dedicated to heat pipes made of polymer (Berut, 2016)

Auteur	Type	Orientation	Polymère(s)	Fluide	Refroidissement	R (K/W)	λ (W/mK)	Rapport Ref	Flux (W/cm² – W)
Oshman (2009)	FHP	H	LCP	eau	eau	-	850	21 (vide)	3,0 – 3,0
Oshman (2011)	FHP	H	LCP	eau	eau	-	830	2 (Cu)	11,94 – 11,94
Oshman (2012)	FHP	H	LCP	eau	eau à 10°C	-	1653	3 (Cu)	62,5 – 40
Shi (2015)	FHP	H	LCP	eau, acétone	air ambiant	1,02	-	4,5 (Cu)	4,58 – 10,3
Wang (2003)	-	-	LCP	-	-	-	-	-	-
Hilderbrand (2007)	FHP	H	PE	eau	eau	1,04	-	-	? – 5
Oshman (2013)	FHP	H	PET, PE	eau	eau à 10°C	1,2	-	3,8 (Cu)	2,88 – 25
Wu (2012)	FHP	H	PET	méthanol	air à 25°C	0,157	13 261	-	? – 26
Chen (2013)	FHP	H	PET	méthanol	air à 25°C	0,146	18 310	-	? – 26
Wu (2012)	FHP	H	PET	méthanol	air à 25°C	0,146	-	-	? – 26
Ogata (2014)	PHP	H	PET	hydrofluoroether	eau	8	-	1,2 (Cu)	? – 7
Ogata (2014)	PHP	H	Résine polymère, PET	hydrofluoroether	eau	10,10	-	0,9 (Cu)	? – 4,11
Oshman (2012)	FHP	H	PET, PI Kapton, tout polymère	eau	air	1,6 1,5 5,1	-	12,5 (vide) 2,3 (Cu) -	- - ? – 20
Tanaka (2009)	Cyl.	V+	PI	eau, butanol, heptanol	eau	-	-	-	-
Lewis (2015)	FHP	H	PI Kapton	eau	eau à 22°C	4,08	-	3,0 (Cu)	5 – 8
Lewis (2015)	FHP	H	PI Kapton	eau	-	11,92	541	1,4 (Cu)	4,77 – 9,54
Ji (2013)	PHP	V+	MQ PDMS	éthanol, Al2O3/éthanol	eau à 40°C	2,56 2,46	-	-	0,65 – 20 0,65 – 20
Lin (2009)	PHP	V+	MQ PDMS	méthanol	eau à 15°C	8	-	-	? – 8

Hsieh (2013)	FHP	H	Q	eau	eau à 15°C	6	-	-	12,7 – 12,7
Yang (2014)	Cyl.	V+	PU	eau	eau à 15°C	0,008	-	1000 (Cu)	0,7 – 12
Yang (2016)	FHP	H	FKM	eau	eau à 10°C	0,09	-	-	0,64 – 12
Yang (2015)	FHP	V-	FR4	eau	eau à 5°C	3,84	-	-	? – 16
Ye (2014)	LHP	H	polymère acrylique	éthanol	-	-	-	-	-
Wits (2006)	FHP	H V+	Multicouches PCB	eau	-	1,4 1,0	3080 4430	-	? – 10 ? – 10
Liu (2003)	Cône	V+	Résine photo-durcissable	isopropanol	air ambiant	-	-	-	4,0 – ?
Liu (2002)	Cône	V-	Résine photo-durcissable	isopropanol	air ambiant	-	20 000	-	-

The LCP have very good properties but are complicated to manufacture and to shape. As a consequence, Elise chose to manufacture various thermosiphon made of PET (figure 2-57). This first experimental study enabled to quantify the contribution of the various thermal resistance in the system (figure 2-58) and to identify the main technical issues. She concluded that the relatively low thermal conductivity of the PET (~ 0.2 W/mK) was not a major issue depending on the heat pipe configuration, but an important effort have to be put on the PET shaping in order to have a perfectly tight heat pipe.

During his internship, realized in 2017, Charles-Emmanuel Bronstein focused on the industrial polymer processes. He highlighted the main advantage and drawback of each technology and concluded that the twin-forming technology, which coupled an extrusion process to a blow molding process, would probably the best suited to realize polymer heat pipes at an industrial level. However, this kind of processes requires important investments and do not seem affordable for preliminary research programs.

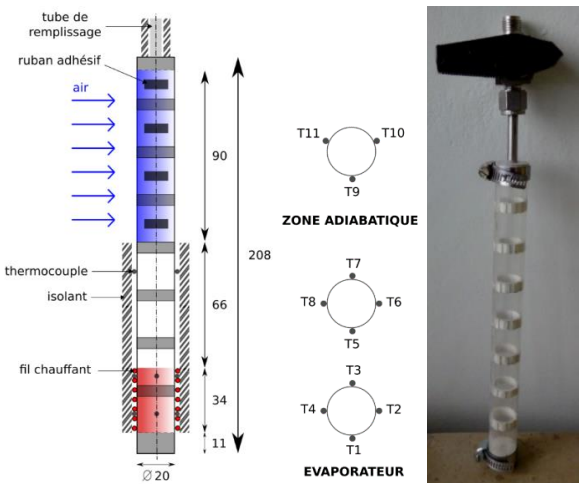

Figure 2-57. Example of prototype manufactured by Elise Berut (Berut, 2016)

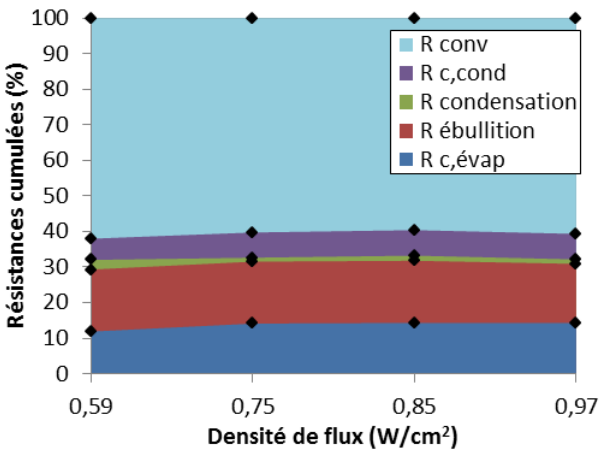

Figure 2-58. Example of contribution of the various thermal resistance of the system (conv: convection ; c,cond: conduction at the condenser ; c,évap: conduction at the evaporator) (Berut, 2016)

These two internships enabled to have a good overview of the state of the art of polymer heat pipes and to understand the related technological challenges. Even if the primary goal of the CETHIL is not to assess this type of issue, it was a necessary step to conceive an adequate research strategy. Thanks to letters of intention of various industrial partners and to the discussions with IPC (technical centers for polymer and composite innovations), we manage to fund with Valérie Sartre a two years research project by the Institut Carnot I@L. The project CAPIT4L started in January 2018 and aims at manufacturing a functional prototype of polymer heat pipe. The goal of IPC will be to assess the shaping of the polymer whereas the CETHIL will focus on his real centre of interest: the study of two-phase heat transfer, in this case in a non-wettable wall and in a confined configuration. The different working regime and the coupling between the various phenomena will be studied in order to understand the global behaviour of this type of system.

2.5 Conclusions and perspectives

The literature review presented at the beginning of this chapter enables to list the significant advances that have been achieved by the heat pipe scientific community during the past years:

- The understanding of evaporation and condensation phenomena on a capillary scale has been improved, thanks mainly to new systems of visualisation and instrumentation.

- New fluids and new materials have been successfully tested and enabled to increase the performance of heat pipes.

- Major progress in the understanding of LHPs have now enabled to develop this technology at an industrial scale. The models are now able to predict the experiments satisfactorily even if improvements could still be achieved in the prediction of transient behaviour and thermal resistances involved in the systems. From a technological point of view, new geometries and types of capillary structure have also been proposed (bi-porous wick, multi-layer wick, ceramic wick …). A new challenge is now the miniaturisation of the systems.

- The more impressive advances are probably related to the PHPs. Ten years ago, even the main phenomena were not well identified. Models are now almost able to reflect their chaotic behaviour and reliable predictive tools can be expected in the coming few years.

Since 2006, I also tried to contribute to the improvement of the heat pipe scientific knowledge through the various projects in which I was involved. However, several scientific questions still need to be answered. Amongst them, we can list:

- The predictive tools strongly depend on the capillary structure properties and on the heat transfer coefficient during condensation and evaporation. Limited progress has been realized in developing satisfactory models or correlations, even for simple geometries.

- Several phenomena still have to be better understood to be correctly taken into account in the models. Boiling in the capillary structure of a flat heat pipe and coalescence and break-up of liquid slugs and vapour plugs in pulsating heat pipes are only two examples.

- The evaporation and condensation processes involving thin liquid films are not yet fully understood, and especially the influence of the wall properties on these phenomena. If the case of fully wetting fluids is supported by some theoretical backgrounds, partial wetting, which is present in real engineering systems, still needs to be understood.

To answer these questions, more studies are required. First of all, experimental studies with visualization are essential because of the need to understand the coupling between the different phenomena involved in these systems. The lack of experimental data is even more acute for the phenomena that act on the micro-scale. For instance, without the knowledge of the accommodation coefficient, the thermal models of phase change heat transfer at the triple contact line cannot be validated. The real mechanisms leading to the onset of nucleate boiling are also not yet fully understood and it strongly limits the predictability of the numerical models as they almost always need to be fitted with experimental data. Besides this, there is a lack of reliable convective condensation models at low flow rates, able to predict the heat transfer coefficients in small and bended tubes such as the LHP condensers. Another challenge will be to couple these microscale models to the system scale models. This difficulty comes partially from the fact that the physical, topological and chemical properties of the materials are often poorly known. To answer this issue, more interactions should be created between the heat pipe research community and the material science research community.

One can also expect that the progresses in other research fields will bring new tools enabling to improve the current systems. For instance, the progress in high frequency micro-electronics opens the way for active control of heat pipes and the continuous development of new materials awake hopes of real flexible and lightweight heat pipes, if the current problems of fluid/material compatibility on plastic heat pipes are solved. Anyway, one can conclude that the study of heat pipes will remain a challenging and exciting topic at least for the next couple of decades.

Chapter 3: Active cooling systems: convective boiling and condensation

When passive systems, as heat pipes, cannot be used for various reasons, active two-phase flow cooling systems can be of a great interest. They enable a very efficient and controllable cooling of the electronic components. However, the design of these systems is of great importance, from the viewpoint of both, pressure drops and heat transfer coefficient. The former will directly affect the electrical consumption of the pump or compressor used to generate the flow. The latter affects both the temperature of the heat sink that need to be used to maintain the electronic component temperature, and the size of the system, which is of great importance for confined configurations, as encountered in automotive or mobile applications, for instance.

My personal research on this field comes from the post-doctoral project I led in the University of Pretoria in South Africa, and on the PhD thesis of Thibaut Layssac, defended in February 2018, and that of Samuel Martel, still ongoing and co-supervised by Remi Revellin. We are mainly interested in the characterization of two-phase flows in inclined configurations, which is a tool to understand the balance between the various forces acting on the system. In the present chapter, a brief scientific context is firstly proposed. The experimental test-benches I had the opportunity to work with are then described and the experimental results are finally presented and discussed.

3.1 Scientific context

The difficulty of studying two-phase flows lies in their complex structure, which strongly depends on the experimental conditions. As a consequence, two-phase flows characteristics are often determined for a given fluid, in a given channel geometry (shape, inclination, dimensions…) and for a given set of mass velocity, vapour quality and saturation temperature. The scientific community mainly follows two approaches to achieve a better understanding of this kind of flows:

- The experimental approach consists in characterizing the flows in various conditions. In a first step, the various phenomena are firstly identified and in a second step, important databases are built in order to collect a maximum of information in order to help the development of models.
- The modelling approach consists in building analytical or numerical models trying to predict the flow characteristics by taking into account the most influencing phenomena.

My research on two-phase flows tries to be in between these two approaches: I mainly conduct experimental works, but more aiming at identifying the weight between the various phenomena than to build important and exhaustive databases. I use very simplified models to verify the experimental conclusions but I never tried to build complex and fully predictive numerical tools, which is completely out of my skills.

The present section does not aim at being an exhaustive state of the art of the two-phase flow studies available in the literature but rather aims at bringing a simple overview of the various phenomena involved in two-phase flows. It should help to understand the general scientific context of the various aspects addressed in the other sections of the present chapter.

3.1.1 General description of two-phase flows

Two-phase flow are generally characterised firstly by their flow pattern. The structure of this kind of flow being complex, discriminating the various flow patterns that can be encountered help to simplify the scientific analysis. To do so, transparent experimental set-ups are designed by the research community and flow pattern maps are drawn by the authors. Figure 3-1 presents an example of flow pattern map proposed by Wojtan et al. (2005). This type of studies are very useful for the community but remains valid only for one specific fluid in a specific geometry and in a given experimental condition. Contrarily to monophasic flows, two-phase flows cannot be fully described by non-dimensional numbers yet, which limits the possibility to generalise or extrapolate the conclusions of the various authors. A flow pattern map like that of Wojtan et al. (2005) can even be subjected to discussions because the definition of the flow patterns themselves are not rigorous and depends on subjective choices of the authors. A given author can even change the way of defining the various flow patterns between two articles. For instance, I personally defined five flow patterns visually during my postdoc in the University of Pretoria (figure 3-2) whereas Thibaut Layssac, who performed his PhD under the supervision of Remi Revellin and myself, use quantitative indicators to delimit only three flow patterns (figure 3-3). However, even with quantitative indicators, the chosen threshold values remain subjective.

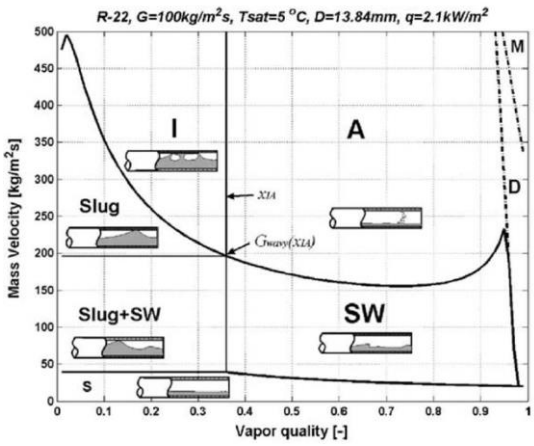

Figure 3-1. Flow pattern map of Wojtan et al. (2005)

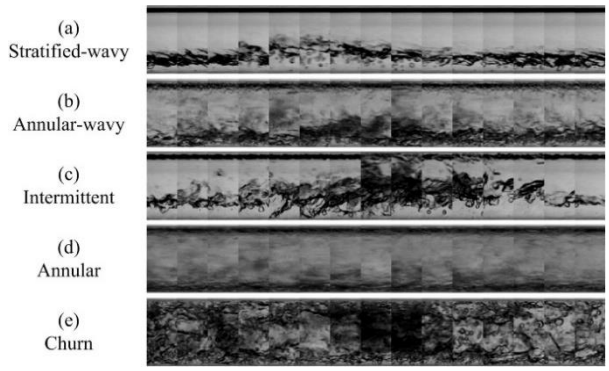

Figure 3-2. The different types of flow patterns considered in the study of Lips and Meyer (2012a). Discrimination were performed only visually

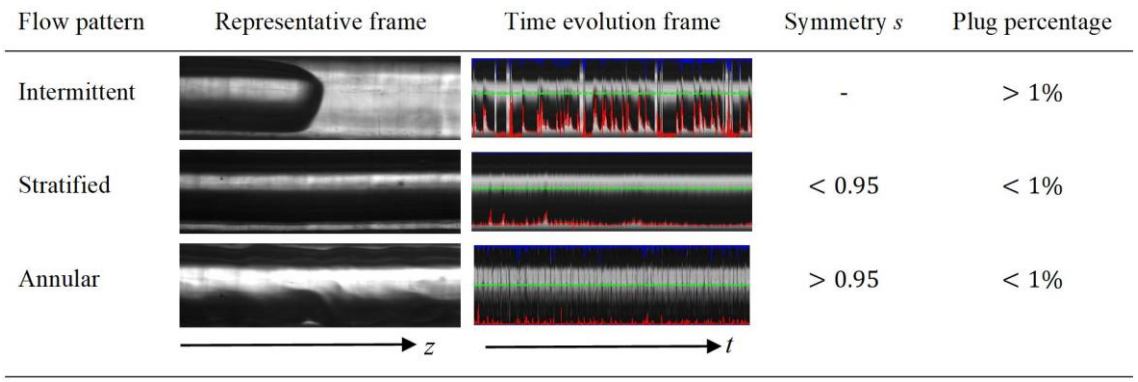

Figure 3-3. Flow patterns considered by Layssac et al. in his PhD (2018a). The determination of the top and bottom liquid thicknesses enables to use quantitative indicators

In the literature, some authors have tried to propose fully objective criterion, like probabilistic flow pattern maps (van Rooyen et al., 2010), but one must admit that the complexity of these tools strongly limit their utilisation by the other authors. The discrepancy between the definition of the various flow patterns can be a problem when trying to build predictive tools (correlations or simplified models), but actually does not affect so much the quality of the scientific results from a phenomenological point of view. When we are interested in experimental conditions corresponding to a well-defined flow pattern, for instance stratified flow presented in figure 3-4 and considered by Taitel and Dukler (1976), we actually consider an ideal model enabling to predict the trends of the evolution of the various flow characteristics as a function of the flow conditions. When we considered boundaries between two flow patterns, the limits are, by definition, blurred and subjective, and the interest of the studies actually lies in the balance between the various phenomena, which can dominate each flow patterns separately, but are affected by other parameters in the transition zone. For instance, to understand the transition from stratified to annular flow regimes, one must consider, amongst others, the pumping action of the disturbance waves (figure 3-5), that have almost no influence in each flow regimes separately.

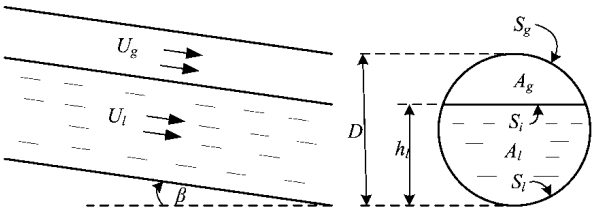

Figure 3-4. Geometry considered by Taitel and Dukler (1976) for stratified flow

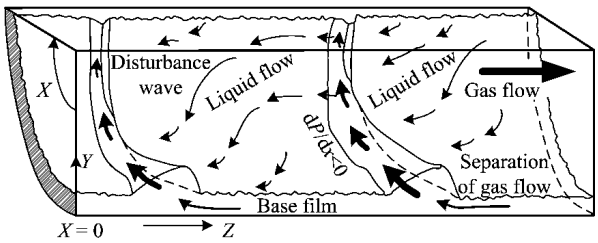

Figure 3-5. Pumping action of the disturbance waves, adapted from Fukano and Ousaka (1989)

This example illustrates my personal way of considering experimental research in two-phase flows. The coupling between these two types of studies (ideal models and transition analyses) enables to get a global overview of the behaviour of two-phase flows. I strongly believe that in a near future, the numerical tools will enable the development of predictive simulations, thanks to both the increasing computer performance and the increasing understanding of the various phenomena. Nowadays, the researchers in the field of CFD manage to simulate quite complex two-phase flows with no phase change (bubbly flows with coalescence and with strong interfacial interactions, for example) and begun to have interesting results when including phase-change. In the recent years, they improved the quality of the simulations in simple geometries but with strongly coupled phenomena (see example of a single growing bubble in a subcooled convective flow in figure 3-6) and start to be able to model more complex flows (see the example of boiling on a heated surface presented on figure 3-7). As a consequence, I consider my own contributions to the two-phase flows scientific community as a way to feed this type of models, both with experimental data and with experimental conclusions highlighting the major phenomena that need to be taken into account to achieve predictive and robust tools in the future.

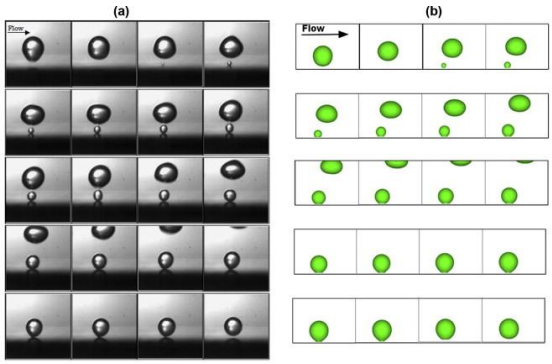

Figure 3-6. Example of comparison between experiments and simulations of a growing bubble in a subcooled convective flow (Lal et al., 2015)

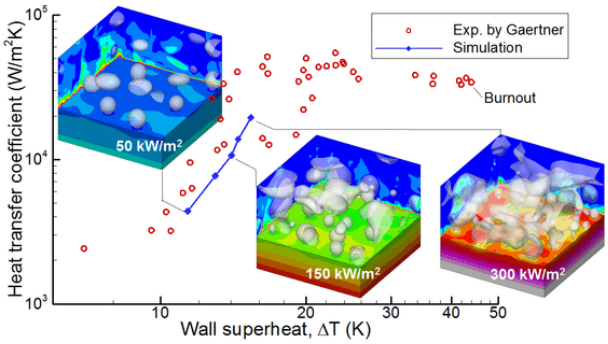

Figure 3-7. Example of boiling modelling taking into account the bubble merging (Sato and Niceno, 2017)

3.1.2 Characterisation techniques for two-phase flows

The major challenge in experimental study is to acquire the pertinent information enabling to characterise the flow. If the measurement of the pressure drop is not really a problem as long as a high-speed acquisition system is available; the flow visualization and the acquisition of the heat transfer coefficient require more material and skills. In order to visualize the flow, the authors usually use a transparent section at the outlet of the real test section on which the heat flux is applied. The relevance of this technic is however discussed in the literature, as it does not enable to visualise the flow directly where the heat flux is applied. To overcome this issue, some authors implement fully transparent test sections, like Narcy et al. (2014), who used an ITO coating to study the effect of the bubble nucleation on a convective boiling flow in microgravity (figure 3-8). The use of an ITO coating also enables to perform IR visualization to measure the temperature field. Other technics, as the utilisation of temperature sensitive liquid crystals enable to have a simultaneous visualisation of the flow configuration and the temperature field (see example on figure 3-13).

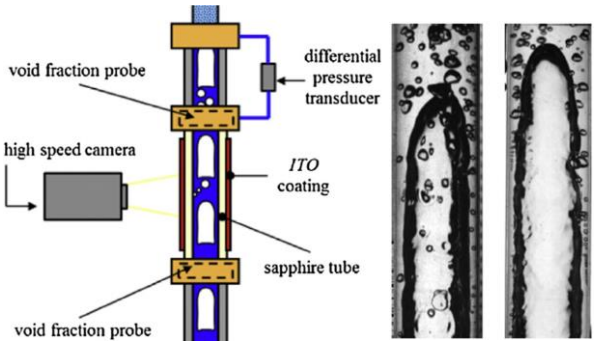

Figure 3-8 Example of heated transparent test section by means of an ITO coating (Narcy et al., 2014)

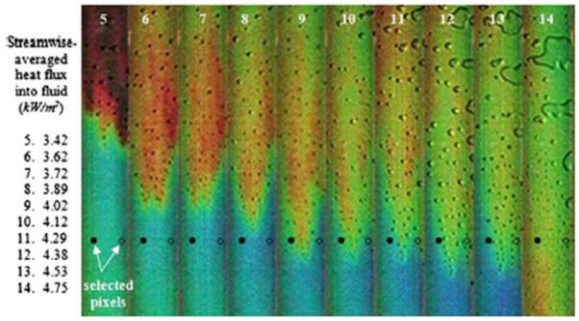

Figure 3-9 Superposition of IR and visible images of a saturated R11 flow for increasing heat fluxes (Ozer et al., 2011)

Fluorescence and phosphorescence techniques can also be used, as the Laser Induced Fluorescence (LIF), for instance, in order to improve the visualization of the two phases of the flow (Figure 3-10), which enables a quantitative and high speed characterisation of the liquid film thickness (Figure 3-11). During his PhD, Samuel Martel, co-supervised by Remi Revellin and myself, performed an intensive literature survey of these techniques for the characterization of two-phase flows (Martel et al., 2018). He concluded that few studies manage to characterise two-phase flows (see Table 3-1), but the use of Molecular Tagging Velocimetry (MTV) could be of a great interest if the experimental constraints associated to the fluorescence phenomena can be addressed.

However, this kind of setup requires synchronisation between lasers and high speed IR and visible cameras, which represents an important investment for the research laboratories. Strong skills in calibration processes and inverse methods are also required to determine accurately the heat transfer coefficient between the internal wall and the fluid. As a consequence, few international research teams are able to provide this kind of information and their outcome is always interesting. In the phase-change research group of the CETHIL, we collectively aim at developing this kind of skills and I try to bring my own contribution to the global effort by focusing on the development of innovative and ambitious experimental set-ups.

Figure 3-10 Example of liquid film LIF visualization (Schubring et al., 2010)

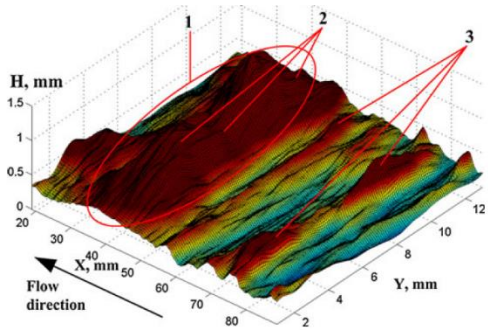

Figure 3-11 Three-dimensional wavy structure for entrainment regimes (Alekseenko et al., 2012)

Table 3-1. Applications of fluorescence and phosphorescence techniques for the two-phase flow characterisation (Martel et al., 2018)

Authors	Technique	Configuration	Measured value	Tracer dye
Ritchie (2006)	LIF	Mixing two-phase sprays	Mixture fraction, droplet size	Acetone + RhB
Castanet et al. (2007)	LIF (two emission bands)	Vaporizing acetone droplets	Mean droplet temperature	Acetone + RhB
Tran (2008)	LIF and LIP	Supercritical multiphase flow	Liquid-vapour interface	Acetone
Frackowiak et al. (2009)	LIF	Monodisperse flow	Liquid-vapour interface, vapour mole fraction	Acetone
Charogiannis and Beyrau (2013)	LIP	Evaporating acetone droplets stream	Liquid-vapour interface	Acetone
Fogg et al. (2009)	DELIF	Liquid-air homogeneous flow	Fluid temperature and void fraction	RhB + Rh110
Schubring et al. (2010)	LIF	Vertical upward air-water annular flow	Film thickness through longitudinal visualisation	RhB
Milan (2012)	LIF	Vertical downward air-water annular flow	Film thickness and void fraction through section visualisation	Rh6G
Farias et al. (2012)	LIF	Annular air-water flow	Film thickness and void fraction through section and longitudinal visualisation	RhB
Alekseenko et al. (2005)	LIF	Vertical downward gas-liquide annular flow	Film thickness	Rh6G
Alekseenko et al. (2012)	LIF	Vertical downward gas-liquide annular flow	Film thickness	Rh6G
Hosokawa et al. (2009)	MTV	Squared duct bubbly flow	Velocity gradient	Fluorescein

3.1.3 Force balance in two-phase flows: effect of tube inclination

The strength of an experimental study compared to a numerical one is to be able to adapt the flow conditions easily, without being affected by the change of flow pattern. A numerical model is indeed often dedicated to a specific kind of flow and is difficult to adapt to other flows with different dominating phenomena. On the other hand, an experimental study is often limited in terms of number of test section geometries and of fluid properties, which limit the range of experimental conditions that can be tested. Other ways to study the balance between the various phenomena thus have to be found. During my postdoctoral position in the University of Pretoria in 2011, I found surprisingly very few studies using the change of inclination angle as a tool to understand the physic of two-phase flows. As a consequence, I choose this method to explore new experimental conditions, for which we expected to have different force balances than in horizontal and vertical orientations.

With Josua Meyer, we proposed a literature review that considered studies dealing with inclined two-phase flows, in terms of flow pattern maps, void fractions, heat transfer coefficients and pressure drops (Lips and Meyer, 2011a). More recent studies were proposed and enable to have a better idea of the inclination effect, but there is still a huge need of experimental and theoretical studies.

In terms of flow patterns, Weisman and Kang (1981) experimentally studied the effect of the inclination on the flow pattern transitions in the case of a R113 saturated flow. The tests were realised for upward flows in channels of 25 mm and 38 mm inner diameter and were completed by the study of Crawford et al. (1985) for downward flows. These studied enabled to develop an empirical model predicting the flow patterns for the whole range of inclination. In diabatic configuration, the studies of Bhagwat and Ghajar (2017, 2016a) and Mohseni and Akhavan-Behabadi (2014) were published more recently. Bhagwat and Ghajar (2017, 2016a) presented a study about heated air-water flow pattern transitions in a 12.7 mm inner diameter channel. As an example, the effect of the inclination angle on the flow pattern map is presented on Figure 3-12 and on Figure 3-13 for upward and downward flows respectively.

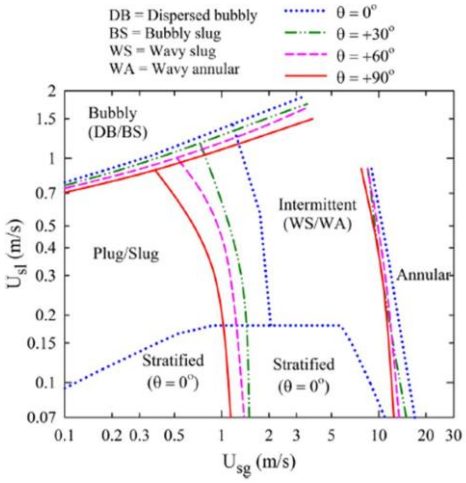

Figure 3-12. Flow pattern amp of Bhagwat et Ghajar (2016b) for upward air-water flow in a 12,7 mm inner diameter smooth tube

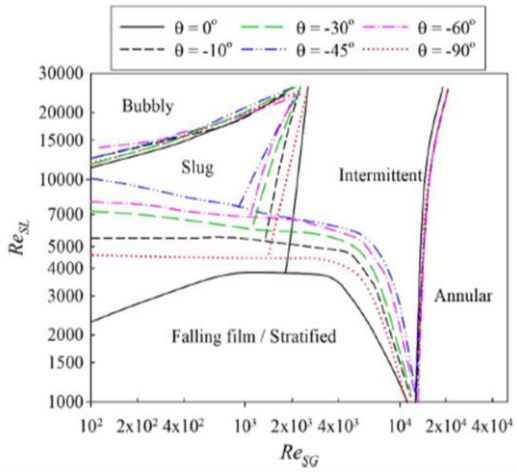

Figure 3-13. Flow pattern amp of Bhagwat et Ghajar (2017) for downward air-water flow in a 12,7 mm inner diameter smooth tube

Like the flow pattern transitions, the effect of the flow parameters on the pressure drops was largely investigated in horizontal and vertical orientations. However, few studies dealing with the role of the gravity force orientation on the pressure drops are available in the literature, but all of them highlight the strong influence of the inclination angle, at least for low-inertia two-phase flows. An example of the evolution of the pressure drop as a function of the inclination angle is presented on figure 3-14 (Spedding et al., 1982). However, there is a lack of diversity in the literature configurations, especially in terms of confinement, and no general conclusion can be drawn yet.

In terms of heat transfer, many studies available in the literature deal with the effect of the experimental conditions on the heat transfer in the cases of heated air-water flows, convective condensation or flow boiling. However, the large majority of these studies were carried out for horizontal or vertical flows. Moreover, the few studies dealing with the effect of the inclination on the heat transfer before 2011 were

focusing on a small range of angles, generally near the horizontal orientation. The studies of Ghajar and Kim (2005), Ghajar and Tang (2007), but also the one from Vaze and Banerjee (2011), were realised with air-water flows in horizontal and upward flows with inclination angles of 2°, 5° and 7° in a 27.9 mm inner diameter channel. All these studies show a very strong dependency of the heat transfer coefficient with the inclination angle. Since 2011, an intensification of the studies in both convective condensation and flow boiling under inclined configurations can be noticed. An example of evolution of the heat transfer coefficient as a function of the tube inclination is given in figure 3-15 for convective boiling of HFE 7100 in a 0.44 mm inner diameter channel.

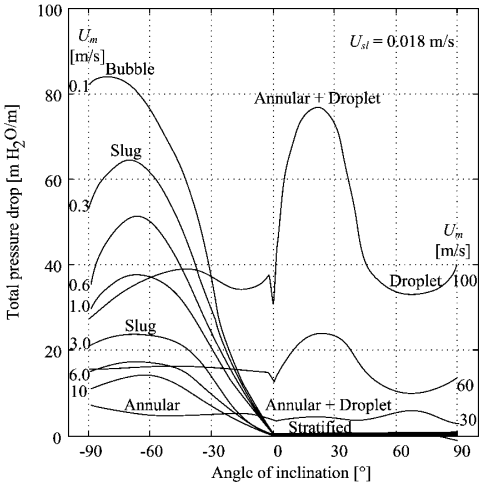

Figure 3-14. Example of pressure drop evolution as a function of the inclination angle (air-water flow in a 4.55 mm inner diameter pipe) (Spedding et al., 1982)

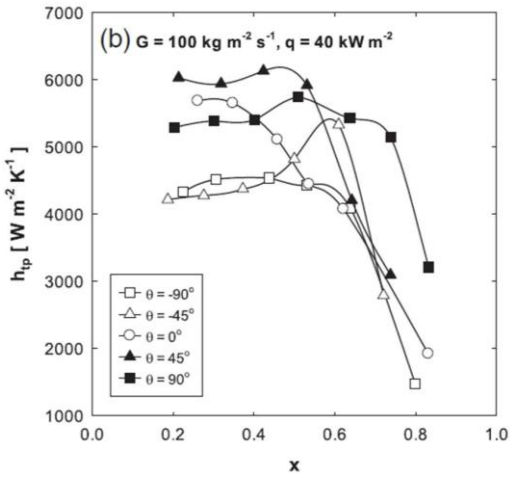

Figure 3-15. Example of evolution of the heat transfer coefficient as a function of the tube inclination for convective boiling of HFE 7100 in a 0.44 mm inner diameter channel (Hsu et al., 2015a)

During his PhD, Thibaut Layssac (2018) proposed a literature review of the studies dealing with the effect of inclination angle on the heat transfer. The main experimental conditions and conclusions of these studies are summarized in table 3-2; $\Delta\alpha$ is the maximum relative difference of heat transfer coefficient when the inclination angle is modified and β_{opt} is the inclination angle that leads to the highest heat transfer coefficient.

Table 3-2. Summary of the studies dealing with the effect of inclination angle on the heat transfer (Layssac, 2018)

	Author	Fluid	d_i [mm]	Geometry	[β_{min} β_{max}]	$\Delta\alpha$	β_{opt}
Condensation	Lips and Meyer (2012b)	R134a	8.38	Smooth	[-90° 90°]	50%	-15°
	Marchuk et al. (2013)	Ethanol	4.8	Smooth	[-90° 0°]	50%	-15°
	Mohseni et al. (2013)	R134a	8.38	Smooth	[-90° 90°]	80%	30°
	Meyer et al. (2014)	R134a	8.38	Smooth	[-90° 90°]	100%	-30°
	Xing et al. (2015)	R245fa	14.81	Smooth	[-90° 90°]	30%	30°
	Adelaja et al. (2016)	R134a	8.38	Smooth	[-90° 90°]	50%	-30°
Air-Water flows	Ghajar and Kim (2005)	Air-water	27.9	Smooth	[0° 7°]	90%	5°
	Ghajar and Tang (2007)	Air-water	27.9	Smooth	[0° 7°]	90%	5°
	Vaze and Banerjee (2011)	Air-water	27.9	Smooth	[0° 7°]	90%	5°
	Bhagwat and Ghajar (2016b)	Air- water	12.5	Smooth	[0° 90°]	100%	75°
	Bhagwat and Ghajar (2017)	Air- water	12.5	Smooth	[-90° 0°]	300%	-90°
Flow boiling	Akhavan-Behabadi et al. (2011)	R134a	8.92	Corrugated	[-90° 90°]	70%	90°
	Wang et al. (2012, p. 7100)	HFE7100	0.825	Multiple	[-90° 90°]	50%	45°
	Akhavan-Behabadi et al. (2014)	R134a	8.3	Corrugated	[-90° 90°]	60%	90°
	Kundu et al. (2014)	R134a	7	Smooth	[0° 90°]	15%	90°
	Kundu et al. (2014)	R407C	7	Smooth	[0° 90°]	15%	90°
	Mohseni and Akhavan-Behabadi (2014)	R134a	8.9	Smooth	[-90° 90°]	70%	90°
	Hsu et al. (2015b)	HFE7100	0.44	Multiple	[-90° 90°]	50%	45°
	Bamorovat Abadi et al. (2016)	R245fa	3	Smooth	[0° 90°]	10%	90°
	Cheng et al. (2017)	R134a	10	Ω grooved	[-90° 90°]	300%	-90°

Depending on the configuration, there is an important discrepancy between the conclusions of the various authors, which justify the importance of this type of studies. In the following of the present chapter, I will try to bring an overview of the main outcomes of the studies in which I was involved since 2011 in terms of inclination effects on the flow pattern (section 3.2), heat transfer (section 3.3) and pressure drops (section 3.4), both for convective condensation and convective boiling.

3.2 Experimental test benches and flow pattern characterisation

3.2.1 Description of the experimental test benches

The results discussed in the present chapter were obtained by means of two different set-ups. During my post-doctoral position, I used a system based on a compression cycle (Figure 3-16) to study convective condensation of R134a in a 8.38 mm tube, whereas Thibaut Layssac used during his PhD a pump based cycle (figure 3-17) previously developed by Romain Charnay during his own PhD to study convective boiling of R245fa. At the beginning of his PhD, Thibaut Layssac used the test section of Romain Charnay, which consisted in a 3 mm inner diameter stainless steel tube, which could only be used in horizontal orientation (figure 3-18). He then developed his own test section made of a transparent sapphire tube of 1.6 mm, coated with ITO and inclinable (figure 3-19). The characteristics and range of experimental conditions are summarised in table 3-3 for each test-sections. The Bond number is defined as:

$$Bo = \frac{g(\rho_l - \rho_v)d^2}{\sigma} \tag{3-1}$$

The condition diversity between the studies enables to draw interesting conclusions when analysing the whole set of experimental results.

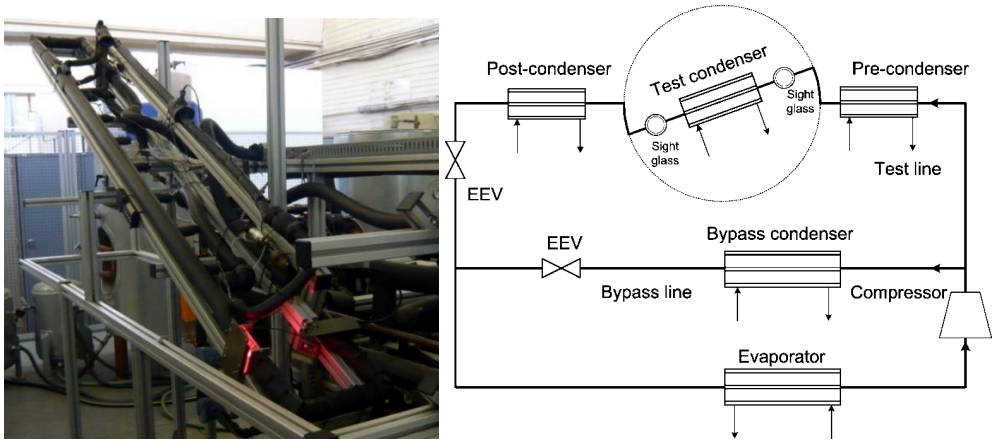

Figure 3-16. Picture and schematic diagram of the experimental setup of Lips and Meyer (2011b) for the study of convective condensation in an inclined orientation

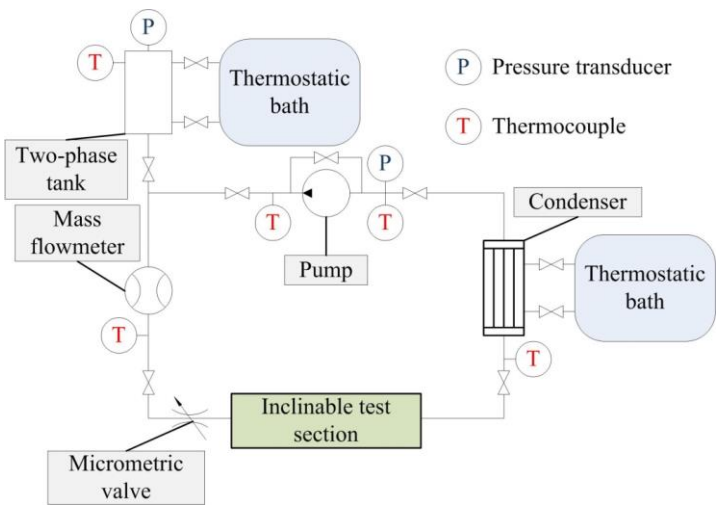

Figure 3-17. Schematic of the test bench of Layssac et al. (2018a) for the study of convective boing in inclined orientation

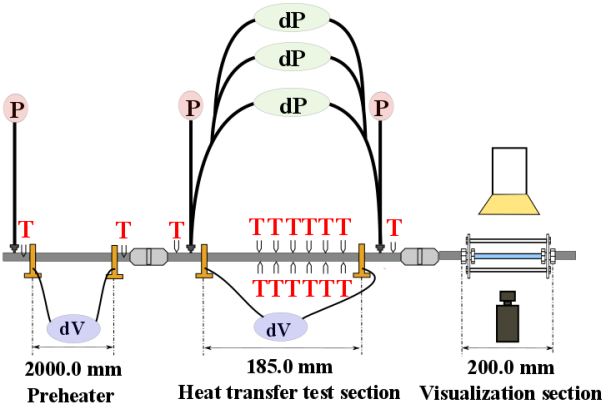

Figure 3-18. Schematic of the test section of Charnay et al. (2014)

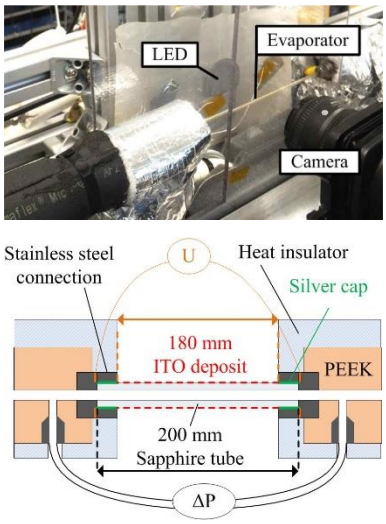

Figure 3-19. Photo and schematic of the evaporator of Layssac et al. (2018a)

Table 3-3. Summary of the characteristics and range of experimental conditions for each test-sections

Set-up	Lips and Meyer (2011b)	Charnay et al. (2014)	Layssac et al. (2018a)
Type of system	Compressor	Pump	Pump
Fluid	R134a	R245fa	R245fa
Tube	8.38 mm	3.0 mm	1.6 mm
Orientation	-90° → + 90°	horizontal	-90° → + 90°
Visualisation section	After the test section	After the test section	Transparent test section
Heating/cooling system	Water heat exchanger	Joule effect in the stainless steel tube	Joule effect in ITO
Wall temperature measurement	Thermocouple	Thermocouple	IR camera
Phenomena	Condensation	Boiling	Boiling
Range of mass flux	200 →600 kg/m²s	50 → 400 kg/m²s	100 →600 kg/m²s
Range of heat flux	5.1 kW/m²	0 → 50 kW/m²	0 → 29.2 kW/m²
Range of Bond number	12.6	7.7 → 19.1	4.1

3.2.2 Effect of tube inclination on flow pattern maps

The difference of Bond number between the studies of Lips and Meyer (2011b) and Layssac et al. (2018a) leads to different flow regimes, as presented in figure 3-2 and figure 3-3 respectively. However, the flow pattern is strongly affected by the inclination angle in both studies. Figure 3-20 and Figure 3-21 present an example of evolution of the flow pattern with the inclination example for the two studies. In general, the flow is more affected for low mass fluxes and low vapour qualities, meaning for low vapour inertia flows. Figure 3-22 and figure 3-23 present two examples of flow pattern maps for the two studies. The difference in terms of flow pattern encountered but also of the inclination effect is very important, even for comparable mass fluxes. Surprisingly, the annular flow regime is more present in the study of Layssac et al. (2018a) despite the fact that the confinement is more important. The stratified flow observed in larger tube is replaced by an annular flow and not by an intermittent flow.

This example highlights the limit of the utility of experimental flow pattern maps: it is a convenient tool to present experimental results but they are difficult to use as a design tool as when one parameter of the flow condition change, the whole flow pattern map can be strongly affected. The development of predictive tools thus has to rely on more complex mechanistic models, which can predict the flow pattern whatever the flow conditions.

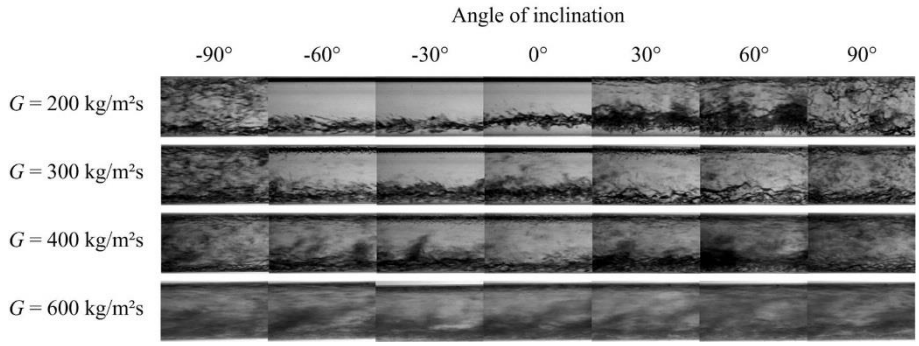

Figure 3-20. Effect of the inclination angle on the flow pattern for different mass fluxes (R134a, d = 8.38 mm, x = 0.5) (Lips and Meyer, 2012a)

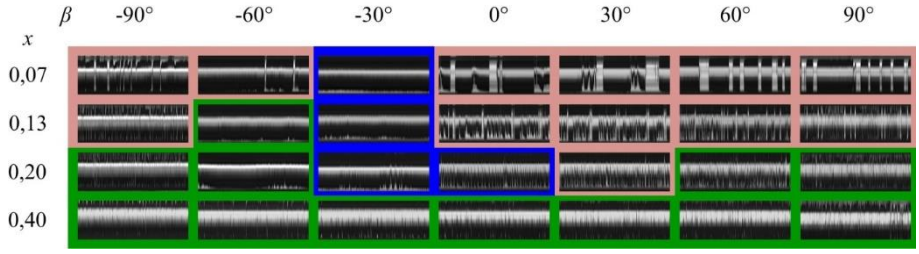

Figure 3-21. Evolution of flow patterns (pink: intermittent; blue: stratified; green: annular) and time representative frames for various vapour qualities and inclination angles (R245fa, d = 1.6 mm, G = 150 kg.m^{-2}.s^{-1}) (Layssac et al., 2018a)

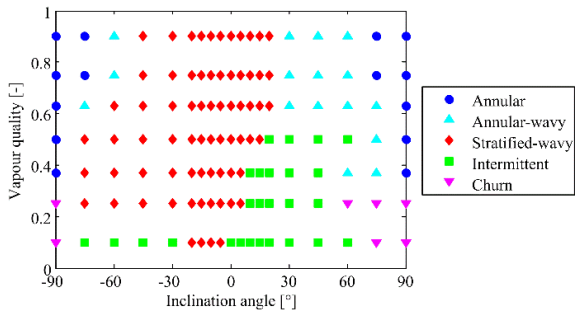

Figure 3-22. Example of experimental flow pattern map of Lips and Meyer (2012c) (R134a, d = 8.38 mm, G = 200 kg/m²s)

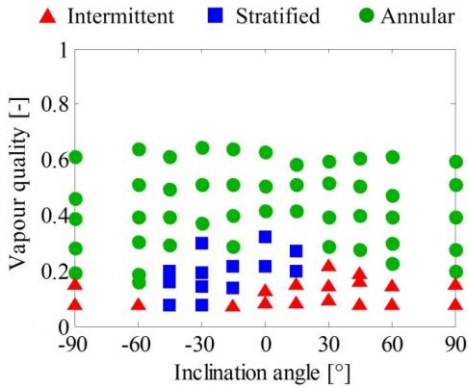

Figure 3-23. Example of experimental flow pattern map of Layssac et al. (2018a) (R245fa, d = 1.6 mm, G = 150 kg.m^{-2}.s^{-1} ; φ = 0 kW.m^{-2})

Lips and Meyer (2011b) and Layssac et al. (2018a) noted that few flow pattern models taking into account the tube inclination exist in the literature. Amongst them, the ones of Barnea (1987) and Crawford et al. (1985; Weisman and Kang, 1981) were the only one usable for the whole range of inclination angle. Despite the fact that the model of Barnea was developed for air-water flows in 2.5 cm and 5.1 cm inner diameter tubes, it enables a rather good prediction of the flow pattern in the various configurations considered in the present studies (figure 3-24). It seems to mean that this model takes into account the relevant physical phenomena involved in the transition between the regimes. The comparison between the experimental results and the predictions of the model of Crawford et al. (1985; Weisman and Kang, 1981) shows that the latter is not able to reproduce the transitions observed for the whole range of inclination angles. This correlation being more empirical, it cannot be used in conditions for which it was not developed.

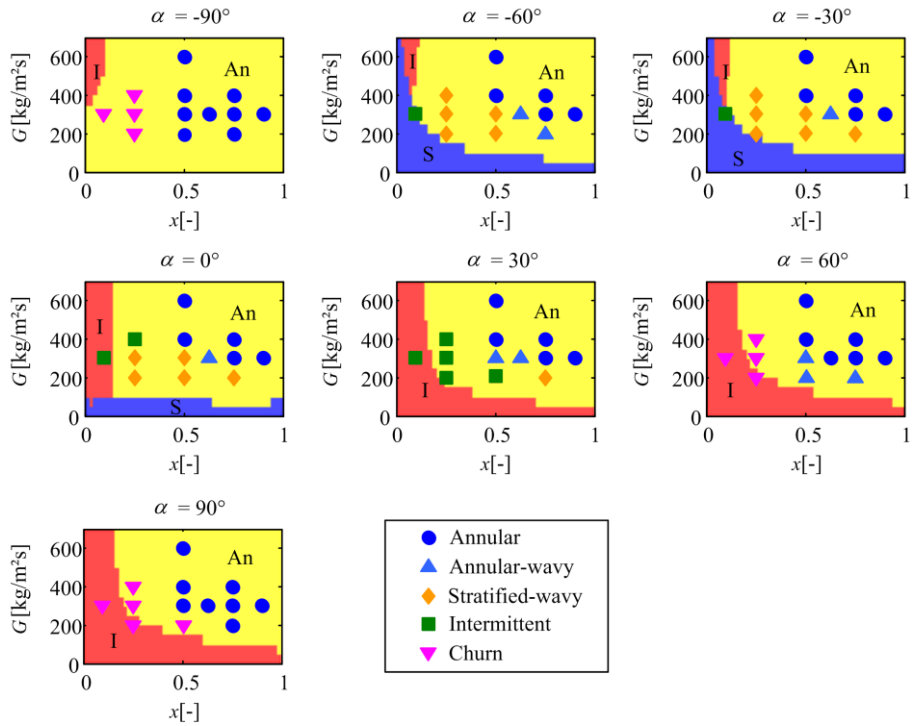

a) flow patterns of Lips and Meyer (2012a) (R134a, d = 8.38 mm)

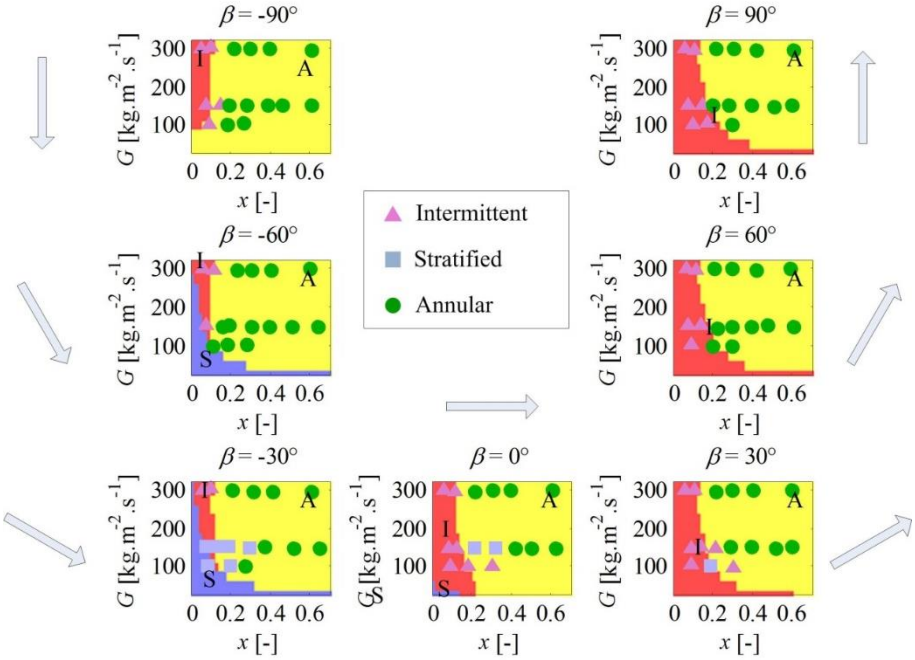

b) flow patterns of Layssac et al. (2018a) (R245fa, d = 1.6 mm, φ = 0 kW.m^{-2})

Figure 3-24. Comparison of experimental flow patterns of Lips and Meyer (2012a) and Layssac et al. (2018a) with the Barnea (1987) flow pattern map (An = Annular, I = Intermittent, S = Stratified)

The experimental flow patterns of Layssac et al. (2018a) presented in figure 3-24 were obtained with no heat flux. Thanks to his transparent test section, Thibaut Layssac showed that the flow pattern was indeed affected by the heat flux. Figure 3-25 presents a comparison of flow patterns with and without heat flux for two experimental conditions corresponding to two flow patterns. The intermittent regime is strongly affected by the bubble nucleation: liquid plugs are smaller and small bubbles are present in the flow. The stratified regime tends to be strongly unstable when nucleation occurs and becomes intermittent. In the conditions tested by Thibaut Layssac, the stratified flow regime completely disappeared when a heat flux of 13.5 kW.m^{-2} is imposed to the tube (figure 3-26).

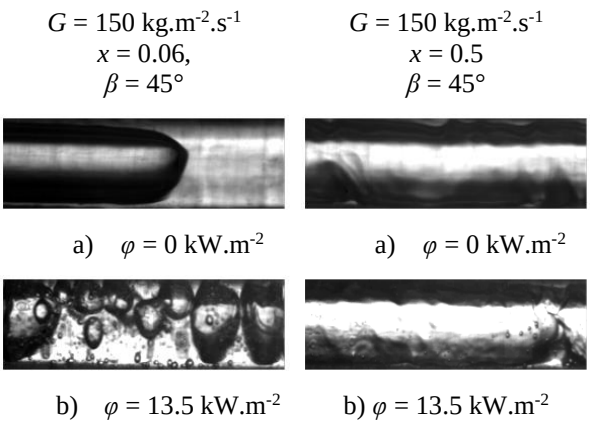

Figure 3-25. Example of the heat flux effect on the flow pattern (Layssac et al., 2018a)

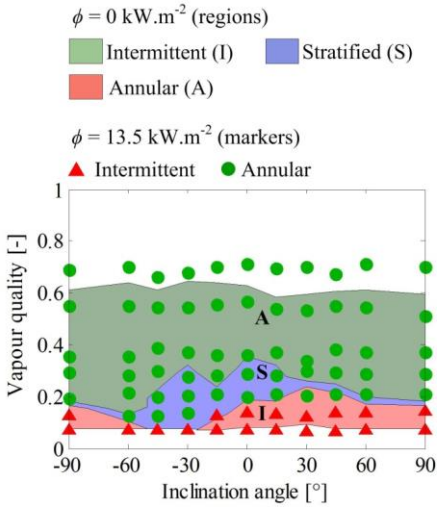

Figure 3-26. Flow patterns with φ = 13,5 kW.m^{-2} compared to the adiabatic conditions (G = 150 kg.m^{-2}.s^{-1}) (Layssac et al., 2018a)

So far, no model of flow patterns taking into account the effect of both the inclination angle and the heat flux is available in the literature. As the flow pattern map of Barnea seems well adapted and robust to the change of flow conditions, it could be used as a base to include the effect of the bubble nucleation in the destabilization of the liquid-vapour interface. However, more experiments are still required to get a better overview of the inclination and heat flux effects on the flow distribution.

3.2.3 Database analysis for the construction of a symmetry correlation

If the number of experimental studies available in the literature does not enable to develop a complete mechanistic model of two-phase flows in inclined tubes, there is enough data to advance on specific phenomena. When studying two-phase flows, a common way to analyse the huge number of experimental data points available in the literature is to develop correlations linking one of the flow characteristic to the various experimental parameters. This approach can be of a great interest for the scientific community for several reasons:

- It enables to compare the experimental data coming from different studies with different fluids, tube diameters and experimental conditions.
- When non-dimensional figures are used, the shape and the relative weight of each figure can give an interesting information on the impact on each phenomena represented by this figures.
- Once the robustness of a proposed correlation is demonstrated, it can be used as a predictive model, either to design a system, or to build other correlations or models for different parameters.

For all these reasons, during his PhD, Thibaut Layssac proposed a correlation for the determination of the symmetry parameter of a two-phase flow in horizontal tubes. The present section summarizes the approach used and its main conclusions.

The study mainly aimed at quantifying the relative effect of each forces affecting the flow stratification. The two-phase flow symmetry was thus considered through the parameter *s*, defined as:

$$s = \frac{d_{top}}{r} \tag{3-2}$$

with *s* the symmetry parameter, d_{top} the distance between the vapour core centre and the top glass-liquid interface and *r* the internal radius as shown in figure 3-27.

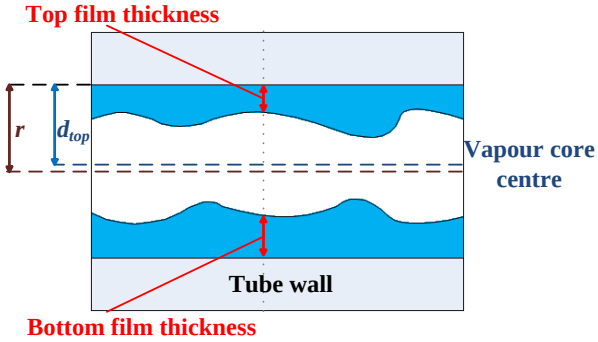

Figure 3-27. Position of the vapour core centre for a horizontal two-phase flow (Layssac et al. (2017))

The first step is the concatenation of the various data points available in the literature. The goal is to widen as much as possible the various experimental conditions in which the data were measured but it appears that few studies present experimental data enabling the determination of the flow symmetry. Table 3-4 summarizes the database Layssac et al. (2017) used for the correlation construction. It involves air-water and two-phase refrigerant flows.

Table 3-4. Database used by Layssac et al. (2017) for the symmetry correlation construction

	Fluid	*d* [mm]	***x* [-]**	*s* [-]	Points [-]	Bd [-]	Fr_v [-]
Hurlburt and Newell (1997)	Air-water	23→95	0.07→0.96	0.82→1.00	105	87→347	0.7→9.8
Schubring and Shedd (2009)	Air-water	8.8→26.3	0.11→0.76	0.99→1.00	206	10→93	2.2→9.7
Cioncolini and Thome (2013)	Air-water	12→95	0.03→0.96	0.82→1.00	182	8.9→1200	0.7→9.8
Masala et al. (2007)	Air-water	21	0.04→0.21	0.84→0.89	6	59	0.3
Ong and Thome (2011)	R-236fa R-245fa	1.03	0.16→0.69	0.71→1.00	12	1.1→1.5	1.2→7.9
Donniacuo et al. (2015)	R-245fa	2.95	0.1→0.82	0.83→1.00	41	9.2→18.6	1.8→11
Layssac et al. (2017)	R-245fa	2.95	0.06→0.99	0.35→1.00	229	7.7→19.1	0.4→8.3
Total		1.03→95	0.03→1.00	0.35→1.00	676	1.1→1200	0.3→11

The second step is to choose the shape of the correlation. This is of a great importance, as it will directly affect the quality of the correlation. The limit cases of 0 for bubble disappearance at the top of the tube and 1 for a centred flow have to be respected. The monotonic evolution of symmetry also suggests choosing a monotonic function. The function used for respecting these mathematical restrictions can then be constructed with the following form:

$$s = \frac{1}{1 + h\prod_{i=1}^{N} P_i^{\alpha_i}} \tag{3-3}$$

where h is the multiplying factor (h>0), P_i is the ith dimensionless physical parameter, α_i the ith exponent to be determined. All the coefficients of the correlation are obtained by means of a nonlinear method based on the minimization of the Mean Squared Error defined as:

$$MSE = \frac{1}{N}\sum_{i=1}^{N}\left(s_{meas,i} - s_{pred,i}\right)^2 \tag{3-4}$$

From a statistical point of view, the best correlation is obtained when the optimization is led directly considering the base parameters, namely the liquid and vapour viscosity and density, the vapour quality, the surface tension, the mass velocity and the diameter (figure 3-28). However, the robustness of this type of correlation is quite low. It means that a small variation in the database values greatly affect the parameter exponents. It can be highlight by a sensibility analysis, as presented in figure 3-29 which represent the evolution of the MSE when fixing one imposed coefficient and running the optimization with the others.

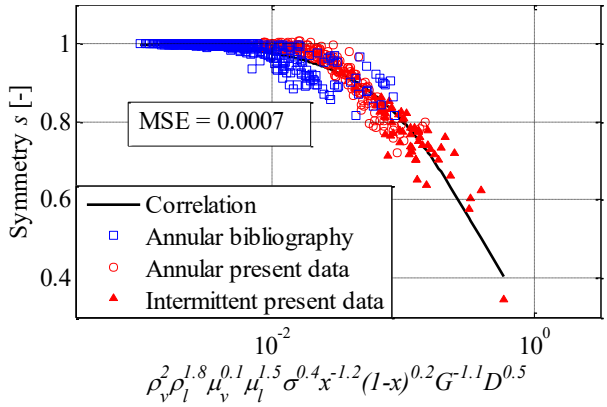

Figure 3-28. Base parameters correlation (Layssac et al., 2017)

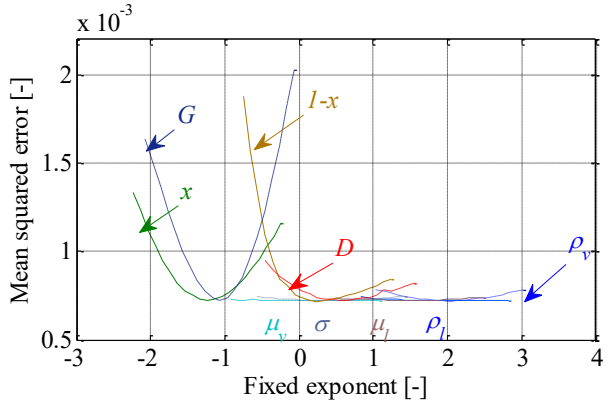

Figure 3-29. Evolution of the Mean Squared Error with the imposed exponents (Layssac et al., 2017)

The evolution of the MSE as a function of the fixed exponent is directly an image of the impact of this exponent on the global optimization. If the MSE is strongly affected by the fixed exponent, it means that the concerned physical parameter has a strong influence on the flow symmetry and that its effect cannot be compensated by the other parameters. On the contrary, if the MSE is slightly affected by the exponent value, it means that either the physical parameter has a low effect on the flow symmetry or that its effect is numerically compensated by the other parameters.

Figure 3-29 shows that the exponent on the fluid properties are strongly linked. It can be confirmed by calculating the correlation coefficients of the database parameters (table 3-5) which shows a strong statistical link between the values of the fluid properties. It actually highlights one of the database weakness, which is to consider not enough fluids to draw real conclusions on the effect of each fluid parameters independently.

Table 3-5. Correlation coefficients of the present database flow parameters (Layssac et al., 2017)

$\lvert Corr(P_i,P_j)\rvert$	ρ_v	ρ_l	μ_v	μ_l	σ	x	G
D	0.49	0.61	0.65	0.70	0.67	0.09	0.21
G	0.05	0.10	0.08	0.06	0.05	0.26	
x	0.22	0.06	0.11	0.16	0.16		
σ	0.78	0.89	0.96	0.99			
μ_l	0.82	0.85	0.94				
μ_v	0.60	0.98					
ρ_l	0.42						

The fact that only a few non-dimensional numbers have been considered enables to compensate partly this weakness, each parameter effect being taken into account in the physical phenomena represented by the non-dimensional numbers. In the case of the symmetry correlation proposed by Layssac et al. (2017) several analyses led to the choice of the Bond number *Bd*, the vapour only Froude number Fr_{vo} and the Martinelli parameter χ, the latters being defined as:

$$Fr_{vo} = \frac{\frac{G}{\sqrt{\rho_{vap}}}}{\sqrt{g(\rho_{liq} - \rho_{vap})d}} \tag{3-5}$$

$$\chi = \sqrt{\frac{f_{liq}\rho_{vap}}{f_{vap}\rho_{liq}}}\left(\frac{1-x}{x}\right) \tag{3-6}$$

with f_i the Fanning friction factor of phase *i* (liquid or vapour), evaluated using Churchill correlation (1975).

The global MSE of the correlation based on these non-dimensional number is slightly higher than that done with the basic parameters (figure 3-30), but the robustness of the parameter exponents is much better (figure 3-31). A new correlation is thus proposed:

$$s = \frac{1}{1 + Bd^{0.1} Fr_{vo}^{-0.9} \chi^{1.1}} \tag{3-7}$$

Symmetry appears to be guided by the relative importance of inertia compared to buoyancy, which is consistent with previous correlations proposed by Hurlburt and Newell (1997), Schubring and Shedd (2009) and Cioncolini and Thome (2013). However, the present correlation reveals the importance of pressure drops for two-phase flow stratification in horizontal circular mini and macro channels. The lower exponent of the Bond number indicates a lower importance of capillarity in this range of diameters, which is consistent with the known behaviour of mini and macro channels.

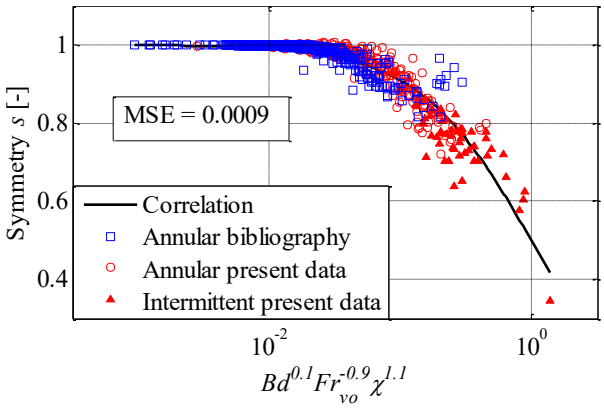

Figure 3-30. Correlation with the Bond number, the Froude number and the Lockhart-Martinelli parameter (Layssac et al., 2017)

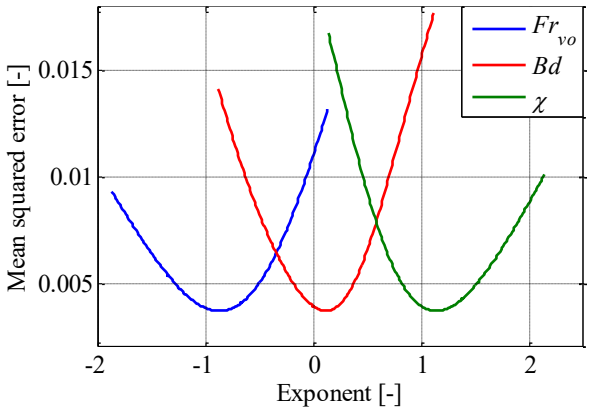

Figure 3-31. Evolution of the Mean Squared Error with imposed dimensionless number exponents (Layssac et al., 2017)

The prediction accuracy of the correlation can be analysed with introduced statistical indicators as shown in figure 3-32. With this set of exponents, 100% of the data points are predicted within a +/- 50% error band whereas 90% of the database is predicted within +/- 10% error band which shows the excellent agreement between the data and the correlation. A more detailed uncertainty analyses of the correlation is given in (Layssac et al., 2017).

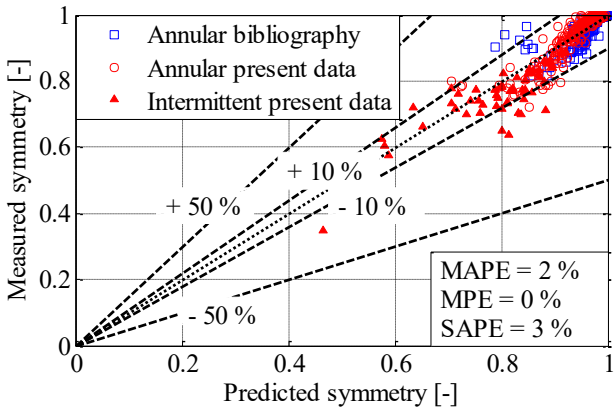

Figure 3-32. Measured symmetry as a function of predicted symmetry for Bd, χ and Fr_{vo} correlation (Layssac et al., 2017)

This example of correlation construction shows how careful one has to be when proposing a new correlation. The basic fitting of a given function with experimental data can always be done, but a great care in the physical and statistical analyses has to be taken to ensure the robustness of the correlation.

3.2.4 Conclusions

The studies of Lips and Meyer (2011b) and Layssac et al. (2018a) showed that the inclination angle has an important effect on the flow distribution in various experimental conditions and that no model available in the literature is able to predict this effect. The flow pattern determination being the first step when aiming at predicting the heat transfer and pressure drops in a system, more experimental and theoretical works are consequently required to achieve a better understanding of two-phase flows in these conditions.

3.3 Effect of tube orientation on heat transfer

When dimensioning a heat exchanger, the knowledge of the heat transfer coefficient between the fluid and the wall is of great consequence. In industrial heat pump or chillers, the refrigeration cycle induces both an evaporator and a condenser. The important size of these systems leads to the question of an optimal design of the complete system by adapting the inclination angles of the various components. In the present section, the experimental determination of the heat transfer coefficient between the fluid and the flow is firstly presented. The experimental results obtained by means of the test bench of Lips and Meyer (2011b) are then discussed for the case of convective condensation. A phenomenological model is proposed to understand the various effects of the inclination angle on the heat transfer. Lastly, the experimental results obtained by Layssac et al. (2018a) are discussed in the case of convective boiling.

3.3.1 Experimental determination of the heat transfer coefficient

The experimental determination of the heat transfer coefficient between the wall and the fluid is never easy when studying two-phase flows. During my post-doc, the test section I used consisted in 1.5 m long tube-in-tube counter-flow heat exchanger, with water in the annulus and refrigerant on the inside. The outer-wall temperature of the inner tube of the test condenser was measured by means of thermocouples at seven stations, equally spaced. The refrigerant and the water temperatures were measured at the inlet and outlet of the test section. At each station, thermocouple measurements were taken with three or four thermocouples, equally spaced and soldered onto the tube perimeter. The heat transfer rate through the test condenser was calculated from an energy balance on the water side. The heat transfer coefficient was calculated considering a constant heat transfer coefficient in the test condenser and considering the mean temperature difference between the mean inner-wall temperature, itself linked to the mean outer-wall temperature of the tube through the thermal resistance of the wall of the copper tube. The mean outer-wall temperature was calculated by averaging the outer-wall temperature measured at the seven different stations along the test condenser by means of a trapezoidal numerical integration method.

As a consequence, despite the use of 40 thermocouples on the test section itself, the experimental set-up did not allow the determination of the local heat transfer coefficient. Averaging the wall and saturation temperature leads to the smoothing of the variation of heat transfer coefficient with the vapour quality (that varied between 3.4 % and 11 % across the test-section), with the temperature difference between the wall and the fluid at saturation (that varies with a few Kelvin because of the water temperature variation on the annulus) and with the position on the tube (the wall temperature difference was about 0.2 K between the top and the bottom of the tube). It also hides the saturation temperature variation due to the pressure drop (typically 0.5 K across the test-section). However, the average heat transfer coefficient on the test-section was still a characteristic parameter of the flow and could be studied and compared to correlations.

During his PhD, Thibaut Layssac used an IR camera that enabled to measure the temperature of the ITO coating. This type of measurement is non-intrusive and enables to measure local temperature. However, it requires the perfect knowledge of the ambient conditions. Thibaut Layssac used polycarbonate plates to control the convective and radiative heat transfer between the test section and surroundings (figure 3-33). The raw measurements of the camera also had to be corrected because of the low emissivity of the ITO coating. The later also depends on the angle of visualisation on the tube (figure 3-34) and thus a complex calibration method had to be developed, by considering an average emissivity for each abscissa of the tube, the latter also depending on the temperature (figure 3-35). In order to determine the heat transfer coefficient from the temperature measurements a thermal nodal model (figure 3-36), associated to another calibration procedure was used to take into account the conduction in the wall and the heat losses to the surroundings (as no insulation could be used because of the IR visualisation).

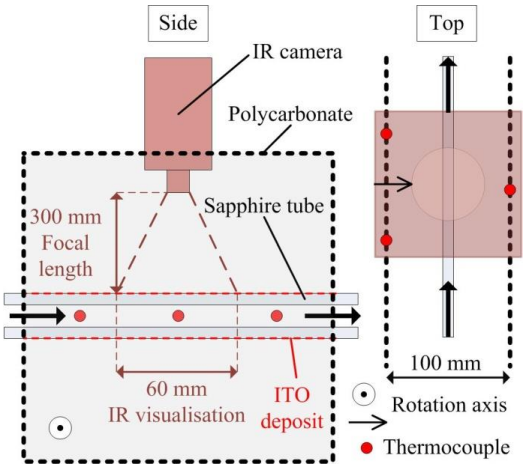

Figure 3-33. Top and side view of the IR test section. Polycarbonate plates enable to measure the equivalent temperature of the test section surroundings (Layssac et al., 2018b)

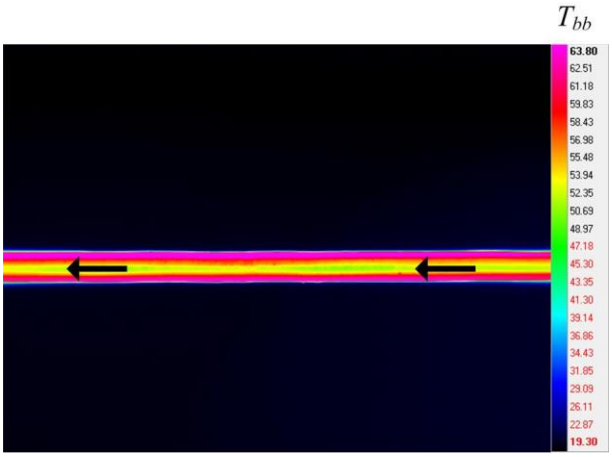

Figure 3-34. Black body temperature field of the test section. The edges of the tube appear hotter because of the angle dependence of the ITO coating emissivity (Layssac et al., 2018b)

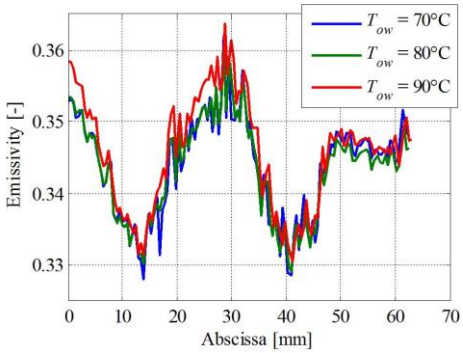

Figure 3-35. Variations of the ITO deposit emissivity with abscissa for sapphire outer wall temperature of 70°C, 80°C and 90°C (Layssac et al., 2018b)

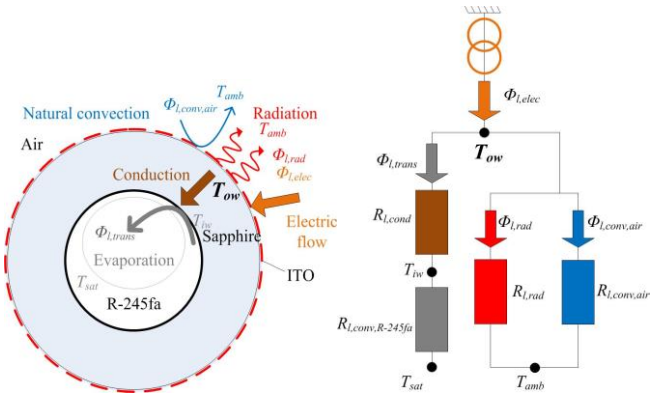

Figure 3-36. Thermal model at abscissa z and electric equivalent schematic (Layssac et al., 2018b)

Whatever the technique used, the determination of the heat transfer coefficient is always complex and requires a great care. A high uncertainty is also associated with the measurements, typically between 10 % and 15% in the two studies considered here. This uncertainty is still acceptable for the analysis of the heat transfer phenomena occurring in two-phase flows but remains a limitation and is a cause of scattering of the experimental data available in the literature.

3.3.2 Convective condensation

The experiments performed for convective condensation of R134a in an 8.38 mm inner diameter tube showed an important effect of the inclination angle on the heat transfer coefficient. Figure 3-37 presents an example of heat transfer coefficient variation as a function of the inclination angle for G = 200 kg/m²s and for various vapour qualities. For low vapour qualities, an optimal inclination angle of -15° (downward flow) is found and the worst conditions were obtained for the vertical downward configuration. The sharp variation of the heat transfer coefficient between -15° and +15° is due to the strong effect of the inclination on the flow pattern in these conditions in terms of both liquid holdup and liquid film thickness at the top of the tube (figure 3-20). The inclination effect decreases when the vapour quality and/or the mass flux increase (figure 3-38). These configurations corresponds to high vapour inertia flows, which lead mainly to annular flows, less sensitive to the inclination angle. This effect is highlighted by the figure 3-39 on which the experimental inclination effect, defined as the relative difference between the highest and lowest heat transfer coefficient for a given mass flux and vapour quality, are drawn on the flow pattern map of Thome-El Hajal-Cavallini (El Hajal et al., 2003), developed for horizontal flows. As expected, the conditions that are the most affected by the inclination angle corresponds to stratified flows.

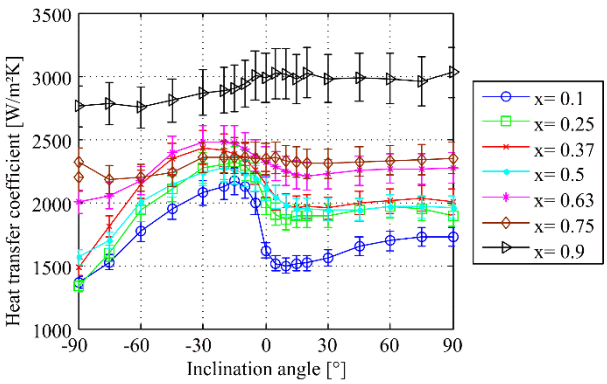

Figure 3-37. Experimental heat transfer coefficient during convective condensation of R134a in a 8.38 mm tube (G = 200 kg/m²s, -90° : downwards, 0° : horizontal; 90° vertical upwards) (Lips and Meyer, 2012c)

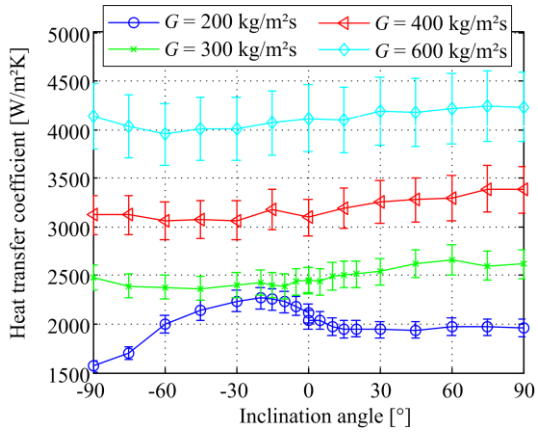

Figure 3-38. Inclination effect on heat transfer coefficients during convective condensation of R134a in a 8.38 mm tube for various mass fluxes (x = 0.5) (Lips and Meyer, 2012a)

In inclined configurations, stratified flows are mainly observed for downward flows. Figure 3-40 highlights the coupling between the variations of heat transfer coefficient and flow patterns. Several phenomena can be observed: For low inclination angles (<45° in absolute values), the liquid-vapour interface is almost flat but the liquid holdup is strongly affected by the inclination angle. For higher inclination angles, the liquid film thickness seems to stabilise but the wetted area at the bottom of the tube increases when the inclination increases. For vertical flows, an annular flow regime is observed.

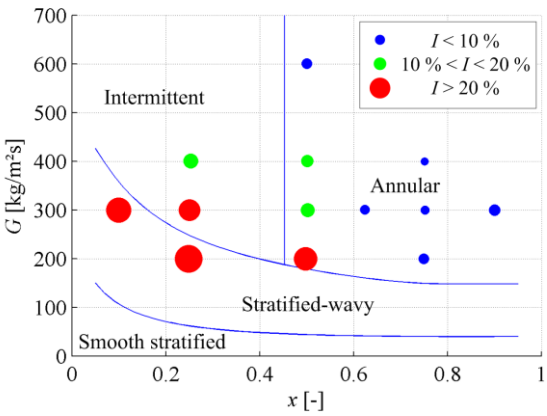

Figure 3-39. Map of the inclination effect on heat transfer coefficients drawn on the Thome-El Hajal-Cavallini (El Hajal et al., 2003) flow pattern map (Lips and Meyer, 2012a)

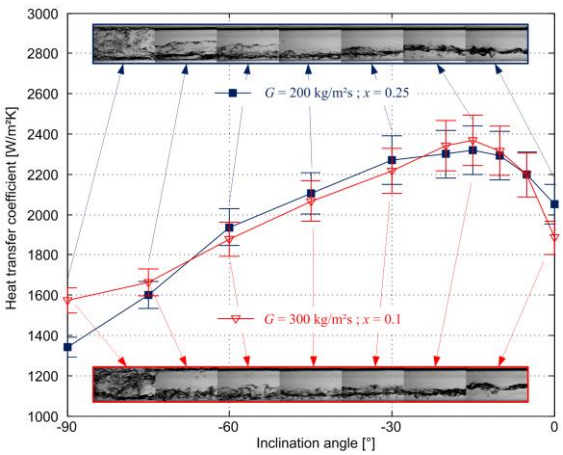

Figure 3-40. Flow patterns and heat transfer coefficients for downward flows at low mass fluxes and low vapour qualities (Lips and Meyer, 2012a)

In order to quantify the relative effect of each phenomenon on the variation of heat transfer coefficient, we proposed a simplified phenomenological model of stratified flows in downward configurations. For this type of flows, the model of Taitel and Dukler (1976) is often considered as very relevant. It takes into account the geometry given in figure 3-4 and is based on the balance of pressure drop in the liquid and vapour phases. In the present study, it was found to predict well the liquid hold up as well as the flow pressure drops (Figure 3-41). However, it was not developed for predicting the heat transfer coefficient during condensing flow.

As a consequence, we proposed a new model, based on that of Taitel and Dukler (1976), but considering a curved liquid-vapour interface instead of a flat one (figure 3-42). Gravitational and capillary forces were considered for the interface shape determination. A thermal model was also associated to the hydrodynamic one. He consisted on the coupling between a conductive model in the liquid pool and a falling liquid film model on the upper part of the tube, calculated with the approach of Fieg and Roetzel (1994) (figure 3-43).

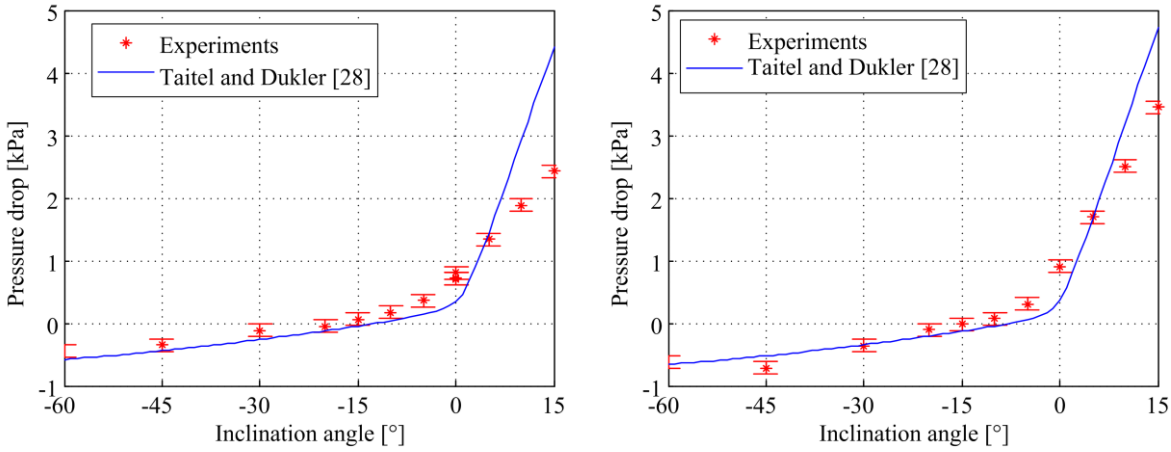

a) G = 200 kg/m²s; x = 0.25; T_{sat} = 40°C

b) G = 300 kg/m²s; x = 0.1; T_{sat} = 40°C

Figure 3-41. Pressure drops predicted by the model of Taitel and Dukler compared with experimental results obtained for convective condensation of R134a in a 8.38 mm tube (Lips and Meyer, 2012b)

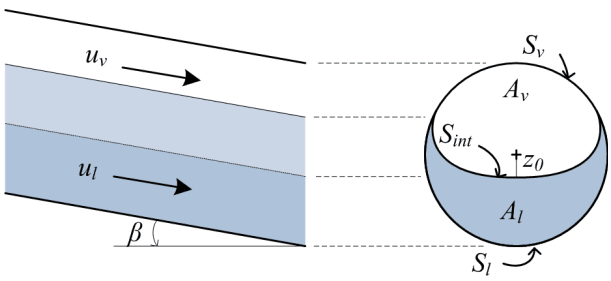

Figure 3-42. Modified model of Taitel and Dukler (1976) for convective condensation in inclined tubes (Lips and Meyer, 2012c)

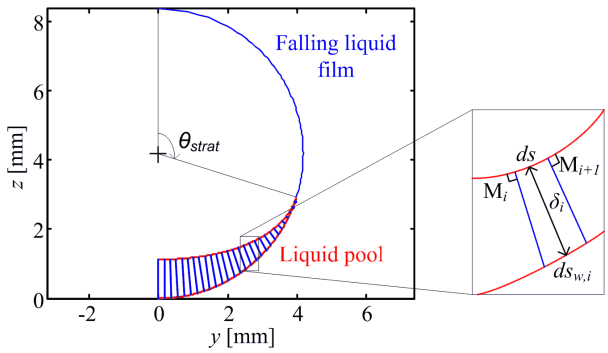

Figure 3-43. Scheme of the thermal model for the heat transfer coefficient determination for convective condensation in inclined tubes (Lips and Meyer, 2012c)

The model is able to determine the liquid hold-up, the liquid-vapour interface shape, the pressure drops and the global heat transfer coefficient between the wall and the fluid. An example of model results and their comparison with experimental data is presented in figure 3-44. When the flow is stratified (solid lines, according to the model of Crawford et al. (1985)), a remarkable agreement is observed between the model predictions and the experimental results. It tends to show that the physics of this type of flow is well understood and well represented by the model hydrodynamic and thermal model. It has to be noted that no empirical parameter is present in the model, the heat transfer being mainly led by the evolution of the liquid film thickness around the tube.

This case is almost an exception, as the stratified flow is maybe the simplest of the flow patterns encountered for two-phase flows. However, once the model is validated, it can be used for studying the balance between the various phenomena. Model predictions are presented in figure 3-45 for various assumptions. Case a) corresponds to the assumption of a flat interface, as considered by Taitel and Dukler (1976) and a constant falling film heat transfer coefficient (FFHTC), equal to the heat transfer coefficient in a horizontal orientation. Case b) corresponds to the assumption of a curved interface and a constant falling film heat transfer coefficient. The validated assumptions corresponds to the case c) in which a curved interface and a varying falling film heat transfer coefficient model is used. It can be seen that if a constant falling film heat transfer coefficient model is used, which is often the case in the literature, the experimental trends would not have been properly represented. In the same way, the consideration of a flat interface would have led to a noticeable shift in the model predictions.

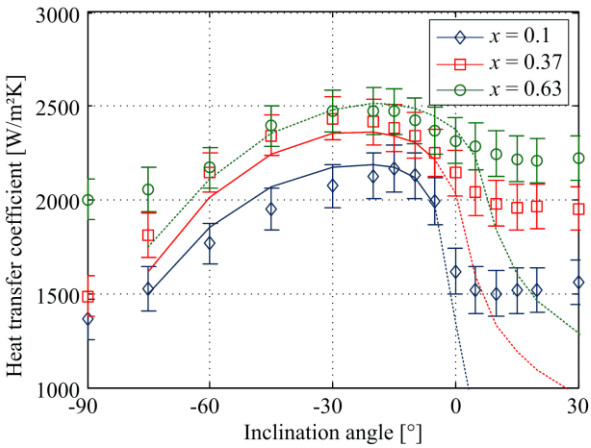

Figure 3-44. Comparison of the model predictions with experimental results (G = 200 kg/m²s). Dashed lines mean that the flow is not stratified according to Crawford et al. (1985)(Lips and Meyer, 2012c)

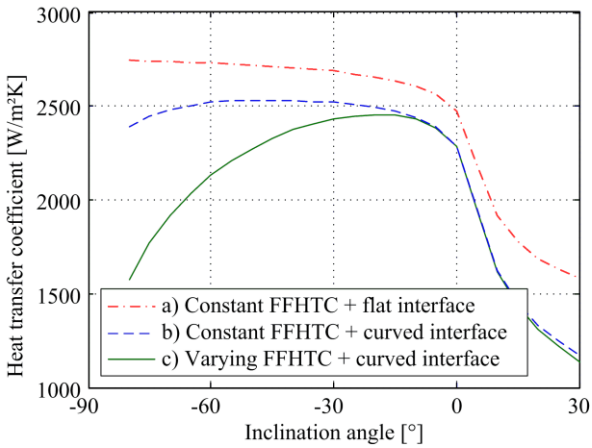

Figure 3-45. Influence of different assumptions on the model predictions. FFHTC: Falling film heat transfer coefficient (G = 200 kg/m²s ; x = 0.3; ΔT = 2 K) (Lips and Meyer, 2012c)

This brief summary of the research I led on heat transfer during convective condensation in inclined tube shows that the heat transfer can be affected through two main phenomena:

- When the inclination angle affects the flow pattern, the heat transfer process is logically affected as well. This conclusion should be true whatever the heat transfer configuration considered (air-water flows, convective condensation, convective boiling…).
- Even when the flow pattern is slightly affected, the inclination angle can affect specific phenomena directly governing the heat transfer, for instance the liquid film thickness at the top of the tube when considering stratified flow during convective condensation. This specific effect should not be encountered in other heat transfer configurations, or even in other flow regimes, but other effects could occur specifically for each considered configuration. More experimental studies are thus required to have a global overview of the inclination effect on two-phase flows.

3.3.3 Convective boiling

During his PhD, Thibaut Layssac measured the heat transfer coefficient between the wall and the fluid during convective boiling of R245fa in a 1.6 mm inner tube diameter made of sapphire. He surprisingly found a very low effect of the inclination angle on the heat transfer coefficient. The variation of the latter as a function the inclination angle for various mass fluxes and various vapour qualities are presented on figure 3-46 and figure 3-47 respectively. The same trend is observed for various heat fluxes (figure 3-48).

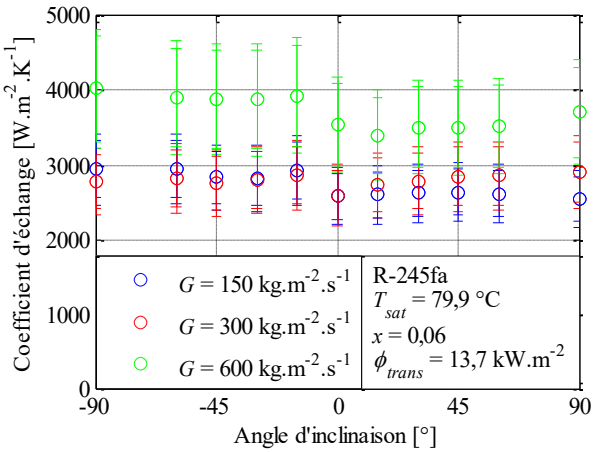

Figure 3-46. Variations of the heat transfer coefficient with the inclination angle for various mass fluxes (x = 0.06) (Layssac, 2018)

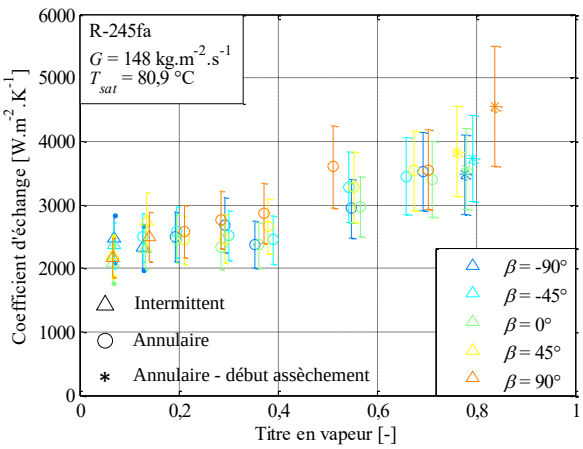

Figure 3-47. Variations of the heat transfer coefficient with the vapour quality for various inclination angle (G = 148 kg/m²s) (Layssac, 2018)

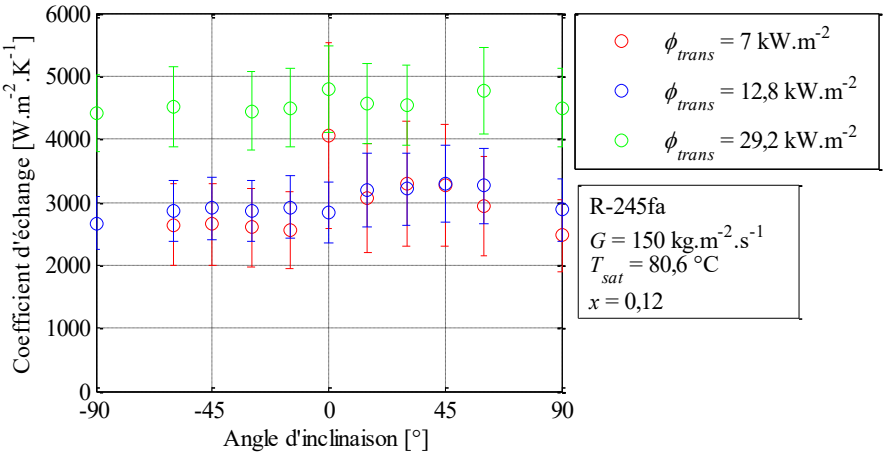

Figure 3-48. Variations of the heat transfer coefficient with the inclination angle for various heat fluxes (x = 0.12; G = 150 kg/m²s) (Layssac, 2018)

The absence of evolution of the heat transfer coefficient with the inclination angle is surprising as an inclination effect was observed on the flow pattern for the same experimental conditions (Figure 3-20). The confinement alone does not explain the observed trends. In order to study the various phenomena involved in two-phase flows, Thibaut Layssac compared his experimental results to various models of heat transfer available in the literature, which are developed for horizontal flows (Table 3-6).

He found that the model of Bertsch et al. (2009) appears to be the best one to predict the variations of the heat transfer coefficient for his dataset. The particularly good agreement of this model may indicates it takes into account correctly the various phenomena involved during convective boiling. The model of Bertsch et al. (2009) is an asymptotic model considering a balance between the heat transfer coefficient due to convective phenomena and the heat transfer coefficient due to the nucleate boiling phenomena. These terms are calculated and represented on figure 3-49 in the case of the data obtained in horizontal configuration with a mass velocity of 150 kg.m^{-2}.s^{-1}. The model of Bertsch et al. (2009) predicts the decrease of the nucleate boiling with the vapour quality. Simultaneously, the convective boiling increases. These variations with the vapour quality result in a transition of dominant heat transfer modes for a vapour quality equal to 0.37.

During his experiments, Thibaut Layssac observed a transition of flow regime from intermittent to annular for a vapour quality of 0.2 a mass velocity of 150 kg.m^{-2}.s^{-1}. It was also observed that for low vapour qualities, a large amount of little bubbles coming from the nucleation were present. When the vapour quality increased, the flow became annular but some bubbles coming from the inner wall were still observed. The flowing liquid film thickness became thinner and the overheat of the inner wall became lower. The intensity of the nucleation lowered as a consequence. Almost no bubbles were observed for a vapour quality higher than 0.7. It can thus be concluded that there exists three kinds of couplings between the heat transfer modes and the flow patterns.

- In the case of a vapour quality lower than about 0.2, the two-phase flow was intermittent and the dominant heat transfer mode was the nucleate boiling. Nucleate boiling is very slightly affected by the inclination and the effect of the inclination on the heat transfer coefficient is weak.

- For a vapour quality between ~ 0.2 and ~ 0.37, the two-phase flow is annular and the dominant heat transfer is nucleate boiling. For the same reason as explained previously, the inclination does not affect much the heat transfer.

- With a vapour quality higher than 0.37, the two-phase flow is annular and the dominant heat transfer mode is convective boiling. The convective boiling is impacted by the type of flow patterns but the two-phase flow is constantly annular. This flow is very slightly affected by the orientation, being inertia-driven. Consequently, the global inclination of the tube has a low effect on heat transfer.

Table 3-6. Heat transfer coefficient prediction accuracy of various models (Layssac et al., 2018b)

	MAPE	MPE	PEDC50	PEDC30	PEDC10
Chen (1964)	57	57	40	10	0
Gungor and Winterton (1986)	79	79	20	15	2
Kandlikar (1990)	46	-42	51	38	6
Liu and Winterton (1991)	32	21	89	36	9
Kandlikar and Balasubramanian (2003)	55	-49	39	16	5
Zhang et al. (2004)	52	49	66	34	11
Saitoh et al. (2007)	34	32	82	34	13
Bertsch et al. (2009)	16	9	100	94	29

MAPE: Mean Absolute Percentage Error; MPE: Mean Percentage Error; PEDCx: Percentage of Experimental Data Captured within ± x%.

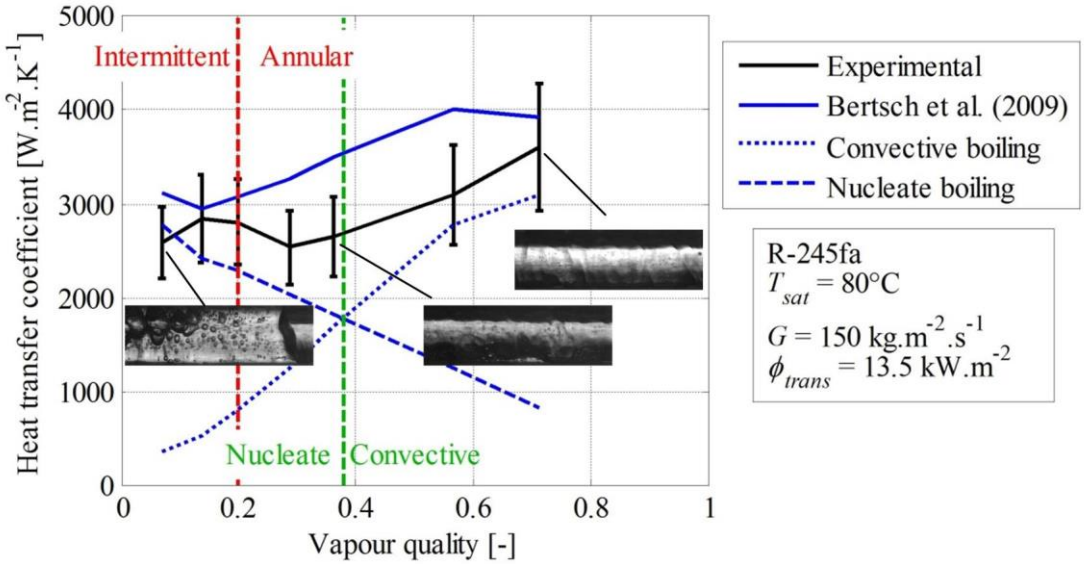

Figure 3-49. Prediction of the variations of the nucleate and convective heat transfer mode with vapour quality from Bertsch et al. (2009) model for a mass velocity of 150 kg.m^{-2}.s^{-1} (Layssac, 2018)

3.3.4 Conclusions

The experimental studies performed for convective condensation and convective boiling highlight the complexity of the coupling between the various phenomena when we incline the test section. Depending on the heat transfer mechanism, the leading phenomena can differ and thus the sensitivity of the heat transfer to the variation of gravitational forces. Besides bringing a better knowledge of the two-phase flows behaviour, this observation is actually very interesting from an experimental point of view as it enables to determine the importance between the various phenomena by segregating the flow that are sensible to the inclination angle from the others.

3.4 Effect of tube orientation on pressure drop

Together with the heat transfer coefficient, the knowledge of the pressures drops in two-phase flows is an important matter when designing an industrial system. Many models are available in the literature for vertical or horizontal orientations, but once more, very few studies deal with inclined configurations. In the present section, the experimental results obtained with the test benches of Lips and Meyer (2011b) and Layssac et al. (2018a) are firstly presented. A discussion on the notion of apparent gravitational pressure drop is then proposed. It opens more widely the question of the physical meaning of the pressure drop decomposition itself. Lastly, an example of entropy analysis will be given in order to try to link the thermal and hydrodynamic performance of an evaporator or a condenser included in a complete heat pump.

3.4.1 Pressure drop measurements

The pressure drop measurements in two-phase flow is less difficult to achieve than that of the heat transfer coefficient. One must pay attention to the quality of the pressure taps and to the presence of gas, vapour or liquid in the pressure lines, but it eventually requires only a classical pressure difference sensor.

Figure 3-50 and figure 3-51 presents the variation of pressure drops for a condensing flow of R134a in an 8.38 mm diameter tube as a function of the inclination angle, for various vapour qualities and various mass fluxes respectively. It can be seen that the pressure drop globally increases when the vapour quality and the mass flux increase, but also when the inclination angle increases. These effects are well known and are due to the increase of the fluid velocities and the gravitational pressure drop respectively.

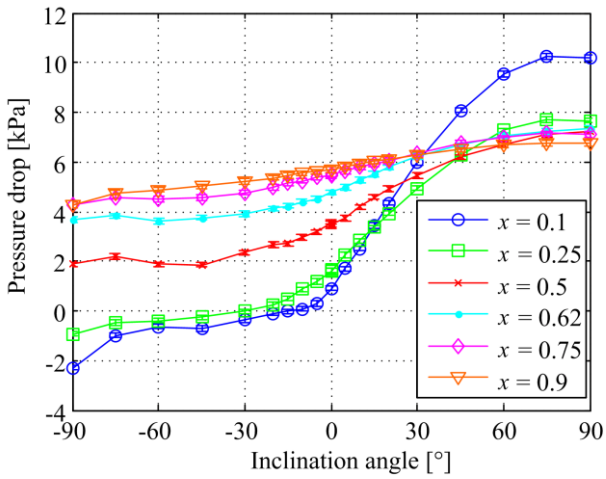

Figure 3-50. Measured pressure drops for different vapour qualities (R134a, d = 8.38 mm; G = 300 kg/m²s) (Lips and Meyer, 2012b)

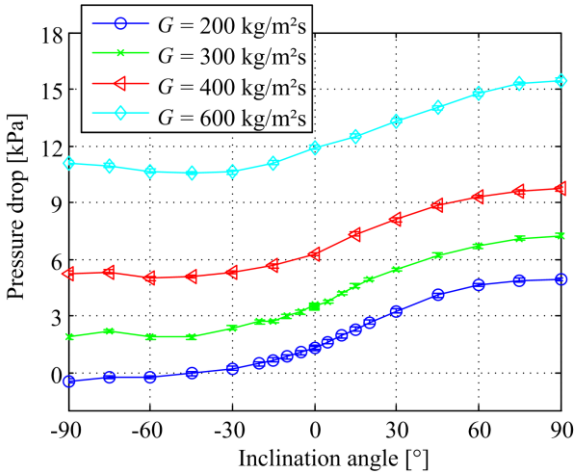

Figure 3-51. Measured pressure drops for different mass fluxes (R134a, d = 8.38 mm; x = 0.5) (Lips and Meyer, 2012b)

What is more interesting is the shape of the variation of pressure drops with the inclination angle for low vapour qualities. It seems that there is a strong change of slope of the curves between -15° and -30° (see, for instance, the curves corresponding to x = 0.1 and x = 0.25 on figure 3-50). This variation of behaviour is also visible on the measurements performed by Layssac et al. (2018a) during convective boiling of R245fa in a 1.6 mm tube (figure 3-52). It seems to be linked to two phenomena: In these conditions, the total pressure are almost equal to zero and the flow pattern is mainly stratified. It seems to behave as an open channel flow. This behaviour seems to be predicted by the model of Taitel and Dukler (see figure 3-41 page 56) but a deeper analysis is required to understand in detail the cause and the consequences of this phenomenon.

More generally, the shape of the curves obtained for convective condensation (figure 3-50) and for convective boiling (figure 3-52) are very similar and it explains why the pressure drop models available in the literature are generally used independently on the heat transfer mechanism. Pressure drop models developed for unsaturated flows can even be used to predict the behaviour of saturated flows. However, Thibaut Layssac showed during his PhD that for convective boiling, the heat flux, and more accurately the bubble nucleation, could affect the pressure drops. This phenomenon is illustrated in figure 3-53: a systematic shift is observed when the pressure drop, with and without heat flux, are compared. The bubble nucleation may affect the shear layer and thus increase the pressure drop. However, more experiments are required to be able to quantify this effect accurately.

In both studies, the experiment results were compared to models or correlations available in the literature, details can be found in (Lips and Meyer, 2012b) and (Layssac et al., 2018a) and are not reported here for the sake of concision. Both studies concluded that if some models were able to predict satisfactory the pressure drop for upward inclinations, none of them were able to predict the pressure drop in downward inclinations, expect for the case of fully vertical downward flows for which specific correlations are provided. This interesting observation requires the notion of pressure drop decomposition to be analysed.

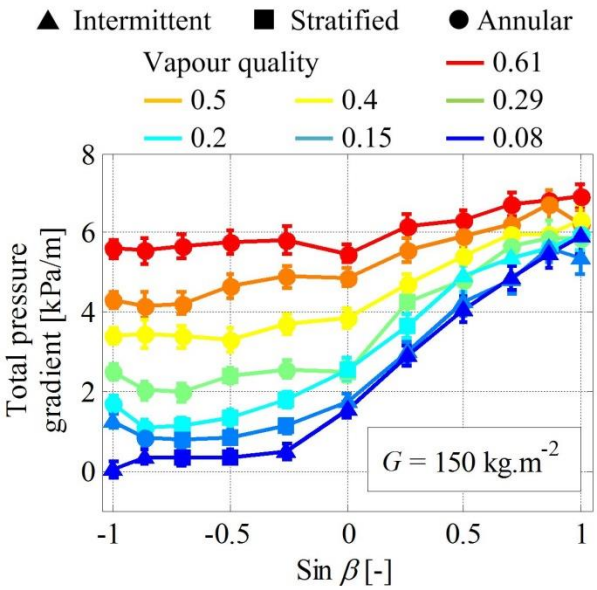

Figure 3-52. Evolution of total pressure gradient as a function of the inclination angle for convective boiling of R245fa in a 1.6 mm tube and a mass velocity of 150 kg.m^{-2}.s^{-1} (Layssac et al., 2018a)

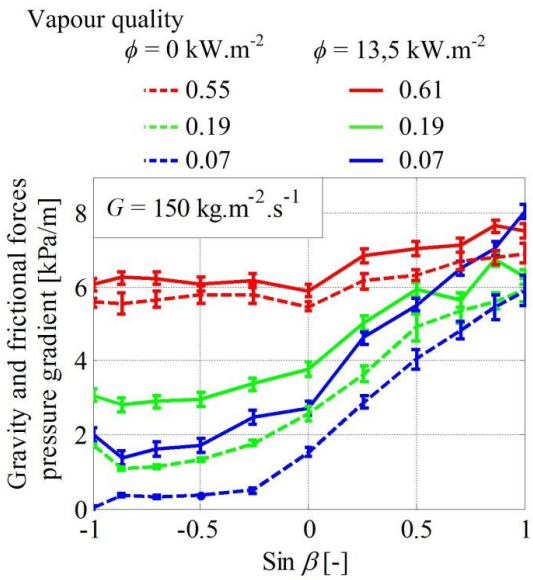

Figure 3-53. Comparison of pressure gradient evolution with inclination angle with an imposed heat flux of 13.5 kW.m^{-2} (filled lines) and without heat flux (dot lines) (Layssac et al., 2018a)

It is commonly admitted in the literature that the total pressure drop of a two-phase flow, ΔP, is the sum of three different terms: the gravitational pressure drop, ΔP_{grav}, the momentum pressure drop, ΔP_{mom}, and the frictional pressure drop, ΔP_{fric}:

$$\Delta P = \Delta P_{fric} + \Delta P_{grav} + \Delta P_{mom} \tag{3-8}$$

The gravitational pressure drop is a consequence of the inclination angle β of the tube. The frictional pressure drop is due to the shear stress between the fluids and the wall. The momentum pressure drop (also called acceleration pressure drop) depends on the variation of kinetic energy of the fluid in the tube.

Authors generally consider that the gravitational and momentum pressure drops can be calculated as:

$$\left(\frac{dP}{dz}\right)_{grav} = -\big(\varepsilon\rho_v + (1-\varepsilon)\big)\rho_l g \sin\beta \tag{3-9}$$

$$\left(\frac{dP}{dz}\right)_{mom} = -G^2 \frac{d}{dz}\left(\frac{x^2}{\rho_v \varepsilon} + \frac{(1-x)^2}{\rho_l(1-\varepsilon)}\right) \tag{3-10}$$

It enables the determination of the frictional pressure drop from the experimental measurements and using a correlation of void fraction available in the literature. Examples of evolution of the frictional pressure drops as a function of the inclination angle are presented in figure 3-54 for convective condensation of R134a in an 8.38 mm tube and in figure 3-55 for the convective boiling of R245fa in a 1.6 mm tube. The shape of these curves is very specific and difficult to explain. In some conditions, the frictional pressure drop seems to increase with the inclination angle (high vapour quality for convective condensation of R134a) but the opposite is also observed (very high or very low vapour quality for convective boiling of R245fa) and there is sometimes a minimum of frictional pressure drop observed for horizontal of slightly downward inclined orientations.

To my knowledge, no model available in the literature enables to explain these trends. In the two next sections, I propose a reflexion on this topic, firstly by introducing the notion of apparent frictional pressure drop and void fraction, and secondly by questioning the physical meaning of this type of decomposition. Surprisingly, the conclusions of these two approaches are contradictory, so I do not pretend to answer this question, but rather to open the discussion.

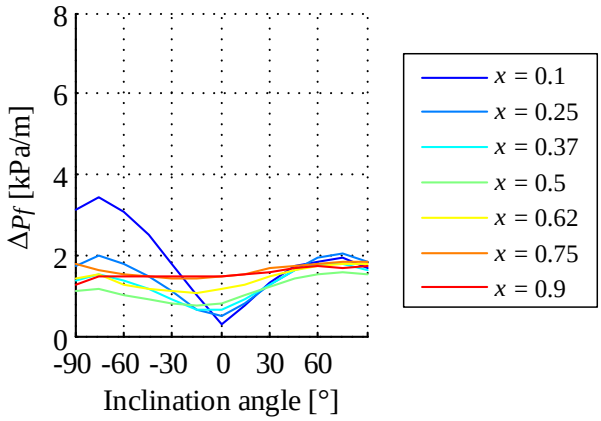

Figure 3-54. Evolution of the frictional pressure gradient as a function of the inclination angle (R134a, d = 8.38 mm; G = 200 kg/m²s)

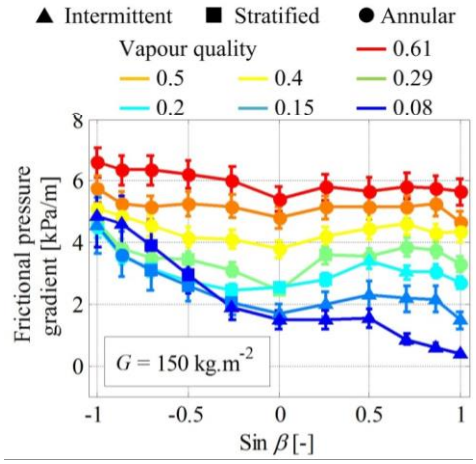

Figure 3-55. Evolution of the frictional pressure gradient as a function of the inclination angle for a mass velocity of 150 kg.m^{-2}.s^{-1} (Layssac et al., 2018a)

3.4.2 The notion of apparent gravitational pressure drop and void fraction

The determination of the frictional pressure drop relies on the prediction of the void fraction of the two-phase flow, which has a huge importance in eq. (3-9). To plot the figure 3-54, the Steiner (1993) version of the correlation of Rouhani and Axelsson (1970) is used. Even if this correlation is considered reliable in the literature, at least for horizontal two-phase flows, we can question its validity in our experimental conditions. An error in the void fraction could explain the shape of the curves of figure 3-54, which present a minimum for the horizontal orientation. To check the sensibility of the total pressure drop evolution, the notion of apparent gravitational pressure drop is thus proposed.

It has previously been noticed that it is not possible to separate the frictional pressure drop and the gravitational pressure drop from the experimental measurements. However, we can define an apparent gravitational pressure drop, ΔP^*_{grav}, which is the difference between the pressure drops in inclined and horizontal orientation:

$$\Delta P^*_{grav} = \Delta P_{test} - (\Delta P_{test})_{\beta=0°} \tag{3-11}$$

The apparent gravitational pressure drop is equal to the actual gravitational pressure drop only if the frictional and momentum pressure drops remain constant, whatever the angle of inclination. Figure 3-56 represents the apparent gravitational pressure drop as a function of the sinus of the inclination angle for various mass fluxes and various vapour qualities. For upward flows, the apparent gravitational pressure drops increase linearly with the sinus of the inclination angles. Assuming that the frictional pressure drops remain constant in these conditions and according to Eq. (3-9), it can mean that the void fraction remains constant, whatever the inclination angle. The apparent gravitational pressure drop also logically increases when the vapour quality decreases as it leads to a decrease of the void fraction. For downward flows, the evolution of the apparent gravitational pressure drops is no longer linear with the sinus of the inclination angle. It shows that the frictional pressure drops and/or the void fraction are dependent on the angle of inclination. We can also note that for upward flows, the apparent gravitational pressure drops are almost insensitive to the mass flux. On the contrary, for downward flows, the mass flux has a strong effect on the pressure drops.

The difference of behaviour between downward and upward flows can be explained by the flow pattern analysis presented in the section 3.2.2. For upward flows, the flow pattern is mainly intermittent or annular. For intermittent flows, there is a strong interaction between the liquid and the vapour phase: the inclination angle has a weak effect on this interaction and the frictional pressure drops and the void fraction remain constant. Annular flows are mainly led by shear forces and the gravitational forces are negligible. As a consequence, the inclination angle has also almost no effect on the flow properties. Furthermore, for these two flow patterns, the void fraction is almost insensitive to the mass flux. On the contrary, for downward flows, stratified flows occur: this kind of flow is strongly dependent on the

gravitational forces and thus on the inclination angle of the tube. As a consequence, the slip ratio between the phases, the void fraction and the frictional pressure drops strongly depend on the inclination angle.

From the apparent gravitational pressure drop, it is then possible to determine an apparent void fraction, which is defined as the void fraction that would have led to the apparent gravitational pressure drop according to the homogeneous model:

$$\varepsilon^* = \frac{\rho_l - \rho_h^*}{\rho_l - \rho_v} \tag{3-12}$$

where ρ_h^* is the apparent density of the flow:

$$\rho_h^* = \frac{\Delta P_{grav}^*}{g L_{\Delta P} \sin\beta} \tag{3-13}$$

The apparent void fraction is equal to the actual void fraction only if the frictional pressure drops for the inclined orientation are the same as those for the horizontal orientation. However, keeping this limitation in mind, it is interesting to study the apparent void fraction as a function of the inclination angle. It is plotted in Figure 3-57 for G = 300 kg/m²s and for different vapour qualities. For upward flows, the apparent void fraction can be considered constant, at least for a void fraction higher than 0.25. For downward flows, the apparent void fraction increases when the inclination angle increases. For each curve, three markers representing different correlations are plotted. For β = 0°, the marker represent the value of the Steiner (1993) version of the correlation of Rouhani and Axelsson (1970). This correlation was developed for horizontal flows. The void fraction correlation of Chisholm (1973), which is supposed to be independent of the tube orientation, is plotted for β = 45°. Lastly, the Rouhani and Axelsson (1970) correlation for vertical tubes is plotted for β = 90°. We can note a relatively good agreement between the different correlations and the apparent void fraction for upward flows. In the same figure is plotted in thick lines the mean apparent void fraction for upward flows, which is determined by doing a linear regression of the apparent gravitational pressure drop as a function of the sinus of the inclination angle. The range of inclination angles used for the linear regression is -5° to 90°, which corresponds to the range where the curves can be considered as linear.

The experimental mean apparent void fractions as a function of the vapour quality for G = 300 kg/m²s are plotted in figure 3-58. The void fractions predicted by different correlations are also presented. A good agreement is observed between the experimental results and the correlations of Friedel (1979) and Chisholm (1973) which tends to show that the apparent void fraction can actually be a good estimation of the real void fraction in these configuration.

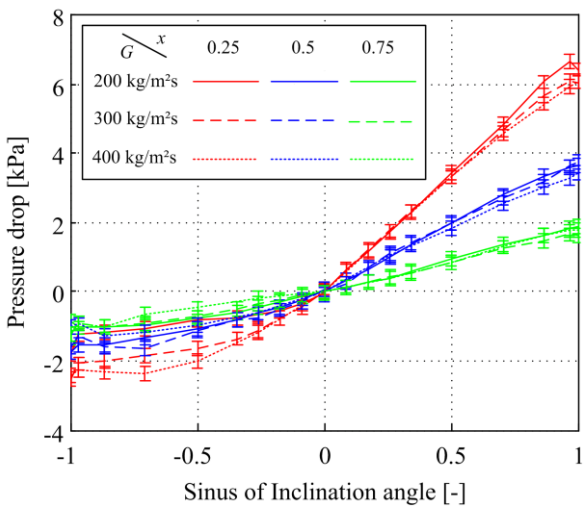

Figure 3-56. Apparent gravitational pressure drops for various vapour qualities and mass fluxes as a function of inclination angle (R134a, d = 8.38 mm) (Lips and Meyer, 2012b)

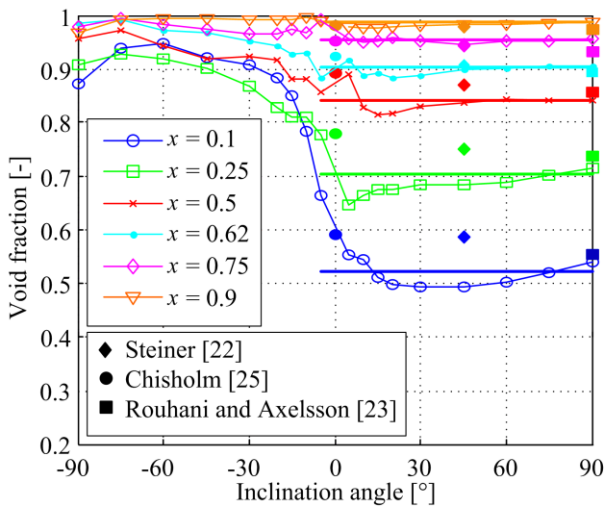

Figure 3-57. Effect of inclination angle on the apparent void fraction and comparison with different correlations (R134a, d = 8.38 mm, G = 300 kg/m²s). The thick horizontal lines represent the mean apparent void fraction between -5° and 90° (Lips and Meyer, 2012b)

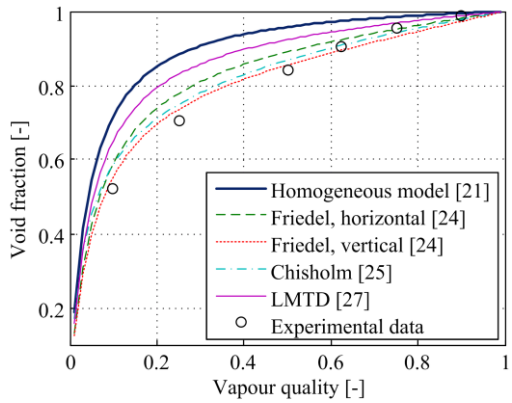

Figure 3-58. Apparent void fraction for horizontal and upward flows and comparison with different correlations (R134a, d = 8.38 mm, G = 300 kg/m²s) (Lips and Meyer, 2012b)

In conclusion, the apparent void fraction may be a possible estimation of the actual void fraction for upward flows. The linearity of the apparent gravitational pressure drops as a function of the sinus of the inclination angle tends to show that the frictional pressure drops and the void fraction can be considered constant in these conditions. This is not the case for downward flows where the inclination angle has a stronger influence on the flow pattern and thus on the frictional pressure drop and void fraction. Thus, for slightly inclined and downward flows, the apparent void fraction has not really any physical significance. This approach does not help either to understand the shape of the curves of figure 3-54 as the correlation of Steiner (1993) seems to predict well the void fraction for the horizontal orientation. Another approach can thus be proposed.

3.4.3 Theory or philosophy? Discussion on the physical meaning of pressure drop decomposition

In the present section, a discussion is proposed about the physical meaning of the pressure drop decomposition presented page 61 eq (3-8) and the way it is used in the literature. This study having not be published yet, the complete reflexion and equations are presented in this section.

3.4.3.1 Pressure drop decomposition by means of a two-phase separated model

Usually, the pressure drop decomposition is illustrated by means of two-phase separated model, as the one presented in figure 3-42. The velocity is supposed to be constant in the cross section of a phase but can be different in the two phases. This model is adapted to a progressive phase-change in a tube as the two phases can be present in one cross section. A_v and A_l are the area occupied in a cross section by the vapour and the liquid respectively. S_v, S_l and S_{int} are the length of vapour-wall, liquid-wall and liquid-vapour interfaces respectively. The void fraction ε is defined as the ratio between the area of a cross section occupied by the vapour A_v and the total area of the cross section A_{tot}. The tube is tilted with an angle β from the horizontal ($\beta > 0$ for upward flows and $\beta < 0$ for downward flows).

In steady-state separated flow, considering that the pressure is equal in the vapour and in the liquid in a cross-sectional area, the following two momentum equations are satisfied:

$$\frac{dP}{dz} = -\frac{\tau_{vw}S_v + \tau_i S_{int}}{A_v} - \rho_v g \sin\beta - \frac{\rho_v}{\varepsilon}\frac{d\varepsilon u_v^2}{dz} \tag{3-14}$$

$$\frac{dP}{dz} = -\frac{\tau_{lw}S_l - \tau_i S_{int}}{A_l} - \rho_l g \sin\beta - \frac{\rho_l}{1-\varepsilon}\frac{d(1-\varepsilon)u_l^2}{dz} \tag{3-15}$$

Note that for each phase, the pressure drop can be decomposed in terms of frictional, gravitational and momentum pressure drops:

$$\Delta P_{fric,v} = -\frac{\tau_{vw}S_v + \tau_i S_{int}}{A_v};\ \Delta P_{grav,v} = -\rho_v g \sin\beta;\ \Delta P_{mom,v} = -\frac{\rho_v}{\varepsilon}\frac{d\varepsilon u_v^2}{dz} \tag{3-16}$$

$$\Delta P_{fric,l} = -\frac{\tau_{lw}S_l - \tau_i S_{int}}{A_l};\ \Delta P_{grav,l} = -\rho_l g \sin\beta;\ \Delta P_{mom,l} = -\frac{\rho_l}{1-\varepsilon}\frac{d(1-\varepsilon)u_l^2}{dz} \tag{3-17}$$

To define a pressure drop decomposition for the two-phase flow, Equations (3-14) and (3-15) can be combined. For instance, a weighed summation of Equations (3-14) and (3-15) can be done with any arbitrarily coefficients w_v and w_v:

$$(w_v + w_l)\frac{dP}{dz} = -w_v\left(\frac{\tau_{vw}S_v + \tau_i S_{int}}{A_v}\right) - w_l\left(\frac{\tau_{lw}S_l - \tau_i S_{int}}{A_l}\right) - (w_v\rho_v + w_l\rho_l)g\sin\beta - \left(w_v\frac{\rho_v}{\varepsilon}\frac{d\varepsilon u_v^2}{dz} + w_l\frac{\rho_l}{1-\varepsilon}\frac{d(1-\varepsilon)u_l^2}{dz}\right) \quad (3\text{-}18)$$

As a result, the pressure drop can be decomposed in three terms:

$$\frac{dP}{dz} = \left(\frac{dP}{dz}\right)^*_{fric} + \left(\frac{dP}{dz}\right)^*_{grav} + \left(\frac{dP}{dz}\right)^*_{mom} \quad (3\text{-}19)$$

With

$$\left(\frac{dP}{dz}\right)^*_{fric} = -\frac{w_v}{w_v + w_l}\left(\frac{\tau_{vw}S_v + \tau_i S_{int}}{A_v}\right) - \frac{w_l}{w_v + w_l}\left(\frac{\tau_{lw}S_l - \tau_i S_{int}}{A_l}\right) \quad (3\text{-}20)$$

$$\left(\frac{dP}{dz}\right)^*_{grav} = -\rho^*_{eq}g\sin\beta \text{ with } \rho^*_{eq} = \frac{w_v\rho_v + w_l\rho_l}{w_v + w_l} \quad (3\text{-}21)$$

$$\left(\frac{dP}{dz}\right)^*_{mom} = -\frac{w_v}{w_v + w_l}\frac{\rho_v}{\varepsilon}\frac{d\varepsilon u_v^2}{dz} - \frac{w_l}{w_v + w_l}\frac{\rho_l}{1-\varepsilon}\frac{d(1-\varepsilon)u_l^2}{dz} \quad (3\text{-}22)$$

Thus, we can define an infinite number of pressure drop decomposition depending on the choice of the coefficients w_v and w_v. All these decompositions are mathematically correct, but they do not have necessarily a physical meaning.

A traditional choice of the coefficient is $w_v = A_v$ and $w_v = A_l$. The decomposition becomes:

$$\left(\frac{dP}{dz}\right)^{trad}_{fric} = -\left(\frac{\tau_{vw}S_v + \tau_{lw}S_l}{A_{tot}}\right) \quad (3\text{-}23)$$

$$\left(\frac{dP}{dz}\right)^{trad}_{grav} = -\rho^{trad}_{eq}g\sin\beta \text{ with } \rho^{trad}_{eq} = \varepsilon\rho_v + (1-\varepsilon)\rho_l \quad (3\text{-}24)$$

$$\left(\frac{dP}{dz}\right)^{trad}_{mom} = -\rho_v\frac{d\varepsilon u_v^2}{dz} - \rho_l\frac{d(1-\varepsilon)u_l^2}{dz} = -G^2\frac{d}{dz}\left(\frac{x^2}{\rho_v\varepsilon} + \frac{(1-x)^2}{\rho_l(1-\varepsilon)}\right) \quad (3\text{-}25)$$

It is possible to show that the traditional momentum pressure drop is also equal to:

$$\left(\frac{dP}{dz}\right)^{trad}_{mom} = -\frac{1}{2}\tilde{\rho}\frac{d\tilde{u}^2}{dz} \quad (3\text{-}26)$$

With $\tilde{u} = xu_v + (1-x)u_l$ and $\tilde{\rho} = \frac{G}{\tilde{u}} = \frac{\varepsilon\rho_v u_v + (1-\varepsilon)\rho_l u_l}{xu_v + (1-x)u_l} = \frac{\varepsilon\rho_v u_v^2 + (1-\varepsilon)\rho_l u_l^2}{(xu_v + (1-x)u_l)^2}$

The physical meaning of ρ^{trad}_{eq} and $\tilde{\rho}$ must be questioned. ρ^{trad}_{eq} would be the ratio between the mass of the fluid present in a portion of the tube and the volume of this portion. Such a definition does not really have any thermodynamic sense because of the vapour and liquid in the tube cannot be considered as a unique fluid as they do not have the same velocity: there are not at equilibrium and the corresponding thermodynamic relations do not apply. The control volume delimited by the portion of the tube must be considered as an open system and the thermodynamic relations applied on each phases, defined by their properties and their mass flux. $\tilde{\rho}$ and $\tilde{u}$ are mathematically defined and represent other equivalent parameters of the fluid, but they do not seem to have a real physical meaning. Note that $\tilde{\rho}$ and ρ^{trad}_{eq} are equal to the thermodynamic definition of the two-phase density only for a homogeneous flow, i. e. for a flow were the slip ratio is equal to 1.

This decomposition is widely used in the literature; however, it does not have more physical meaning than any other decomposition obtained with other coefficients w_v and w_v. For Collier and Thome (1996) this decomposition is based on the conservation of momentum but they did not accord any importance to the physical meaning of their mathematical approach. Collier and Thome (1996) also proposed a different decomposition, based on the energy conservation. The result of this decomposition can be found using the coefficients $w_v = \varepsilon_h$ and $w_v = 1- \varepsilon_h$, where ε_h is the void fraction considering an homogenous flow. It gives:

$$\left(\frac{dP}{dz}\right)_{fric}^{energy} = -\varepsilon_h \frac{(\tau_{vw}S_v+\tau_i S_i)}{A_v} - (1-\varepsilon_h)\frac{(\tau_{lw}S_l-\tau_i S_i)}{A_l} \tag{3-27}$$

$$\left(\frac{dP}{dz}\right)_{grav}^{energy} = -\rho_{tp} g \sin\beta \text{ with } \rho_{tp} = \frac{1}{v_{tp}} = \frac{1}{xv_v+(1-x)v_l} \tag{3-28}$$

$$\left(\frac{dP}{dz}\right)_{mom}^{energy} = -\frac{1}{2}\rho_{tp}\frac{du_{tp}^2}{dz} \text{ with } u_{tp}^2 = xu_v^2 + (1-x)u_l^2 \tag{3-29}$$

The two-phase density ρ_{tp} is equal to the equivalent density calculated with the homogeneous model. It corresponds to the definition of the density in the two-phase zone of a thermodynamic diagram. For an open system, ρ_{tp} can also be seen as the ratio between the total mass flux $\dot{m}_t$ and the total volumetric flow rate $\dot{V}_t$ in a cross-section of the tube:

$$\rho_{tp} = \frac{1}{v_{tp}} = \frac{1}{xv_v + (1-x)v_l} = \frac{\dot{m}_t}{v_v\dot{m}_v + v_l\dot{m}_l} = \frac{\dot{m}_t}{\dot{V}_t} \tag{3-30}$$

These two approaches give different results in terms of momentum and gravitational pressure drops, and thus on the experimental determination of the frictional pressure drops. For instance, in the case of the experimental results presented in (Lips and Meyer, 2012a, 2012b) for condensing flow of R134a in a 8.38 mm inner diameter tube, frictional pressure drop were calculated with the traditional approach (using the Steiner (1993) version of the correlation of Rouhani and Axelsson (1970)). If the difference of momentum pressure drop calculated with the traditional (momentum) and energy approach was relatively low (figure 3-59), the gravitational pressure drop can be multiplied by more than 2 when using the traditional approach compared to the traditional one (figure 3-60). As a consequence, the frictional pressure drop determination would have been different (figure 3-61).

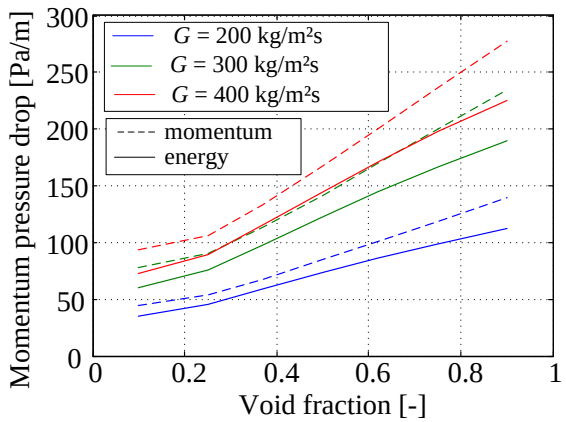

Figure 3-59. Comparison of the momentum pressure drop calculated by the traditional and the energy approach (Lips and Revellin, 2013)

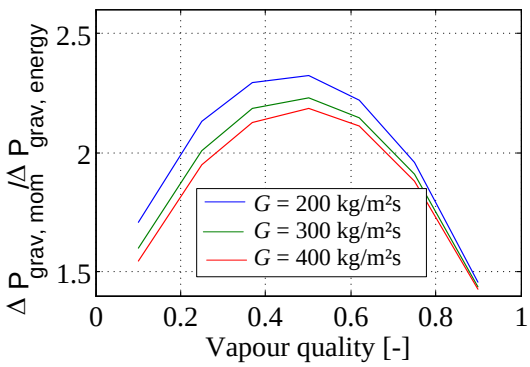

Figure 3-60. Comparison of the gravitationnal pressure drop calculated by the traditional and the energy approach (Lips and Revellin, 2013)

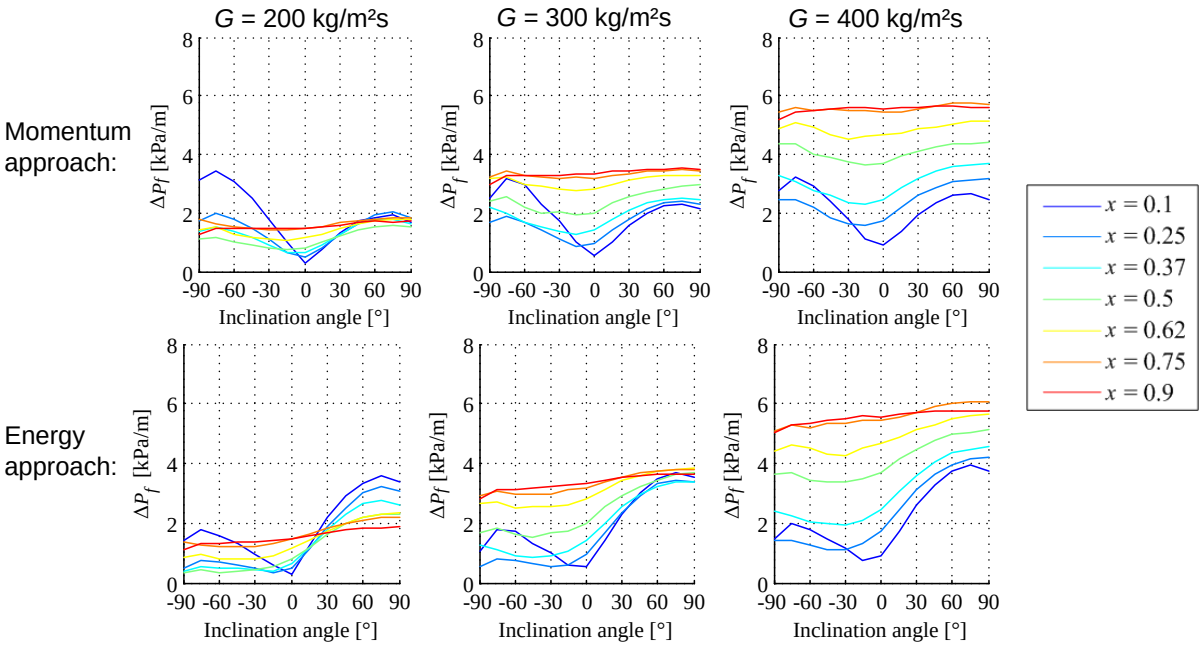

Figure 3-61. Impact of the approach for the frictional pressure drop determination (Lips and Revellin, 2013)

As a conclusion, the two decompositions are different and the value of the frictional, gravitational and momentum pressure drops are not the same depending on which approach is chosen. Collier and Thome (1996) do not really conclude about the validity of each decomposition. The equivalent density that appears in the second approach (energy conservation) has a physical meaning whereas it is not the case for the traditional approach (momentum conservation). However, another criterion has to be chosen to discuss the validity of each approach.

3.4.3.2 Pressure drop decomposition for single-phase non-compressible flow

To understand the notion of pressure drop decomposition, it is important to refer firstly to the case of a non-compressible flow with the 1-D approximation. This case is well known in the literature but is useful in the present study to introduce the concept of the pressure drop decomposition.

The first law of thermodynamics for single-phase flow with a constant mass flux $\dot{m}$ can be written as:

$$\dot{m}d(h^0) = \delta W_t + \delta Q \tag{3-31}$$

$\delta\dot{W}_t$ and $\delta\dot{Q}$ are the mechanical work and the heat exchanged with the surroundings respectively. h^0 is the total enthalpy of the fluid, defined in the 1-D approximation as:

$$h^0 = h + gz + \frac{1}{2}u^2 \tag{3-32}$$

The second law of thermodynamics enables to write the entropy generation dS':

$$dS' = \dot{m}ds - \frac{\delta Q}{T_w} \tag{3-33}$$

T_w is the wall temperature. For a non-compressible flow ($\rho = \text{cst}$) with reversible heat transfer ($T_w = T$, T being the fluid temperature), without exchange of mechanical work with the surroundings ($\delta\dot{W}_t = 0$), and using the thermodynamic relation: $dh = vdP - Tds$, equations (3-33) can be written as:

$$dS' = -\frac{\dot{m}v}{T}d\left(P + \rho gz + \frac{1}{2}\rho u^2\right) \tag{3-34}$$

The sum of the terms in the brackets is called the total pressure of the fluid. It is the sum of the thermodynamic pressure P (also called static pressure), the gravitational pressure P_{grav} and the dynamic pressure P_{dyn}:

$$P_{tot} = P + P_{grav} + P_{dyn} \tag{3-35}$$

With:

$$P_{grav} = \rho g z \tag{3-36}$$

$$P_{dyn} = \frac{1}{2}\rho u^2. \tag{3-37}$$

It is possible to define an irreversible pressure drop $\left(\frac{dP}{dx}\right)_{irr}$, which is the part of pressure drop that participates to the entropy generation. As a result of equation (3-34), for a non-compressible flow, the irreversible pressure drop is equal to the variation of total pressure in the flow. Another concept widely used is the total hydraulic head of a fluid which is defined by: $H_{tot} = \frac{P_{tot}}{\rho g} = \frac{P}{\rho g} + z + \frac{u^2}{2g}$. For a inviscid flow (no friction), the total hydraulic head is constant in a fluid along a streamline. This result is called in the literature as the Bernoulli's principle.

From the total pressure definition, the irreversible pressure drop can be expressed as:

$$\left(\frac{dP}{dx}\right)_{irr} = \frac{d}{dx}(P_{tot}) = \frac{d}{dx}(P) + \frac{d}{dx}(P_{grav}) + \frac{d}{dx}(P_{dyn}) \tag{3-38}$$

Note that the distinction is done in the mathematical notations between the variations of a type of pressure $\frac{d}{dx}(P_i)$, where *i* can refer to thermodynamic, dynamic, gravitational or total pressure, and a part of the variation of the thermodynamic pressure due to specific phenomena $\left(\frac{dP}{dx}\right)_j$, where *j* can refer to the gravitational, acceleration or frictional forces.

The variation of the actual thermodynamic pressure *P*, called total pressure drop in the present paper despite the fact that it is not the variation of the total pressure, can be decomposed in three terms:

$$\frac{dP}{dx} = \frac{d}{dx}(P) = \left(\frac{dP}{dx}\right)_{irr} + \left(\frac{dP}{dx}\right)_{grav} + \left(\frac{dP}{dx}\right)_{mom} \tag{3-39}$$

$\left(\frac{dP}{dx}\right)_{irr}$ is the pressure drop due to the irreversibilities (frictions) .

$\left(\frac{dP}{dx}\right)_{grav}$ is the pressure drop due to the gravitational forces. It is related to the variation of the gravitational pressure. For a tube tilted with an angle β from the horizontal ($\beta > 0$ for upward flows and $\beta < 0$ for downward flows), Eq. (3-38) gives:

$$\left(\frac{dP}{dx}\right)_{grav} = -\frac{d}{dx}(P_{grav}) = -\rho g \sin\beta \tag{3-40}$$

$\left(\frac{dP}{dx}\right)_{mom}$ is the pressure drop due to the change of momentum of the fluid. It is related to the variation of the dynamic pressure:

$$\left(\frac{dP}{dx}\right)_{mom} = -\frac{d}{dx}(P_{dyn}) = -\frac{1}{2}\rho\frac{du^2}{dx} \tag{3-41}$$

In non-compressible single phase flows, the decomposition of the pressure drop comes directly from the variation of the different terms of the total pressure decomposition, the actual thermodynamic pressure being only one of these terms. Each term of the decomposition has directly a physical sense: In absolute value, the gravitational and momentum pressure drops are equal to the variation of the gravitational and dynamic pressure respectively. The frictional, or irreversible, pressure drop is the residue.

The total pressure definition itself is based on the entropy generation equations and the Bernoulli's principle. The next section deals with the adaptation of the notions developed for non-compressible single-phase flows to two-phase flows.

3.4.3.3 Entropy generation analysis as a criterion of choice

The first law of thermodynamics for an open two-phase flow system, with no work exchange with its environment, can be written as:

$$d\left(\dot{m}_l h_l^0\right) + d(\dot{m}_v h_v^0) = \delta Q \tag{3-42}$$

Note that $\delta Q > 0$ for evaporation and $\delta Q < 0$ for condensation. h^0 is the total enthalpy of the fluid: $h^0 = h + \frac{1}{2}u^2 + gz$. Equation (3-42) can be rewritten as:

$$(1-x)dh_l^0 + xdh_v^0 + \left(h_v^0 - h_l^0\right)dx = \frac{\delta Q}{\dot{m}_t} \tag{3-43}$$

With the definition of the total enthalpy, it gives:

$$(1-x)dh_l + xdh_v + h_{lv}dx + g\sin\beta\, dz + \frac{1}{2}\left((1-x)du_l^2 + xdu_v^2 + \left(u_v^2 - u_l^2\right)dx\right) = \frac{\delta Q}{\dot{m}_t} \tag{3-44}$$

We can define a two-phase enthalpy, h_{tp}, and a two-phase velocity, u_{tp}, as $h_{tp} = xh_v + (1-x)h_l$ and $u_{tp}^2 = xu_v^2 + (1-x)u_l^2$. Eventually, the first law of thermodynamic can be written as:

$$dh_{tp} = \frac{\delta Q}{\dot{m}_t} - g\sin\beta\, dz - \frac{1}{2}du_{tp}^2 \tag{3-45}$$

The second law of thermodynamics can be written as:

$$dS'dz = d(\dot{m}_v s_v + \dot{m}_l s_l) - \frac{\delta Q}{T_w} \tag{3-46}$$

With $s_{tp} = xs_v + (1-x)s_l$ and thus $ds_{tp} = xds_v + (1-x)ds_l + s_{lv}dx$, the equation becomes:

$$dS'dz = \dot{m}_t ds_{tp} - \frac{\delta Q}{T_w} \tag{3-47}$$

Moreover, by definition, we have: $ds_v = \frac{dh_v - v_v dP}{T_{sat}}$ and $ds_l = \frac{dh_l - v_l dP}{T_{sat}}$, so:

$$ds_{tp} = \frac{xdh_v + (1-x)dh_l - (xv_v + (1-x)v_l)dP + T_{sat}s_{lv}dx}{T_{sat}} \tag{3-48}$$

Considering that $dh_{tp} = xdh_v + (1-x)dh_l + h_{lv}dx$, and $h_{lv} - T_{sat}s_{lv} = 0$, it gives:

$$ds_{tp} = \frac{dh_{tp} - v_{tp}dP}{T_{sat}} \tag{3-49}$$

with $v_{tp} = xv_v + (1-x)v_l$. Thus, using the result of the first law of thermodynamic, the entropy generation can be written as:

$$dS'dz = \delta Q\left(\frac{1}{T_{sat}} - \frac{1}{T_w}\right) - \frac{\dot{m}_t}{T_{sat}}\left(v_{tp}dP + g\sin\beta\, dz + \frac{1}{2}du_{tp}^2\right) \tag{3-50}$$

The first term of the right side of the equation can be written as a function of the heat flux and the heat transfer coefficient by assuming that $|T_w - T_{sat}|/T_{sat} \ll 1$. Dividing both sides by *dz*, it gives:

$$dS' = \frac{q^2 p}{hT_{sat}^2} - \frac{\dot{m}_t}{T_{sat}}\left(v_{tp}\frac{dP}{dz} + g\sin\beta + \frac{1}{2}\frac{du_{tp}^2}{dz}\right) \tag{3-51}$$

wich can be written as:

$$dS' = \frac{q^2 p}{hT_{sat}^2} - \frac{\dot{m}_t v_{tp}}{T_{sat}}\left(\frac{dP}{dz} + \rho_{tp}g\sin\beta + \frac{1}{2}\rho_{tp}\frac{du_{tp}^2}{dz}\right) \tag{3-52}$$

As a conclusion, the entropy generation is the sum of two different terms:

- The entropy generation due to the thermal resistance during the heat transfer: $\frac{q^2 p}{hT_{sat}^2}$.
- The entropy generation due to the pressure drops: $-\frac{\dot{m}_t v_{tp}}{T_{sat}}\left(\frac{dP}{dz}+\rho_{tp} g \sin\beta+\frac{1}{2}\rho_{tp}\frac{du_{tp}^2}{dz}\right)$.

The first term represents the degradation of the thermal exergy of the heat because of the temperature drop. It will not be further considered in the present study.

The second term enables to add a physical meaning of the pressure drop decomposition. Equation (3-52) states that only a part of the pressure drops, $\left(\frac{dP}{dz}\right)_{irr}$, participates to the creation of entropy:

$$\left(\frac{dP}{dz}\right)_{irr}=\frac{dP}{dz}+\rho_{tp} g \sin\beta+\frac{1}{2}\rho_{tp}\frac{du_{tp}^2}{dz} \tag{3-53}$$

The traditional pressure drop decomposition leads to unphysical results as it would imply than a part of the gravitational and momentum pressure drops would participate to the entropy creations. We get:

$$\left(\frac{dP}{dz}\right)_{irr}=\left(\frac{dP}{dz}\right)_{fric}^{trad}+\left(\rho_{tp}-\rho_{eq}^{trad}\right) g \sin\beta+\frac{1}{2}\left(\rho_{tp}\frac{du_{tp}^2}{dz}-\tilde{\rho}\frac{d\tilde{u}^2}{dz}\right) \tag{3-54}$$

As a consequence, the entropy generation due to the pressure drop would be the sum of three different terms:

- The entropy generation due to the frictional pressure drops:
  $dS'_{fric}=-\frac{\dot{m}_t v_{tp}}{T_{sat}}\left(\frac{dP}{dz}\right)_{fric}^{trad}$.
- The entropy generation due to the gravitational energy variation:
  $dS'_{grav}=-\frac{\dot{m}_t v_{tp}}{T_{sat}}\left(\rho_{tp}-\rho_{eq}^{trad}\right) g \sin\beta$.
- The entropy generation due to the kinetic energy variation:
  $dS'_{mom}=\frac{1}{2}\left(\rho_{tp}\frac{du_{tp}^2}{dz}-\tilde{\rho}\frac{d\tilde{u}^2}{dz}\right)$

On the other hand, according to the decomposition based on the energy conservation, we get:

$$\left(\frac{dP}{dz}\right)_{irr}=\left(\frac{dP}{dz}\right)_{fric}^{energy} \tag{3-55}$$

The entropy generation is only due to the frictional pressure drop, which is a logical result as the pressure drops due to gravitational forces and acceleration are due to reversible phenomena. This decomposition corresponds to a thermodynamic valid decomposition, contrary to the traditional pressure drop.

As a conclusion, the expressions of the frictional, gravitational and momentum pressure drops defined from this thermodynamic point of view (equations (3-27)-(3-29)) are different than the expressions usually used in the literature (equations (3-23)-(3-25)). The two set of expressions are only equal for a homogeneous flow, where the slip ratio is equal to 1. Under these conditions, we have $\rho_{eq}=\rho_{tp}=\tilde{\rho}=\rho_h$ and $u_l=u_v$. For non-homogeneous flows, it appears than the definitions of the pressure drop used in the literature do not seem to have an actual physical or thermodynamic signification. The logic would thus enforce the use of the energy approach decomposition. In order to validate this approach, more experiments are required to measure the void fraction of two-phase flows in inclined configuration. Building an important database would help to highlight the difference between the two approaches.

However, both approaches are mathematically correct and they can be seen as an engineering tool for the development of models and correlations. As all correlations were performed with the momentum approach, the validity of the results presented in the literature is not questioned. The use of a more physical decomposition could maybe have helped to improve the accuracy of the correlations but the coexistence of the two approaches may be dangerous for the scientific community. As a consequence, the present discussion may remain more philosophical than practical...

3.4.4 An optimum inclination angle in terms of Entropy generation?

Whatever the physical meaning of the pressure drop decomposition, the entropy generation analysis remains an interesting tool to study the performance of an evaporator or a condenser. In the present section, a study dedicated to the inclination optimisation of a condenser is summarizes as an example of potential application.

Usually, when performing an entropy analyses, one tries to minimize the entropy generation of the process (eq (3-52)). In the case of a condenser included in a heat pump, it can be shown (Lips and Meyer, 2012d) that the minimization of the entropy generation in a condenser is equivalent to the minimization of the difference between the hot source temperature and the saturation temperature at the condenser inlet, called $\Delta T_{cond,init}$ in the following (figure 3-62).

This difference of temperature is due to two phenomena: the heat transfer between the working fluid and the hot source and the pressure drop along the condenser itself. In (Lips and Meyer, 2012d), we proposed both an analytical model and a numerical model to predict the value of $\Delta T_{cond,init}$ in various configurations.

The analytical model enables to determine $\Delta T_{cond,init}$ to get full condensation with a specific condenser length L:

$$\Delta T_{cond,init} = \frac{\dot{m} h_{lv}}{\bar{h} L p} - \frac{L}{2}\frac{T_{sat}}{h_{lv}}\left(\frac{1}{\rho_v} - \frac{1}{\rho_l}\right)\frac{\overline{dP}}{dz} \tag{3-56}$$

$\bar{h}$ and $\overline{dP/dz}$ are the average heat transfer coefficient and pressure drop during the fluid condensation. Note that this expression is equivalent to what Cavallini et al. (2010) call Total Temperature Penalization (TTP). Thereby, the present study gives another signification to this parameter.

The numerical model is based on the discretisation along the tube, the irreversibilites being calculated for each section, taking into account the local heat transfer coefficient and pressure drops.

The measurements of heat transfer coefficients and pressure drops as a function of the vapour quality, the mass velocity and the tube inclination presented in sections 3.3.2 and 3.4.1 enable to calculate the value of $\Delta T_{cond,init}$ for a condenser length of 5 m as a function of the tube inclination and for various mass velocities (figure 3-63). This example shows that it exists, from a thermodynamic point of view, an optimum inclination angle that leads to the lowest temperature difference between the hot source and the fluid at the condenser inlet. In the present study, it ranges between -15° and -30° and is more significant for lower mass fluxes and for lower condenser length (figure 3-64). This optimization approach can also be seen as a way to minimize the condenser length for a fix temperature difference at the inlet of the condenser (figure 3-65), this one being often chosen by a rule of thumb when designing a heat pump system. This example deals only with the design of the condenser, but the whole system would have to be optimized, especially from a geometrical point of view, because of the difference of altitude induced by tilted tubes.

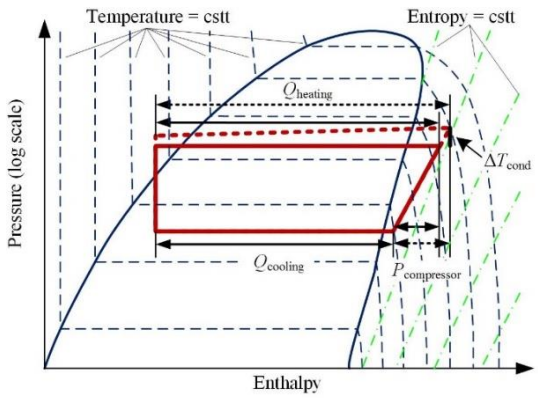

Figure 3-62. Thermodynamic cycle of a heat pump. Solid lines: optimal cycle. Dashed lines: cycle considering irreversibilities in the condenser (Lips and Meyer, 2012d)

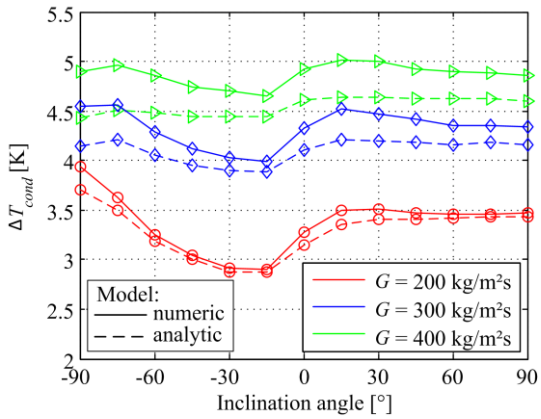

Figure 3-63. Determination of the initial temperature difference of condensation for L = 5 m (Lips and Meyer, 2012d)

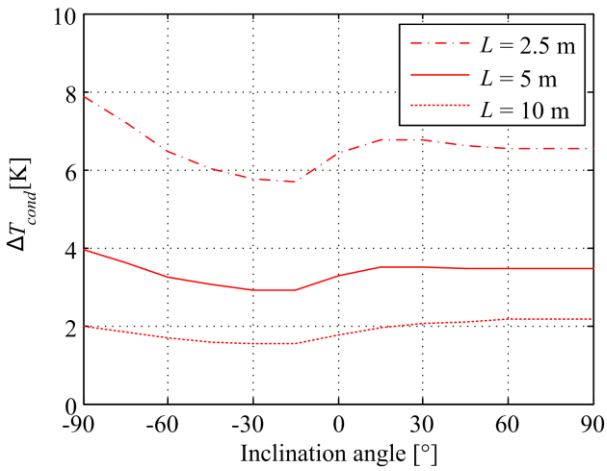

Figure 3-64. Effect of the condenser length (G = 200 kg/m²s) (Lips and Meyer, 2012d)

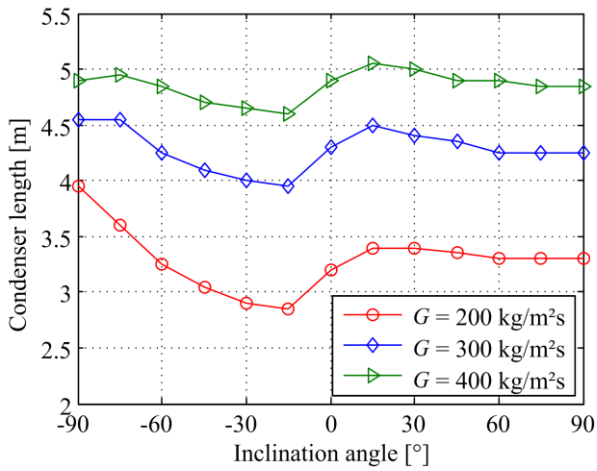

Figure 3-65. Determination of the condenser length for an initial temperature difference of condensation equal to 5 K (Lips and Meyer, 2012d)

As a conclusion, entropy generation studies can help to design a system by considering simultaneously the heat transfer coefficient and the pressure drop of the two-phase flow. It has been chosen in the present example to use the difference between the hot source temperature and the saturation temperature at the condenser inlet, but it can enlarged to any system if considering directly the entropy generation. This kind of study becomes to be more common in the scientific literature, but there is still a need for transferring this type of tool to the engineering community.

3.5 Conclusions and perspectives

The study of two-phase flows in inclined tubes is an interesting way to analyse the balance of the various forces involved in various configurations. From an experimental point of view, the inclination effect can be summarized by the drawing of maps corresponding to the flow pattern inclination effect (figure 3-66), the heat transfer coefficient inclination effect (figure 3-67), or the apparent void fraction inclination effect (figure 3-68). The latter is defined by the relative variation of apparent void fraction when the inclination angle varies. By considering arbitrarily that the flow is not getting affected by the gravity forces when the inclination effect is lower than 10%, it is thus possible to draw an overall map of the gravity independent and gravity dependent two-phase flow zones (figure 3-69). This kind of map would be interesting to know in which conditions specific correlations, which take into account the inclination angle, should be used, or developed if not available.

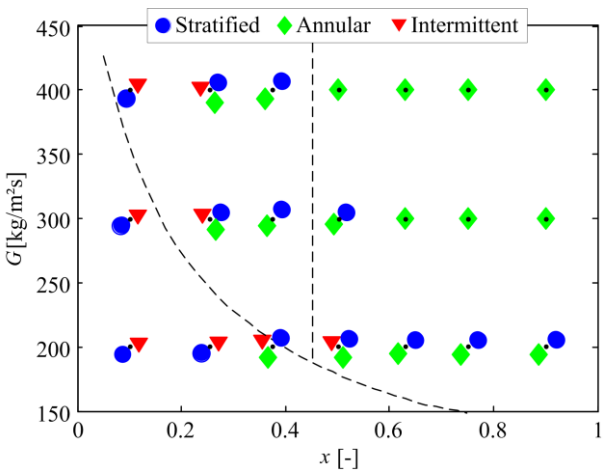

Figure 3-66. Map of the inclination effect on the flow pattern (R134a, d = 8.38 mm) (Lips and Meyer, 2012e)

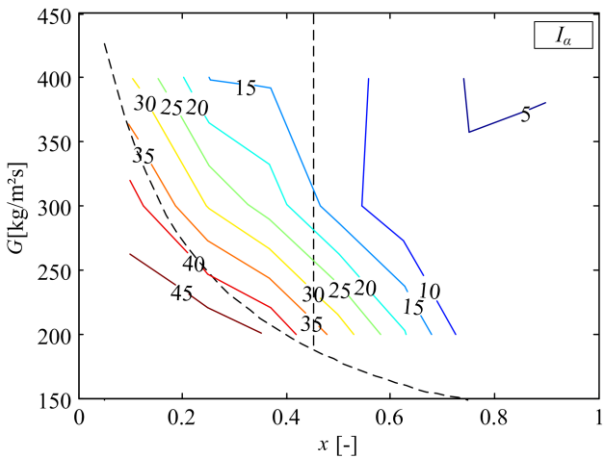

Figure 3-67. Map of the inclination effect on the heat transfer coefficient (R134a, d = 8.38 mm) (Lips and Meyer, 2012e)

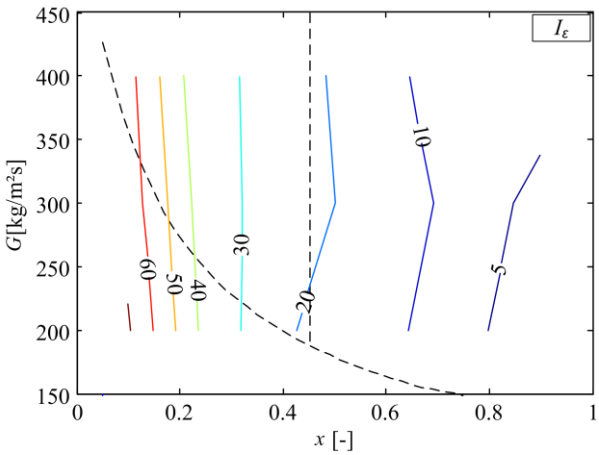

Figure 3-68. Map of the inclination effect on the apparent void fraction (R134a, d = 8.38 mm) (Lips and Meyer, 2012e)

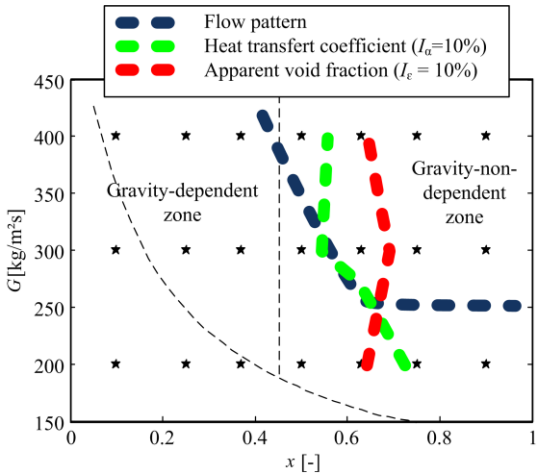

Figure 3-69. General map of the inclination effect (R134a, d = 8.38 mm) (Lips and Meyer, 2012e)

This type of studies open many research perspectives.

In my point of view, it is of major importance to continue to perform experimental studies in various configurations. Besides the inclination angle, the effect of the tube shape and singularities and that of specific fluids (mixture, self-rewetting fluids, non-Newtonian fluids) still need to be better understood.

These experimental set-ups must include advanced and innovative systems for the flow characterisation. The utilisation of transparent test sections is a first step, but new void fraction detectors and other sensors enabling to study the velocity profiles in each phase of the flows should also be developed. There is a strong lack of information, which limit the possibility of validation of the mechanistic models available in the literature. Others methods as X-ray visualisations and fluorescence and phosphorescence techniques could also be used.

The further development of numerical models should also help to improve the understanding of the two-phase flow behaviour. Various models, at various space and time scales, can still be improved. We need models able to predict the onset of nucleation or the dropwise/filmwise condensation but also models able to take into account correctly the interfacial interactions and the merging/splitting of the bubbles. Even at the scale of the phase change heat transfer itself, model can be improved, for instance through dynamic molecular simulations. Of course, all these models require more experiments in order to validate them.

I also strongly believe that quick major advances could be obtained if there were more exchanges between the scientific communities of saturated two-phase flows (mainly linked to the thermal sciences), gas-liquid two-phase flows (mainly linked to fluid mechanic sciences) and to liquid-liquid two-phase flows (mainly linked to chemical sciences). The convergence between the various approaches should be of a great interest.

Besides experimental and numerical studies, I also believe in the strength of purely theoretical studies. A major limitation in the field of saturated two-phase flow is the absence of complete non-dimensional analyses. If this situation can be explained by the high number of phenomena involved in these systems, it does not mean it is impossible and I think the limitation is today more cultural than physical. The scientific community of two-phase flows is used to correlations and empirical models. They actually proved their utility and efficiency, but on my point of view, it remains a limitation today. Maybe this situation will evolve in a close future, as the need for theoretical models is also highlighted by the fact that many new studied configurations can often no longer be considered as in a thermodynamic equilibrium. The outcomes of the non-equilibrium thermodynamic scientific field could thus be of a great use for a better understanding of two-phase flows.

To conclude, the study of two-phase flows will probably remain an amazing playing field for many researchers for a long time: there is room for every approaches, from that of the “plumber” to that of the nano-scale study of nucleation process and dynamic molecular!

Chapter 4: Passive systems using the solid-liquid phase change: the notion of thermal damper

4.1 Principle and general overview of the applications

Liquid-vapour phase change cooling systems enable to dissipate high heat fluxes with a low temperature gradient. However, in many applications, electronic components are subjected to highly transient heat fluxes. In the latter, it can be interesting to smooth the component temperature variation by means of a thermal storage system, typically based on a phase change material (PCM). Amongst all types of PCM (figure 4-1), paraffins are well adapted for the electronic components thermal management, thanks to their range of solid-liquid phase change temperature (30 - 120°C) and to their high latent heat of phase change (100 kJ kg^{-1} to 300 kJ kg^{-1}).

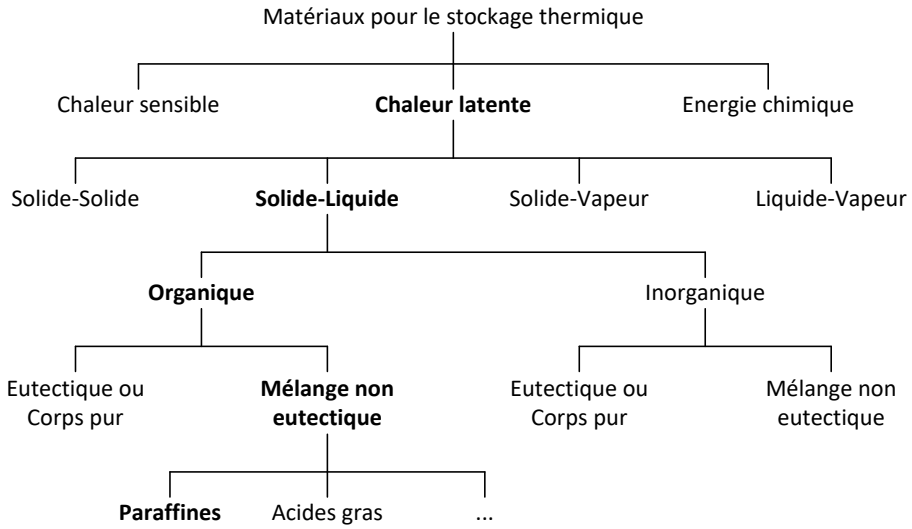

Figure 4-1. Classification of the various material used for thermal storage applications (Kinkelin, 2016; after Zalba et al., 2003)

However, the main drawback of PCMs is their low thermal conductivity. Thermal conductivity enhancement through insertion of dispersed high-conductivity nanostructures into PCMs (carbon-based nanostructures, carbon nanotubes, metallic and metal oxide nanoparticles and silver nanowires) leads to an effective thermal conductivity up to only twice that of PCMs (Khodadadi et al., 2013). The thermal conductivity of such composite PCMs remains small because of the high thermal resistance between neighboring high-conductivity elements. A much better thermal conductivity enhancement is reported when a thermal link exists between the particles, thus forming a single non-moving conductive matrix like graphite nanofibers with a high aspect-ratio (Fan et al., 2015),with controlled graphite plane orientation (Weinstein et al., 2008) or a graphite matrix (Mills et al., 2006). However, the interactions between the PCM, the nanoparticles and a potential additional structure are far from being completely understood and further numerical and experimental studies are still necessary (Hossain et al., 2015).

Ling et al. (2014) and Sahoo et al. (2016) performed two extensive literature reviews on the use of PCM for electronic cooling and it appears that the most recent studies on passive cooling of electronics with PCM are based on the addition of PCM in an external structure. PCM can be embedded between the fins of a traditional heat sink (Gharbi et al., 2015; Jaworski, 2012; Kandasamy et al., 2008; Setoh et al., 2010; Wang et al., 2007) or between high conductivity carbon walls with CNTs added into the PCM (Shaikh and Lafdi, 2010). In this configuration, the main issue is to predict the heat transfer in the PCM and particularly the evolution of the phase-change front in the system. PCM integration in an array of micro-reservoirs etched in a silicon substrate in order to stabilize the surface temperature during short transient thermal solicitations is also reported but this type of studies is very rare. For instance Muratore et al. (Muratore et al., 2012) studies micro-inclusions of PCM, but the areal thermal energy storage density remained small (about 800 J/m²). The design, fabrication and characterization of such systems remain very challenging.

Based on these considerations, the goal of the ANR THERMA3D project (2011-2014) was to design, manufacture and characterize a thermal damper directly implemented in the silicon substrate of the electronic component. Paraffin was inserted in a cavity in which an array of densified carbon nanotubes (CNT) was firstly grown. The CNT structure was supposed to decrease the transversal thermal resistance of the system thanks to their high thermal conductivity (figure 4-2).

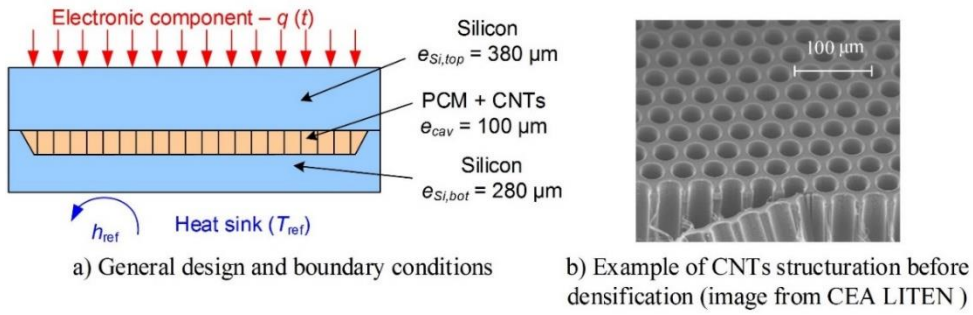

Figure 4-2. Design of the thermal damper (Kinkelin et al., 2017)

Several scientific and technologic challenges justified this project and the involvement of the various partners:

- The development of the process flow enabling to manufacture à silicon cavity standing the thermal and mechanical constraints of the application (IEMN)
- The manufacturing of the densified CNT array (CEA LITEN)
- The understanding of the interactions between the CNT array and the paraffin, in particular the wettability and the capillarity phenomena (CETHIL).
- The characterization and the understanding of the thermal damper behaviour in order to optimize its performance (CETHIL)

On the CETHIL side, the design and manufacturing of the test bench and the characterization and analyses were performed by Christophe Kinkelin during his PhD. He was co-supervised by Prof. Frederic Lefèvre and myself.

In the present chapter, a summary of the research strategy used in the THERMA3D is presented. It mainly consisted in three steps, corresponding to the three next chapter sections:

- The formalization of the thermal damper principle by means of the notion of ideal thermal damper
- The experimental characterization of the thermal performance of the prototypes manufactured by the IEMN and the CEA LITEN.
- The understanding of the phenomena governing the thermal damper behaviour by means of optical non-destructive methods.

4.2 The need for the notion of an ideal thermal damper

A thermal damper can be used in various applications, from the electronic component cooling to the storage of thermal energy in solar power plant. Despite the huge differences of size, mass, solicitation period and amplitude of the various systems, the principle is always based on a given amount of PCM inserted in a high thermal conductivity structure. The determination of the optimum mass of PCM in the system is one of the first step when designing a thermal damper. At the beginning of the THERMA3D project, it was observed that no general model was available in the literature, each thermal damper being specifically designed for the target application. This is why the notion of ideal thermal damper was proposed.

A thermal damper is considered as ideal when all of its components have an infinite thermal conductivity and when the PCM has a fixed phase change temperature T_{fusion}. It means there is no thermal resistances involved in the system and its temperature can be considered as uniform. An ideal thermal damper can thus be modelled with a very simple network model and its energy balance can be written as:

$$\frac{dH}{dt} = qS - h_{ref}S(T - T_{ref}) \tag{4-1}$$

with:

$$dH = (mc_p)_{tot}dT + m_{PCM}h_{ls}dx \tag{4-2}$$

where H and T are the enthalpy and the temperature of the ideal thermal damper, q is the heat flux imposed on the thermal damper of area S. h_{ref} is the heat transfer coefficient between the thermal damper and the heat sink, which is supposed to be constant. h_{ls} is the latent heat of phase change of the PCM, x is its liquid fraction and $(mc_p)_{tot}$ is the sum of the thermal capacity of all the components of the system.

Considering the single-phase and the two-phase zones independently, equation (4-1) can be written as:

$$\begin{cases} \dfrac{dT}{dt} = \dfrac{qS - h_{ref}S(T - T_{ref})}{(mc_p)_{tot}} & \text{if } T \neq T_{fus} \text{ (single-phase zone)} \\ \dfrac{dx}{dt} = \dfrac{qS - h_{ref}S(T - T_{ref})}{m_{PCM}h_{ls}} & \text{if } T = T_{fus} \text{(two-phase zone)} \end{cases} \tag{4-3}$$

To study the behaviour of a thermal damper, a frequency analysis can be performed. The heat flux is assumed to be sinusoidal:

$$q(t) = q_0 + \delta q \cos(2\pi f t + \varphi) \tag{4-4}$$

δq, f and φ are the amplitude, the frequency and the phase of the heat flux oscillation respectively. To perform a frequency analysis, the concept of thermal impedance can be used. It is the ratio between the temperature variation amplitude and the heat flux variation amplitude:

$$Z_{th} = \frac{\delta T}{\delta q} \tag{4-5}$$

with $\delta T = max|T(t) - T_m|$

In the single phase zone, it can be shown (Kinkelin et al., 2017) that the thermal impedance is equal to:

$$Z_{th} = \frac{1}{\sqrt{(h_{ref})^2 + \dfrac{(2\pi f (mc_p)_{tot})^2}{S}}} \tag{4-6}$$

The thermal impedance does not depend on the heat flux. An example of thermal impedance variation as a function of the frequency is plotted on figure 4-3. It decreases when the frequency increases. A higher frequency solicitation induces a smaller thermal damper temperature variation: even without phase change, any system will damp a high frequency solicitation because of its own thermal capacity.

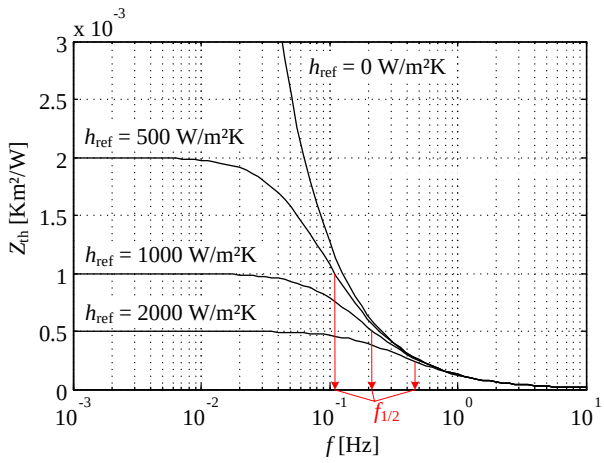

Figure 4-3. Thermal impedance in the single-phase zone of the ideal thermal damper associated to the geometry considered in figure 4-2 (Kinkelin et al., 2017)

The behaviour of an ideal thermal damper corresponds to that of a low-pass filter: the variation of heat flux imposed on the system is transferred to heat sink after being damped. In order to characterize this filter, the thermal impedance can also be written under the non-dimensional parameter G:

$$G = \frac{h_{ref}\delta T}{\delta q} = h_{ref} Z_{th} \tag{4-7}$$

G is the gain of the equivalent low-pass filter corresponding to the ideal thermal damper. When $G = 1$, there is no damping of the output heat flux variation and the temperature variation is maximum. When $G = 0$, the variation of the imposed heat flux is totally damped and the thermal damper temperature remains constant.

In the single phase zone, the filter gain depends only on the parameter N_{mcp}:

$$G = \frac{1}{\sqrt{1 + {N_{mcp}}^2}} \tag{4-8}$$

with $N_{mcp} = \frac{2\pi f (mc_p)_{tot}}{h_{ref} S}$. This term corresponds to a non-dimensional total thermal capacity of the thermal damper.

In the two-phase zone, it can be shown that the gain filter depends only on two non-dimensional parameters, N_{mcp} and $N_{mhls} = \frac{2\pi f \mathrm{m_{PCM}} h_{ls}}{\delta q S}$ (Kinkelin et al., 2017). N_{mhls} represents the latent heat of phase-change of the thermal damper in a dimensionless form.

In practice, the mean temperature of the thermal damper depends on the boundary conditions and is therefore not always equal to the phase-change temperature of the PCM. If both temperatures are far from each other, no phase change occurs and the thermal damper behaviour corresponds to the single-phase zone. If the thermal damper mean temperature is close to the PCM phase change temperature, only a part of the PCM is used to store heat. Figure 4-4 summarizes different cases of the thermal damper temperature evolution depending on the value of the mean temperature compared to the phase change temperature and on the amplitude of the imposed heat flux compared to the PCM latent heat. For low heat flux amplitude, an ideal thermal damper can be viewed as a thermal barrier that prevents the thermal damper temperature to become higher than the phase change temperature. For high heat flux amplitudes, the thermal damper can only damp the temperature variation partly.

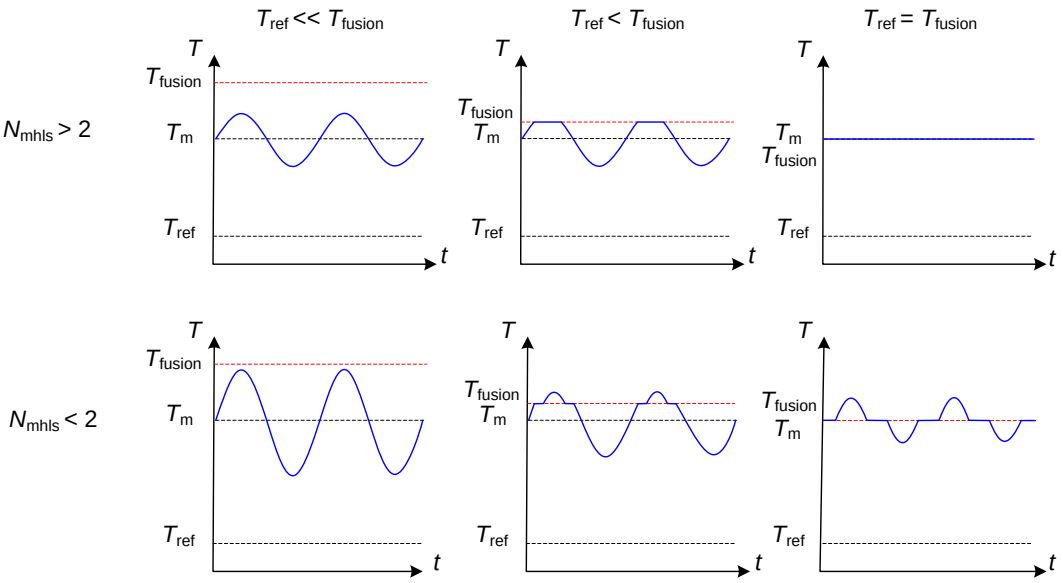

Figure 4-4. Thermal behaviour of an ideal thermal damper subjected to a sinusoidal heat flux (Kinkelin et al., 2017)

The case $N_{\text{mhls}} = 2$ corresponds to the situation for which the energy corresponding to half a period of the imposed heat flux variation is equal to the energy stored into the PCM during phase change. As a consequence, and contrary to the single-phase zone, the temperature variations are totally damped for a frequency higher than a threshold value f_0:

$$N_{mhls} \geq 2 \Leftrightarrow f \geq f_0 \text{ with } \mathrm{f}_0 = \frac{\delta q\, S}{2\pi m_{\mathrm{PCM}} h_{ls}} \tag{4-9}$$

Figure 4-5 presents the evolution of G in the case $T_{ref} = T_{fusion}$, as a function of N_{mcp} and N_{mhls}. Figure 4-6 presents the thermal impedance of the ideal thermal damper in the two-phase zone as a function of the oscillation frequency, for various heat transfer coefficients and for various heat flux amplitudes. It can be seen that the cut-off frequency depends strongly on the amplitude of the heat flux oscillations whereas the steady state depends only on the thermal resistance between the thermal damper and the heat sink.

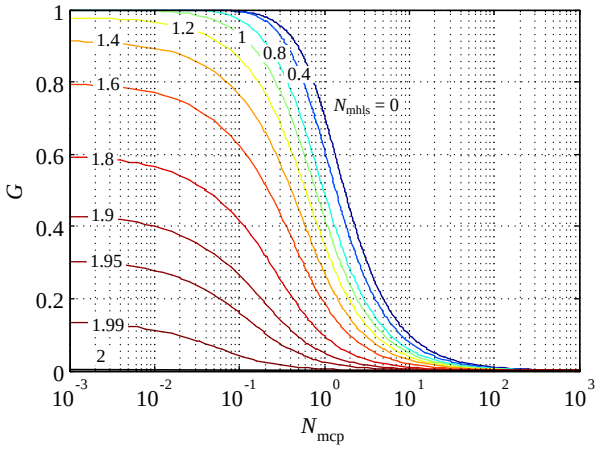

Figure 4-5. Gain of the equivalent filter of an ideal thermal damper (Kinkelin et al., 2017)

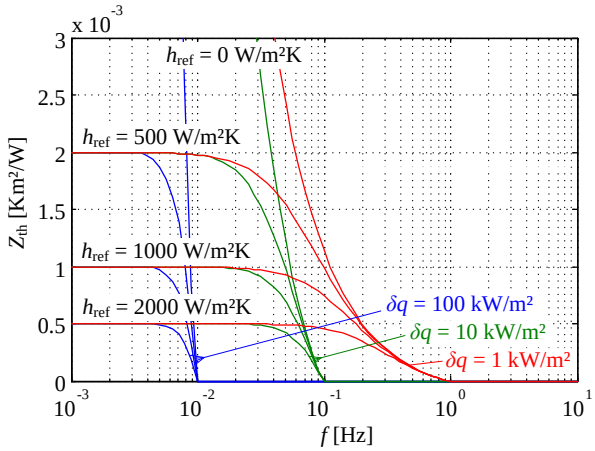

Figure 4-6. Impedance of an ideal thermal damper in the two-phase zone (Kinkelin et al., 2017)

The use of a thermal damper is worthwhile only if the thermal impedance in the two-phase zone is much lower than the thermal impedance in the single-phase zone. The comparison between figure 4-3 and figure 4-6 shows that it is verified for a limited range of frequency that depends on the heat flux amplitude and on the total latent heat of PCM. For small frequencies, the amount of PCM is too small to damp significantly the temperature variations whereas for high frequencies, the temperature variation is always damped by the thermal capacity of the materials composing the thermal damper even without phase change. This result can also be highlighted using non-dimensional parameters. Figure 4-7 presents the part of the attenuation due to the phase change only, represented by $G_0 - G$, where G_0 is the filter gain with no phase change ($N_{\text{mhls}} = 0$). The attenuation can be significant only for $N_{\text{mhls}} > 1$ and is larger for N_{mcp} around 1. For $N_{\text{mhls}} < 1$, $G_0 - G$ is limited to about 0.3 in the best configuration.

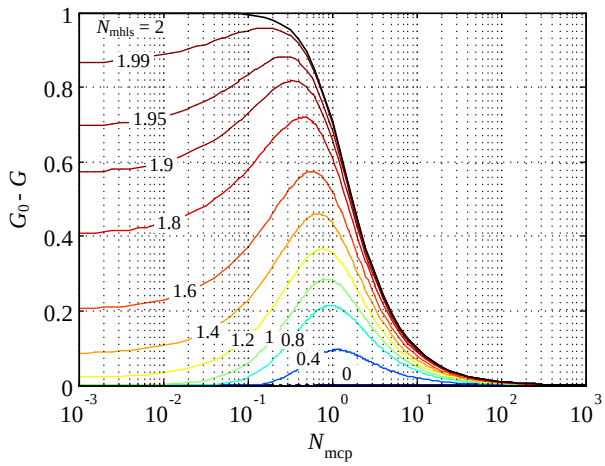

Figure 4-7. Attenuation due to the phase change (Kinkelin et al., 2017)

This graph is very useful to design a thermal damper for a known thermal solicitation. Based on non-dimensional parameters, it does not depend on the applications or on the scale of the system.

In practice, a thermal damper is rarely ideal. A temperature glide can occur during the phase change of the PCM and temperature gradients can exist in the various parts of the thermal damper. As a consequence, the study of the effect of the various thermal resistances have to be studied, mainly to design the high thermal conductivity structure. In the THERMA3D project, it was performed by means of a 2D numerical model that enables to theoretically study the difference of behaviour between an ideal and a non-ideal thermal damper for a given geometry (figure 4-8) and to optimize the geometry of the densified CNT structuration (figure 4-9). In the configuration of the project, it was concluded that the potential interface thermal resistances involved in the system would have probably a greater impact than the conductive thermal resistance in the CNT themselves. The temperature glide during the PCM phase change would also have a great impact on the thermal damper behaviour.

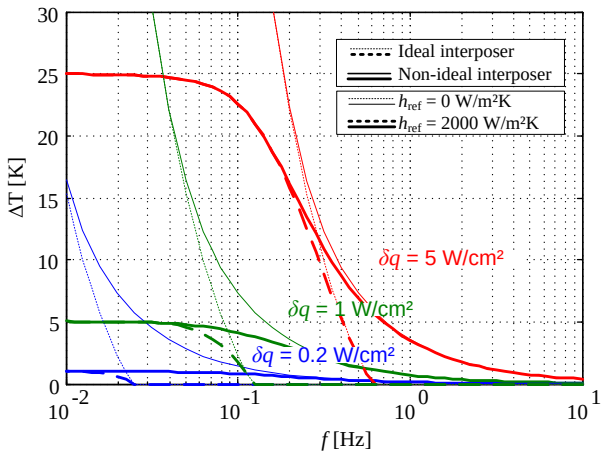

Figure 4-8. Non-ideal thermal damper behavior compared to the ideal one (p = 25 µm, σ_T = 5 K) (Kinkelin et al., 2017)

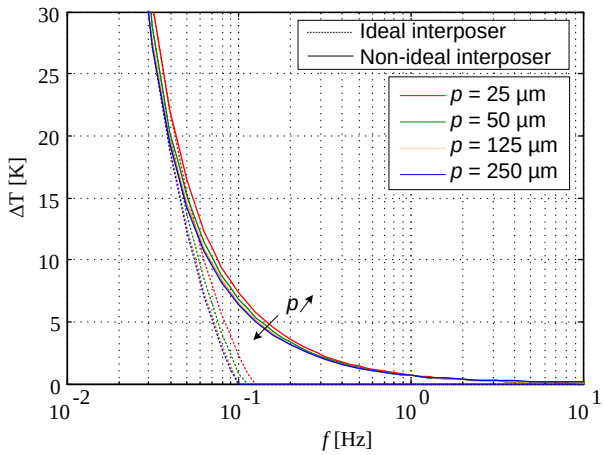

Figure 4-9. Effect of the honeycomb dimension p (δq = 1 W cm^{-2}; h_{ref} = 0 W m^{-2} K^{-1}; σ_T = 5 K) (Kinkelin et al., 2017)

4.3 Experimental characterisation of a thermal damper

The analytical and numerical models used to design a thermal damper are based on a theoretical behaviour of the PCM. However, the latter depends on numerous parameters (temperature glide during phase change, supercooling and hysteresis effect, aging of the material…) and is rather difficult to predict accurately. In the THERMA3D project, CETHIL was in charge of characterizing the thermal dampers behaviour in order to understand the interactions between the various components of the prototypes.

4.3.1 Samples and test benches

About forty prototypes were manufactured by the IEMN and the CEA LITEN. They corresponded to various manufacturing processes with various fabrication parameters. As a general description, they consisted on two silicon plates, with or without sealing, with or without PCM and with or without CNTs (figure 4-10). When existing, the CNTs were non-densified or densified with various patterns (figure 4-11). The reader can refer to (Kinkelin, 2016) for further details.

In order to characterize the prototypes, an optical test bench was designed and manufactured. The heating was provided by a 808 nm laser and a set of leness and the temperature of both sides of the prototypes was recorded by an infrared (IR) camera and a set of four mirrors (figure 4-12). The cooling of the thermal damper was ensured either by natural convection or by forced convection (figure 4-13). This configuration has been chosen in order to perform non-intrusive solicitations and characterization while ensuring a very low response time of the system. The whole apparatus was inserted in a black enclosure that enables to control the thermal and optical boundary conditions of the prototypes.

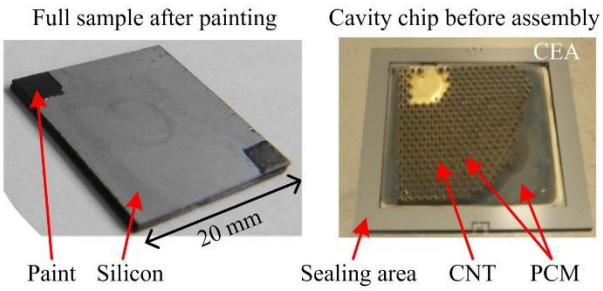

Figure 4-10. Typical pictures of the studied thermal dampers (Kinkelin et al., 2017)

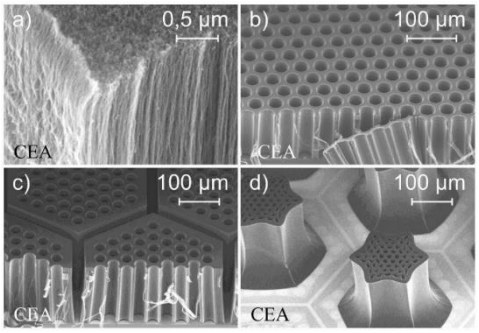

Figure 4-11. SEM images of different configurations of the CNT array: edge of a standard CNT array (a), array with holes (b), array with holes and hexagonal splits before (c) and after (d) densification (images and fabrication: CEA-Liten) (Kinkelin et al., 2017)

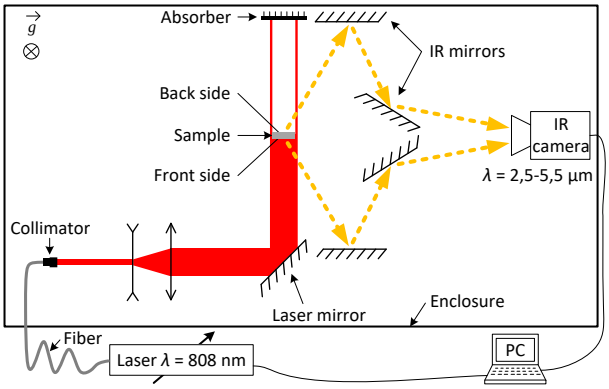

Figure 4-12. Main components of the test bench (top view, not to scale) (Kinkelin et al., 2017)

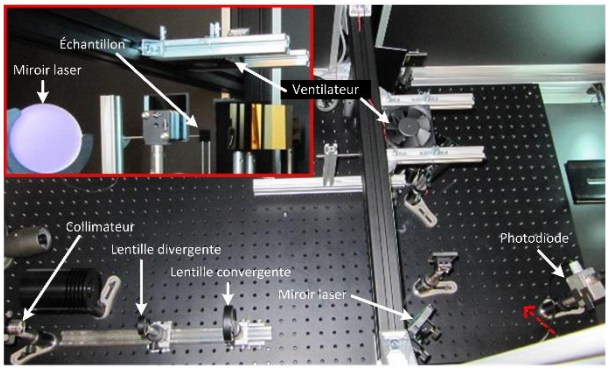

Figure 4-13. Picture of the test bench for the thermal cycle characterization (Kinkelin, 2016)

4.3.2 Optical approach and calibration

The choice of using a laser and an IR camera to heat and characterize the thermal dampers involves the use of a black paint and requires an elaborated calibration process. Moreover, the silicon being semi-transparent in the IR wavelengths, the use of an IR camera enables to visualize the phenomena occurring inside the thermal damper when no paint is used. Therefore, the images recorded by the IR camera are very rich of information but can be very difficult to analyse. As an example, figure 4-14 summarizes the various contributions to the IR camera measurements for plain silicon and for a silicon coated with black paint. This type of configuration enables to calibrate the IR camera, and especially to determine the transmittance of the black paint layer and the equivalent emissivity of the painted silicon plate. The latter enables to link the digital level (DL) measured by the camera to the temperature of the silicon plate. It has to be noted that the equivalent emissivity also depends on the characteristics of the IR camera and thus on the chosen integration time and acquisition frequency of the camera (figure 4-15). The use of a black paint also slightly affects the thermal response of the thermal dampers but the temporal shift has been estimated to about 10 ms in the tested configuration and was thus concluded to be acceptable (figure 4-16).

As a conclusion, an IR camera can be a very powerful tool to characterize a system but requires a very rigorous approach to obtain quantitative information. During his PhD, Christophe Kinkelin managed to develop the calibration and measurement procedures with a great care for the details, which strengthen the analyses and conclusions drawn from his measurements.

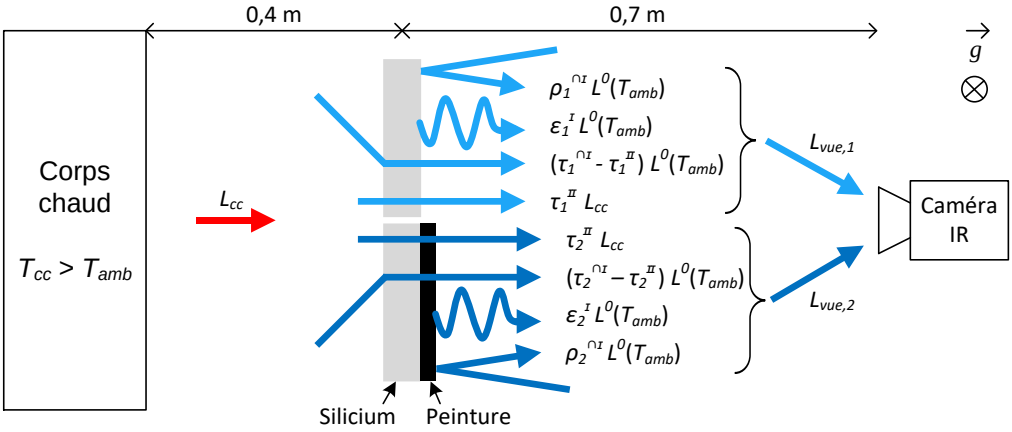

Figure 4-14. Schematic view of an experimental configuration used to measure the transmittance of the black paint layer and summarizing the various contributions seen by the IR camera (Kinkelin, 2016)

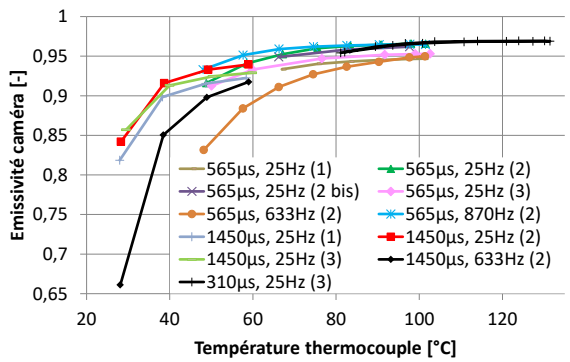

Figure 4-15. Equivalent emissivity of the painted silicon plate as a function of the plate temperature, for various integration times, acquisition frequency and various dates (day 1, 2 or 3) (Kinkelin, 2016)

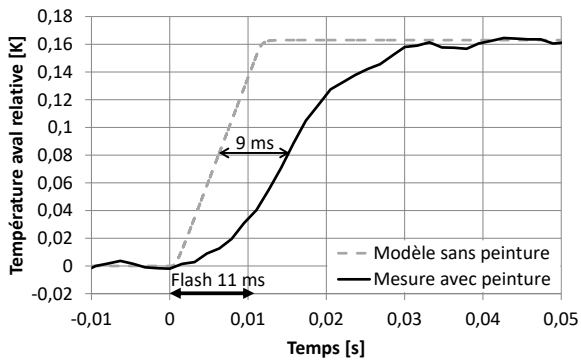

Figure 4-16. Estimation of the temporal shift due to the black paint layer (solid line: measured thermogramm after a laser crenel of 11 ms. dotted line: simulation of the behaviour without the paint layer) (Kinkelin, 2016)

4.3.3 Heat storage capacity characterisation

The first goal of a thermal damper is to store a given amount of thermal energy during transient thermal solicitations. CETHIL developed an experimental procedure to estimate the heat storage capacity of the various samples. It consists of imposing a laser crenel of about 20 s to heat the prototypes up to about 100°C and then let their temperature decreases by natural convection. The energy balance of the sample located in the test bench (figure 4-17) can be written as:

$$(mc_p)_{tot} \frac{dT_m}{dt} = Q_{abs} - G_{env}(T_m - T_{amb}) \tag{4-10}$$

with Q_{abs} being the laser flux absorbed by the sample; T_m and T_{amb} are the sample and ambient temperatures respectively. G_{env} is the equivalent thermal conductance between the sample and its environment and $(mc_p)_{tot}$ is the total thermal capacity of the sample.

Figure 4-18 provides an example of thermogram measured for two samples, respectively with and without PCM. This type of curve enables to determine the apparent thermal capacity of the sample, as a function of its temperature. An example of characterization is presented on figure 4-19 (solid lines). The apparent thermal capacity correspond to the thermal capacity of the solid materials included in the sample as well as the latent heat of phase change of the PCM, spread along its specific temperature glide. The apparent thermal capacity differs in the heating and cooling modes because of the supercooling effect. The results were also compared to a DSC characterisation (dotted lines). One can note that the supercooling effect is similar for both the DSC measurements and the measurements on our test bench, which is consistent with the fact that the quantity of PCM is of the same order of magnitude in both cases.

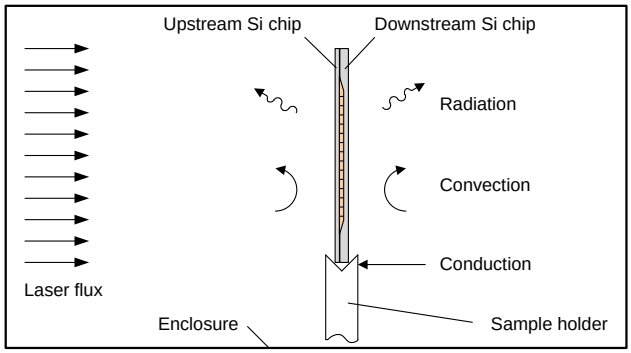

Figure 4-17. Thermal boundary conditions for the TIM-TS (Kinkelin et al., 2015)

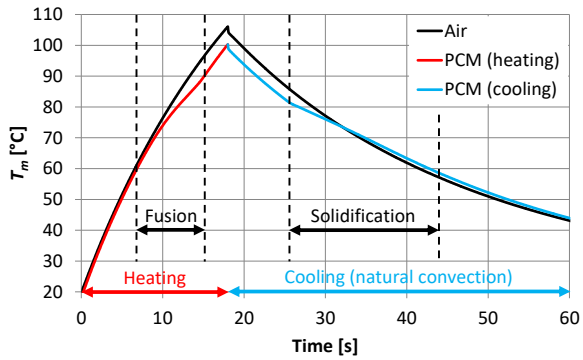

Figure 4-18. Temperature history of prototype thermal dampers with and without PCM (Kinkelin et al., 2017)

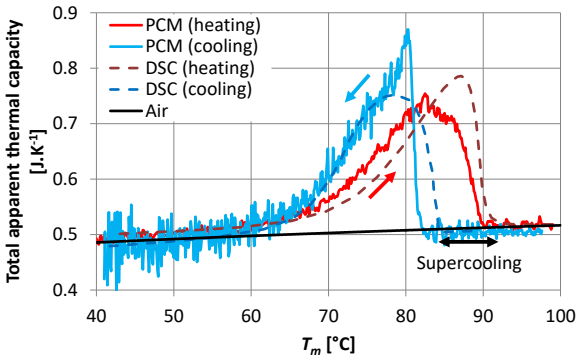

Figure 4-19. Estimated total apparent thermal capacity $(mc_p)_{tot}$ of the samples with and without PCM versus DSC measurements (Kinkelin et al., 2017)

The test bench developed for THERMA3D enabled to characterize each sample. For instance, the PCM filling ratio of the various prototypes, which is difficult to estimate during the manufacturing process, was determined thanks to this procedure. It also permitted to study the phase-change phenomena inside the system. For instance, it has been shown that the PCM behaviour was very reproducible and that the amplitude of supercooling was of the same order of magnitude for samples containing no CNT, undensified CNTs or densified CNTs. A thermal cycling procedure was also develop to estimate the aging of the PCM. It was shown that the thermal storage capacity remains constant, even after 1000 fusion/solidification cycles (figure 4-20).

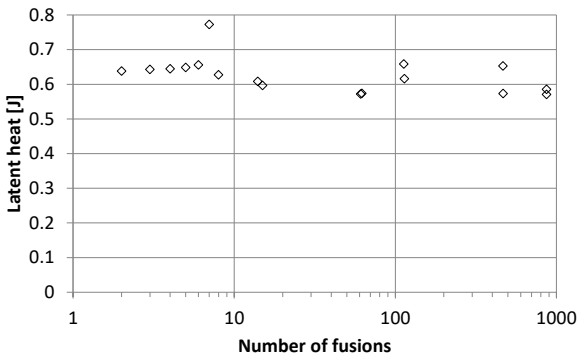

Figure 4-20. Latent heat storage capacity of the CNT/PCM material as a function of the number of fusion/solidification cycles (Kinkelin et al., 2017)

4.3.4 Thermal resistance characterisation

In the configuration imagined by ST-Microelectronics, the thermal damper is located between the electronic component (heat source) and the PCB (heat sink). Its thermal resistance is thus of a great importance and the main challenge of the THERMA3D project was indeed to reduce it as much as

possible. The test bench was thus used with a procedure close to a flash method. A 10 ms flash was imposed on the sample front side and the back side temperature was recorded (figure 4-21). A simple network model, presented on figure 4-22, enabled to estimate the thermal resistance R_{ff} from the characteristic times $t_{1/2}$:

$$R_{ff} = \frac{t_{1/2}}{0.693\ c_{p,Si}} \left(\frac{1}{m_f} + \frac{1}{m_b} \right) \tag{4-11}$$

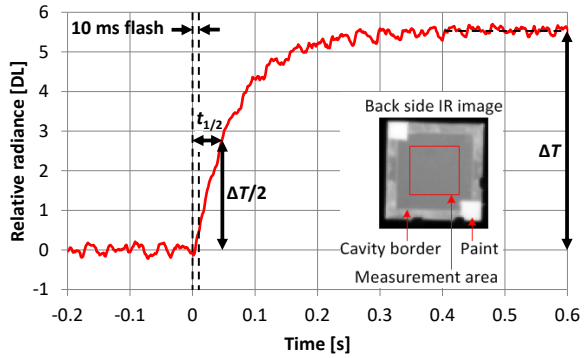

Figure 4-21. Measured temperature history of the back side of a prototype thermal damper subjected to a 10 ms laser crenel (DL: digital level of the IR camera) (Kinkelin et al., 2017)

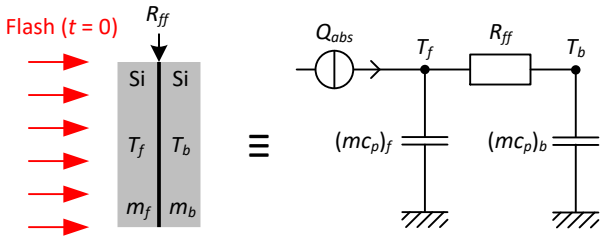

Figure 4-22. Thermal model of the thermal damper subjected to a laser flash (Kinkelin et al., 2017)

The accuracy of this procedure is rather low but enables a fast and robust estimation of the sample thermal resistance. Moreover, it enables to compare the performance of the samples and thus to study the effect of the various manufacturing parameters. For instance, the Table 4-1 summarizes the thermal resistance of various prototypes made of two silicon plates and linked with non-densified CNTs. It was shown that the main parameter influencing the thermal resistance was the pressure applied on the plates during the manufacturing process.

Table 4-1. Influence of the manufacturing process on the thermal resistance of two silicon plates linked by non-densified CNTs (Kinkelin, 2016)

Ech.	Avant scellement	Scellement	Après scellement	Force arracht.	Après test d'arrachement	NTC transférés	Ech.	R_{ff}
1a		Temp.: 150 °C Pression : 1 kg Durée : 60 s		294 gf cm^{-2}		0 %	1c	3,6 K W^{-1}
2a		Temp.: 150 °C Pression : 1 kg Durée : 600 s		-		0 %	2c	3,4 K W^{-1}
3a		Temp.: 150 °C Pression : 5 kg Durée : 60 s		2357 gf cm^{-2}		60 %	3c	0,7 K W^{-1}
4a		Temp.: 150 °C Pression : 5 kg Durée : 600 s		2883 gf cm^{-2}		68 %	4c	0,8 K W^{-1}
5a		Temp.: 300 °C Pression : 1 kg Durée : 60 s		442 gf cm^{-2}		0 %	5c	0,7 K W^{-1}
6a		Temp.: 300 °C Pression : 1 kg Durée : 600 s		540 gf cm^{-2}		0 %	6c	1,5 K W^{-1}
7a		Temp.: 300 °C Pression : 5 kg Durée : 60 s		2128 gf cm^{-2}		100 %	7c	0,5 K W^{-1}
8a		Temp.: 300 °C Pression : 5 kg Durée : 600 s		1130 gf cm^{-2}		100 %	8c	0,6 K W^{-1}

Several other parametric studies were also performed. For instance, the thermal resistance of an array of non-densified CNTS was measured for prototypes with difference CNT length. The results are presented on figure 4-23 and shows a weak link between the thermal resistance and the CNTs length. It can thus be concluded that the conduction heat transfer resistance in the CNT is negligible and that the total thermal resistance mainly depends on the various interfacial thermal resistances involved in the systems.

The performance of the THERMA3D samples were also compared to the results available in the literature and it showed that their performance were quite good compared to samples having similar CNT length (figure 4-24).

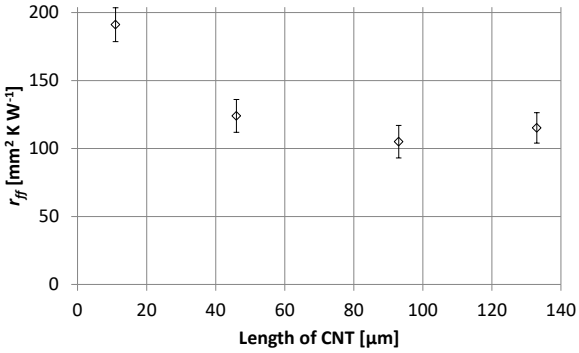

Figure 4-23. Total thermal resistance of Si/CNT/Si samples with various lengths of CNTs (Kinkelin et al., 2017)

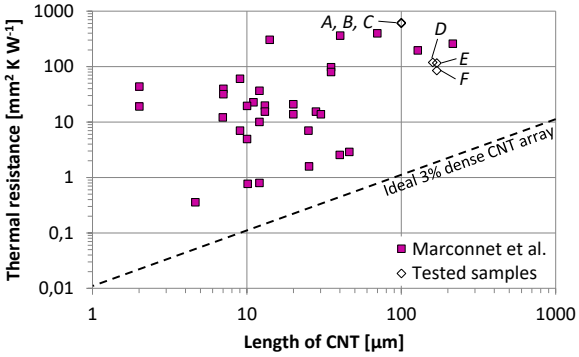

Figure 4-24. Estimated total thermal resistance of the best THERMA3D samples (A-F) compared to those of the CNT arrays reported in the review article of Marconnet et al. (2013) (Kinkelin et al., 2017)

4.4 Optical non-destructive testing

The characterization of the samples, both in terms of energy storage capacity and of thermal resistance, enabled to study the effect of the manufacturing parameters on the global performance of the thermal dampers but it gave relatively little information on the phenomena occurring inside the systems. During his PhD, Christophe Kinkelin developed the skills and the knowledge enabling to take advantage of the semi-transparency of the silicon. He characterized many samples before coating them with black paint, which enables to get useful additional information. For instance, Figure 4-25 present the visualization of three samples with various cavity thickness, filled with PCM but with no CNT. They were placed in vertical orientation and heated with the laser. It is possible to visualize the evolution of the location of the PCM in the cavity. For thin cavity thicknesses, the capillary effect are dominant and the PCM remains in the centre of the thermal damper. For large cavity thicknesses, the gravity effects are dominants and the PCM tends to flow at the bottom of the thermal damper. This type of visualization also enabled to study qualitatively the front of phase change of the PCM.

When CNTs are grown in the silicon cavity, the analyses of the IR visualization is more complex because of the presence of various metallic layers coated in the inner sides of the cavity. They are required in order to promote the CNTs growing (catalyst layer) and/or to strengthen the mechanical and thermal link between the CNT and the silicon plates (stamping layer). Figure 4-26 present an example of IR visualization of a sample containing CNTs. Several zones can be delimited, which corresponds to the CNT, the silicon and the tape zones, seen from both the front and the back plates. Depending on the plates, the NTC can be seen, or not. The tape zone appears lighter than the NTC zone in the front plate but darker in the back plate. This difference of behaviour can be explained when considering all the contributions seen by the IR camera (figure 4-27). It appears that the stamping layer, which corresponds to two titanium/gold layer and one indium layer, acts mainly as a mirror in the IR wavelength. On the other side, the CNT themselves act as a black body. The catalyst layer, the silicon, the PCM and the tapes are semi-transparent with various level of transmittance.

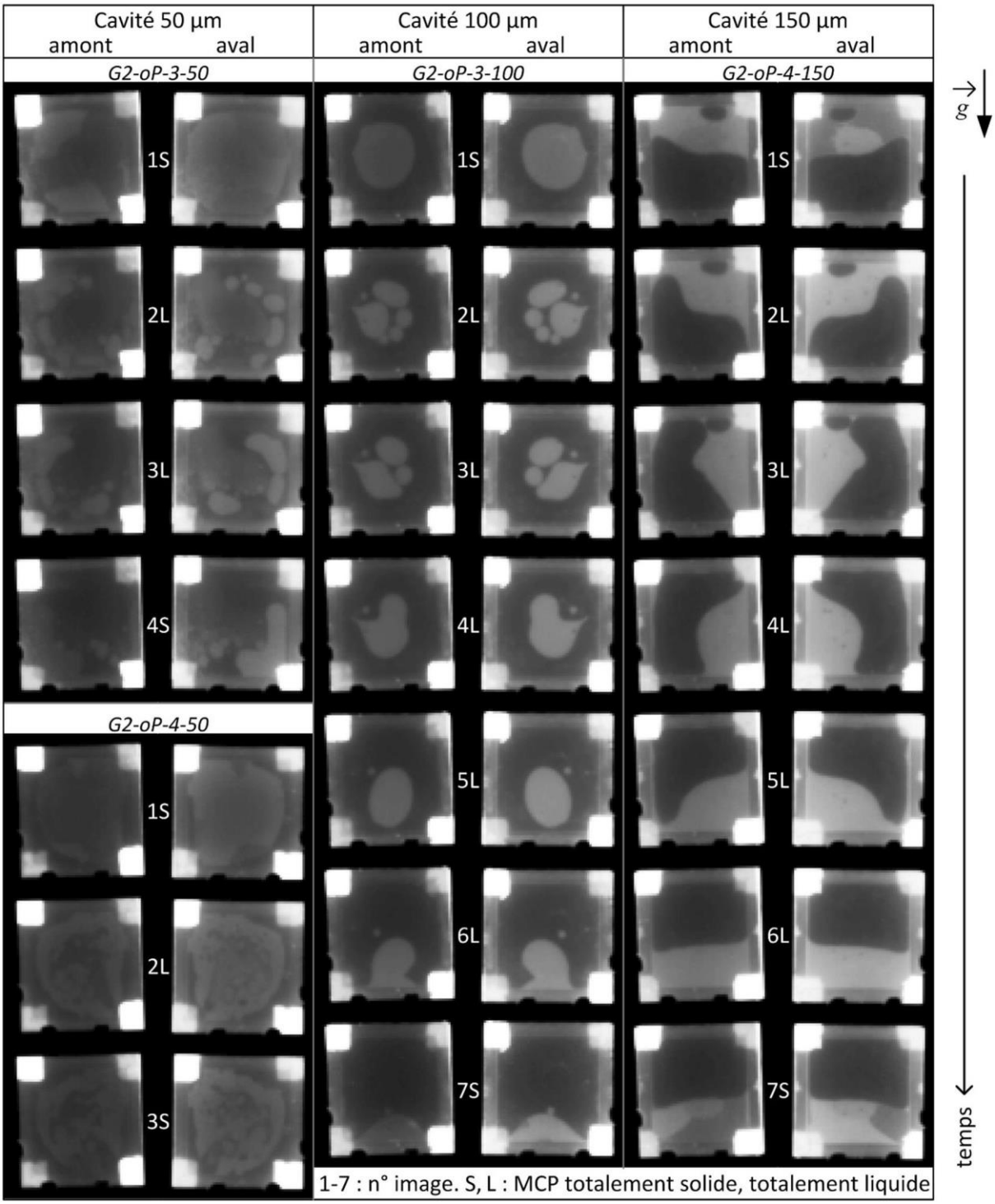

Figure 4-25. Samples SI-PCM-SI placed in vertical orientation and heated up to the complete fusion of the PCM. The IR visualization of the front and back side are presented as a function of the time (Kinkelin, 2016)

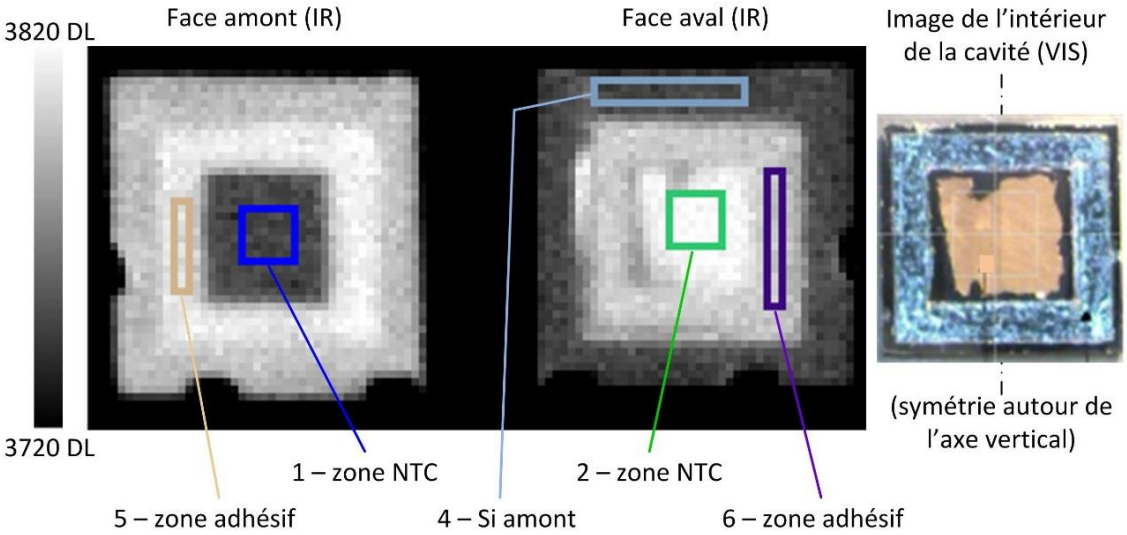

Figure 4-26. Example of IR visualization for a sample above the ambient temperature (Kinkelin, 2016)

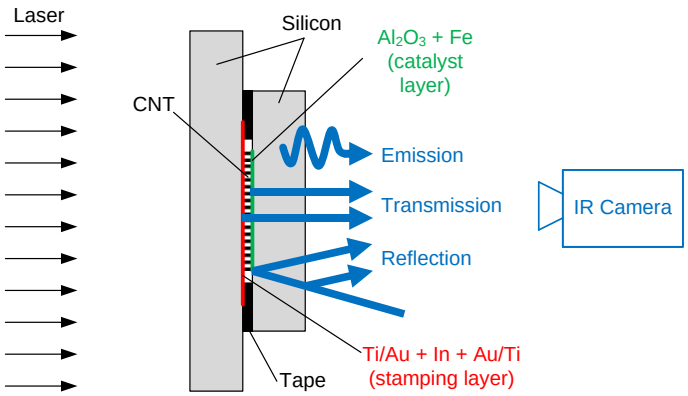

Figure 4-27. Schematic illustration of the contributions to the infrared signal measured by the IR camera (Kinkelin et al., 2015)

Because of their manufacturing process, the various samples were rarely symmetric which complicated the image analyses on one side, but enabled to perform additional studies on the other side. For instance, Christophe Kinkelin managed to detect the location of the main thermal resistance in some samples by performing a flash method on non-painted samples and corresponding to the figure 4-27. Figure 4-28 presents the thermogram measured on the front side of two samples ("CNT-P" is filled with PCM and "CNT-A" contains only CNTs) after a laser crenel of 10 ms. The relative radiance seen by the camera is mainly an image of the temperature of the front plate because of the presence of the stamping layer. The thermogram are very similar and shows that the front plates is heated up almost immediately by the laser. The thermograms measured on the backside of the two samples are presented on figure 4-29. For this side, the relative radiance is mainly an image of the NTC temperature because all others layers are semi-transparent. It can be seen that the NTC temperature of the sample CNT-P increases almost immediately whereas that of the sample CNT-A is much delayed. It means that in the case of the sample CNT-A, the stamping layer generates an important interface thermal resistance. The presence of PCM could thus reduce the thermal resistance between the CNTs and the silicon plates. Further measurements showed that for these samples, the catalyst layers also generates a high interface thermal resistance.

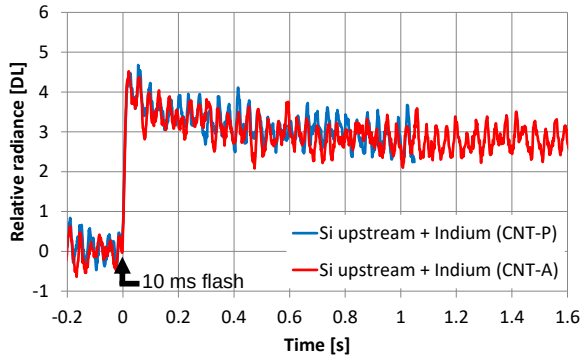

Figure 4-28. IR radiation of the upstream silicon and the stamping layer of unpainted samples “CNT-P” and “CNT-A” (Kinkelin et al., 2015)

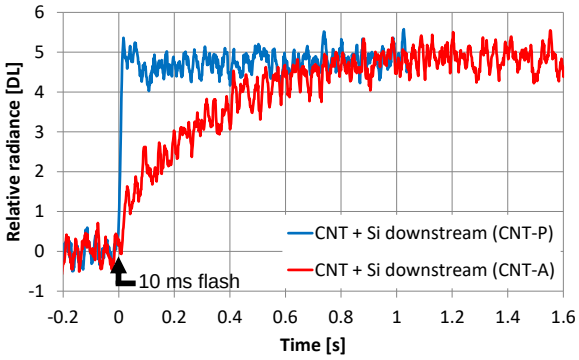

Figure 4-29. IR radiation of the downstream silicon and the CNT array of unpainted samples “CNT-P” and “CNT-A” (Kinkelin et al., 2015)

The same kind of analyses performed on other thermal dampers with different structures enables to draw other conclusions. For instance, Christophe Kinkelin developed a specific optical procedure enabling to characterize the quality of the stamping between the silicon plates and the densified CNTs. All these characterizations enables to improve the manufacturing process during the THERMA3D project. Their limitations lie in the fact that they were all developed for a specific structure of thermal damper and it was very difficult to perform a rigorous parametric study during the project because of the disparity between the various samples manufactured by the partners.

4.5 Conclusions and perspectives

The use of PCM for the thermal management of electronic components can be of great interests to increase the lifetime of the systems but many drawbacks exist and explain why this type of systems is not yet encountered in real applications. A better knowledge of the PCM behaviour is still needed and especially their interactions with the high thermal conductive structure that have to be used to compensate for their low thermal conductivity. In the THERMA3D project, the use of CNTs shows the limitations of this type of material, but silicon structures can still be used and should exhibit good enough thermal performance if the technical issues linked to the whole industrial process of the electronic components can be addressed. From a thermal sciences point of view, specific problems as enhancement of PCM thermal conductivities or coupling between the PCM and other phase change cooling systems, as convective boiling or heat pipes, are worth being investigating. This is the topic of the FUI project OUMOUSS, involving the CETHIL and started in January 2018, which aims at coupling PCM with metal foams and heat pipes in order to improve the thermal performance of mouldings for polymer injection and metal casting applications. The results of this type of study will probably be transferable to the field of the thermal management of electronic components as many of the theoretical aspects and scientific problems can be addressed independently of the application field, even if it requires to developed new concepts, as the one of ideal thermal damper developed in THERMA3D.

Chapter 5: Conclusions and perspectives

From the various studies presented in the present manuscript, many conclusions and perspectives can be drawn. Global perspectives were given at the end of each chapter, but there are here summarized and, more important, prioritized according to the research strategy I will try to follow in the next couples of years.

5.1 Conclusions of the present analysis

I tried in the present document to draw an overview of the research in which I was involved since my PhD defence in 2009. Even if the main application motivating these studies was the cooling of electronic components, I had the opportunity to work on various systems, belonging to three different categories: the heat pipes, the two-phase flows and the thermal dampers. Despite the risk of dispersion, I believe the diversity of these systems enabled me to broaden my scientific culture and skills.

The works related to heat pipes gave me a global view of the various scientific problems that can be encountered in two-phase systems. It goes from fundamental phenomena, as the bubble nucleation, to the understanding of the system behaviour in various configurations. The latter involves the coupling between the various phenomena, which can be a very rich research field, due to the diversity of the systems called “heat pipes”. In this field, I tried to follow a phenomenological approach, mostly by experimental works, but as often as possible followed by simplified models in order to check the validity of the experimental conclusions. The studies of heat pipes enables to cover a large scale of scientific problems because of their direct utilisation in industrial processes. I had the opportunity to cover TRL 3 to 6, which enables to get a permanent motivation by actual applications, while being able to spend time and energy on specific scientific problems. The diversity of the applications induces a diversity in the people involved in this field. In the CETHIL, I worked mainly with Frederic Lefèvre, Valerie Sartre and Jocelyn Bonjour, but I also really enjoyed the meetings and discussions with other french and international scientists, especially in the frame of the previous GDR Syredossi.

My research on two-phase flows are more fundamental and quite limited in terms of scientific questions. I mainly focused on two-phase flows in inclined configurations, but this simple idea brought me further than I expected. Experimental studies of two-phase flows require complementary skills to the studies of heat pipes, but some of the constraints are obviously similar and I found very rich to go from one field to the other. Once more, I focused my research on experiments and phenomenological analyses. Having the chance to work on both convection condensation and flow boiling, the diversity of the configurations helped me to step back, even if I admit I am far from being a specialist of the field. In the CETHIL, I performed my research on two-phase flows with Remi Revellin and I believe our complementary skills and approaches helped a lot in our studies.

When I joined the CETHIL, Frederic Lefèvre associated me quickly to the ANR Therma3D dealing with thermal damper. This project was an opportunity for me to broaden even more my field of research, with the common thread of phase-change, capillary phenomena and electronic cooling. This project enables me to develop my experimental skills using lasers and IR visualisations. The specificity of studying transient thermal solicitations and responses also improved my understanding of the heat transfer phenomena in these conditions. I discovered the world of solid-liquid phase-change and all his complexity and chemical aspects. To finish, the utilisation of carbon nano-tubes gave me a brief overview of the heat transfer at the nano-scale. The collaboration with the CEA, the IEMN and ST microelectronics also enabled me to achieve a better understanding of the problematic linked to electronic components, so even if the Therma3D project was not followed by another one, it was a very rich experience.

Based on all these experiences, I try to draw continuously a research strategy for the oncoming years. Even if the topics I choose are of course also dependant on unexpected opportunities, this guideline help me not to disperse myself too much in the wide field of phase-change heat transfer.

5.2 Research perspectives

In the next years, I plan to continue the study of phenomena involved in heat pipes through various approaches:

The fundamental understanding of phase-change heat transfer is not completely achieved in many applications. I will firstly try to improve the understanding of the evaporation process at the surface of a capillary structure. This study is a direct following of the project 2Mather but with more controlled structures in order to avoid the repeatability issues we faced. The goal would be to get enough experimental data to eventually identify the limiting heat transfer phenomena in these configurations.

I also planned to focus on the study of condensation phenomena in heat pipes. In the project CAPIT4L, we are trying to develop polymer heat pipes, which will be a good object for the study of film-wise and drop-wise condensation in various configurations.

I will try to pursue the studies of heat pipe in confined configuration, in confined flat thermosiphons, but also in other confined geometries, at the condenser for instance. Preliminary tests showed very interesting heat pipe behaviours that worth to be understood in more details.

The studies on heat pipe will also be drawn by the diversification of the applications in which there are used. Thanks to the skills developed in therma3D and the polymer heat pipes developed in CAPIT4L, we should be able to study the behaviour of heat pipes submitted to thermal chocks. In these conditions, the heat pipe cannot be considered in thermodynamic equilibrium any longer and so far, no models are able to predict their behaviour for this type of solicitation. This topic will be fed by the FUI project Oumouss, dealing with the insertion of heat pipes in mouldings.

If opportunities occur, I will of course be happy to contribute to the study of other types of heat pipes, like pulsating and loop heat pipes as it always feeds the scientific community with interesting questions. To finance the research on heat pipes, applied projects at the local, national or European scale are very pertinent as it enables to keep the application constraints in mind.

Besides heat pipe research, I did not plan to give up the field of two-phase flows. Without specialising in this field, I am really interested in developing new characterization technics as I believe the CETHIL has a chance to regroup many people with very complimentary skills. Of course, I will continue to try to answer the questions opened by my previous research. In this field, funding from calls that are more fundamental are required but are also more difficult to obtain. So far, we managed to progress without important external funding, except PhD bursaries. However, depending on the research strategy of the group, we can try to be more ambitious. One possible extension of the current work is the study of the behaviour of non-azeotropic mixture during convective boiling or condensation.

The study I led on thermal dampers was very enriching and I would like to continue to apply this kind of system, but by coupling them directly to heat pipes. Heat pipes are indeed systems having a very high equivalent thermal diffusivity whereas phase change materials are completely the opposite. The coupling between the two systems should open a new way of thinking the thermal management of a system subjected to transient solicitations. We proposed this kind of approach in the frame of the project Oumouss for the thermal optimisation of the cooling process during metal moulding and polymer injection. Depending on the results of this study, we will eventually try to go further.

As a conclusion, it seems I will keep very active and busy in the future… There is so many scientific questions to be answered; I will just try to contribute to the general increase of knowledge provided by the research community. Each individual contribution is modest, but I am always impressed by the global scientific advances that are achieved years after years, thanks to the energy and the willing of all researchers, professors, assistant professors, post-doc, PhD student, master students, engineers, technicians and administrative staffs involved all together in research!

References

Ababneh, M.T., Gerner, F.M., Chamarthy, P., Bock, P. de, Chauhan, S., Deng, T., 2014. Thermal-fluid modeling for high thermal conductivity heat pipe thermal ground planes. J. Thermophys. Heat Transf. 28, 270–278. https://doi.org/10.2514/1.T4107

Adelaja, A.O., Dirker, J., Meyer, J.P., 2016. Convective condensation heat transfer of R134a in tubes at different inclination angles. Int. J. Green Energy 13, 812–821. https://doi.org/10.1080/15435075.2016.1161633

Akhavan-Behabadi, M.A., Esmailpour, M., 2014. Experimental study of evaporation heat transfer of R-134a inside a corrugated tube with different tube inclinations. Int. Commun. Heat Mass Transf. 55, 8–14. https://doi.org/10.1016/j.icheatmasstransfer.2014.03.003

Akhavan-Behabadi, M.A., Mohseni, S.G., Razavinasab, S.M., 2011. Evaporation heat transfer of R-134a inside a microfin tube with different tube inclinations. Exp. Therm. Fluid Sci. 35, 996–1001. https://doi.org/10.1016/j.expthermflusci.2011.01.020

Alawi, O.A., Sidik, N.A.C., Mohammed, H.A., Syahrullail, S., 2014. Fluid flow and heat transfer characteristics of nanofluids in heat pipes: A review. Int. Commun. Heat Mass Transf. 56, 50–62. https://doi.org/10.1016/j.icheatmasstransfer.2014.04.014

Al-Dadah, R.K., Karayiannis, T.G., James, R.W., Allen, P.H.G., 1992. EHD enhanced heat transfer : effect on the performance of a refrigeration system. Heat Transf. 1st Eur. Conf. Therm. Sci. Birm. ICHEME Symp. N°129 2, 1229–1236.

Alekseenko, S., Cherdantsev, A., Cherdantsev, M., Isaenkov, S., Kharlamov, S., Markovich, D., 2012. Application of a high-speed laser-induced fluorescence technique for studying the three-dimensional structure of annular gas–liquid flow. Exp. Fluids 53, 77–89. https://doi.org/10.1007/s00348-011-1200-5

Ameli, M., Agnew, B., Leung, P.S., Ng, B., Sutcliffe, C.J., Singh, J., McGlen, R., 2013. A novel method for manufacturing sintered aluminium heat pipes (SAHP). Appl. Therm. Eng. 52, 498–504. https://doi.org/10.1016/j.applthermaleng.2012.12.011

Arab, M., Abbas, A., 2014. A model-based approach for analysis of working fluids in heat pipes. Appl. Therm. Eng. 73, 751–763. https://doi.org/10.1016/j.applthermaleng.2014.08.001

Asfia, J.F., Cai, Q., Chen, C.-L., 2014. Multi-layer wick in loop heat pipe. US8720530 B2.

Bamorovat Abadi, G., Moon, C., Kim, K.C., 2016. Effect of gravity vector on flow boiling heat transfer, flow pattern map, and pressure drop of R245fa refrigerant in mini tubes. Int. J. Multiph. Flow 83, 202–216. https://doi.org/10.1016/j.ijmultiphaseflow.2016.04.007

Barnea, D., 1987. A unified model for predicting flow-pattern transitions for the whole range of pipe inclinations. Int. J. Multiph. Flow 13, 1–12. https://doi.org/10.1016/0301-9322(87)90002-4

Becker, S., Vershinin, S., Sartre, V., Laurien, E., Bonjour, J., Maydanik, Y.F., 2011. Steady state operation of a copper–water LHP with a flat-oval evaporator. Appl. Therm. Eng. 31, 686–695. https://doi.org/10.1016/j.applthermaleng.2010.02.005

Bertsch, S.S., Groll, E.A., Garimella, S.V., 2009. Effects of heat flux, mass flux, vapor quality, and saturation temperature on flow boiling heat transfer in microchannels. Int. J. Multiph. Flow 35, 142–154.

Berut, E., 2016. Étude théorique et expérimentale de la faisabilité de caloducs en polymère (Rapport de SIRD). CETHIL.

Bhagwat, S.M., Ghajar, A.J., 2017. Experimental investigation of non-boiling gas-liquid two phase flow in downward inclined pipes. Exp. Therm. Fluid Sci. 89, 219–237. https://doi.org/10.1016/j.expthermflusci.2017.08.020

Bhagwat, S.M., Ghajar, A.J., 2016a. Experimental investigation of non-boiling gas-liquid two phase flow in upward inclined pipes. Exp. Therm. Fluid Sci. 79, 301–318. https://doi.org/10.1016/j.expthermflusci.2016.08.004

Bhagwat, S.M., Ghajar, A.J., 2016b. Experimental investigation of non-boiling gas-liquid two phase flow in upward inclined pipes. Exp. Therm. Fluid Sci. 79, 301–318. https://doi.org/10.1016/j.expthermflusci.2016.08.004

Bisetto, A., Torresin, D., Tiwari, M.K., Del Col, D., Poulikakos, D., 2014. Dropwise condensation on superhydrophobic nanostructured surfaces: literature review and experimental analysis, in: Journal of Physics: Conference Series. IOP Publishing, p. 012028.

Bonjour, J., Lefevre, F., Sartre, V., Siedel, B., 2013. Improved device for closed-loop heat transport. WO2013174856 A1.
Boo, J.H., Chung, W.B., 2005. Experimental Study on the Thermal Performance of a Small-scale Loop Heat Pipe with Polypropylene Wick. J. Mech. Sci. Technol. 19, 1052–1061. https://doi.org/10.1007/BF02919189
Bryan, J.E., Seyed-Yagoobi, J., 1997. Heat transport enhancement of monogroove heat pipe with electrohydrodynamic pumping. J. Thermophys. Heat Transf. 11, 454–460.
Buschmann, M.H., 2013. Nanofluids in thermosyphons and heat pipes: Overview of recent experiments and modelling approaches. Int. J. Therm. Sci. 72, 1–17. https://doi.org/10.1016/j.ijthermalsci.2013.04.024
Cardin, N., El Mehdi Brik, M., Lips, S., Siedel, S., Bonjour, J., Davoust, L., 2017. Effect of a DC electric field on the liquid-vapor interface in a grooved flat heat pipe, in: 13th International Conference on Heat Transfer, Fluid Mechanics and Thermodynamics. Portoroz, Slovenia.
Cardin, N., Lips, S., Siedel, S., Davoust, L., Bonjour, J., 2018. Theoretical and experimental investigations of the effect of an electric field on the performance of a grooved flat heat pipe, in: Joint 19th IHPC and 13th IHPS. Pisa, Italy.
Cavallini, A., Brown, J.S., Del Col, D., Zilio, C., 2010. In-tube condensation performance of refrigerants considering penalization terms (exergy losses) for heat transfer and pressure drop. Int. J. Heat Mass Transf. 53, 2885–2896. https://doi.org/10.1016/j.ijheatmasstransfer.2010.02.007
Charnay, R., 2014. Experimental study of flow boiling in horizontal minichannels at high saturation temperature. Lyon, INSA.
Charnay, R., Revellin, R., Bonjour, J., 2014. Flow boiling characteristics of R-245fa in a minichannel at medium saturation temperatures. Exp. Therm. Fluid Sci. 59, 184–194. https://doi.org/10.1016/j.expthermflusci.2014.01.011
Chauris, N., Ayel, V., Bertin, Y., Romestant, C., 2015. Evaporation of a liquid film deposited on a capillary heated tube: Experimental analysis by infrared thermography of its thermal footprint. Int. J. Heat Mass Transf. 86, 492–507. https://doi.org/10.1016/j.ijheatmasstransfer.2015.03.013
Chen, J.C., 1964. A correlation for boiling heat transfer to saturated fluids in convective flow. ASME Publ.
Cheng, W.-L., Chen, H., Yuan, S., Zhong, Q., Fan, Y.-F., 2017. Experimental study on heat transfer characteristics of R134a flow boiling in "Ω"-shaped grooved tube with different flow directions. Int. J. Heat Mass Transf. 108, 988–997. https://doi.org/10.1016/j.ijheatmasstransfer.2016.12.053
Chi, S.W., 1976. Heat pipe theory and practice: a sourcebook. Hemisphere Pub. Corp., Washington DC.
Chisholm, D., 1973. Pressure gradients due to friction during the flow of evaporating two-phase mixtures in smooth tubes and channels. Int. J. Heat Mass Transf. 16, 347–358. http://dx.doi.org/10.1016/0017-9310(73)90063-X
Churchill, S.W., Chu, H.H.S., 1975. Correlating equations for laminar and turbulent free convection from a horizontal cylinder. Int. J. Heat Mass Transf. 18, 1049–1053. https://doi.org/10.1016/0017-9310(75)90222-7
Cioncolini, A., Thome, J.R., 2013. Liquid film circumferential asymmetry prediction in horizontal annular two-phase flow. Int. J. Multiph. Flow 51, 44–54. https://doi.org/10.1016/j.ijmultiphaseflow.2012.12.003
Collier, J.G., Thome, J.R., 1996. Convective boiling and condensation. Oxford University Press.
Cooper, P., 1990. EHD enhancement of nucleate boiling. J. Heat Transf. 112, 458–464.
Crawford, T.J., Weinberger, C.B., Weisman, J., 1985. Two-phase flow patterns and void fractions in downward flow. Part I: steady-state flow patterns. Int. J. Multiph. Flow 11, 761–782. https://doi.org/10.1016/0301-9322(85)90023-0
Damianidis, C., Collins, M.W., Karayiannis, T.G., Allen, P.H.G., 1990. EHD effect in condensation of dielectric fluids, in: Proceeding Second International Symposium on Condensers and Condensation. Bath, UK, pp. 505–518.
Deng, D., Liang, D., Tang, Y., Peng, J., Han, X., Pan, M., 2013. Evaluation of capillary performance of sintered porous wicks for loop heat pipe. Exp. Therm. Fluid Sci. 50, 1–9. https://doi.org/10.1016/j.expthermflusci.2013.04.014

Donniacuo, A., Charnay, R., Mastrullo, R., Mauro, A.W., Revellin, R., 2015. Film thickness measurements for annular flow in minichannels: Description of the optical technique and experimental results. Exp. Therm. Fluid Sci. 69, 73–85. https://doi.org/10.1016/j.expthermflusci.2015.07.005

Dullien, F.A., 2012. Porous media: fluid transport and pore structure. Academic press, New-York.

El Achkar, G., Lavieille, P., Miscevic, M., 2012. Loop heat pipe and capillary pumped loop design: About heat transfer in the isolated bubbles zone of condensers. Appl. Therm. Eng. 33–34, 253–257. https://doi.org/10.1016/j.applthermaleng.2011.09.011

El Hajal, J., Thome, J.R., Cavallini, A., 2003. Condensation in horizontal tubes. Part 1: two-phase flow pattern map. Int. J. Heat Mass Transf. 46, 3349–3363. https://doi.org/10.1016/S0017-9310(03)00139-X

Fan, L.-W., Zhu, Z.-Q., Zeng, Y., Xiao, Y.-Q., Liu, X.-L., Wu, Y.-Y., Ding, Q., Yu, Z.-T., Cen, K.-F., 2015. Transient performance of a PCM-based heat sink with high aspect-ratio carbon nanofillers. Appl. Therm. Eng. 75, 532–540. https://doi.org/10.1016/j.applthermaleng.2014.10.050

Fieg, G.P., Roetzel, W., 1994. Calculation of laminar film condensation in/on inclined elliptical tubes. Int. J. Heat Mass Transf. 37, 619–624. https://doi.org/10.1016/0017-9310(94)90133-3

Fornells-Vernet, A., 2012. Etude expérimentale, hydrodynamique et thermique de l'évaporation dans les structures capillaires de caloduc (PIRD No. 13).

Fried, S.S., Maydanik, Y.F., Kozhin, V.A., 2013. Liquid cooled condensers for loop heat pipe like enclosure cooling. Google Patents.

Friedel, L., 1979. Improved friction pressure drop correlations for horizontal and vertical two-phase pipe flow, in: European Two-Phase Flow Group Meeting. Ispra, Italy.

Fukano, T., Ousaka, A., 1989. Prediction of the circumferential distribution of film thickness in horizontal and near-horizontal gas-liquid annular flows. Int. J. Multiph. Flow 15, 403–419. https://doi.org/10.1016/0301-9322(89)90010-4

Ghajar, A.J., Kim, J., 2005. A non-boiling two-phase flow heat transfer correlation for different flow patterns and pipe inclination angles, in: Proceedings of the 2005 ASME Summer Heat Transfer Conference. pp. 17–22.

Ghajar, A.J., Tang, C.C., 2007. Heat Transfer Measurements, Flow Pattern Maps, and Flow Visualization for Non-Boiling Two-Phase Flow in Horizontal and Slightly Inclined Pipe. Heat Transf. Eng. 28, 525–540. https://doi.org/10.1080/01457630701193906

Gharbi, S., Harmand, S., Jabrallah, S.B., 2015. Experimental comparison between different configurations of PCM based heat sinks for cooling electronic components. Appl. Therm. Eng. 87, 454–462. https://doi.org/10.1016/j.applthermaleng.2015.05.024

Giraudon, R., 2017. Contribution à la fabrication et la compréhension du comportement thermique de structures capillaires optimales pour les boucles diphasiques à pompage thermo-capillaire (Thèse de doctorat). INSA de Lyon, Université de Lyon.

Giraudon, R., Lips, S., Fabregue, D., Gremillard, L., Maire, E., Sartre, V., 2017a. Design and optimization of the sintering process of a bi-layer capillary structure for loop heat pipes. Heat Pipe Sci. Technol. Int. J. 8, 27–49. https://doi.org/10.1615/HeatPipeScieTech.2017018805

Giraudon, R., Lips, S., Sartre, V., Gremillard, L., Fabregue, D., Maire, E., 2017b. Thermohydraulic characterization of sintered copper powder wicks for loop heat pipes, in: 9th World Conference on Experimental Heat Transfer, Fluid Mechanics and Thermodynamics. Igazu Falls, Brazil.

Gully, P., 2015. Superfluid Helium Heat Pipe. Phys. Procedia, Proceedings of the 25th International Cryogenic Engineering Conference and International Cryogenic Materials Conference 2014 67, 625–630. https://doi.org/10.1016/j.phpro.2015.06.106

Gungor, K.E., Winterton, R.H.S., 1986. A general correlation for flow boiling in tubes and annuli. Int J Heat Mass Transf. 29, 351–358.

Hansen, G., Naess, E., Kristjansson, K., 2015. Sintered nickel powder wicks for flat vertical heat pipes. Energies 8, 2337–2357. https://doi.org/10.3390/en8042337

Hodot, R., 2015. Modélisation et tests d'une boucle diphasique capillaire (LHP) pour applications avioniques civile et militaire. Thèse de doctorat, Université de Lyon.

Hossain, R., Mahmud, S., Dutta, A., Pop, I., 2015. Energy storage system based on nanoparticle-enhanced phase change material inside porous medium. Int. J. Therm. Sci. 91, 49–58.

Hsu, L.-C., Cion, S.-W., Lin, K.-W., Wang, C.-C., 2015a. An experimental study of inclination on the boiling heat transfer characteristics of a micro-channel heat sink using HFE-7100. Int. Commun. Heat Mass Transf. 62, 13–17. https://doi.org/10.1016/j.icheatmasstransfer.2015.01.007

Hsu, L.-C., Cion, S.-W., Lin, K.-W., Wang, C.-C., 2015b. An experimental study of inclination on the boiling heat transfer characteristics of a micro-channel heat sink using HFE-7100. Int. Commun. Heat Mass Transf. 62, 13–17. https://doi.org/10.1016/j.icheatmasstransfer.2015.01.007

Hu, Y., Liu, T., Li, X., Wang, S., 2014. Heat transfer enhancement of micro oscillating heat pipes with self-rewetting fluid. Int. J. Heat Mass Transf. 70, 496–503. https://doi.org/10.1016/j.ijheatmasstransfer.2013.11.031

Hurlburt, E.T., Newell, T.A., 1997. Prediction of the circumferential film thickness distribution in horizontal annular gas-liquid flow, ACRC Report TR-111. Air Conditioning and Refrigeration Center. College of Engineering. University of Illinois at Urbana-Champaign.

Irissou, E., Legoux, J.-G., Ryabinin, A.N., Jodoin, B., Moreau, C., 2008. Review on cold spray process and technology: part I—intellectual property. J. Therm. Spray Technol. 17, 495–516.

Iverson, B.D., Davis, T.W., Garimella, S.V., North, M.T., Kang, S.S., 2007. Heat and mass transport in heat pipe wick structures. J. Thermophys. Heat Transf. 21, 392–404. https://doi.org/10.2514/1.25809

Jaworski, M., 2012. Thermal performance of heat spreader for electronics cooling with incorporated phase change material. Appl. Therm. Eng. 35, 212–219. https://doi.org/10.1016/j.applthermaleng.2011.10.036

Ji, Y., Liu, G., Ma, H., Li, G., Sun, Y., 2013. An experimental investigation of heat transfer performance in a polydimethylsiloxane (PDMS) oscillating heat pipe. Appl. Therm. Eng. 61, 690–697. https://doi.org/10.1016/j.applthermaleng.2013.09.001

Kaled, A., Dutour, S., Platel, V., Lachassagne, L., Ayel, V., 2012. A theoretical analysis of the transient behavior of a CPL for terrestrial application, in: 16th International Heat Pipe Conference. Presented at the 16th International Heat Pipe Conference, Lyon, France.

Kandasamy, R., Wang, X.-Q., Mujumdar, A.S., 2008. Transient cooling of electronics using phase change material (PCM)-based heat sinks. Appl. Therm. Eng. 28, 1047–1057. https://doi.org/10.1016/j.applthermaleng.2007.06.010

Kandlikar, S. Balasubramanian, P., 2003. Extending the applicability of the flow boiling correlation to low Reynolds number flows in microchannels. ASME - First Int. Conf. Microchannels Minichannels April 21-23 Rochester N. Y. USA 603–608.

Kandlikar, S.G., 1990. A General Correlation for Saturated Two-Phase Flow Boiling Heat Transfer Inside Horizontal and Vertical Tubes. J. Heat Transf. 112, 219–228. https://doi.org/10.1115/1.2910348

Karthikeyan, M., Vaidyanathan, S., Sivaraman, B., 2013. Heat transfer analysis of two-phase closed thermosyphon using aqueous solution of n-butanol. Int. J. Eng. Technol. 3, 661–667.

Karthikeyan, V.K., Khandekar, S., Pillai, B.C., Sharma, P.K., 2014. Infrared thermography of a pulsating heat pipe: Flow regimes and multiple steady states. Appl. Therm. Eng. 62, 470–480. https://doi.org/10.1016/j.applthermaleng.2013.09.041

Khandekar, S., Joshi, Y.M., Mehta, B., 2008. Thermal performance of closed two-phase thermosyphon using nanofluids. Int. J. Therm. Sci. 47, 659–667. https://doi.org/10.1016/j.ijthermalsci.2007.06.005

Khandekar, S., Panigrahi, P.K., Lefèvre, F., Bonjour, J., 2010. Local hydrodynamics of flow in a pulsating heat pipe: a review. Front. Heat Pipes 1, 023001–1 ; 023001–20.

Khodadadi, J.M., Fan, L., Babaei, H., 2013. Thermal conductivity enhancement of nanostructure-based colloidal suspensions utilized as phase change materials for thermal energy storage: A review. Renew. Sustain. Energy Rev. 24, 418–444.

Kim, D.E., Yu, D.I., Jerng, D.W., Kim, M.H., Ahn, H.S., 2015. Review of boiling heat transfer enhancement on micro/nanostructured surfaces. Exp. Therm. Fluid Sci. 66, 173–196.

Kim, N., Kim, S., 2014. Self-convectional three-dimensional integrated circuit cooling system using micro flat heat pipe for portable devices. Heat Transf. Eng. 35, 924–932. https://doi.org/10.1080/01457632.2014.859514

Kinkelin, C., 2016. Etude expérimentale d’un amortisseur thermique composite MCP-NTC. Université de Lyon, INSA Lyon.

Kinkelin, C., Lips, S., Lefevre, F., Soupremanien, U., Remondiere, V., Dijon, J., Le Poche, H., Ollier, E., Zegaoui, M., Rolland, N., Rolland, P.-A., Lhostis, S., Descouts, B., Kaplan, Y., 2015. Experimental study of a hybrid CNT/PCM structure for the transient thermal management of electronics, in: 11th International Conference on Heat Transfer, Fluid Mechanics and Thermodynamics. Skukuza, South Africa, pp. 839–844.

Kinkelin, C., Lips, S., Soupremanien, U., Remondière, V., Dijon, J., Poche, H.L., Ollier, E., Zegaoui, M., Rolland, N., Rolland, P.-A., Lhostis, S., Descouts, B., Kaplan, Y., Lefèvre, F., 2017. Theoretical and experimental study of a thermal damper based on a CNT/PCM composite structure for transient electronic cooling. Energy Convers. Manag. 142, 257–271. http://dx.doi.org/10.1016/j.enconman.2017.03.034

Kundu, A., Kumar, R., Gupta, A., 2014. Flow boiling heat transfer characteristics of R407C inside a smooth tube with different tube inclinations. Int. J. Refrig. 45, 1–12. https://doi.org/10.1016/j.ijrefrig.2014.06.009

Kunkelmann, C., Ibrahem, K., Schweizer, N., Herbert, S., Stephan, P., Gambaryan-Roisman, T., 2012. The effect of three-phase contact line speed on local evaporative heat transfer: Experimental and numerical investigations. Int. J. Heat Mass Transf. 55, 1896–1904. https://doi.org/10.1016/j.ijheatmasstransfer.2011.11.044

Lachassagne, L., Ayel, V., Romestant, C., Bertin, Y., 2012. Experimental study of capillary pumped loop for integrated power in gravity field. Appl. Therm. Eng. 35, 166–176. https://doi.org/10.1016/j.applthermaleng.2011.10.019

Lachassagne, L., Bertin, Y., Ayel, V., Romestant, C., 2013. Steady-state modeling of Capillary Pumped Loop in gravity field. Int. J. Therm. Sci. 64, 62–80. https://doi.org/10.1016/j.ijthermalsci.2012.09.007

Lachassagne, L., DELALANDRE, N., AYEL, V., ROMESTANT, C., BERTIN, Y., 2009. Modélisation transitoire d'une boucle fluide diphasique à pompage thermocapillaire.

Lal, S., Sato, Y., Niceno, B., 2015. Direct numerical simulation of bubble dynamics in subcooled and near-saturated convective nucleate boiling. Int. J. Heat Fluid Flow, Theme special issue celebrating the 75th birthdays of Brian Launder and Kemo Hanjalic 51, 16–28. https://doi.org/10.1016/j.ijheatfluidflow.2014.10.018

Larsen, P.O., von Ins, M., 2010. The rate of growth in scientific publication and the decline in coverage provided by Science Citation Index. Scientometrics 84, 575–603. https://doi.org/10.1007/s11192-010-0202-z

Launay, S., Sartre, V., Bonjour, J., 2010. Selection criteria for fluidic and geometrical parameters of a LHP based on analytical approach., in: 15th International Heat Pipe Conference. Presented at the Proc. 15th International Heat Pipe Conference, Clemson, USA.

Layssac, T., 2018. Contribution à l'étude phénoménologique de l'ébullition convective en mini-canal (Thèse de doctorat). INSA de Lyon, Université de Lyon.

Layssac, T., Capo, C., Lips, S., Mauro, A.W., Revellin, R., 2017. Prediction of symmetry during intermittent and annular horizontal two-phase flows. Int. J. Multiph. Flow 95, 91–100.

Layssac, T., Lips, S., Revellin, R., 2018a. Experimental study of flow boiling in an inclined mini-channel: effect of inclination on flow pattern transitions and pressure drops. Exp. Therm. Fluid Sci.

Layssac, T., Lips, S., Revellin, R., 2018b. Effect of inclination on heat transfer coefficient during flow boiling in an inclined mini-channel. Int. J. Heat Mass Transf.

Lin, Z., Wang, S., Shirakashi, R., Winston Zhang, L., 2013. Simulation of a miniature oscillating heat pipe in bottom heating mode using CFD with unsteady modeling. Int. J. Heat Mass Transf. 57, 642–656. https://doi.org/10.1016/j.ijheatmasstransfer.2012.09.007

Ling, Z., Zhang, Z., Shi, G., Fang, X., Wang, L., Gao, X., Fang, Y., Xu, T., Wang, S., Liu, X., 2014. Review on thermal management systems using phase change materials for electronic components, Li-ion batteries and photovoltaic modules. Renew. Sustain. Energy Rev. 31, 427–438.

Lips, S., 2015. Recent progress and challenges in heat pipes science, in: 11th International Conference on Heat Transfer, Fluid Mechanics and Thermodynamics. Skukuza, South Africa.

Lips, S., 2009. Analyse phénoménologique du fonctionnement de diffuseurs thermiques diphasiques (caloducs plats) par voies expérimentale et numérique (Thèse doctorat). Institut national des sciences appliquées (Lyon).
Lips, S., Barrière, A., Narcy, M., Sartre, V., 2017a. Dispositif de diffusion thermique. 1750129.
Lips, S., Bonjour, J., 2007. Oscillating two-phase flow in a capillary tube: Experiments and modeling, in: Proc. 14th International Heat Pipe Conference (IHPC),. Florianopolis, Brazil.
Lips, S., Fornells-Vernet, A., Lefèvre, F., 2013. Utilisation de mèches métalliques comme structure capillaire pour des caloducs plats., in: Congrès Français de Thermique. Gerardmer, France.
Lips, S., Lefèvre, F., 2014. A general analytical model for the design of conventional heat pipes. Int. J. Heat Mass Transf. 72, 288–298. https://doi.org/10.1016/j.ijheatmasstransfer.2013.12.068
Lips, S., Lefèvre, F., Bonjour, J., 2010a. Investigation of evaporation and condensation processes specific to grooved flat heat pipes. Front. Heat Pipes 1, 023001–1 ; 023001–8. https://doi.org/10.5098/fhp.v1.2.3001
Lips, S., Lefèvre, F., Bonjour, J., 2010b. Thermohydraulic study of a flat plate heat pipe by means of confocal microscopy: application to a 2D capillary structure. J. Heat Transf. 132, 019008. https://doi.org/10.1115/1.4001930
Lips, S., Lefèvre, F., Bonjour, J., 2010c. Combined effects of the filling ratio and the vapour space thickness on the performance of a flat plate heat pipe. Int. J. Heat Mass Transf. 53, 694–702. https://doi.org/10.1016/j.ijheatmasstransfer.2009.10.022
Lips, S., Lefèvre, F., Bonjour, J., 2009a. Thermal and hydrodynamic study of a flat plate heat pipe, in: Proc. 7th Experimental Heat Transfer, Fluid Mechanics and Thermodynamics (ExHFT), Krakow, Poland.
Lips, S., Lefèvre, F., Bonjour, J., 2009b. Nucleate boiling in a flat grooved heat pipe. Int. J. Therm. Sci. 48, 1273–1278. https://doi.org/10.1016/j.ijthermalsci.2008.11.011
Lips, S., Meyer, J.P., 2012a. Experimental study of convective condensation in an inclined smooth tube. Part I: Inclination effect on flow pattern and heat transfer coefficient. Int. J. Heat Mass Transf. 55, 395–404. https://doi.org/10.1016/j.ijheatmasstransfer.2011.09.033
Lips, S., Meyer, J.P., 2012b. Experimental study of convective condensation in an inclined smooth tube. Part II: Inclination effect on pressure drop and void fraction. Int. J. Heat Mass Transf. 55, 405–412. https://doi.org/10.1016/j.ijheatmasstransfer.2011.09.034
Lips, S., Meyer, J.P., 2012c. Stratified flow model for convective condensation in an inclined tube. Int. J. Heat Fluid Flow 36, 83–91. https://doi.org/10.1016/j.ijheatfluidflow.2012.03.005
Lips, S., Meyer, J.P., 2012d. Global optimisation of tube inclination during convective condensation, in: 8th International Conference on Boiling and Condensation Heat Transfer (ECI 8th). Lausanne, Switzerland.
Lips, S., Meyer, J.P., 2012e. Effect of gravity forces on heat transfer and pressure drops during condensation of R134a. Microgravity Sci. Technol. 24, 157–164. https://doi.org/10.1007/s12217-011-9292-3
Lips, S., Meyer, J.P., 2011a. Two-phase flow in inclined tubes with specific reference to condensation: A review. Int. J. Multiph. Flow 37, 845–859. https://doi.org/10.1016/j.ijmultiphaseflow.2011.04.005
Lips, S., Meyer, J.P., 2011b. Experimental study of Convective condensation of R134A in an inclined Tube, in: 8th International Conference on Heat Transfer, Fluid Mechanics and Thermodynamics. Pointe Aux Piments, Ile Maurice.
Lips, S., Narcy, M., Barrière, A., Sartre, V., 2017b. Définition d'un critère d'utilité appliqué aux diffuseurs thermiques diphasiques pour le refroidissement de composants électroniques, in: Congrès de La SFT. Marseille, France.
Lips, S., Revellin, R., 2013. Physical meaning of the pressure drop decomposition in two-phase flows, in: 51th European Two-Phase Group Meeting. Lyon, France.
Liu, X., Chen, Y., 2013. Transient thermal performance analysis of micro heat pipes. Appl. Therm. Eng. 58, 585–593. https://doi.org/10.1016/j.applthermaleng.2013.04.025
Liu, Z., Winterton, R.H.S., 1991. A general correlation for saturated and subcooled flow boiling in tubes and annuli, based on a nucleate pool boiling equation. Int J Heat Mass Transf. 34, 2759–2766.

Liu, Z.-H., Li, Y.-Y., 2012. A new frontier of nanofluid research–Application of nanofluids in heat pipes. Int. J. Heat Mass Transf. 55, 6786–6797. https://doi.org/10.1016/j.ijheatmasstransfer.2012.06.086

MacGregor, R.W., Kew, P.A., Reay, D.A., 2013. Investigation of low global warming potential working fluids for a closed two-phase thermosyphon. Appl. Therm. Eng. 51, 917–925. https://doi.org/10.1016/j.applthermaleng.2012.10.049

Mallik, S., Ekere, N., Best, C., Bhatti, R., 2011. Investigation of thermal management materials for automotive electronic control units. Appl. Therm. Eng. 31, 355–362.

Mameli, M., Araneo, L., Filippeschi, S., Marelli, L., Testa, R., Marengo, M., 2014. Thermal response of a closed loop pulsating heat pipe under a varying gravity force. Int. J. Therm. Sci. 80, 11–22. https://doi.org/10.1016/j.ijthermalsci.2014.01.023

Mameli, M., Marengo, M., Zinna, S., 2012a. Thermal Simulation of a Pulsating Heat Pipe: Effects of Different Liquid Properties on a Simple Geometry. Heat Transf. Eng. 33, 1177–1187. https://doi.org/10.1080/01457632.2012.677695

Mameli, M., Marengo, M., Zinna, S., 2012b. Numerical Investigation of the Effects of Orientation and Gravity in a Closed Loop Pulsating Heat Pipe. Microgravity Sci. Technol. 24, 79–92. https://doi.org/10.1007/s12217-011-9293-2

Marchuk, I., Lyulin, Y., Kabov, O.A., 2013. Theoretical and experimental study of convective condensation inside a circular tube. Interfacial Phenom. Heat Transf. 1.

Marconnet, A.M., Panzer, M.A., Goodson, K.E., 2013. Thermal conduction phenomena in carbon nanotubes and related nanostructured materials. Rev. Mod. Phys. 85, 1295.

Martel, S., Lips, S., Kuhni, M., Galizzi, C., Revellin, R., 2018. Characterisation of saturated two-phase flows by means of fluorescence and phosphorescence techniques: a review, in: 10th International Conference on Boiling and Condensation Heat Transfer. Nagasaki, Japan.

Masala, T., Harvel, G., Chang, J.-S., 2007. Separated two-phase flow regime parameter measurement by a high speed ultrasonic pulse-echo system. Rev. Sci. Instrum. 78, 114901. https://doi.org/10.1063/1.2804117

Maydanik, Y.F., Chernysheva, M.A., Pastukhov, V.G., 2014. Review: Loop heat pipes with flat evaporators. Appl. Therm. Eng. 67, 294–307. https://doi.org/10.1016/j.applthermaleng.2014.03.041

Mehta, B., Khandekar, S., 2014. Measurement of local heat transfer coefficient during gas–liquid Taylor bubble train flow by infra-red thermography. Int. J. Heat Fluid Flow 45, 41–52. https://doi.org/10.1016/j.ijheatfluidflow.2013.12.001

Meyer, J.P., Dirker, J., Adelaja, A.O., 2014. Condensation heat transfer in smooth inclined tubes for R134a at different saturation temperatures. Int. J. Heat Mass Transf. 70, 515–525.

Michels, V., Milanez, F.H., Mantelli, M.B.H., 2012. Vapor chamber heat sink with hollow fins. J. Braz. Soc. Mech. Sci. Eng. 34, 233–237. https://doi.org/10.1590/S1678-58782012000300002

Michels, V., Milanez, F.H., Mantelli, M.H., 2007. Analytical model to predict thermal resistances of hollow fin heat sinks, in: 19th International Congress of Mechanical Engineering. Brasilia, Brazil.

Mills, A., Farid, M., Selman, J.R., Al-Hallaj, S., 2006. Thermal conductivity enhancement of phase change materials using a graphite matrix. Appl. Therm. Eng. 26, 1652–1661.

Miscevic, M., El Achkar, G., Lavieille, P., Kaled, A., Dutour, S., 2012. About flow regime and heat transfer in low diameter condenser of LHP and CPL, in: 16th International Heat Pipe Conference. Lyon, France.

Mishkinis, D., Prado, P., Sanz, R., Torres, A., 2010. Development of LHP for Intermediate Temperature Range, in: 15th International Heat Pipe Conference. Presented at the Clemson, USA.

Mohseni, S.G., Akhavan-Behabadi, M.A., 2014. Flow pattern visualization and heat transfer characteristics of R-134a during evaporation inside a smooth tube with different tube inclinations. Int. Commun. Heat Mass Transf. 59, 39–45. https://doi.org/10.1016/j.icheatmasstransfer.2014.10.018

Mohseni, S.G., Akhavan-Behabadi, M.A., Saeedinia, M., 2013. Flow pattern visualization and heat transfer characteristics of R-134a during condensation inside a smooth tube with different tube inclinations. Int. J. Heat Mass Transf. 60, 598–602.

Monier-Vinard, E., Rogie, B., Bissuel, V., Laraqi, N., Daniel, O., Kotelon, M.-C., 2017. State of the art of thermal characterization of electronic components using computational fluid dynamic tools. Int. J. Numer. Methods Heat Fluid Flow 27, 2433–2450. https://doi.org/10.1108/HFF-10-2016-0380

Monier-Vinard, E., Rogie, B., Nguyen, N.-M., Laraqi, N., Bissuel, V., Daniel, O., 2016. Practical steady-state temperature prediction of active embedded chips into high density electronic board. J. Phys. Conf. Ser. 745, 032095. https://doi.org/10.1088/1742-6596/745/3/032095

Mottet, L., Coquard, T., Prat, M., 2015. Three dimensional liquid and vapour distribution in the wick of capillary evaporators. Int. J. Heat Mass Transf. 83, 636–651. https://doi.org/10.1016/j.ijheatmasstransfer.2014.12.048

Muratore, C., Aouadi, S.M., Voevodin, A.A., 2012. Embedded phase change material microinclusions for thermal control of surfaces. Surf. Coat. Technol. 206, 4828–4832.

Narcy, M., de Malmazet, E., Colin, C., 2014. Flow boiling in tube under normal gravity and microgravity conditions. Int. J. Multiph. Flow 60, 50–63. https://doi.org/10.1016/j.ijmultiphaseflow.2013.11.011

Narcy, M., Lips, S., Barrière, A., Sartre, V., 2017. Experimental investigation of a confined flat two-phase thermosyphon for electronics cooling, in: 9th World Conference on Experimental Heat Transfer, Fluid Mechanics and Thermodynamics. Igazu Falls, Brazil.

Nikolayev, V.S., 2011. A dynamic film model of the pulsating heat pipe. J. HeatTransfer 133, 081504. https://doi.org/10.1115/1.4003759

Nikolayev, V.S., 2010. Dynamics of the triple contact line on a nonisothermal heater at partial wetting. Phys. Fluids 22, 082105. https://doi.org/10.1063/1.3483558

Nishikawara, M., Nagano, H., Kaya, T., 2013. Transient thermo-fluid modeling of loop heat pipes and experimental validation. J. Thermophys. Heat Transf. 27, 641–647. https://doi.org/10.2514/1.T3888

Ong, C.L., Thome, J.R., 2011. Macro-to-microchannel transition in two-phase flow: Part 1 – Two-phase flow patterns and film thickness measurements. Exp. Therm. Fluid Sci. 35, 37–47. https://doi.org/10.1016/j.expthermflusci.2010.08.004

Ozer, A.B., Oncel, A.F., Hollingsworth, D.K., Witte, L.C., 2011. A method of concurrent thermographic–photographic visualization of flow boiling in a minichannel. Exp. Therm. Fluid Sci. 35, 1522–1529. https://doi.org/10.1016/j.expthermflusci.2011.07.002

Plawsky, J.L., Fedorov, A.G., Garimella, S.V., Ma, H.B., Maroo, S.C., Chen, L., Nam, Y., 2014. Nano- and Microstructures for Thin-Film Evaporation—A Review. Nanoscale Microscale Thermophys. Eng. 18, 251–269. https://doi.org/10.1080/15567265.2013.878419

Poniewski, M.E., Thome, J.R., 2008. Nucleate boiling on micro-structured surfaces. Heat Transfer Research, Inc. (HTRI), College Station.

Price, D.C., 2003. A review of selected thermal management solutions for military electronic systems. IEEE Trans. Compon. Packag. Technol. 26, 26–39.

Qu, J., Wang, Q., 2013. Experimental study on the thermal performance of vertical closed-loop oscillating heat pipes and correlation modeling. Appl. Energy 112, 1154–1160. https://doi.org/10.1016/j.apenergy.2013.02.030

Qu, X., Zhang, L., Mao, W.U., Ren, S., 2011. Review of metal matrix composites with high thermal conductivity for thermal management applications. Prog. Nat. Sci. Mater. Int. 21, 189–197.

Ranjan, R., Garimella, S.V., Murthy, J.Y., Yazawa, K., 2011. Assessment of nanostructured capillary wicks for passive two-phase heat transport. Nanoscale Microscale Thermophys. Eng. 15, 179–194.

Ranjan, R., Patel, A., Garimella, S.V., Murthy, J.Y., 2012. Wicking and thermal characteristics of micropillared structures for use in passive heat spreaders. Int. J. Heat Mass Transf. 55, 586–596. https://doi.org/10.1016/j.ijheatmasstransfer.2011.10.053

Rao, M., Lefèvre, F., Khandekar, S., Bonjour, J., 2015. Heat and mass transfer mechanisms of a self-sustained thermally driven oscillating liquid–vapour meniscus. Int. J. Heat Mass Transf. 86, 519–530. https://doi.org/10.1016/j.ijheatmasstransfer.2015.03.015

Rao, Z., Wang, S., 2011. A review of power battery thermal energy management. Renew. Sustain. Energy Rev. 15, 4554–4571.

Revil-Baudard, L., Lips, S., 2015. A non-invasive method for thermal and hydrodynamic characterisation of flat plate heat pipes, in: 9th International Conference on Boiling and Condensation Heat Transfer. Boulder, Colorado.

Rouhani, S.., Axelsson, E., 1970. Calculation of void volume fraction in the subcooled and quality boiling regions. Int. J. Heat Mass Transf. 13, 383–393. https://doi.org/10.1016/0017-9310(70)90114-6

Sahoo, S.K., Das, M.K., Rath, P., 2016. Application of TCE-PCM based heat sinks for cooling of electronic components: A review. Renew. Sustain. Energy Rev. 59, 550–582. https://doi.org/10.1016/j.rser.2015.12.238

Saidur, R., Leong, K.Y., Mohammad, H., 2011. A review on applications and challenges of nanofluids. Renew. Sustain. Energy Rev. 15, 1646–1668.

Saitoh, S., Daiguji, H., Hihara, E., 2007. Correlation for boiling heat transfer of R-134a in horizontal tubes including effect of tube diameter. Int. J. Heat Mass Transf. 50, 5215–5225. https://doi.org/10.1016/j.ijheatmasstransfer.2007.06.019

Santos, P.H.D., Bazzo, E., Oliveira, A.A.M., 2012. Thermal performance and capillary limit of a ceramic wick applied to LHP and CPL. Appl. Therm. Eng. 41, 92–103. https://doi.org/10.1016/j.applthermaleng.2012.02.042

Sato, Y., Niceno, B., 2017. Nucleate pool boiling simulations using the interface tracking method: Boiling regime from discrete bubble to vapor mushroom region. Int. J. Heat Mass Transf. 105, 505–524. https://doi.org/10.1016/j.ijheatmasstransfer.2016.10.018

Savino, R., Di Paola, R., Cecere, A., Fortezza, R., 2010. Self-rewetting heat transfer fluids and nanobrines for space heat pipes. Acta Astronaut. 67, 1030–1037. https://doi.org/10.1016/j.actaastro.2010.06.034

Schubring, D., Ashwood, A.C., Shedd, T.A., Hurlburt, E.T., 2010. Planar laser-induced fluorescence (PLIF) measurements of liquid film thickness in annular flow. Part I: Methods and data. Int. J. Multiph. Flow 36, 815–824. https://doi.org/10.1016/j.ijmultiphaseflow.2010.05.007

Schubring, D., Shedd, T.A., 2009. Critical friction factor modeling of horizontal annular base film thickness. Int. J. Multiph. Flow 35, 389–397. https://doi.org/10.1016/j.ijmultiphaseflow.2008.12.002

Senthilkumar, R., Vaidyanathan, S., Sivaraman, B., 2012. Comparative study on heat pipe performance using aqueous solutions of alcohols. Heat Mass Transf. 48, 2033–2040. https://doi.org/10.1007/s00231-012-1046-2

Setoh, G., Tan, F.L., Fok, S.C., 2010. Experimental studies on the use of a phase change material for cooling mobile phones. Int. Commun. Heat Mass Transf. 37, 1403–1410. https://doi.org/10.1016/j.icheatmasstransfer.2010.07.013

Shaikh, S., Lafdi, K., 2010. C/C composite, carbon nanotube and paraffin wax hybrid systems for the thermal control of pulsed power in electronics. Carbon 48, 813–824.

Siedel, B., 2014. Analysis of heat transfer and flow patterns in a LHP: modelling by analytical and numerical approaches and experimental observations. PhD thesis, INSA de Lyon.

Siedel, B., Sartre, V., Lefèvre, F., 2015a. Literature review: Steady-state modelling of loop heat pipes. Appl. Therm. Eng. 75, 709–723.

Siedel, B., Sartre, V., Lefèvre, F., 2015b. Complete analytical model of a loop heat pipe with a flat evaporator. Int. J. Therm. Sci. 89, 372–386. https://doi.org/10.1016/j.ijthermalsci.2014.11.014

Sikarwar, B.S., Battoo, N.K., Khandekar, S., Muralidhar, K., 2011. Dropwise condensation underneath chemically textured surfaces: simulation and experiments. J. Heat Transf. 133, 021501.

Singh, R., Nguyen, T., Mochizuki, M., 2014. Capillary evaporator development and qualification for loop heat pipes. Appl. Therm. Eng. 63, 406–418. https://doi.org/10.1016/j.applthermaleng.2013.10.059

Smith, K., Kempers, R., Robinson, A.J., Siedel, S., 2014. Flow visualisation in a transparent thermosyphon: influence of internal pressure, in: 15th International Heat Transfer Conference. Kyoto, Japan. https://doi.org/10.1615/IHTC15.hpp.008985

Spedding, P.L., Chen, J.J.J., Nguyen, V.T., 1982. Pressure drop in two phase gas-liquid flow in inclined pipes. Int. J. Multiph. Flow 8, 407–431. https://doi.org/10.1016/0301-9322(82)90050-7

Srimuang, W., Amatachaya, P., 2012. A review of the applications of heat pipe heat exchangers for heat recovery. Renew. Sustain. Energy Rev. 16, 4303–4315. https://doi.org/10.1016/j.rser.2012.03.030

Srinivasan, V., Marty-Jourjon, V., Khandekar, S., Lefèvre, F., Bonjour, J., 2015. Evaporation of an isolated liquid plug moving inside a capillary tube. Int. J. Heat Mass Transf. 89, 176–185. https://doi.org/10.1016/j.ijheatmasstransfer.2015.05.039

Steiner, D., 1993. Heat transfer to boiling saturated liquids. VDI-Wārmeatlas VDI Heat Atlas Ver. Dtsch. Ingenieure VDI-Ges. Verfahrenstechnik Chemieingenieurwesen GCV Düsseld. Chapter Hbb.

Stutz, B., Morceli, C.H.S., da Silva, M. de F., Cioulachtjian, S., Bonjour, J., 2011. Influence of nanoparticle surface coating on pool boiling. Exp. Therm. Fluid Sci. 35, 1239–1249. https://doi.org/10.1016/j.expthermflusci.2011.04.011

Suman, B., 2006. A steady state model and maximum heat transport capacity of an electrohydrodynamically augmented micro-grooved heat pipe. Int. J. Heat Mass Transf. 49, 3957–3967. https://doi.org/10.1016/j.ijheatmasstransfer.2006.04.011

Sureshkumar, R., Mohideen, S.T., Nethaji, N., 2013. Heat transfer characteristics of nanofluids in heat pipes: A review. Renew. Sustain. Energy Rev. 20, 397–410. https://doi.org/10.1016/j.rser.2012.11.044

Tadrist, L., 2007. Review on two-phase flow instabilities in narrow spaces. Int. J. Heat Fluid Flow 28, 54–62.

Taitel, Y., Dukler, A.E., 1976. A model for predicting flow regime transitions in horizontal and near horizontal gas-liquid flow. AIChE J. 22, 47–55. https://doi.org/10.1002/aic.690220105

Tong, X.C., 2011. Advanced Materials for Thermal Management of Electronic Packaging. Springer.

van Rooyen, E., Christians, M., Liebenberg, L., Meyer, J.P., 2010. Probabilistic flow pattern-based heat transfer correlation for condensing intermittent flow of refrigerants in smooth horizontal tubes. Int. J. Heat Mass Transf. 53, 1446–1460. https://doi.org/10.1016/j.ijheatmasstransfer.2009.12.005

Vaze, M.J., Banerjee, J., 2011. Effect of inclination on flow and thermal characteristics of air-water two-phase flow: an experimental investigation. pp. 213–224. https://doi.org/10.2495/MPF110181

Vivet, P., Guérin, V., 2011. A Three-Layers 3D-IC Stack including Wide-IO and 3D NoC (Network on Chip)–Practical Design Perspective, in: Proceedings of 3D-Architectures for Semiconductor Integration and Packaging (3D-ASIP). San Francisco, California.

Waldrop, M.M., 2016. The chips are down for Moore's law. Nat. News 530, 144.

Wang, C.-C., Chang, W.-J., Dai, C.-H., Lin, Y.-T., Yang, K.-S., 2012. Effect of inclination on the convective boiling performance of a microchannel heat sink using HFE-7100. Exp. Therm. Fluid Sci. 36, 143–148. https://doi.org/10.1016/j.expthermflusci.2011.09.006

Wang, J.-C., 2012. 3-D numerical and experimental models for flat and embedded heat pipes applied in high-end VGA card cooling system. Int. Commun. Heat Mass Transf. 39, 1360–1366. https://doi.org/10.1016/j.icheatmasstransfer.2012.07.030

Wang, X.-Q., Mujumdar, A.S., Yap, C., 2007. Effect of orientation for phase change material (PCM)-based heat sinks for transient thermal management of electric components. Int. Commun. Heat Mass Transf. 34, 801–808. https://doi.org/10.1016/j.icheatmasstransfer.2007.03.008

Wang, Z., Zhang, X., Li, Z., Luo, M., 2015. Analysis on energy efficiency of an integrated heat pipe system in data centers. Appl. Therm. Eng. 90, 937–944. https://doi.org/10.1016/j.applthermaleng.2015.07.078

Weinstein, R.D., Kopec, T.C., Fleischer, A.S., Addio, E.D., Bessel, C.A., 2008. The Experimental Exploration of Embedding Phase Change Materials With Graphite Nanofibers for the Thermal Management of Electronics. J. Heat Transf. 130, 040301.1-044503.4.

Weisman, J., Kang, S.Y., 1981. Flow pattern transitions in vertical and upwardly inclined lines. Int. J. Multiph. Flow 7, 271–291. https://doi.org/10.1016/0301-9322(81)90022-7

Wojtan, L., Ursenbacher, T., Thome, J.R., 2005. Investigation of flow boiling in horizontal tubes: Part I - A new diabatic two-phase flow pattern map. Int. J. Heat Mass Transf. 48, 2955–2969.

Xing, F., Xu, J., Xie, J., Liu, H., Wang, Z., Ma, X., 2015. Froude number dominates condensation heat transfer of R245fa in tubes: Effect of inclination angles. Int. J. Multiph. Flow 71, 98–115. https://doi.org/10.1016/j.ijmultiphaseflow.2015.01.005

Xu, J., Zhang, L., Xu, H., Zhong, J., Xuan, J., 2014. Experimental investigation and visual observation of loop heat pipes with two-layer composite wicks. Int. J. Heat Mass Transf. 72, 378–387. https://doi.org/10.1016/j.ijheatmasstransfer.2014.01.016

Yeo, J., Yamashita, S., Hayashida, M., Koyama, S., 2014. A loop thermosyphon type cooling system for high heat flux. J. Electron. Cool. Therm. Control 4, 128–137. https://doi.org/10.4236/jectc.2014.44014

Yu, Z., Hallinani, K., Bhagat, W., Kashani, R., 2002. Electrodynamically augmented micro heat pipes. J. Thermophys. Heat Transf. 16, 180–186.

Zalba, B., Marín, J.M., Cabeza, L.F., Mehling, H., 2003. Review on thermal energy storage with phase change: materials, heat transfer analysis and applications. Appl. Therm. Eng. 23, 251–283. https://doi.org/10.1016/S1359-4311(02)00192-8

Zhang, W., Hibiki, T., Mishima, K., 2004. Correlation for flow boiling heat transfer in mini-channels. Int. J. Heat Mass Transf. 47, 5749–5763. https://doi.org/10.1016/j.ijheatmasstransfer.2004.07.034

Zhang, X., Zhao, X., Shen, J., Xu, J., Yu, X., 2014. Dynamic performance of a novel solar photovoltaic/loop-heat-pipe heat pump system. Appl. Energy 114, 335–352. https://doi.org/10.1016/j.apenergy.2013.09.063

List of publications

- **Articles in international journals (24)**

[1] M. Narcy, S. Lips, V. Sartre, Experimental investigation of a confined flat two-phase thermosyphon for electronics cooling, Experimental Thermal and Fluid Science (2018) In press, corrected proof. https://doi.org/10.1016/j.expthermflusci.2018.01.018.

[2] T. Layssac, C. Capo, S. Lips, A.W. Mauro, R. Revellin, Prediction of symmetry during intermittent and annular horizontal two-phase flows, International Journal of Multiphase Flow. 95 (2017) 91–100.

[3] C. Kinkelin, S. Lips, U. Soupremanien, V. Remondière, J. Dijon, H.L. Poche, E. Ollier, M. Zegaoui, N. Rolland, P.-A. Rolland, S. Lhostis, B. Descouts, Y. Kaplan, F. Lefèvre, Theoretical and experimental study of a thermal damper based on a CNT/PCM composite structure for transient electronic cooling, Energy Conversion and Management. 142 (2017) 257–271. doi:http://dx.doi.org/10.1016/j.enconman.2017.03.034.

[4] R. Giraudon, S. Lips, D. Fabregue, L. Gremillard, E. Maire, V. Sartre, Design and optimization of the sintering process of a bi-layer capillary structure for loop heat pipes, Heat Pipe Science and Technology, An International Journal. 8-1 (2017) 27–49. Doi:10.1615/HeatPipeScieTech.2017018805

[5] C. Capo, T. Layssac, S. Lips, A.W. Mauro, R. Revellin, Asymmetry during a horizontal annular flow in a micro-channel: optical measurements and effect of dimensionless numbers, J. Phys.: Conf. Ser. 796 (2017) 12045. doi:10.1088/1742-6596/796/1/012045.

[6] N. Blet, S. Lips, V. Sartre, Heats pipes for temperature homogenization: A literature review, Applied Thermal Engineering. 118 (2017) 490–509. doi:10.1016/j.applthermaleng.2017.03.009.

[7] S. Lips, V. Sartre, F. Lefèvre, S. Khandekar, J. Bonjour, Overview of heat pipe studies during the period 2010-2015, Interfacial Phenomena and Heat Transfer. 4 (2016) 33–53.

[8] E. Ollier, U. Soupremanien, V. Remondière, J. Dijon, H. Le Poche, A.L. Seiler, F. Lefevre, S. Lips, C. Kinkelin, N. Rolland, P. Rolland, M. Zegaoui, S. Lhostis, P. Ancey, B. Descouts, Y. Kaplan, Thermal Management of Electronic Devices by Composite Materials Integrated in Silicon, Microelectronic Engineering. 127 (2014) 28–33. doi:10.1016/j.mee.2014.03.016.

[9] S. Lips, F. Lefèvre, A general analytical model for the design of conventional heat pipes, International Journal of Heat and Mass Transfer. 72 (2014) 288–298. doi:10.1016/j.ijheatmasstransfer.2013.12.068.

[10] R. Revellin, S. Lips, P. Neveu, J. Bonjour, A comprehensive non-equilibrium thermodynamic analysis applied to a vapor–liquid two-phase flow of a pure fluid, International Journal of Multiphase Flow. 42 (2012) 184–193. doi:10.1016/j.ijmultiphaseflow.2012.02.008.

[11] S. Lips, J.P. Meyer, Stratified flow model for convective condensation in an inclined tube, International Journal of Heat and Fluid Flow. 36 (2012) 83–91. doi:10.1016/j.ijheatfluidflow.2012.03.005.

[12] S. Lips, J.P. Meyer, Experimental study of convective condensation in an inclined smooth tube. Part I: Inclination effect on flow pattern and heat transfer coefficient, Int. J. Heat Mass Transfer. 55 (2012) 395–404. doi:10.1016/j.ijheatmasstransfer.2011.09.033.

[13] S. Lips, J.P. Meyer, Experimental study of convective condensation in an inclined smooth tube. Part II: Inclination effect on pressure drop and void fraction, Int. J. Heat Mass Transfer. 55 (2012) 405–412. doi:10.1016/j.ijheatmasstransfer.2011.09.034.

[14] S. Lips, J.P. Meyer, Effect of gravity forces on heat transfer and pressure drops during condensation of R134a, Microgravity Sci. Technol. 24 (2012) 157–164. doi:10.1007/s12217-011-9292-3.

[15] F. Lefèvre, S. Lips, R. Rullière, J.-B. Conrardy, M. Raynaud, J. Bonjour, Flat plate heat pipes: from observations to the modeling of the capillary structure, Frontiers in Heat Pipes. 3 (2012). doi:10.5098/fhp.v3.1.3001.

[16] S. Lips, J.P. Meyer, Two-phase flow in inclined tubes with specific reference to condensation: A review, Int. J. Multiphase Flow. 37 (2011) 845–859. doi:10.1016/j.ijmultiphaseflow.2011.04.005.

[17] S. Lips, F. Lefèvre, J. Bonjour, Physical mechanisms involved in grooved flat heat pipes: Experimental and numerical analyses, Int. J. Therm. Sci. 50 (2011) 1243–1252. doi:10.1016/j.ijthermalsci.2011.02.008.

[18] S. Lips, F. Lefèvre, J. Bonjour, Thermohydraulic study of a flat plate heat pipe by means of confocal microscopy: application to a 2D capillary structure, J. Heat Transfer. 132 (2010) 19008. doi:10.1115/1.4001930.

[19] S. Lips, F. Lefèvre, J. Bonjour, Investigation of evaporation and condensation processes specific to grooved flat heat pipes., Frontiers in heat pipes. 1 (2010) 23001-1-8. doi:10.5098/fhp.v1.2.3001.

[20] S. Lips, F. Lefèvre, J. Bonjour, Combined effects of the filling ratio and the vapour space thickness on the performance of a flat plate heat pipe, Int. J. Heat Mass Transfer. 53 (2010) 694–702. doi:10.1016/j.ijheatmasstransfer.2009.10.022.

[21] S. Lips, A. Bensalem, Y. Bertin, V. Ayel, C. Romestant, J. Bonjour, Experimental evidences of distinct heat transfer regimes in pulsating heat pipes (PHP), Appl. Therm. Eng. 30 (2010) 900–907. doi:10.1016/j.applthermaleng.2009.12.020.

[22] F. Lefèvre, R. Rullière, S. Lips, J. Bonjour, Confocal microscopy for capillary film measurements in a flat plate heat pipe, J. Heat Transfer. 132 (2010) 31502. doi:10.1115/1.4000057.

[23] R. Revellin, S. Lips, S. Khandekar, J. Bonjour, Local entropy generation for saturated two-phase flow, Energy. 34 (2009) 1113–1121. doi:10.1016/j.energy.2009.03.014.

[24] S. Lips, F. Lefèvre, J. Bonjour, Nucleate boiling in a flat grooved heat pipe, Int. J. Therm. Sci. 48 (2009) 1273–1278. doi:10.1016/j.ijthermalsci.2008.11.011.

- **Book chapter (1)**

[1] J. Bonjour, S. Lips, V. Sartre, M. Woloszyn, Transferts avec changement de phase fluide-fluide, in: Transferts Thermiques - Initiation et Approfondissement, Lavoisier, 2015: pp. 359–438.

- **Patent (1)**

[1] S. Lips, A. Barrière, M. Narcy, V. Sartre, Dispositif de diffusion thermique, 1750129, 2017.

- **Communications in international conferences with proceedings (20, including 1 invited talk)**

[1] N. Cardin, L. Davoust, S. Lips, S. Siedel, J. Bonjour. Theoretical and experimental investigations of the effect of an electric field on the shape of a meniscus in a square groove. in : 5th European Conference on Microfluidics – µFlu18 3rd European Conference on Non-Equilibrium Gas Flows – NEGF18. Strasbourg, France, 2018.

[2] S. Martel, S.Lips, M. Kuhni, C. Galizzi, R. Revellin. Characterisation of saturated two-phase flows by means of fluorescence and phosphorescence techniques: a review. in : 10th International Conference on Boiling and Condensation Heat Transfer. Nagasaki, Japan, 2018.

[3] N. Cardin, M. El Mehdi Brik, S. Lips, S. Siedel, J. Bonjour, L.Davoust. Effect of a DC electric field on the liquid-vapor interface in a grooved flat heat pipe. in : 13th International Conference on Heat Transfer, Fluid Mechanics and Thermodynamics. Portoroz, Slovenia, 2017.

[4] M. Narcy, S. Lips, A. Barrière, V. Sartre, Experimental investigation of a confined flat two-phase thermosyphon for electronics cooling, in: 9th World Conference on Experimental Heat Transfer, Fluid Mechanics and Thermodynamics, Igazu Falls, Brazil, 2017.

[5] R. Giraudon, S. Lips, V. Sartre, L. Gremillard, D. Fabregue, E. Maire, Thermohydraulic characterization of sintered copper powder wicks for loop heat pipes, in: 9th World Conference on Experimental Heat Transfer, Fluid Mechanics and Thermodynamics, Igazu Falls, Brazil, 2017.

[6] N. Cardin, M. El Mehdi Brik, S. Lips, S. Siedel, J. Bonjour, L. Davoust, Effect of a DC electric field on the liquid-vapor interface in a grooved flat heat pipe, in: 13th International Conference on Heat Transfer, Fluid Mechanics and Thermodynamics, Portoroz, Slovenia, 2017.

[7] T. Layssac, S. Lips, R. Revellin, Prediction of asymmetry during intermittent and annular flows of R-245fa in an horizontal mini-channel, in: 9th International Conference on Multiphase Flow, Firenze, Italy, 2016.

[8] C. Capo, T. Layssac, S. Lips, A.W. Mauro, R. Revellin, Asymmetry during a horizontal annular flow in a micro-channel: optical measurements and effect of dimensionless numbers, in: 34rd UIT Heat Transfer Conference, Ferrara, Italy, 2016.

[9] R. Giraudon, S. Lips, D. Fabregue, L. Gremillard, E. Maire, V. Sartre, Fabrication and characterization of efficient wicks for LHPs, in: Joint 18th IHPC and 12th IHPS, Jeju, Korea, 2016.

[10] L. Revil-Baudard, S. Lips, A non-invasive method for thermal and hydrodynamic characterisation of flat plate heat pipes, in: 9th International Conference on Boiling and Condensation Heat Transfer, Boulder, Colorado, 2015.

[11] S. Lips, Recent progress and challenges in heat pipes science, in: 11th International Conference on Heat Transfer, Fluid Mechanics and Thermodynamics, Skukuza, South Africa, 2015 (conference invitee).

[12] C. Kinkelin, S. Lips, F. Lefevre, U. Soupremanien, V. Remondiere, J. Dijon, H. Le Poche, E. Ollier, M. Zegaoui, N. Rolland, P.-A. Rolland, S. Lhostis, B. Descouts, Y. Kaplan, Experimental study of a hybrid CNT/PCM structure for the transient thermal management of electronics, in: 11th International Conference on Heat Transfer, Fluid Mechanics and Thermodynamics, Skukuza, South Africa, 2015: pp. 839–844.

[13] E. Ollier, U. Soupremanien, V. Remondière, J. Dijon, H. Le Poche, F. Lefevre, S. Lips, C. Kinkelin, N. Rolland, P.A. Rolland, M. Zegaoui, S. Lhostis, P. Ancey, B. Descouts, Y. Kaplan, Thermal management of electronic devices by composite materials integrated in silicon, in: Microtherm, Lodz, Poland, 2013.

[14] S. Lips, F. Lefèvre, Contribution of Fourier series expansion to conventional heat pipe modeling: towards a universal analytical model, in: International Heat Pipe Conference, Kanpur, India, 2013.

[15] S. Lips, J.P. Meyer, Global optimisation of tube inclination during convective condensation, in: 8th International Conference on Boiling and Condensation Heat Transfer (ECI 8th), Lausanne, Switzerland, 2012.

[16] S. Lips, J.P. Meyer, Experimental study of Convective condensation of R134A in an inclined Tube, in: 8th International Conference on Heat Transfer, Fluid Mechanics and Thermodynamics, Pointe Aux Piments, Ile Maurice, 2011.

[17] S. Lips, J.P. Meyer, Effect of gravity forces on heat transfer and pressure drops during condensation of R134a, in: Eurotherm Seminar n°92, Presqu'îles de Giens, France, 2011.

[18] S. Lips, F. Lefèvre, J. Bonjour, What have brought observations inside the capillary structure to the knowledge on flat plate heat pipes?, in: 15th International Heat Pipe Conference (15th IHPC), Clemson, Etats-Unis, 2010.

[19] S. Lips, F. Lefèvre, J. Bonjour, Thermal and hydrodynamic study of a flat plate heat pipe, in: Proc. 7th Experimental Heat Transfer, Fluid Mechanics and Thermodynamics (ExHFT), Krakow, Poland, 2009.

[20] S. Lips, J. Bonjour, Oscillating two-phase flow in a capillary tube: Experiments and modeling, in: Proc. 14th International Heat Pipe Conference (IHPC), Florianopolis, Brazil, 2007.

- **Communications in national conferences with proceedings (5)**

[1] S. Lips, M. Narcy, A. Barrière, V. Sartre, Définition d'un critère d'utilité appliqué aux diffuseurs thermiques diphasiques pour le refroidissement de composants électroniques, in: Congrès de La SFT, Marseille, France, 2017.

[2] R. Giraudon, S. Lips, L. Gremillard, D. Fabregue, E. Maire, V. Sartre, Caractérisation thermo-hydraulique de structures capillaires frittées pour une utilisation dans les boucles diphasiques, in: Congrès de La SFT, Marseille, France, 2017.

[3] T. Layssac, S. Lips, R. Revellin, Assessment of stratification during horizontal two-phase flow of R-245fa: intermittent and annular flows, in: 22ème Congrès Français de Mécanique, Lyon, France, 2015.

[4] S. Lips, A. Fornells-Vernet, F. Lefèvre, Utilisation de mèches métalliques comme structure capillaire pour des caloducs plats., in: Congrès Français de Thermique, Gerardmer, France, 2013.

[5] S. Lips, J.P. Meyer, A model for stratified flow during convective condensation in an inclined tube, in: 12th UK National Conference on Heat Transfer, Leeds, Angleterre, 2011.

- **Communication in conferences without proceeding (4)**

[1] Giraudon, Remi, Stéphane Lips, Laurent Gremillard, Damien Fabregue, Eric Maire, et Valérie Sartre. « Manufacturing and thermohydraulic characterization of sintered capillary structure ». In Euromat2017. Thessaloniki, Greece, 2017.

[2] R. Revellin, S. Lips, T. Layssac, W. mauro, Stratification assessment during evaporative annular flow of R-245fa in a horizontal minichannel, in: 53rd European Two-Phase Flow Group Meeting, Zermatt, Switzerland, 2015.

[3] S. Lips, R. Revellin, Physical meaning of the pressure drop decomposition in two-phase flows, in: 51th European Two-Phase Group Meeting, Lyon, France, 2013.

[4] J.P. Meyer, S. Lips, A. Adelaja, J. Dirker, Condensation heat transfer in aerospace, (2012).

- **Citation reports**

Database	Google Scholar (https://scholar.google.fr/citations?user=tmHRYKEAAAAJ&hl=fr)		Scopus (https://www.scopus.com/authid/detail.uri?authorId=32167626800)
Number of publications	51 references		19 references
	All	Since 2013	All
Number of citations	578	468	348
H index	13	12	10
I10 Index	14	13	-

Curriculum Vitae (in French)

Stéphane LIPS, 35 ans
☏ tel : +33 (0)6 72 43 02 91
stephane.lips@insa-lyon.fr

Centre d'Energétique et de Thermique de Lyon (CETHIL)
UMR5008, CNRS, INSA Lyon, Univ. Lyon 1,
Université de Lyon
Bat. Sadi Canot, INSA-Lyon
F69621 Villeurbanne Cedex, France

Maître de conférences en thermique et énergétique :
Transferts thermiques avec changement de phase

Formation

Depuis septembre 2011	Maître de Conférences à l'INSA de Lyon : - Recherche au laboratoire CETHIL - Enseignement au département Génie Energétique et Environnement (GEN)
Jan. 2010 à juillet 2011	Post-doctorat à l'Université de Pretoria (Afrique du Sud) au sein du Thermofluids Research Group. *Etude expérimentale du phénomène de condensation convective en tubes lisses inclinés.*
Oct. 2006 à nov. 2009	Doctorat au Centre de Thermique de Lyon (CETHIL - UMR 5008). *Analyse phénoménologique du fonctionnement de diffuseurs thermiques diphasiques (caloducs plats) par voies expérimentale et numérique.*
2005-2006	Master Recherche MEGA. Spécialité Thermique-Energétique, en double cursus avec la 5ème année INSA.
2001-2006	Cycle ingénieur de l'INSA de Lyon. Département Génie Energétique et Environnement (GEN).

Activités de recherches

Etude des transferts thermiques avec changement de phase

- Etude des transferts thermiques avec changement de phase liquide-vapeur dans des structures capillaires innovantes.
- Etude de l'utilisation de matériaux à changement de phase solide-liquide pour le contrôle thermique de composants électroniques.
- Analyse thermodynamique des écoulements convectifs avec changement de phase.
- Etude expérimentale de la condensation et de l'ébullition convectives en tubes lisses inclinés : effet de la gravité sur le régime d'écoulement, les pertes de charge et les transferts thermiques.

Analyse phénoménologique du fonctionnement de différents types de caloducs

- Etudes des écoulements oscillants liquide-vapeur adiabatiques dans des tubes capillaires pour une application aux caloducs de type PHP (Pulsating Heat Pipe).
- Etudes expérimentale et théorique des écoulements et des transferts thermiques dans la structure capillaire de diffuseurs thermiques diphasiques et de LHP.
- Etudes expérimentale et théorique du comportement des caloducs soumis à des solicitations extremes (haute temperature, regime transitoire forts, choc thermiques…)

Activités d'enseignement

Interventions dans les cours du département GEN en équivalent L3 et M1 :

- Cours magistral, TD et TP d'échangeurs thermiques.
- Cours magistral, TD et TP de mesures physiques.
- TD de génie climatique et thermique du bâtiment.
- TP de mesures physiques, transferts thermiques, machines thermiques et mécanique des fluides
- Suivi de 6 à 8 étudiants en stage ou en PIRD à l'étranger par an.

Participation aux P2I du premier cycle de l'INSA de Lyon (équivalent L2)

Implications dans les formations d'énergetique et thermique d'INSAValor.

Rayonnement scientifique

- **Publications (voir liste complète des publications page 103)**

24 publications dans des revues internationales

Int. J. Heat Mass Transfer, Int. J. Multiphase Flow, Int. J. Therm. Sci., Energy, J. Heat Transfer, Appl. Therm. Eng., Frontiers in Heat Pipes, Microgravity Science and Technology, Int. J. Heat Fluid Flow

29 communications dans des congrès avec actes dont 25 conférences internationales

- **Expertises d'articles scientifiques**

Environ 35 expertises entre 2011 et 2018 pour une quinzaine de journaux internationaux et de conferences internationales

- **Relations internationales (par ordre alphabétique)**

Pr. Sameer Khandekar, IIT Kanpur (Inde) échanges réguliers, professeur invités au CETHIL, participation au projet Indien CEFIPRA2 (2 publications communes).

Pr. William Mauro, Federico II University of Naples (Italie), professeur invité au CETHIL d'Avril à Aout 2017 (4 publications communes).

Pr. Yu F. Maydanik, Institute of Thermal Physics of Ekaterinburg (Russie) accueil au sein du CETHIL de Eric Bartuli en 2012 et 2013 , doctorant de l'Institute of Thermal Physics of Ekaterinburg.

Pr. Josua Meyer, University of Pretoria (Afrique du Sud) échanges réguliers suite à mon post-doctorat, suivi de 4 stagiaires GEN à l'Université de Pretoria en tant que tuteur enseignant (10 publications communes).

Pr. Tony Robinson, Trinity College Dublin (Irlande), échanges réguliers, professeur invité au CETHIL, suivi de 3 stagiaires GEN au Trinity College en tant que tuteur enseignant.

Encadrements

- **Co-directions et co-encadrements de thèse (5)**

Samuel Martel, depuis Octobre 2016, *Application des méthodes de fluorescence et de phosphorescence à l'étude des écoulements diphasiques*.
Bourse ministérielle MEGA, co-direction avec Rémi Revellin

Nicolas Cardin, depuis Octobre 2015, *Etude expérimentale et théorique de l'application des effets EHD aux caloducs plats.*
Financement Arc région Rhône-Alpes, co-encadrement avec Jocelyn Bonjour, Laurent Davoust (SIMAP) et Samuel Siedel (SIMAP)

Remi giraudon, Janvier 2015 à Décembre 2017 (36 mois), *Contribution à la fabrication et la compréhension du comportement thermique de structures capillaires optimales pour les boucles diphasiques à pompage thermo-capillaire.*

Finacement Carnot I@L, co-encadrement avec Valérie Sartre, Laurent Gremillard (MATHEIS), Eric Maire (MATHEIS)

Thibaut Layssac, Octobre 2014 à Février 2018 (41 mois), *Etude expérimentale de l'ébullition convective en tubes inclinés.*
Bourse Ministérielle MEGA, co-direction avec Rémi Revellin

Christophe Kinkelin, Octobre 2012 à Septembre 2016 (48 mois), *Etude expérimentale d'un amortisseur thermique composite MCP-NTC.*
Projet ANR Therma 3D, co-direction avec Frédéric Lefèvre

- **Encadrements de post-doctorants et d'ATER (4)**

Antoine Voirand, depuis septembre 2017, *Etudes expérimentale et théorique de caloduc en polymères à ailettes intégrées.*
Post-doctorat, Projet CAPIT4L

Mostafa El Mehdi Brick, Septembre 2016 à Aout 2017 (12 mois), *Etude numérique de l'implémentation sous Comsol de champs électriques au sein d'une rainure rectangulaire.*
ATER INSA CETHIL-GEN

Marine Narcy, Juillet 2015 à Aout 2017 (26 mois), *Etude expérimentale de thermosiphons plats confinés pour le refroidissement de composants électroniques.*
Post-doctorat, Projet Européen I2mpect

Nicolas Blet, Juillet 2015 à Juillet 2017 (25 mois), *Contribution à l'implantation de systèmes diphasiques au sein d'un réacteur d'avion.*
Post-doctorat, Projet Airbus Optima

- **Encadrements d'Ingénieur d'études (2)**

Elise Berut, depuis Septembre 2017, soutien aux projets I2mpect et Capit4L

Antoine Barrière, Mars 2016 à Mars 2017, (12 mois), soutien au projet Européen I2mpect

- **Encadrements de niveau Master 1 et 2 (8)**

Charles Emmanuel Bronstein, Octobre 2016 à Janvier 2017 (3 mois), *Étude théorique et expérimentale de la faisabilité de caloducs en Polymère.*
Projet d'Initiation au développement (PID GMPP)

Elise Berut, Avril à Septembre 2016 (5 mois), *Étude théorique et expérimentale de la faisabilité de caloducs en Polymère.*
Stage d'Initiation à la recherche et au développement (SIRD GEN)

Léa Rigaud et **Jiaqi Ruan**, Février à Juin 2016 (4 mois), *Conception de la tête d'extrusion de nouvelle génération pour la technique de fabrication additive FDM.*
Projet de fin d'étude (PFE GMC)

Leo Revil Baudard, Avril à octobre 2014 (7 mois), *Etude expérimentale et théorique du comportement thermique et des limites capillaires des diffuseurs thermiques diphasiques.*
Stage d'Initiation à la recherche et au développement (SIRD GEN)

Christina Dominguez, Février à juin 2013 (5 mois), *Etudes expérimentales et théoriques de structures capillaires innovantes pour des applications de type caloducs plats.*
Projet d'Initiation à la recherche et au développement (PIRD GEN)

Hamza Hannachi, Décembre 2012 à avril 2013 (5 mois), *Etude expérimentale, hydrodynamique et thermique de l'évaporation dans les structures capillaires de caloduc.*
Projet d'Initiation à la recherche et au développement (PIRD GEN)

Alba Fornells-Vernet, Février à juillet 2012 (6 mois), *Etude expérimentale, hydrodynamique et thermique de l'évaporation dans les structures capillaires de caloduc.*
Projet d'Initiation à la recherche et au développement (PIRD GEN)

François Bocquet, Avril à Septembre 2010 (5 mois), *Single-phase heat transfer and pressure drop of water inside horizontal circular Smooth tube in the transitional flow regime.*
Master 1 internship, University of Pretoria (Afrique du Sud)

Contrats de recherche

- **INTENSIFILM** – ANR Blanc 2006-2009 (36 mois)
  Films liquides et intensification des transferts dans les systèmes et micro-systèmes à changement de phase et les milieux poreux.
  Partenaires : CETHIL, Univ. Toulouse, Univ. Marseille, INP Toulouse
  Aide de l'ANR : 550 k€
- **THERMA3D** – ANR P2N 2012-2015 (36 mois)
  Interposeur 3D pour le management thermique
  Partenaires : CETHIL, IEMN, CEA LITEN, Kaplan energy, ST Microelectronics
  Aide de l'ANR : 871 k€
- **2MATHER** – Projet Carnot Ingéniere@Lyon 2014-2017 (36 mois)
  Matériaux poreux structurés pour le management thermique
  Partenaires : CETHIL , MATEIS
  Aide de l'institut Carnot : 230 k€
- **OPTIMA -** Projet DGA (42 mois)
  Optimisation Thermique de l'Intégration de Moteurs d'Avions
  Partenaires : CETHIL , Airbus, ATHERM, PPrime, Cerfacs, Pulswer
  Budget financement : 2 503 k€
- **I2MPECT -** Projet Européen H2020 (36 mois)
  Integrated, Intelligent modular power electronic converter
  Partenaires : CETHIL , AMPERE, Airbus, Siemens, Univ. Zurich, Dynex, Safran,
  Budget total : 7 180 k€ dont 6 735 k€ de fonds europpéens
- **CAPIT4L** – Projet Carnot Ingéniere@Lyon 2018-2020 (24 mois)
  Caloduc à Ailettes en Polymère pour l'Industrie, le Transport et les Télécommunications couplant Transferts Thermiques avancés et Légèreté
  Partenaires : CETHIL , IPC
  Aide de l'institut Carnot : 210 k€
- **OUMOUSS** – Projet FUI 2018-2021 (36 mois)
  Conception innovante d'OUtillages combinant allègement et performances thermiques par l'utilisation de MOUSSes métalliques
  Partenaires : CETHIL, SANDEN, CASTMETAL, ARRK SHAPERS', INNOMOLDS, CETHIL, CTIF, IPC
  Budget total : 3 112 k€ dont 1 230 k€ d'aides

Responsabilités administratives

- **Responsable de la plateforme de TP énergétique du département GEN (depuis juillet 2013)**
- **Membre élu du conseil de département de GEN (depuis mai 2015)**
- **Coordinateur de la commission scientifique du CETHIL (d'avril 2013 à janvier 2015)**